

# **Synthesis of Multistable Equilibrium Compliant Mechanisms**

**by**

**Youngseok Oh**

A dissertation submitted in partial fulfillment  
of the requirements for the degree of  
Doctor of Philosophy  
(Mechanical Engineering)  
in The University of Michigan  
2008

Doctoral Committee:

Professor Sridhar Kota, Chair  
Professor Yogesh B. Gianchandani  
Professor Gregory M. Hulbert  
Assistant Professor Shorya Awtar

© Youngseok Oh

---

All Rights Reserved

2008

For my Mother, Father, sister and brother,  
and  
My beloved wife, Jihea, and my son, Isaac.  
Thank you for your support and love.

## Acknowledgments

I especially wish to express my gratitude to my advisor, Professor Sridhar Kota, who from the outset encouraged me in my work, provided me with many details and suggestions for my research. I was not able to complete this dissertation without his support and instruction. I was able to become a better researcher and in turn a real engineer because of his mentorship. His broad knowledge of mechanism design, including compliant mechanism design, gives me incredible advice whenever I discussed with him. His insights in engineering design and enthusiasm for the topic of multistable compliant mechanism inspired me to have an extensive vision in this area.

I wish also to record my appreciation to my other committee members. The thoughtful recommendations and suggestions of Professors Yogesh Gianchandani, Gregory Hulbert and Shorya Awtar have been extremely helpful in revising this dissertation.

I have also learned a lot from previous and current colleagues working in the Compliant Systems Design Laboratory (CSDL). My colleagues in the Compliant Systems Design Laboratory (CSDL) at the University of Michigan have also played an important role in the completion of this dissertation. I would like to thank Professor Charles Kim, Dr. Tanakorn (Tony) Tanakorn, Dr. Brian Trease, Dr. Christine Vehar Jutte, Mr. Michael Cherry, Mr. Dragan Maric, Mr. Girish Krishnan, Mr. Zachary Kreiner, Ms. Audrey Plinta, Mr. Joshua Bishop-Moser, Mr. Michael Manolidis, Mr. Rahul Sangole, Mr. David Lax, and Ms. Froukje Euwe. In particular, I would like to thank Michael Cherry for having read and commented on parts of the dissertation. I would also like to thank Michael Cherry and Girish Krishnan for the insightful conversation regarding the design of compliant mechanisms. I have learned a great deal from these discussions and was able to apply them even

to the research in this dissertation.

Finally, I would like to thank my family members. As always, my family members have been there, providing all sorts of tangible and intangible support. I know I would not have accomplished my work without their encouragement and support. My parents have always been my biggest fans and have never hesitated to support me. My sister and brother have also encouraged me to overcome the difficulties I had while I was pursuing the degree. I send gratitude separately to my sister, Kyungseok Oh, for having read and commented on parts of the dissertation. I would like to thank to my wife, Jihea who has assisted me in innumerable ways. She has been my friend, companion, and supporter. I was able to spend more time on my research because she devoted herself to taking care of our family.

# Table of Contents

<b>Dedication</b> . . . . .	ii
<b>Acknowledgments</b> . . . . .	iii
<b>List of Tables</b> . . . . .	viii
<b>List of Figures</b> . . . . .	ix
<b>List of Appendices</b> . . . . .	xiv
<b>Abstract</b> . . . . .	xv
<b>Chapter 1 Introduction</b> . . . . .	1
1.1 Compliant Mechanisms . . . . .	2
1.2 Bistable and Multistable Compliant Mechanisms . . . . .	4
1.2.1 Advantages . . . . .	5
1.2.2 Applications . . . . .	6
1.2.3 Nonlinearities and Stabilities . . . . .	8
1.3 Conclusion . . . . .	11
1.4 Organization of the Dissertation . . . . .	12
<b>Chapter 2 Literature Review</b> . . . . .	13
2.1 Synthesis of Compliant Mechanisms . . . . .	13
2.1.1 Lumped Compliant Mechanisms . . . . .	13
2.1.2 Distributed Compliant Mechanisms . . . . .	17
2.2 Nonlinearity in Compliant Mechanisms . . . . .	20
2.2.1 Buckling and Snap-through Behaviors . . . . .	21
2.3 Bistable and Multistable Compliant Mechanisms . . . . .	22
<b>Chapter 3 Overview of Synthesis Methodologies</b> . . . . .	26
3.1 Motivation . . . . .	26
3.2 General Approach . . . . .	27
3.2.1 Synthesis Procedures . . . . .	28
3.2.2 Design Domain Decomposition . . . . .	30
3.3 Scope of Research . . . . .	31

<b>Chapter 4 Synthesis of Bistable Compliant Mechanisms Using Buckled Configurations</b>	34
4.1 Introduction	34
4.2 Organization of This Chapter	34
4.3 Understanding the Characteristics of Bistable Compliant Mechanisms	35
4.4 Exploiting Bistability in Conventional Four-bar Linkage Mechanisms	38
4.4.1 Bistability of Grashof Four-bar Linkage Mechanisms	38
4.4.2 Bistability of Slider-crank Mechanisms	44
4.4.3 Tristable Four-bar Linkage Mechanism	50
4.5 Bistability of Buckled Configurations	51
4.5.1 Modal Strain Energy	52
4.5.2 Finite Element Model	55
4.5.3 Topology Synthesis Using Buckling Configurations	59
4.5.4 Effect of Imperfections	65
4.6 Conclusions	68
<b>Chapter 5 Robust Design of Bistable Compliant Mechanisms Using the Bistability of a Clamped-Pinned Beam</b>	70
5.1 Introduction	70
5.2 Organization of This Chapter	71
5.3 Bistability of a Clamped-Free Beam	72
5.3.1 Reverse-lateral Deformation	72
5.3.2 Solution for a Clamped-free Beam with a Reverse-lateral Deformation	73
5.4 Design of Bistability Using a Clamped-Pinned Beam	84
5.4.1 Design of Bistability Using Two RL Deformations	86
5.4.2 Design of a Rotational Bistable Compliant Mechanism Using RL Deformation	92
5.4.3 Design of Tristable Compliant Mechanisms Using RL Deformation	97
5.5 Conclusions	98
<b>Chapter 6 Synthesis of Multistable Compliant Mechanisms (MSCM)</b>	100
6.1 Introduction	100
6.2 Organization of This Chapter	101
6.3 Understanding the Characteristics of MSCMs	101
6.3.1 Understanding the Characteristics of MSCMs	101
6.3.2 Nonlinear Behavior of MSCM	104
6.3.3 Simplified Mathematical Expression of Bistable Behavior	107
6.4 Combining Multiple Bistable Behaviors in Series	109
6.4.1 Combining Bistable Behaviors with Different Actuation Loads	111
6.4.2 Numerical Procedure to Determine the Combined Multistable Behavior	112
6.5 Case Study 1: Combining Two Bistable Behaviors	113
6.6 Case Study 2: Combining Three Bistable Behaviors	118
6.7 Case Study 3: Combining Four Bistable Behaviors	121

6.8	Example: Quadristable Equilibrium Rotational Compliant Mechanism . . . .	123
6.9	Design of Tristable and Quadristable Compliant Mechanisms by Combin- ing Two Bistable Compliant Mechanisms . . . . .	127
6.9.1	Experimental Verification of the Two Combination Types, <b>TYPE<sub>21</sub><sup>21</sup></b> and <b>TYPE<sub>12</sub><sup>21</sup></b> . . . . .	129
6.9.2	Digitizing Multistable Behaviors . . . . .	130
6.9.3	Combining Two Rotational Bistable Compliant Mechanisms . . . .	131
6.9.4	Combining Four Bistable Compliant Mechanisms . . . . .	137
6.9.5	Combining Two Bistable Mechanisms Orthogonally . . . . .	140
6.10	Conclusions . . . . .	142
<b>Chapter 7 Design Examples . . . . .</b>		<b>144</b>
7.1	Meso-scale Rotational Multistable Compliant Mechanisms . . . . .	144
7.1.1	Design Specifications . . . . .	145
7.1.2	Design of Two Rotational Bistable Compliant Mechanisms . . . . .	146
7.1.3	Design of a Rotational Multistable Compliant Mechanism . . . . .	152
7.1.4	Discussion . . . . .	156
7.2	Multistable Cargo Door Design using a Multistable Compliant Joint . . . .	159
7.2.1	Design Specifications . . . . .	159
7.2.2	Design of a Rotational Multistable Compliant Mechanism . . . . .	160
7.2.3	Discussion . . . . .	164
<b>Chapter 8 Conclusions, Contributions and Future Work . . . . .</b>		<b>165</b>
8.1	Conclusions . . . . .	165
8.1.1	Summary of the Synthesis Methodologies . . . . .	166
8.1.2	Contributions . . . . .	167
8.2	Future Work . . . . .	169
8.2.1	Improving Design Methodologies of Multistable Compliant Mech- anisms . . . . .	170
8.2.2	Areas of Applications . . . . .	171
<b>Appendices . . . . .</b>		<b>172</b>
<b>Bibliography . . . . .</b>		<b>187</b>



## List of Tables

### Table

4.1	Design requirements and initial values of two design problems for bistable four-bar linkage mechanisms . . . . .	42
4.2	Classification of bistable Grashof four-bar linkage mechanisms. . . . .	45
4.3	Load-displacement curves for various stiffness ratio, $k_\theta/k_\delta$ . . . . .	49
5.1	Comparison of the results from Fig. 5.12 and experimental tests for various values of the included angle, $\Gamma$ . . . . .	88
6.1	Actuation loads and equilibrium positions defined in two bistable systems. .	111
6.2	Summary table for the combination of two bistable behaviors in series ( $n = 2$ ). . . . .	119
6.3	Matrix for number of stable equilibria for combinations of three bistable mechanisms. . . . .	122
6.4	Summary table for the combination of two bistable behaviors in series ( $n = 4$ ). .	123
6.5	Digitizing bistability. . . . .	131
6.6	An example of digitizing multistability: 1011. . . . .	131
7.1	Ratios of yield stress to elastic modulus of metals. . . . .	161

## List of Figures

Figure		
1.1	Bent trees: (a) a tree bent by wind and (b) a wind-bent tree. . . . .	2
1.2	Classification of compliant mechanisms [57]. . . . .	3
1.3	Compliant grippers : (a) a distributed compliant gripper [57] and (b) a lumped compliant gripper [61]. . . . .	4
1.4	Applications of bistable compliant mechanisms: (a) a stent [14], (b) a bottle lid [81], and (c) a switch [40]. . . . .	6
1.5	Electro-statically actuated micro-mirror array, from Integrated Photonics Lab. at U. C. Berkeley. . . . .	8
1.6	A typical load-displacement response [24]. . . . .	9
1.7	Nonlinear response patterns : (a) stiffening, (b) softening, (c) snap-through, and (d) snap-back [24]. . . . .	10
2.1	XY flexure mechanism [9]. . . . .	16
2.2	Pseudo-Rigid-Body-Model: (a) A flexible segment and (b) its pseudo-rigid-body model . . . . .	17
2.3	A hinge feature: (a) a gripper design using SIMP [61], (b) point connections between elements, and (c) a flexure after a post-processing step. . . . .	20
2.4	A schematic overview of the design of compliant mechanisms: (a) topology synthesis and (b) dimensional synthesis [57]. . . . .	21
2.5	A bistable compliant slider-crank mechanism [37]. . . . .	23
2.6	A multistable system consisting of an array of magnets [48]. . . . .	24
2.7	Multistable four-bar linkage demonstration problem [49]. . . . .	24
2.8	A pin-jointed multistable compliant mechanism [64]. . . . .	25
3.1	Flowchart for the design process of multistable compliant mechanisms . . . . .	29
3.2	Design domain decomposition procedures. . . . .	31
4.1	Potential energy curve and load-displacement curve of a bistable equilibrium system. . . . .	36
4.2	Four-bar linkage mechanism with rotational springs at each joint. . . . .	38
4.3	Classification of four-bar linkage mechanisms. . . . .	39
4.4	Load-displacement curve of a typical bistable four-bar linkage mechanism. . . . .	40
4.5	Two optimal solutions of Case 1: (a) <i>Type 1</i> and (b) <i>Type 2</i> . . . . .	43
4.6	Two optimal solutions of Case 2: (a) <i>Type 1</i> and (b) <i>Type 2</i> . . . . .	43
4.7	A slider-crank mechanism with two springs: (a) initial configuration and (b) buckled configuration. . . . .	46
4.8	Initial configuration of a slider-crank mechanism with two springs. . . . .	48

4.9	A multistable behavior by applying contact conditions. . . . .	51
4.10	Tristable four-bar switching mechanism. . . . .	51
4.11	Bistability of a buckled beam (an oil-canning problem). . . . .	52
4.12	Buckling analysis procedure to obtain buckled configurations. (a) desired buckled configuration, (b) applying load to the initial shape, (c) performing static analysis, (d) applying load to the deformed shape, (e) applying internal forces to the initial shape in order to determine the buckled configuration. . . . .	53
4.13	Strain Energy change when one of the buckled configurations is used as an initially unstressed configuration. . . . .	53
4.14	(a) static analysis: $\mathbf{Ku} = \mathbf{f}$ , (b) static analysis with unit load input: $\mathbf{Kv} = \mathbf{1}$ , and (c) buckling analysis: $(\mathbf{K} + \lambda_i \mathbf{K}_G) \bar{\mathbf{x}}_i = \lambda \mathbf{p}$ . . . . .	54
4.15	2-D beam element in the $x - y$ plane. . . . .	56
4.16	Rigid member (MPC) in the $x - y$ plane. . . . .	58
4.17	Bistable compliant mechanisms design: (a) rotational bistable compliant mechanism, and (b) translational bistable compliant mechanism. . . . .	60
4.18	Design domain discretization: (a) the right-top corner of the design domain in Fig. 4.17 (a), and (b) the upper half of the design domain in Fig. 4.17 (b) . . . . .	61
4.19	The optimal topology of the right-top corner of a bistable compliant mechanism (SQP). . . . .	62
4.20	The optimal topology of a rotational bistable compliant mechanism. . . . .	63
4.21	The optimal topology of the right-top corner of a rotational bistable compliant mechanism (GA): (a) $V_M = 0.23461$ (b) $V_M = 0.22842$ . . . . .	63
4.22	The optimal topology of the right-top corner of a translational bistable compliant mechanism (GA): (a) $V_M = 0.25522$ (b) $V_M = 0.23594$ . . . . .	64
4.23	A rotational bistable compliant mechanism: The initial stable and the second stable configurations [ME551 design project: a bistable trunk latch]. . . . .	64
4.24	A translational bistable compliant mechanism: (a) the initial stable configuration, and (b) the second stable configuration. . . . .	65
4.25	Implementing buckling modes to the original geometry: (a) preparing nonlinear analysis to obtain the bistable behavior of a perfect geometry, (b) solving for linear buckling modes, (c) accumulating obtained modes to the original geometry. . . . .	66
4.26	Load-displacement curves with and without imperfections. . . . .	67
5.1	Two stable stages of a beam with a force applied at the tip. . . . .	72
5.2	Problem definition of a reverse-lateral deformation. . . . .	74
5.3	Illustration of the relationship between $\theta_e$ and $n$ . . . . .	75
5.4	Dimensionless displacement of the free-end vs. dimensionless load for the loading direction, $n = 0.0 \cdots 1.2$ . . . . .	80
5.5	Minimum dimensionless load for the loading direction, $n = -2.0 \cdots 2.0$ . . . . .	81
5.6	Feasible deflection paths of the free-end for the loading direction: (a) $n = -2.0 \cdots 0.0$ , (b) $n = 0.0 \cdots 2.0$ . . . . .	82
5.7	Deflected shapes for (a) $n = -1.0$ and (b) $n = 1.0$ . . . . .	83
5.8	Feasible range of the deflection when load $P$ applied with an angle of $45^\circ$ . . . . .	84
5.9	Conceptual drawing of a bistable compliant mechanism with a clamped-pinned beam. . . . .	85

5.10	Relationship between $\gamma$ and $d/L$ for various values of $n$ .	86
5.11	Both stable configurations of a symmetrical bistable mechanism.	87
5.12	Relationship between $\gamma$ and $d/L$ for a symmetrical condition.	87
5.13	Load-displacement plots for four symmetric problems [ANSYS]	89
5.14	Bistable mechanisms using symmetric RL deformed beams. = (a) $160^\circ$ , (b) $140^\circ$ , (c) $120^\circ$ , and (d) $95^\circ$ .	90
5.15	Two stable configurations of an asymmetric bistable mechanism.	91
5.16	(a) Deformed result of an asymmetrical problem, and (b) load-displacement curve for the asymmetrical example.	92
5.17	Rotational bistable compliant mechanism design	93
5.18	(a) The relationship between $R_d$ and $\theta_{inc}$ , and (b) the relationship between $L$ and $n$ when $\theta_s = 17^\circ$ and $R = 20[\text{mm}]$ .	94
5.19	A rotational bistable compliant mechanism using RL deformed beams.	95
5.20	A rotational bistable compliant mechanism design tool.	96
5.21	A tristable compliant switching mechanism.	97
5.22	A multistable rotational compliant mechanism using RL deformed beams.	98
6.1	Potential energy and load-displacement curves of a multistable system.	102
6.2	A simple bistable compliant mechanism.	105
6.3	Load-displacement curves of : (a) solved using path following method, (b) solved using displacement-control method, and (c) solved using load- control method. (ABAQUS).	106
6.4	Illustration of the nonlinear behavior of a multistable compliant mechanism with four stable equilibria.	107
6.5	Piecewise-continuous function representing the key parameters (stable po- sitions and actuation loads).	108
6.6	(a)(b) Two bistable systems and (c) a combined multistable system.	110
6.7	Load-displacement curves of two bistable behaviors ( <b>TYPE<sub>21</sub><sup>21</sup></b> ).	111
6.8	Potential energy contour plot and potential energy (PE) path for <b>TYPE<sub>21</sub><sup>21</sup></b> . (b) represents the two axes ( $x_1$ and PE) isolated from the normal three axes, i.e. ( $x_1, x_2, \text{PE}$ ). The vertical lines, in (b) correspond to the jumps of $x_2$ in (a).	114
6.9	Deformed configurations of $\text{BES1}(x_1)$ and $\text{BES2}(x_2)$ of <b>TYPE<sub>21</sub><sup>21</sup></b> when $x_1$ increases steadily.	116
6.10	Load-displacement curves of the combined multistability: (a) displacement control and (b) load control.	117
6.11	Potential energy contour plot and potential energy path for <b>TYPE<sub>21</sub><sup>12</sup></b> and <b>TYPE<sub>12</sub><sup>21</sup></b> .	118
6.12	Combined multistable system consisting of three bistable systems.	119
6.13	Load-displacement curves of three different bistable behaviors ( <b>TYPE<sub>312</sub><sup>231</sup></b> ).	120
6.14	Potential Energy vs. displacement curve of combined multistable system behaviors ( <b>TYPE<sub>312</sub><sup>231</sup></b> ).	120
6.15	Load-Displacement curve of the combined multistability with controlling the load behaviors ( <b>TYPE<sub>312</sub><sup>231</sup></b> ).	121
6.16	Load-displacement curves of four bistable behaviors.	122
6.17	Two bistable compliant mechanisms of different dimensions (size and pro- portion)	124

6.18	Load-displacement curves for the bistable compliant mechanisms. (a) BiCM-inner, and (b) BiCM-outer. Key parameters are marked as circles. (ABAQUS)	124
6.19	Combined multistable equilibrium rotational compliant mechanism with four stable equilibria. . . . .	125
6.20	(a) Simplified mathematical functions of the two bistable behaviors, and (b) the combined results from Maple software. . . . .	126
6.21	Load-displacement curves for the combined multistable compliant mechanism using nonlinear analysis (ABAQUS). . . . .	127
6.22	Four stable configurations of the rotational multistable compliant mechanism.	128
6.23	Rotational bistable compliant mechanism. . . . .	130
6.24	Two combinations of the rotational bistable compliant mechanisms. . . . .	132
6.25	Combining two bistable compliant mechanisms in series: {01} . . . . .	132
6.26	Load-displacement responses of the two bistable mechanisms. . . . .	133
6.27	Potential energy contour plot and the equilibrium paths of the combined multistable mechanism, <b>TYPE<sub>21</sub><sup>21</sup></b> . . . . .	134
6.28	Potential energy curve of the combined multistable mechanism, <b>TYPE<sub>21</sub><sup>21</sup></b> . . . . .	134
6.29	Load-displacement behavior of the combined multistable mechanism, <b>TYPE<sub>21</sub><sup>21</sup></b> , using the load-control method. . . . .	135
6.30	Four stable configuration of the combined multistable mechanism, <b>TYPE<sub>21</sub><sup>21</sup></b> : (a) 0°, (b) 28°, (c) 33°, and (d) 61°. . . . .	135
6.31	Load-displacement responses of the two bistable mechanisms. . . . .	136
6.32	Potential energy curve of the combined multistable mechanism, <b>TYPE<sub>12</sub><sup>21</sup></b> . . . . .	137
6.33	Potential energy contour plot and the equilibrium paths of the combined multistable mechanism, <b>TYPE<sub>12</sub><sup>21</sup></b> . . . . .	138
6.34	Load-displacement behavior of the combined multistable mechanism, <b>TYPE<sub>12</sub><sup>21</sup></b> , using the load-control method. . . . .	138
6.35	Four stable configuration of the combined multistable mechanism, <b>TYPE<sub>12</sub><sup>21</sup></b> : (a) 0°, (b) 33°, (c) -28°, and (d) 5°. . . . .	139
6.36	Combining four bistable compliant mechanisms in series. . . . .	139
6.37	Multistable compliant mechanisms using four bistable compliant mechanisms. . . . .	140
6.38	Two axes rotational multi-bistable compliant mechanism. . . . .	141
6.39	Biaxial rotational multistable mechanism. . . . .	141
6.40	Four stable configurations of the combined multistable mechanism, <b>TYPE<sub>21</sub><sup>21</sup></b> : (a) 0°, (b) -18°, (c) -36°, and (d) -54°. . . . .	142
7.1	A rotational bistable compliant mechanism using RL deformation. . . . .	147
7.2	Design and analysis results of Rotational Bistable CM Design Tool for <b>BES2</b>	147
7.3	Nonlinear FE analysis for <b>BES2</b> : (a) load-displacement response and (b) strain energy plot [Ansys]. . . . .	149
7.4	Two stable positions of a RL beam of <b>BES2</b> and stress results. . . . .	150
7.5	<b>BES2</b> : a rotational bistable compliant mechanism with a 30° angle between stable positions . . . . .	151
7.6	Design and Analysis results of Rotational Bistable CM Design Tool for <b>BES1</b> . . . . .	151

7.7	Nonlinear FE analysis for <b>BES1</b> : (a) load-displacement response and (b) strain energy plot. . . . .	153
7.8	Bistable behavior related to slenderness ratio. . . . .	154
7.9	Two stable positions of a RL beam of <b>BES1</b> and stress results. . . . .	154
7.10	BES1: a rotational bistable compliant mechanism with a 40° angle between stable positions . . . . .	155
7.11	The combined rotational multistable compliant mechanism. . . . .	155
7.12	Nonlinear FE analysis for the combined rotational multistable compliant mechanism : (a) load-displacement response , and (b) strain energy plot. . . . .	157
7.13	The first and the fourth stable positions of the combined rotational multistable compliant mechanism and its stress results. . . . .	158
7.14	Minivan cargo-door: (a) rigid-link mechanism with a pneumatic door opening system, and (b) rotational multistable compliant mechanism. . . . .	160
7.15	Desired behavior of the multistable compliant mechanism and the door. . . . .	161
7.16	Load-displacement curves of the multistable compliant mechanism and the door. . . . .	162
7.17	Load-displacement curves of the multistable compliant mechanism and the door. . . . .	163
7.18	A combined rotational multistable compliant mechanism. (diameter 23cm, length 36cm) . . . . .	163
7.19	A cargo door that has two rotational multistable compliant mechanisms located at both ends. . . . .	164
1	Beam buckling analysis: (a) a single beam and (b) two beams in series. . . . .	173
2	Buckling modes and their critical loads: (a) one beam, (b)(c) two beams. . . . .	174
3	Relationship chart between the two out of three bistable behaviors. . . . .	175
4	Load-Displacement curve of <b>TYPE<sub>312</sub><sup>231</sup></b> and behaviors for two bistabilities in the curve. . . . .	176

## List of Appendices

### Appendix

A	Combining Bistable Behaviors with Identical Actuation Loads. . . . .	173
B	Alternative Approach to Obtain Multistable Behavior. . . . .	175
C	Combinations of Three Bistable Behaviors ( $n = 3$ ). . . . .	177
D	Elliptic Integral Solution for Reverse Lateral Deformation. . . . .	183
E	Sensitivity of Buckling Load and Corresponding Mode. . . . .	185

## Abstract

Whenever an engineering system operates far from its equilibrium position, the control and actuation scheme can become excessively complicated and power consuming. However, in a multistable compliant mechanism (MSCM), a passive subsystem can be integrated to afford discrete adaptability in function by providing additional equilibria thereby simplifying the actuation and control scheme. This dissertation explores the design and application of devices that exhibit multistability by exploiting compliance in design.

MSCMs have the essential advantages of compliant mechanisms including reduced part-count, assembly time, wear, and increased precision, durability and reliability. However, there is no systematic method to design MSCMs and the majority of prior research is limited to design of specific types of bistable mechanisms. This is due to the fact that design of MSCMs is not intuitive and it requires enormous computational time to overcome the complexity of nonlinear behaviors. This study is motivated by the need to design MSCMs systematically without excessive computational time and complexity.

The design methodology developed in this dissertation has two major components: (i) generalized methods for synthesizing bistable mechanisms and (ii) synthesis of multistable mechanisms by combining multiple bistable mechanisms. A mathematical formalism to ensure bistable behavior is first introduced. Two methods for synthesizing bistable mechanism are developed (i) by choosing “buckled” shape as initial configuration and (ii) by utilizing a reverse-lateral deformation of a clamped-pinned beam to provide bistability. Each bistable compliant mechanism works as a building block, providing either one or two additional stable states. A simplified mathematical scheme is introduced to capture essential parameters of bistable behaviors to aid in synthesis of more sophisticated multistable mecha-



nisms. The methodology enables designers to capture design requirements mathematically, decompose the problem into feasible sub-problems, synthesize the desired MSCMs from pre-compiled combination libraries, and efficiently evaluate the designs without computationally intensive nonlinear FEA. The method also yields robust designs that are insensitive to manufacturing and other imperfections. The synthesis methodology can benefit a variety of applications including MEMS, space mechanisms, ergonomic devices, and general product design. Several novel designs and working prototypes of MSCMs are developed to demonstrate the effectiveness of the synthesis methods.

# Chapter 1

## Introduction

Strength and stiffness coexist in most engineered artifacts. However, strength and flexibility, the two seemingly opposite properties, coexist within balance in the creatures of the nature. For instance, trees are capable of bending in strong wind, and this is a clever way for them to reduce the drag force of wind (Fig. 1.1(a)). Trees grow tall and strong but also withstand the strong winds with their flexibility [76]. When there is no wind, trees tend to return to their equilibrium in order to minimize their potential energy.

However, the need to survive strong winds sometimes shifts trees equilibrium to prevent the tree from collapsing. This is due to the fact that, by nature, objects driven far from equilibrium tend to develop local states[60] in order to minimize their potential energy. Equilibrium of a system can shift in either a continuous manner or discrete increments. For example, a wind-bent tree shown in Fig. 1.1(b) shifts its equilibrium shape adaptively in a continuous manner to strong wind. A fluid when heated shifts its equilibrium discretely by vaporizing. The concept of *adaptive equilibrium* is also included in Darwin's model[54].

In engineering systems design, when one attempts to create a system that operates far from a given equilibrium status, the control and actuation system can become excessively complicated and power-consuming. Such situation can be resolved once the equilibrium within the system shifts to the current operating range. The idea of a multistable equilibrium compliant mechanism is described in which a passive subsystem is integrated to afford *discrete* adaptability in function by providing additional equilibrium states, while the actuation and control system remain simple. This dissertation explores the design and



(a)

(b)

**Figure 1.1** Bent trees: (a) a tree bent by wind and (b) a wind-bent tree.

application of devices that exhibit multistability by exploiting compliance in design.

## 1.1 Compliant Mechanisms

Stiffness and compliance, two inversely proportional properties of man-made systems, are utilized and designed separately by different elements in conventional mechanisms. Conventional mechanisms deliver desired force and motion by using rigid links (large stiffness), kinematic joints (large compliance), and discrete springs. Design theories for conventional mechanisms have been studied for several decades, and their synthesis methods are well developed and even extended to design other kinds of mechanisms such as compliant mechanisms.

Compliant mechanisms also transfer force and motion by resembling nature's balancing tendency of the stiffness and compliance. These mechanisms are ideally designed to be monolithic, i.e. having no conventional joint. The absence of joints provides the following benefits [52, 42].

1. Reducing the friction, wear, weight, and backlash.
2. Requiring no lubricant.

3. Eliminating need for a separate spring to store elastic energy.
4. Resulting fewer links and interconnections, so compliant mechanisms are simpler, more economical and reliable.

The overall class of compliant mechanisms fits into two main categories depending on their material continuity (Fig. 1.2): *monolithic* and *non-monolithic*. Monolithic compliant mechanisms are single-piece or jointless flexible mechanisms. The compliant mechanisms can also be classified into two sub-classes based on the distribution of their compliance: *distributed* and *lumped compliant mechanisms*.

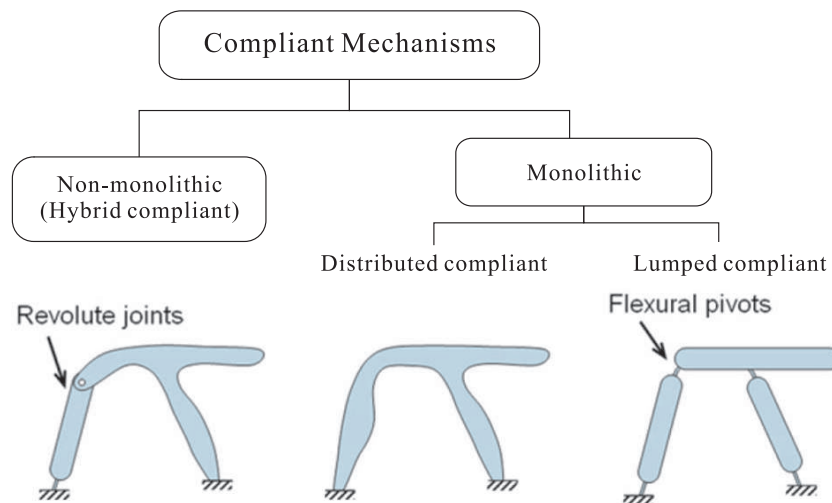


**Figure 1.2** Classification of compliant mechanisms [57].

A lumped compliant mechanism is characterized by flexures working as the joints between rigid members. Since rigid members of these mechanisms can only store a limited amount of energy, the flexural regions are increasingly subjected to concentrated stress. On the other hand, a distributed compliant mechanism utilizes most of its material to store elastic energy; thus, the stress is more evenly distributed throughout the mechanism. Examples of a distributed compliant mechanism and a lumped compliant mechanism are shown in Fig. 1.3.

A non-monolithic or hybrid compliant mechanism usually consists of traditional joints

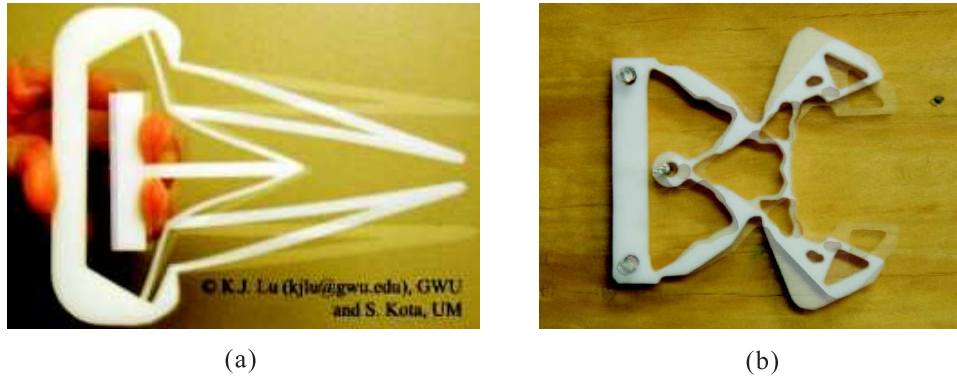


**Figure 1.3** Compliant grippers : (a) a distributed compliant gripper [57] and (b) a lumped compliant gripper [61].

(i.e. revolute joints in Fig. 1.2), rigid links and at least one flexible member. Assembly processes are typically required to manufacture the mechanisms in this category. Lumped and non-monolithic compliant mechanisms are sometimes called partially compliant mechanisms.

## 1.2 Bistable and Multistable Compliant Mechanisms

The term, *multistability*, is broadly used in many different fields including physics, dynamics, chemistry, and even in vision science. Some of the definitions of multistability in these fields are as following:

- Multistability is the property of having more than one stable fixed point [1].
- Multistability means the coexistence of several final states (attractors) for a given set of parameters [3].
- Multistability is a system property. It refers to systems that are neither stable nor totally unstable, but that alternate between two or more mutually exclusive states over time [2].

Although researchers in different fields define multistability in different ways, the underlying concept that they describe is essentially the same. Multistability is a system property representing the coexistence of two or more stable states for a given condition; thus, bistability is a subset of multistability with only two stable states.

The term, ‘multistable compliant mechanism’, is based on the concept that a mechanism can achieve multiple stable positions within its range of motion through compliance, i.e., elastic deformation of one or more of its members. Since multistable compliant mechanisms are a subclass of compliant mechanisms, they offer all the benefits described in the previous section. *The focus of this research is the design of monolithic multistable compliant mechanisms.*

### **1.2.1 Advantages**

Multistable equilibrium compliant mechanisms still have the essential advantages of compliant mechanisms. Such advantages are reduced part count, reduced assembly time, increased precision, increased reliability, reduced wear, reduced maintenance, etc. More importantly, the three main advantages are related to their stability, efficiency, and accuracy. They are stable because they remain in a stable position over time without a load from an actuator, and small disturbances do not change the stable position. They are efficient because each stable position can be reached by relatively uniform actuation forces, so it is not required to use a proportional actuator. They are accurate because the stable position will not change once the system is configured, so an open loop motion control is adequate. Thus, introducing multistability to a system reduces complexity, saves power and also improves the performance and functionality of a variety of devices, including conventional and compliant mechanisms in micro-systems and macro-systems [40, 27, 30, 7].

## 1.2.2 Applications

The majority of known applications for multistable compliant mechanisms are bistable. Fig. 1.4 shows some examples of bistable compliant mechanisms. Fig. 1.4 (a) shows two configurations of a bistable stent, a medical device that is inserted into a natural conduit of the body to prevent a disease-induced localized flow obstruction. This device requires at least two stable configurations because it must be inflated after the insertion, and is usually too small to use traditional joints. Fig. 1.4 (b) is a well-know bistable bottle lid that has two stable positions: opened and closed. Fig. 1.4 (c) is a bistable compliant switch which mimics the existing bistable conventional switching mechanism. These examples are monolithic. Some of them exhibit distributed compliance, and some are partially compliant.

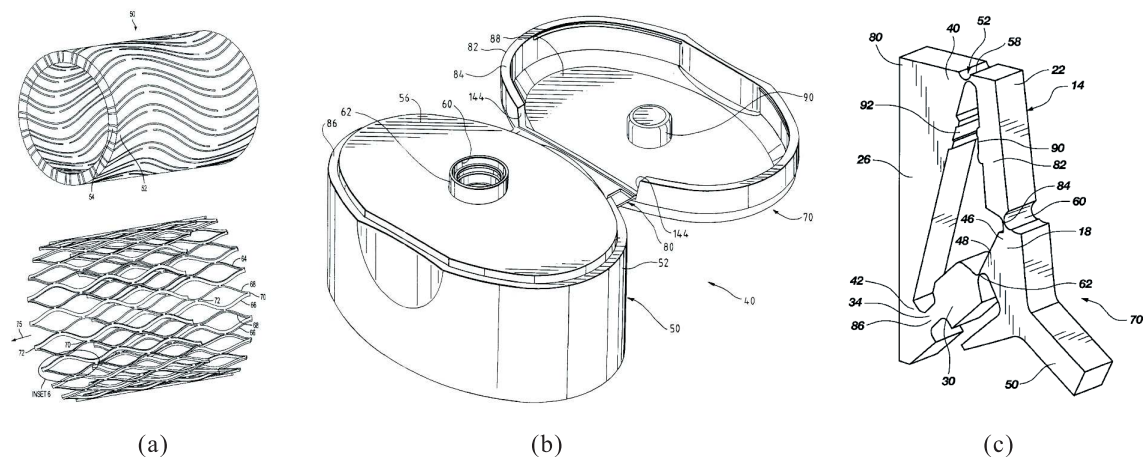


**Figure 1.4** Applications of bistable compliant mechanisms: (a) a stent [14], (b) a bottle lid [81], and (c) a switch [40].

A few multistable compliant mechanisms with more than two stable positions have been designed (e.g. bendable straws [26]). Such multistable compliant mechanisms are not very prevalent because they are difficult to design. Some of the potential applications of multistable compliant mechanisms are

- Multistable switches

- Multistable micro-electro-mechanical systems (MEMS)
- Multi-positioning devices
- Mechanical fuses

Multistable equilibrium mechanisms present a number of advantages in switching applications. They are used broadly as electrical/mechanical switches, and most traditional examples are rigid-body mechanisms consisting of springs, rigid links and joints. A multistable compliant mechanism drastically reduces part count. Therefore, a method of synthesizing multistable compliant equilibrium mechanisms would be very valuable in engineering designs for a broad variety of applications.

MEMS is another area in which multistable equilibrium compliant mechanisms perform well. There are many proven advantages of compliant mechanisms at the micro-level. They can be batch fabricated in a plane requiring no assembly, no need for lubrication, reduced friction and wear, and absence of joint clearance. For example, a MEMS fastener with multistability is used to assemble micro-parts [27]. MEMS switches and micro-mirrors are good examples of the applications of multistable equilibrium compliant mechanisms. An example of micro-mirror arrays is shown in Fig. 1.5. These devices normally consist of top and bottom electrodes. By applying electric potential between the electrodes, the electrostatic force pulls the top electrode down. Generally, pull-in voltage is used to maintain the positions. However, by integrating multistable equilibrium compliant mechanisms into such devices, the switches and mirrors maintain desired positions without expending energy.

Compliant mechanisms which require variable geometry or power are another promising area to apply multistability concepts. An adjustable toggle clamp and snap-fits are examples in this area. Additional stable equilibria give these devices the ability to adjust the opening size by applying different loads.

In recent years, the collision safety for service robots has become an important issue.



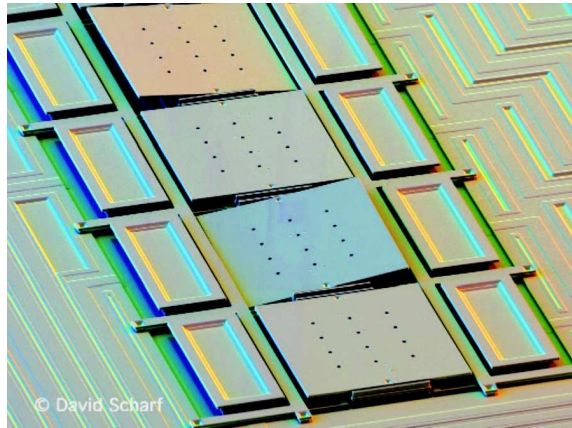


**Figure 1.5** Electro-statically actuated micro-mirror array, from Integrated Photonics Lab. at U. C. Berkeley.

To resolve the issue, passive compliance is preferred to active compliance because it can provide faster and more reliable responses to dynamic collision [65, 66]. Snap-through behavior, one of the nonlinear behaviors of multistable compliant mechanisms, can provide the required responses for collision safety.

### 1.2.3 Nonlinearities and Stabilities<sup>1</sup>

A fishing pole is very flexible and easy to bend when a perpendicular load is applied at the end of the pole. When the load on the pole is increased, a fisherman usually pulls the pole backwards to reduce the moment arm so that the pole can support the additional load. This is a stiffening effect which can be described as one of the nonlinear behaviors of the fishing pole.

The main differences between linear and nonlinear behaviors are:

- Linear behavior satisfies the properties of superposition.
- Linear behavior has one equilibrium point at the initial state. Nonlinear behaviors may have more than one equilibrium points including the initial state.
- Nonlinear behavior depends on the loading history. The loading history is critical to

---

<sup>1</sup>The terminology and figures used in this section are either taken or modified from [24].

estimate the final states of the systems.

These differences can also be explained by their response curves (Fig. 1.6).

The overall static behavior of compliant structures can be characterized by a *load-displacement* response. The load-displacement response can be drawn in a 2-D plot with a vertical and horizontal axis. The vertical axis usually represents the load quantity or load factor, which is a scaling factor of the given input load. The horizontal axis represents displacement quantity. When the displacement is very small at the initial state, the response can be approximated as a linear behavior. The constant value of the slope of the response curve is used to estimate the stiffness of the linearized system (Fig. 1.6). Note that a positive value of stiffness represents stable status and that the initial state of the compliant mechanism is always stable due to the positive stiffness of its linearized behavior.

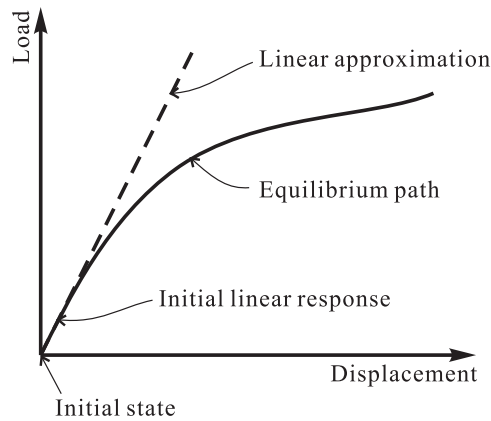


**Figure 1.6** A typical load-displacement response [24].

However, in general, the actual behavior of compliant mechanisms is nonlinear, and the nonlinear behavior arises from a number of causes, which can be grouped into the following three main categories[8].

1. Geometric nonlinearity.
2. Material nonlinearity.
3. Changing status (boundary conditions including contact).

There are three classes of geometric nonlinearity: large strains, small strains with finite displacements and/or rotations, and linearized prebuckling. Geometric nonlinearity is usually represented by small strains with large displacements and/or rotations, and is the most common source of nonlinear behaviors in compliant mechanisms. Large strains and linearized prebuckling cause geometric nonlinearity, but these are not common in compliant mechanisms. Material nonlinearity is related to the nonlinear behaviors of material, such as plastic, hyperelastic, viscoelastic, and yielding responses. Changing status is usually caused by changing the boundary conditions, such as follower forces and changes in contact status (e.g. contact to no-contact). A follower force is a force whose direction depends on the deformed shape. A pressure applied on a surface, in general, is considered as a follower force because it acts normal to both the undeformed and deformed surfaces.

Among the three sources, the nonlinear behavior in this dissertation represents geometric nonlinearity. Fig. 1.7 shows some of the nonlinear behavior of compliant structures.  $R$  and  $F$  denote the initial or reference state and the failure state, which are the starting and ending points of the curves.  $L$  and  $T$  denote the limit and turning points [24].

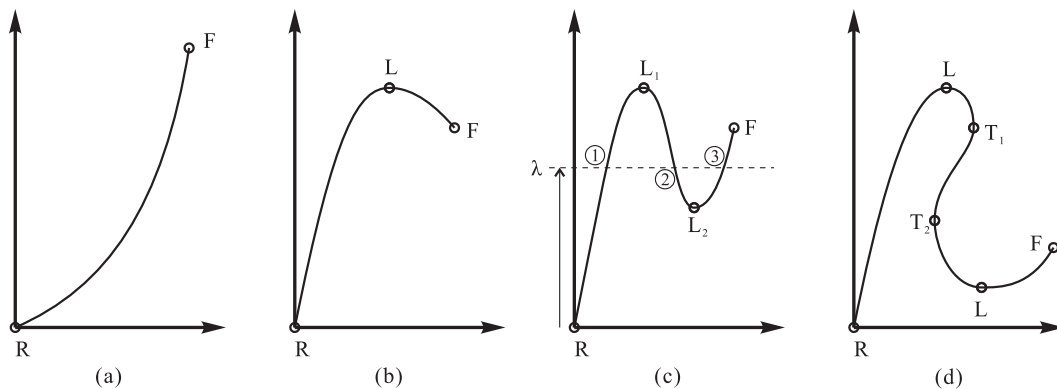


**Figure 1.7** Nonlinear response patterns : (a) stiffening, (b) softening, (c) snap-through, and (d) snap-back [24].

Figs. 1.7 (a) and (b) are well-know nonlinear responses called stiffening and softening behaviors.

The snap-through response in Fig. 1.7 (c) combines softening with stiffening (after the second limit point,  $L_2$ ). The response branch between the two limit points,  $L_1$  and  $L_2$ ,

has a negative stiffness and is, therefore, unstable [24]. Multistability in this response can be explained by applying a load factor,  $\lambda$ , that represents a preloading condition. The horizontal line at  $\lambda$  crosses the response curve three times with two positive slopes and one negative slope between the two. The first positive slope (or positive stiffness) at ① represents the first stable status, and the second positive slope at ③ represents the second stable status. The system is unstable at ② because the slope is negative, (or negative stiffness). In the snap-back response in Fig. 1.7 (d), the response curve turns back between the two turning points. The positive equilibrium (slope) between the two turning points,  $T_1$  and  $T_2$ , may be stable and consequently physically reliable [24].

Load-displacement behaviors of multistable compliant mechanisms are subcases of either Fig. 1.7 (c) or (d), but much more complicated. Note that for multistable compliant mechanisms, the two positive slopes of the curve cross the horizontal axis at  $\lambda=0$ .

## 1.3 Conclusion

The objective of this research is to create an engineering framework to synthesize multistable compliant mechanisms that achieve desired stable positions.

In spite of the attractive benefits of multistable compliant mechanisms, only few products have been developed because of complete lack of design methods. Due to the complex nature of nonlinear behaviors and multistable response, there is no intuitive approach to design multistable compliant mechanisms. In this dissertation, the following two approaches are developed and investigated.

1. Simplification of nonlinear behavior.
2. Decomposition of multistable behaviors.

The first approach captures the essential nature of nonlinear behavior in a simple math-

emational form. The second approach decomposes the multistable behaviors into multiple bistable behaviors which are relatively easy to design.

## **1.4 Organization of the Dissertation**

This chapter introduced the concept of a multistable compliant mechanism as well as benefits of compliant mechanisms. The next chapter reviews the relevant work in the area of compliant mechanism design and multistable systems. Chapter 3 addresses research issues for designing multistable compliant mechanisms. It also addresses a general approach to synthesis multistable compliant mechanisms. Chapters 4 and 5 offer two different approaches to design bistable compliant mechanisms. Chapter 6 provides a method to synthesize multistable compliant mechanisms by combining bistable mechanisms. Chapter 7 presents two design examples of multistable compliant mechanisms with extreme design requirements. Finally, Chapter 8 summarizes the contributions, and future work of this research.

## Chapter 2

### Literature Review

This chapter reviews some of the past work published in the areas related to synthesis of compliant mechanisms and bistable and multistable equilibrium systems. This chapter is organized as follows. The following section includes reviews of literature in compliant mechanisms as well as their synthesis methods. Section 2 is a review of the literature in compliant mechanisms focusing on nonlinear behaviors. Section 3 is a review of the literature in multistable mechanisms including bistable compliant mechanisms.

#### 2.1 Synthesis of Compliant Mechanisms

Compliant mechanisms can be classified into two categories depending on the distribution of their compliance: *lumped compliant mechanisms* and *distributed compliant mechanisms*. A lumped compliant mechanism exploits its elastic deformation at a limited number of locations, while the rest of its body is rigid. On the other hand, a distributed compliant mechanism fully utilizes the material elasticity in all members of the system.

The historical backgrounds of the two categories, lumped and distributed compliant mechanisms, are discussed in the following two subsections.

##### 2.1.1 Lumped Compliant Mechanisms

The use of compliant mechanisms to transmit force and motion has been studied for many decades. Because the deformable members in compliant mechanisms increase the com-

plexity of design, researchers have developed appropriate methods to apply existing conventional mechanism design methodologies to design compliant mechanisms. Classical *kinematics design methods* can be implemented to design lumped compliant mechanisms as well as mechanisms with cantilever-like flexible links. This is due to the fact that the design methodologies of conventional mechanisms have been well developed. Additionally, the majority of conventional mechanical devices have been designed to be rigid, and the rigid members in the conventional mechanisms can conveniently simplify the design approaches because of their limited number of kinematic degrees of freedom.

### **Flexure Hinges**

The earliest kinds of compliant mechanisms were designed based on flexures. Since flexures or flexure hinges were well established by Paros and Weisbord [67], they have been broadly applied in many compliant mechanisms. The advantages of flexure hinges are their high tolerances to manufacturing error, repeatability, and stability in their ranges of motion. These advantages are extremely useful in many compliant mechanisms in precision machinery and instrumentation which require loads that are not high and displacements that are very small [75].

More detailed study of traditional flexures has been conducted by Lobontiu [56], including design methods, material selection, and geometry optimization. Analysis and synthesis of these mechanisms simply represent an extension of the theory that has already been developed for rigid link mechanisms. Traditional flexures are broadly used in MEMS devices such as micro-grippers and micro-parallel mechanisms [53, 47, 46]. The most critical disadvantage is the stress concentration in the flexures because the lumped members cannot carry the strain energy when the structure is deformed. Since the range of motion is typically limited by the stress constraint, traditional flexures are limited to small motion devices.

The availability of living hinges, which are pivot-like short and thin flexures, with plas-

tic material (e.g. polypropylene) extends the functionalities of traditional flexure mechanisms with less accuracy. A living hinge usually joins two rigid plastic parts together and works like a rotational joint. This type of hinge is typically manufactured in an injection molding process that fabricates the three parts simultaneously and monolithically. It is also possible to use the living hinge to reduce the moment applied to flexible members in compliant mechanisms[63]. Despite the inaccurate motion behavior, it has been widely employed in less-demanding applications such as plastic bottle lids.

As an alternative to living hinges, for the design of large-displacement flexures with higher accuracy, compliant revolute joints that perform the function of bearings have been developed by Trease, Moon, and Kota [78].

### **Constraint Based Design**

The basic concepts of constraint-based design for general machine design have been introduced by Blanding [16]. The fundamental principle of constraint based design is achieving desired degrees of freedom by applying the minimum number of constraints required. The same principle can be applied to design compliant mechanisms. Beam flexures are broadly used for constraint based design because of their absolute rigidity in certain directions and absolute compliance in other directions [16]. For example, a beam flexure is used as a means of distributing stress in flexure mechanisms with constraint based design [10, 9, 20]. A parallel kinematic XY flexure mechanism is designed by applying the concepts of constraint-based design (Fig. 2.1).

### **Pseudo-Rigid-Body-Model**

Howell and Midha [33, 32] introduced the idea of a pseudo-rigid-body model to simplify compliant mechanism analysis. In this model, a flexible mechanism is modeled by utilizing the synthesis method of conventional rigid-link mechanisms. Response behaviors of flexible beams are estimated by equivalent links, joints and spring. The pseudo-rigid-body



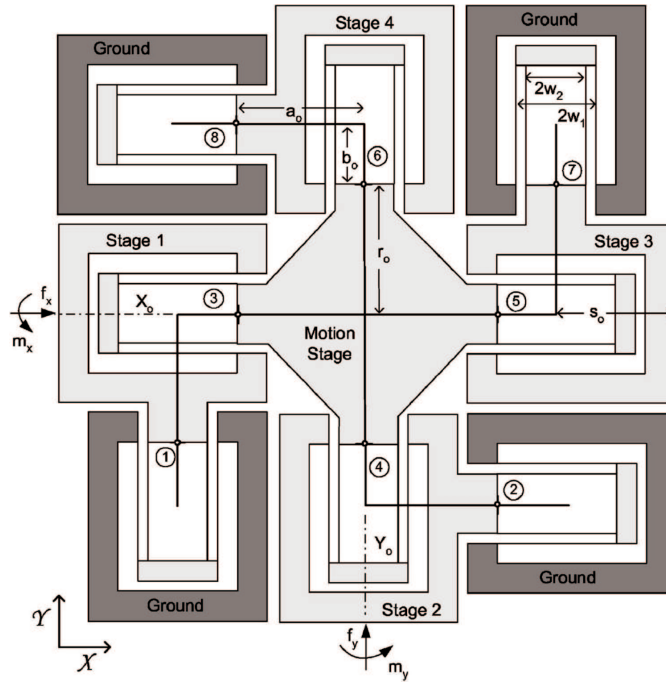
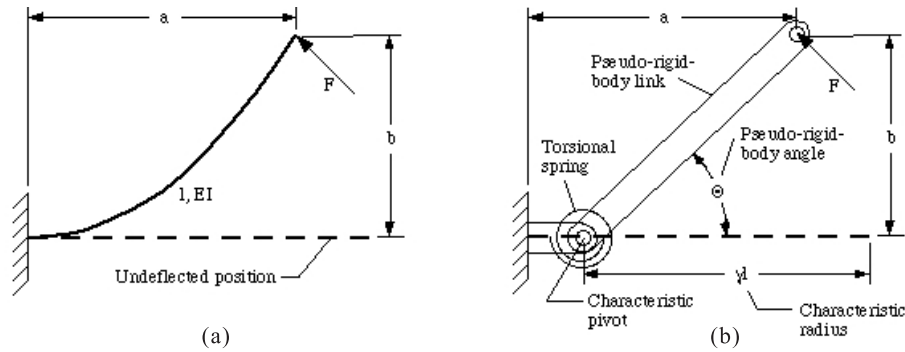


Figure 2.1 XY flexure mechanism [9].

model approach employs the same advantages of kinematic-based design methods. Additionally, the model is applicable to large deformation analysis of compliant mechanism since it uses a set of parametric equations that approximate the nonlinear load-displacement behaviors of flexible members; therefore, the large deformation of a compliant mechanism with a given topology can be predicted without nonlinear finite element analysis.

An example of a flexible segment is shown in Fig. 2.2 with its corresponding pseudo-rigid-body model. The approximated behavior of the segment can be determined based on the characteristic pivot,  $\gamma$ , and spring constant, which can be obtained by the geometry and loading conditions.

In the years following its introduction, pseudo-rigid-body models for many types of flexible links have been presented [34, 35, 36]. This model has enabled many compliant mechanisms to be designed and analyzed much more easily than in the past. For example, snap-fit micro-devices have been designed using the pseudo-rigid-body model [61].



**Figure 2.2** Pseudo-Rigid-Body-Model: (a) A flexible segment and (b) its pseudo-rigid-body model

### 2.1.2 Distributed Compliant Mechanisms

For many decades, structural optimization methods have been broadly used largely to design strong and stiff structures (maximizing the stiffness) with limited volume or weight of materials (volumetric constraints). Topology optimization identifies the topology of the structure which can be defined as the number of holes in the solid structure and their arrangement. This *optimization approach* has been adapted to design compliant mechanisms and is carried out in two stages to yield distributed compliance: (i) topology synthesis and (ii) dimensional synthesis.

Typically, the synthesis procedures of compliant mechanisms using the optimization-based approaches contain the following four steps [59]: (1) design domain specification, (2) design domain parameterization, (3) topology optimization, and (4) size/shape optimization. Two different optimization schemes are used based on the two different parameterizations of the design problems. This section provides further details on the two optimization schemes and the two parameterizations.

#### Optimization Types

The following two optimization schemes are most widely used for structural optimizations.

1. Gradient-based Optimization.
2. Discrete Optimization.

Gradient-based optimization is applicable when the design variables are continuous. Such design variables are material distribution as well as dimensions of components or members and locations of nodes. Two well known material distribution methods are HDM (homogenization design method [13]) and SIMP (Solid Isotropic Microstructure with Penalization [12]).

Since the material distribution methods were introduced for numerical implementations of the topology design for continuum structures, extensive research to design problems of compliant mechanisms was conducted by extending the methods. The first applications of compliant mechanisms synthesis using topology optimization appeared in the work of Ananthasuresh, Kota, and Gianchandani [6] and Ananthasuresh, Kota, and Kikuchi [7]. The approach based on the maximization of the ratio of mutual strain energy (MSE) and strain energy (SE) was initiated in Frecker, Ananthasuresh, Nishiwaki, and Kota [25]. Additionally, the robustness of optimization convergence is improved by using the spring approach suggested in Hetrick, Kikuchi, and Kota [31].

The genetic algorithm or GA is the most commonly used method for discrete optimization of structural design [29]. GAs have also been used to find the optimal topology in compliant mechanism designs [77, 79]. Although GAs have been used broadly for their flexibility in selecting design variables and objective functions, they have encountered difficulties when the connectivity of the structure is not handled properly.

When using a GA, the load-path approach that relies on the connection paths of the boundaries and load locations as the design variables resolves this issue [57]. This method is also utilized for the synthesis of shape morphing compliant mechanisms [58]. A shape morphing compliant mechanism changes its shape through structural deformation, which is independent of the problem scale. The least square error between the deformed shape

and the target shape is used as a design objective. The shape control of external surfaces has been dealt with in Saggere and Kota [71].

### **Design Parameterizations**

Once the design domain is specified in the first step of the design process, the domain can be discretized based on either continuous or discrete variables. The continuous or discrete design variables are used for the gradient based or discrete optimization schemes respectively. When the design domain is discretized, there are two types of design parameterizations which are commonly used in structural optimization [29].

1. Homogenization approach.
2. Ground structure approach.

In the homogenization approach, the design domain is meshed with a 2-D plane or 3-D solid elements. For gradient-based optimization, either the homogenization method or SIMP is commonly used. On the other hand, in the ground structure approach, the design domain is meshed with 2-D or 3-D beam elements. For the gradient-based optimization, the design variables are the thickness of the beam elements. For GA, the design variable is the existence of each member which can be defined in binary number (0 and 1). The advantages and disadvantages of the two approaches are clearly explained by Lu and Kota [59].

One of the well-known drawbacks of the homogenization approach is the point connection between two elements (Fig. 2.3(a)). The point acts as a rotational joint, and the resulting ultra-thin structural elements create high stress concentrations and pose manufacturing challenges (Fig. 2.3(b)). In many cases, additional post-processing is required for the final design interpretation [68, 69].

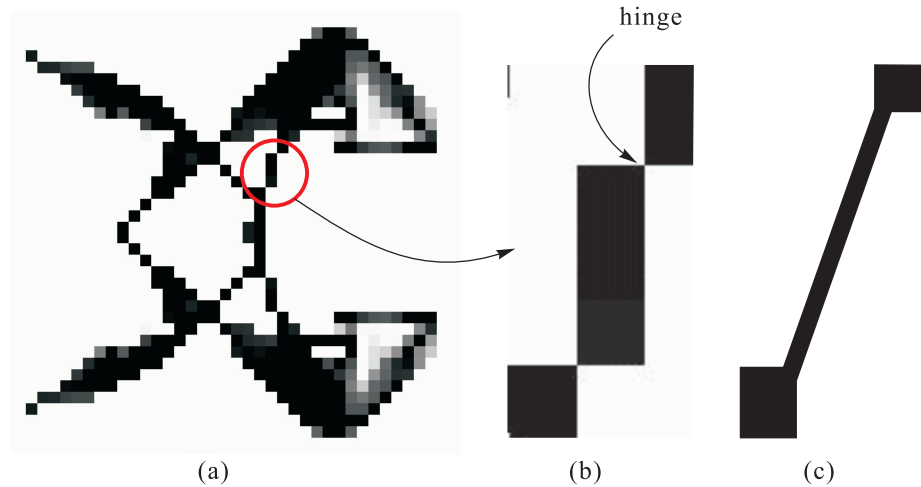


**Figure 2.3** A hinge feature: (a) a gripper design using SIMP [61], (b) point connections between elements, and (c) a flexure after a post-processing step.

In the ground structure approach, since beam elements cannot utilize the full design space, node locations as well as beam thicknesses can be design variables. Because there can be an excessively large number of design variables, the synthesis process is divided into two processes: 1) topology synthesis and 2) dimensional synthesis. Topology synthesis provides a functional design that satisfies the input/output or force/motion specifications within a specified space. Dimensional synthesis completes the design to comply with performance requirements such as maximum stresses, geometrical advantage or mechanical advantage, size constraints, and buckling constraints [42].

The schematic overviews of the two processes are shown in Fig. 2.4.

## 2.2 Nonlinearity in Compliant Mechanisms

Researchers have used linear beam elements and considered bending to improve the analysis accuracy for 2-D compliant mechanisms [44]. In many cases, a significant number of structures in compliant mechanisms are under nonlinear deformation due to geometry nonlinearity, material nonlinearity, or boundary nonlinearity. However, nonlinearity in compliant mechanisms has been explored only by a few researchers [45, 43]. Joo and Kota

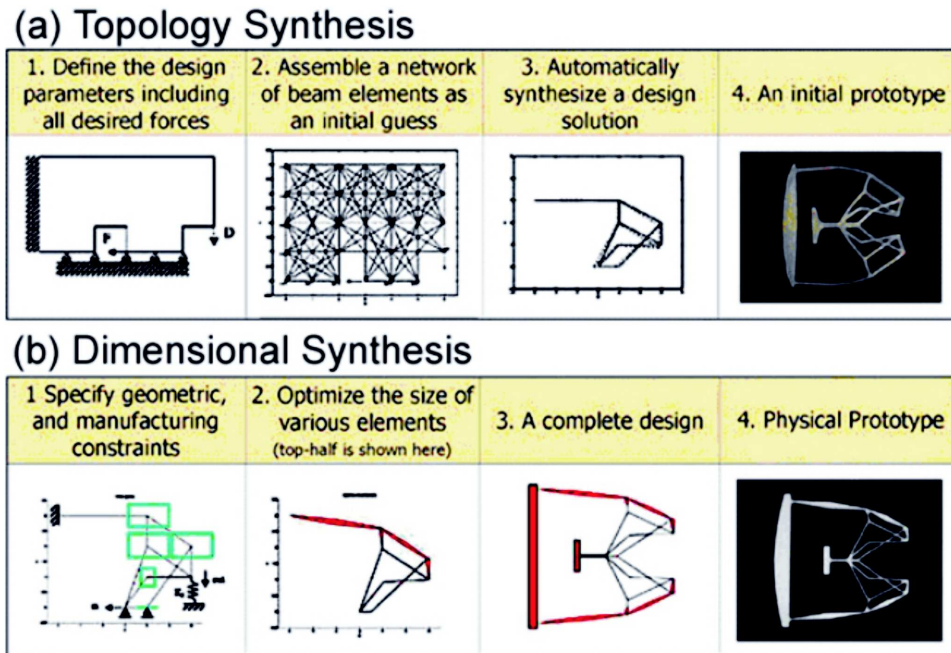


**Figure 2.4** A schematic overview of the design of compliant mechanisms: (a) topology synthesis and (b) dimensional synthesis [57].

presented a nonlinear formulation for the dimensional synthesis of compliant mechanisms using tapered beam elements. Since mechanisms intrinsically provide large deflections, they should be modeled using large displacement theory. Path generating mechanisms have been treated in Saxena and Ananthasuresh [72]. A design methodology for nonlinear springs that match a prescribed stiffness has been studied by Vehar and Kota [80, 79].

### 2.2.1 Buckling and Snap-through Behaviors

When beams undergo compression, snap-through behavior can occur. This is also a geometric nonlinearity problem. However, snap-through behavior in compliant mechanisms has not been studied sufficiently. Some of the MEMS literature mentions designing snap-through behaviors on the micro-level by utilizing bistable equilibria. Because of the dominance of surface friction forces inherent at the micro-scale, many MEMS devices cannot use hinges or joints. Thus, they rely on compliance to allow motion, and one must account for their elastic strain energy [41]. Some designs incorporating bistability use the concept

of buckling [74].

In general, bistability is induced by buckling phenomena. The associated snap through behavior depends on imperfections of the system. In other words, when a system is unstable, it can be sensitive to the imperfections in manufacturing processes, operating conditions, and boundary conditions. In order to reduce sensitivity to the imperfections, many designs in the literature rely on one or more of the following conditions: (a) using rigid members [38, 70], (b) inducing residual stress [23], and (c) using multiple living hinges [40]. These are the conditions which effectively reduce their sensitivity toward imperfections, ensuring bistability. For example, a mechanism designed with symmetric boundary condition without any of the aforementioned conditions may not be able to exhibit bistable behavior since the first buckling mode of a symmetrical mechanism is anti-symmetrical and will destroy the potential energy barrier between the stable positions [70]. Additionally, using rigid members and multiple living hinges increases stress concentrations, and relying on residual stress makes it difficult to control the accuracy of the stress level.

## 2.3 Bistable and Multistable Compliant Mechanisms

Depending of the number of stable equilibria, multistabilities in compliant systems can be divided into two categories: 1) bistabilities and 2) multistabilities with more than two stable configurations. A considerable amount of research has been done on multistable linkage mechanisms, including rigid-link and pinned-truss mechanisms, but MSCMs are essentially different from multistable linkage mechanisms. Rigid-link mechanisms have finite degrees-of-freedom (DOFs) whereas compliant mechanisms have virtually infinite DOFs. The literature on multistable compliant mechanisms is mostly restricted to bistable mechanisms. Most of the bistable-related literature has been presented for decades. Howell and Midha used a pseudo-rigid-body model to design a bistable compliant slider-crank mechanism (Fig. 2.5)[37]. In their model, a flexible mechanism link was modeled by utilizing

the synthesis method of conventional rigid-link mechanisms. A theory to generate bistable behavior in a certain class of compliant structures that directly resemble four-bar linkages has been established [40, 39]; however, the theory deals with each energy storage spring separately.

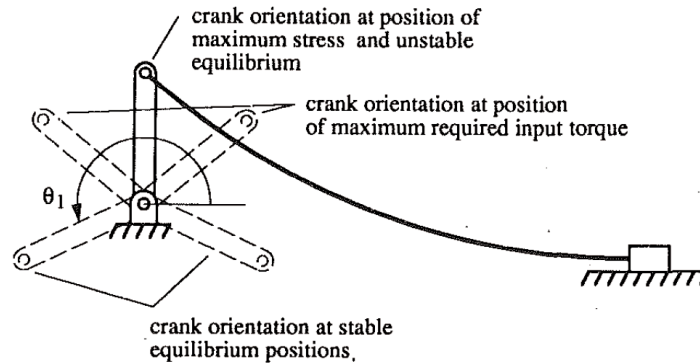


**Figure 2.5** A bistable compliant slider-crank mechanism [37].

Kollata, King, and Campbell [51] demonstrated the bistable behaviors of distributed compliant structures. However, there is a design limitation because topology information must be specified before optimization. Dixit and Campbell developed a bistable compliant MEMS relay [21]. However, in this method, beams cross into each other at the second stable configuration. To generate multistable equilibria without difficulties, magnetic fields have been applied to the systems. Limaye, King and Campbell [55] demonstrated multistability in a magneto-static field. Fig. 2.6 shows a multistable system with an array of magnets [48].

King et al. [48] described the numerical optimization and synthesis of a system composed of energy storage elements from energy domains, including magnetism and mechanical rotation and translation. With only mechanical springs and linkages, King et al. [49] used an optimization approach to demonstrate a specific four-bar linkage problem with more than two stable equilibria. A four-bar linkage mechanism with eight springs attached to the links for the demonstration is shown in Fig. 2.7.

The approach utilizes Monte Carlo mapping to acquire data that can be used as a base-



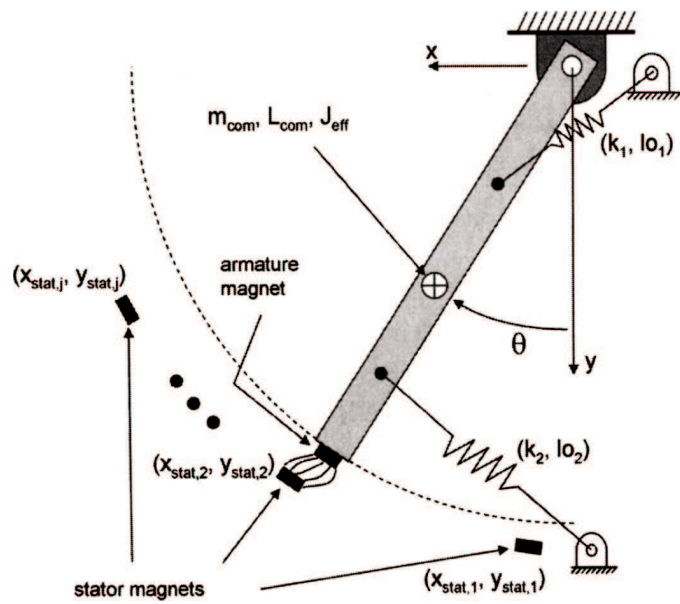


**Figure 2.6** A multistable system consisting of an array of magnets [48].

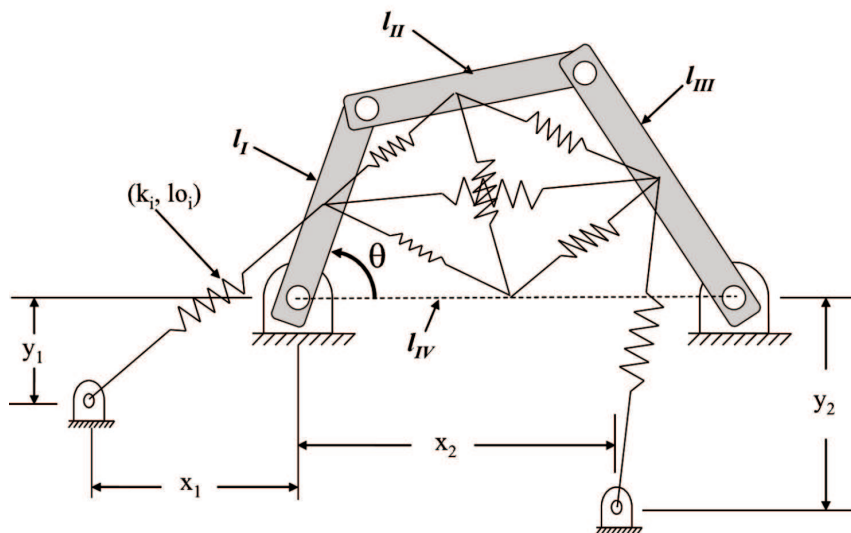


**Figure 2.7** Multistable four-bar linkage demonstration problem [49].

line case for optimization. However, the enormous computational time demanded by the complexity with infinite DOF compliant mechanisms makes it difficult to take advantage of the approach. Using pin-jointed bar elements, Ohsaki and Nishiwaki [64] presented an approach that generates pin-jointed multistable compliant mechanisms. In their approach, an unstable equilibrium state acts like a pseudo-stable state by locking the actuator. Fig. 2.8 shows three "stable" positions of a multistable gripping mechanism.

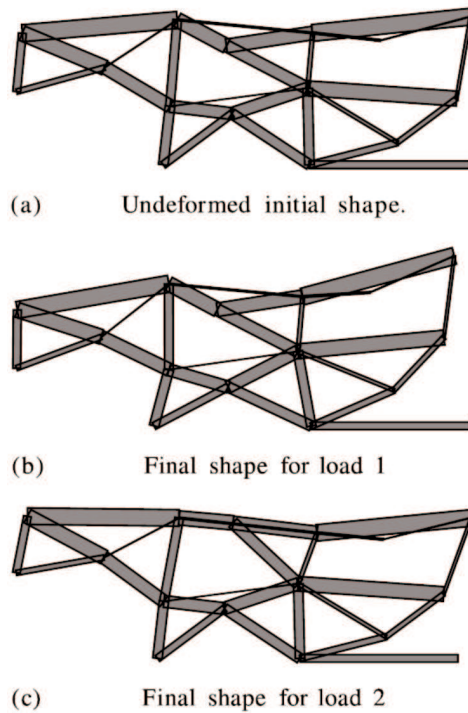


**Figure 2.8** A pin-jointed multistable compliant mechanism [64].

Although some research on design syntheses of bistable has appeared in the literature [51, 40, 33, 39, 55, 48, 49, 64], there is a lack of any demonstration of multistable (specially greater than two stable equilibria) compliant mechanisms.

With the handicap imposed by the computational time and complexity particularly due to complex nonlinear behavior, it is necessary to find an efficient method that can be applied to multistable compliant mechanisms. In this dissertation, a simplified mathematical approach that enables multistable compliant mechanisms to be synthesized by a combination of multiple bistabilities is developed.

## Chapter 3

### Overview of Synthesis Methodologies

The purpose of this research is to synthesize compliant mechanisms which yield multistable equilibrium positions. This chapter outlines general considerations in the synthesis of multistable compliant mechanisms and defines various steps and objectives of the methodologies presented in the subsequent chapters.

#### 3.1 Motivation

In engineering systems design, a fundamental challenge remains: *how do engineers design systems to achieve high accuracy and efficiency when the systems are in different operating modes?* This challenge is even critical when a system is operated far from its equilibrium state because its control system can be excessively complicated and the actuation system often requires a great deal of power to hold the state. Introducing multistability can not only reduce complexity and save power, but can also improve performance and expand the functionality of a variety of mechanical devices including conventional and compliant mechanisms in various systems.

A multistable system has more than one stable equilibrium configuration in which it can remain without any external input. The idea of multistable systems is that a passive subsystem (i.e. a multistable mechanism) is integrated to provide adaptability in function, while the actuation and control system remain unchanged.

Multistable mechanisms provide three main advantages. First, they are stable; the stable position can be maintained without expending energy from the actuator and small distur-

bances do not change the stable position. Secondly, they are efficient; each stable position can be reached by relatively uniform actuation forces, so a proportional actuator is not required to reach each stable position. Finally, they are accurate; the stable position will remain unchanged once the system is configured, so an open loop motion control is possible.

These advantages can be enhanced when multistable mechanisms are integrated with compliant mechanisms. Such mechanisms are called multistable compliant mechanisms (MSCMs). Each stable configuration of a MSCM is defined when its potential energy is at one of its local minima, so the amount of energy stored in the MSCM must be a nonlinear function of its position in order to have such multiple local minima. Design of such devices is not yet intuitive and requires the enormous computational time demanded by the complexity of the nonlinear finite element analysis.

Therefore, this study is motivated by the need to design MSCMs logically and systematically without the handicap imposed by the computational time and complexity.

## **3.2 General Approach**

Although researchers have broadly used topological and structural optimization methods to design compliant mechanism, designing MSCM presents difficult challenges in these methods because of the limitations in obtaining all statically stable and unstable configurations. Therefore, it is necessary to divide a problem to sub-problems which have fewer stable and unstable positions. Thus, the overall procedure of the methodology is divided into two steps: (1) synthesizing bistabilities and (2) synthesizing multistability from the multiple bistabilities.

To perform the first step, two approaches are introduced in this dissertation. First, bistabilities can be obtained by choosing the "buckled" configurations as initial stable configurations, and by letting unbuckled shapes be unstable configurations. When a structure is unstable, it buckles in one of two symmetric buckling modes in order to be in a stable

state. When the unstable structure buckles with finite displacements, the strain energy in both stable states is the same and is smaller than the strain energy in its unstable state. Therefore, in a bistable structure, an unstable state always exists between two stable states. A bistable compliant mechanism can be designed using one of the buckled configurations as an initially unstressed configuration. This approach is discussed in Chapter 4.

The other approach utilizes a clamped-pinned beam. In certain loading conditions, a clamped-pinned beam provides bistability. By using the clamped-pinned beam, which provides bistability, as a part of a compliant mechanism, the compliant mechanism can be bistable. This method is introduced in Chapter 5.

Once a bistable mechanism is generated, multistability is realized by combining multiple bistabilities in series in conjunction with rigid members to constrain relative displacements. Each bistable mechanism works as a building block, producing *either one or two additional stable configurations* when combined with other building blocks. Therefore,  $n$  bistable building blocks generate up to  $2^n$  stable positions. For example, two bistable building blocks provide either three ( $2 + 1$ ) or four ( $2^2$ ) stable positions. A simplified mathematical scheme was developed to capture essential parameters of bistable behaviors, such as load-thresholds that cause the jump from one to the next stable position, and to derive multistable behavior.

### 3.2.1 Synthesis Procedures

Fig. 3.1 shows the overall flowchart of the synthesis approach for multistable compliant mechanisms. It contains three main components: (1) decomposing multistability requirements into multiple bistable compliant mechanism designs, (2) designing bistable compliant mechanisms, and (3) combining the bistable compliant mechanisms to achieve desired multistable mechanisms. First, a design domain is decomposed to several sub-domains for bistable compliant mechanisms, and is combined after obtaining the sub-solutions. This process includes two components, (1) and (3). Second, the sub-domains are designed sep-

arately to obtain desired bistabilities. This process corresponds to component (2).

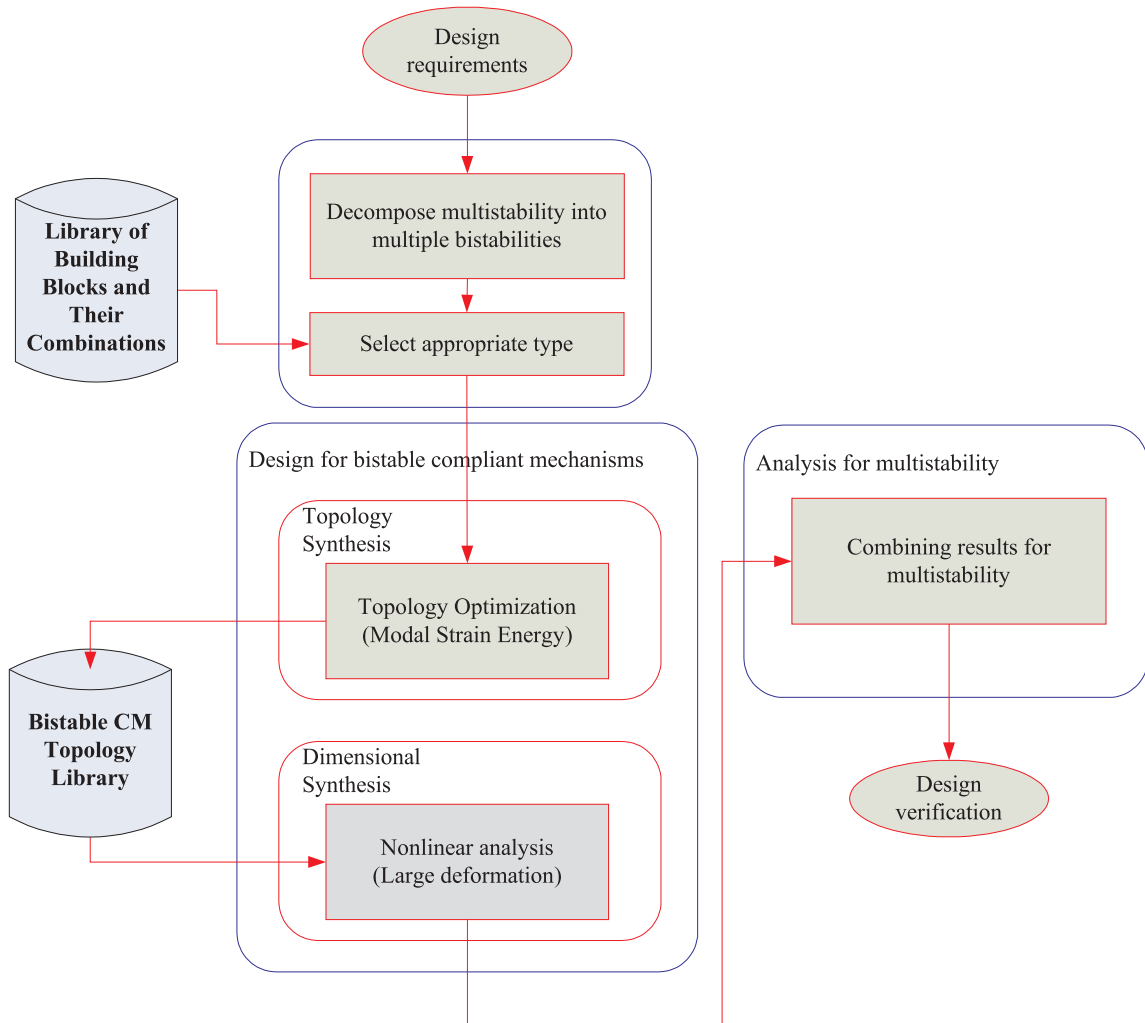


**Figure 3.1** Flowchart for the design process of multistable compliant mechanisms

*Step 1.* Define a design domain and design requirements. Design requirements can include the number of stable equilibria, corresponding actuation loads, equilibrium positions, etc.

*Step 2.* Decide the number of bistable behaviors that need to be combined to synthesize desired multistability. Based on the number of bistable behaviors, a combination type that satisfies the design requirements is selected from the combination type library. The library contains combination tables described in Chapter 6 and Appendix C.

- Step 3.* Divide the design domain into several sub-domains. The number of the sub-domains must be same as the number of the bistable behaviors chosen in *Step 2*. Fig. 3.2 depicts a design domain that is divided into three sub-domains. This step is explained in the next subsection.
- Step 4.* Design bistable compliant mechanisms. If there are topologies that satisfy the design requirements in the design library, a designer can use them to perform dimensional synthesis. If there is no proper topology in the library, bistable compliant mechanisms for the sub-domains are designed in this step. In this dissertation, two approaches for topology synthesis are introduced: using topology optimization and using bistability of a clamped-pinned beam. Details are explained in the chapters 4 and 5.
- Step 5.* Finalize the design of a multistable compliant mechanism. The designed bistable compliant mechanisms are placed to the equivalent sub-domains. The multistable behavior of the final design can be obtained from the combination type library.

### 3.2.2 Design Domain Decomposition

To acquire multistability from multiple bistable compliant mechanisms, the following decomposition procedure is applied. Fig. 3.2(a) shows a design problem of a multistable compliant mechanism (MSCM) which has a load input,  $F$ , and  $n$  stable equilibria,  $e_1 \sim e_n$ . Fig. 3.2(b) shows the MSCM which consists of three sub-domains of bistable equilibrium system (or compliant mechanisms), BES1, BES2, and BES3. Two rigid connectors (R-C) are used to divide the design domain of MSCM to sub-domains. As shown in Fig. 3.2(b), only one bistable compliant mechanism contains the load input, and only one of the other bistable compliant mechanisms contains a fixed boundary. Fig. 3.2(c) depicts how each design problem of the three bistable compliant mechanisms is defined separately. BES1 is

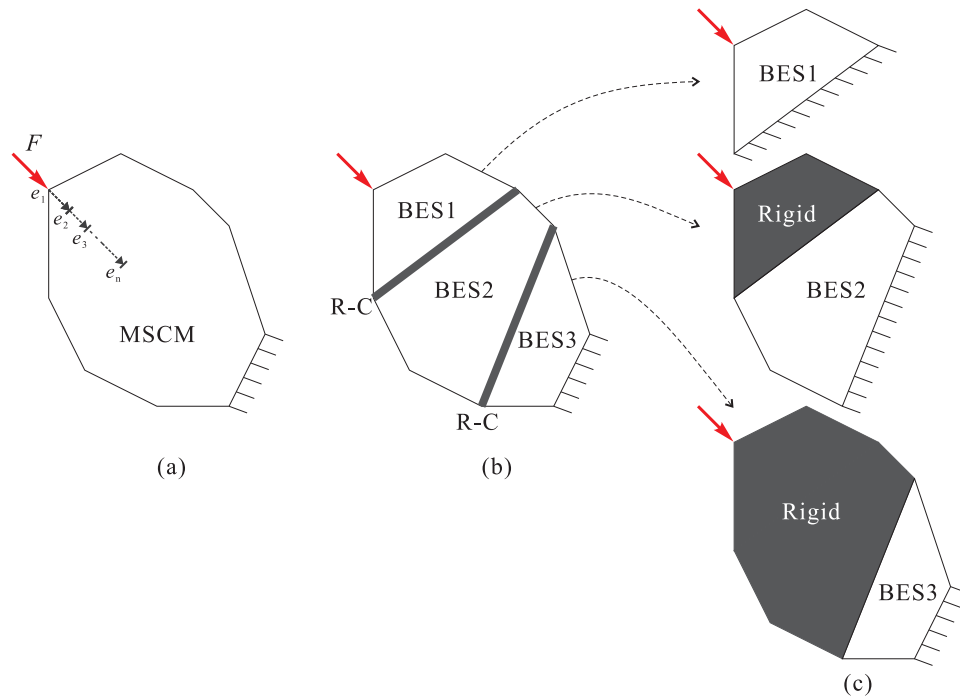


**Figure 3.2** Design domain decomposition procedures.

designed by treating the other two bistable compliant mechanisms as rigid bodies. The load input,  $F$ , locates at the same location of Fig. 3.2(a). BES2 and BES3 can be designed by applying the same assumptions. By combining the three bistable compliant mechanisms, a desired multistable behavior can be obtained. The details of combining multiple bistable behaviors to synthesize a multistable behavior are discussed in Chapter 6.

### 3.3 Scope of Research

The goal of this research is to develop a generalized methodology for synthesizing multistable systems, focusing on compliant mechanisms which have more complex nonlinearity than conventional mechanisms. The focus of this research lies in the two synthesis problems: (1) the synthesis of bistable compliant mechanisms and (2) the synthesis of multistability from combination of multiple bistable compliant mechanisms.

The scope of this research is defined by the following:



**Static Analysis** The synthesis approaches and analysis methods considered in this dissertation are limited to static responses. Considering static responses is more effective and efficient to identify all stable equilibria than considering dynamic responses. Static jumps in static responses requires extremely short period of time to jump in dynamic responses. Considering dynamic responses may miss the next stable equilibrium due to inertia effects.

**Synthesis of Bistable Compliant Mechanisms** In the design of compliant mechanisms, typical procedures include two processes: topology synthesis and dimensional synthesis. In this dissertation, topology optimization is applied to synthesis of bistable compliant mechanisms. Dimensional synthesis to match desired bistable behaviors can be performed by using size and shape optimization with nonlinear analysis [79, 42].

**2-D Planar Compliant Mechanism** A two-dimensional frame, which is the simplest form of an element, can be used to model the nonlinear response, including large deformation and buckling analysis is used in this dissertation. A planar multistable compliant mechanism can provide either in-plane translational or rotational multistable behavior which are used as example examples in subsequent chapters. Understanding two-dimensional problems allows us to extend the approach to general three-dimensional problems.

**Finite Element Model** Beam elements are formulated based on Euler-Bernoulli (slender) beam theory. The Euler-Bernoulli beam has the slenderness, a dimensional ratio of cross-section to the length, which is typically less than 1/15. If the slenderness is greater than 1/15, we cannot ensure the multistability of designed multistable compliant mechanisms. In order to verify the final design, Timoshenko beam elements which satisfy for both thick as well as slender beams are used to consider the transverse shear deformation [5]. The difference between the Timoshenko beam and the

Bernoulli beam is that the Timoshenko beam includes the effect of the shear stresses on its deformation. In other words, Timoshenko beam theory is an extension of the Euler-Bernoulli beam theory to allow for the effect of transverse shear deformation. Implementing Timoshenko beam theory will improve the design approaches introduced in this dissertation.

**Effect of Imperfection** An unstable system can be sensitive to imperfections in manufacturing processes, operating conditions, boundary conditions, and etc. Multistable compliant mechanisms always encounter unstable status because an unstable status exists between two stable states at all time. Some imperfection sensitivity analyses are included to analyze bistable compliant mechanisms. The synthesis methodologies in this dissertation do not consider sensitivity analysis. However, a robust design method that is insensitive to imperfections is introduced.

## **Chapter 4**

# **Synthesis of Bistable Compliant Mechanisms Using Buckled Configurations**

### **4.1 Introduction**

The behavior of multistable mechanisms is by nature very complex compared to mechanisms which have a single stable position. The least complex response can be obtained from bistable mechanisms, which are a subset of multistable mechanisms. The simplest conventional rigid-link mechanism with two stable equilibria is studied in this chapter. Similar studies have been done before [41, 32, 39]; but they are limited to application of pseudo-rigid-body modeling to the existing rigid link mechanisms. The study in this chapter not only provides a basic understanding of behaviors of bistable mechanisms but also supports the introduction of a unique approach applying buckling phenomena to the design of bistable compliant mechanisms.

### **4.2 Organization of This Chapter**

In the next section, the characteristics of bistable compliant mechanisms are discussed, and then four-bar linkage mechanisms with torsional springs on each joint are introduced. Two case studies, (i) bistable four-bar mechanisms and (ii) slider-crank mechanisms, are then presented and the results are compared to the beam buckling problem. Finally, a new approach for the topology synthesis of bistable compliant mechanisms is introduced with

two design examples; (i) rotational bistable compliant mechanisms and (ii) translational bistable compliant mechanisms.

### 4.3 Understanding the Characteristics of Bistable Compliant Mechanisms

A bistable system is a system with two stable equilibrium states. Its stable positions correspond to the local minima of the potential energy curve of the system. This is analogous to the ‘ball on the hill’ shown in the Fig. 4.1. The potential energy of the ball depends on its position on the hill and hence on  $x$ . The potential energy,  $U$ , is

$$U(x) = mgh(x) = -F_g h(x). \quad (4.1)$$

where  $m$  is the mass of the ball,  $g$  is the acceleration of gravity and  $y = h(x)$  is the equation that defines the height of the hill at  $x$ . Thus, the equilibrium positions are located where  $\partial h(x)/\partial x = 0$ . Hence,

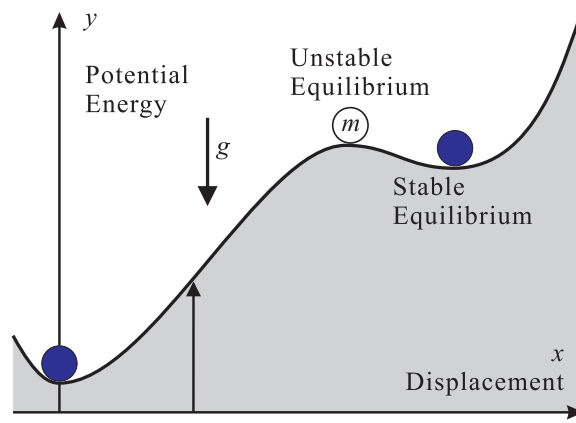
$$\frac{\partial U}{\partial x} = mg \frac{\partial h}{\partial x} = 0 \quad (4.2)$$

The stable positions (solid balls) are located at the local minima of the hill, i.e., locations where

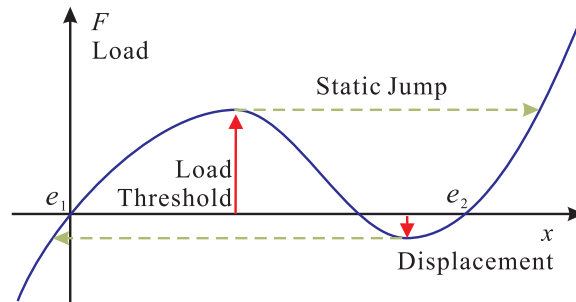
$$\frac{\partial^2 U}{\partial x^2} = mg \frac{\partial^2 h}{\partial x^2} > 0. \quad (4.3)$$

Eqn.(4.2) and (4.3) are the *necessary* and *sufficient* conditions for local minima of the potential energy function,  $U$ , respectively.

The gravitational force,  $F_g$ , acting on the ball can be seen as the action of the gravitational field that is present at the location of the ball. Since the gravitational force is in the



(a) Potential energy



(b) Load-displacement

**Figure 4.1** Potential energy curve and load-displacement curve of a bistable equilibrium system.

potential field, it is a conservative force equal and opposite to the gradient of a potential. By ignoring the friction on the surface, the external force applied to the ball to hold the stable position can be obtained by Eqn. (4.2).

$$F_{\text{external}} = -F_g \frac{\partial h}{\partial x} = \frac{\partial U}{\partial h} \frac{\partial h}{\partial x} = 0 \quad (4.4)$$

The derivative of Eqn. (4.4) at stable positions can be obtained by Eqn. (4.3).

$$\frac{\partial F_{\text{external}}}{\partial x} = \frac{\partial^2 U}{\partial x^2} > 0 \quad (4.5)$$

So far we have only discussed about the gravitational force, but this limitation is not necessary. Eqn. (4.4) and (4.5) must be satisfied for any conservative force including a

spring force,  $F_s$ . Since the external load applied to a spring is equal and opposite to the spring force, the following equations can be derived for the stable equilibria of the spring.

$$\begin{aligned} F_{\text{external}} &= -F_s = \frac{\partial U}{\partial x} = 0 \\ \frac{\partial}{\partial x} F_{\text{external}} &= -\frac{\partial F_s}{\partial x} = \frac{\partial^2 U}{\partial x^2} > 0. \end{aligned} \quad (4.6)$$

The equilibria,  $e_1$  and  $e_2$ , in Fig. 4.1(b) satisfy the conditions described in Eqn. (4.6). Therefore, *load-displacement responses* can be used to identify *stable equilibria*: they are located where the *load input is zero* and the *slope is positive*. In other words, each stable configuration of the system is defined when its potential energy is at one of its local minima; alternatively, the stiffness of the system is positive without an external load input.

As shown in Fig. 4.1(b), in general, bistability requires snap-through behavior to transition from one stable configuration to the other. Snap-through behavior can be characterized by the static jump shown in Fig. 4.1(b). A static jump occurs when the load is increased and reaches the load threshold which is defined as the required load to jump from one stable position to the other. Snap-through behavior normally causes a large amount of displacement and rotations and, therefore, should be considered as a geometrically nonlinear problem. This is true for all bistable mechanisms including rigid-link and compliant.

Snap-through behavior also corresponds to the phenomenon of buckling or instability of structures. The similarity and relationship between the buckling of structures and bistability of four-bar linkage mechanisms is discussed in the remainder of this chapter.

## 4.4 Exploiting Bistability in Conventional Four-bar Linkage Mechanisms

The four-bar linkage mechanism is the simplest possible closed-loop mechanism with one degree of freedom, and has numerous uses in industry ranging from automobile engines to small toys. A general four-bar linkage mechanism with torsional springs on each joint is shown in Fig. 4.2. In the figure,  $r_i$  and  $k_i$  are defined as the length of a given link and the stiffness of a torsional spring respectively.  $M_{in}$  is the moment applied to the input link or driver,  $r_2$ .  $r_1$  is called the ground link or frame,  $r_3$  is called the coupler link, and  $r_4$  is called the follower link.

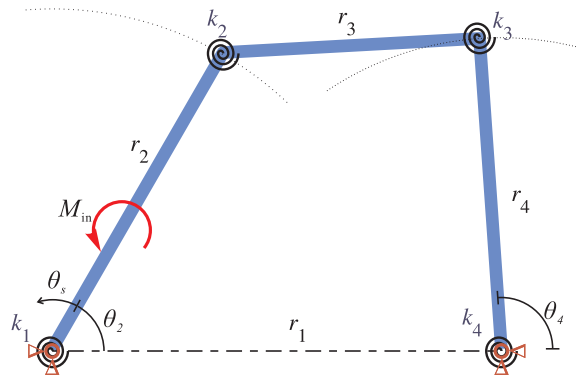


**Figure 4.2** Four-bar linkage mechanism with rotational springs at each joint.

### 4.4.1 Bistability of Grashof Four-bar Linkage Mechanisms

Four-bar linkage mechanisms with springs at each joint can provide bistability. These mechanisms can be classified based on Grashof's criterion [22] as shown in Fig. 4.3: Grashof and Non-Grashof mechanisms. At least one of the links in a Grashof mechanism can rotate through a full revolution, but no link can do in a non-Grashof mechanism. A Grashof mechanism satisfies the following inequality condition.

$$s + l \leq p + q, \quad (4.7)$$

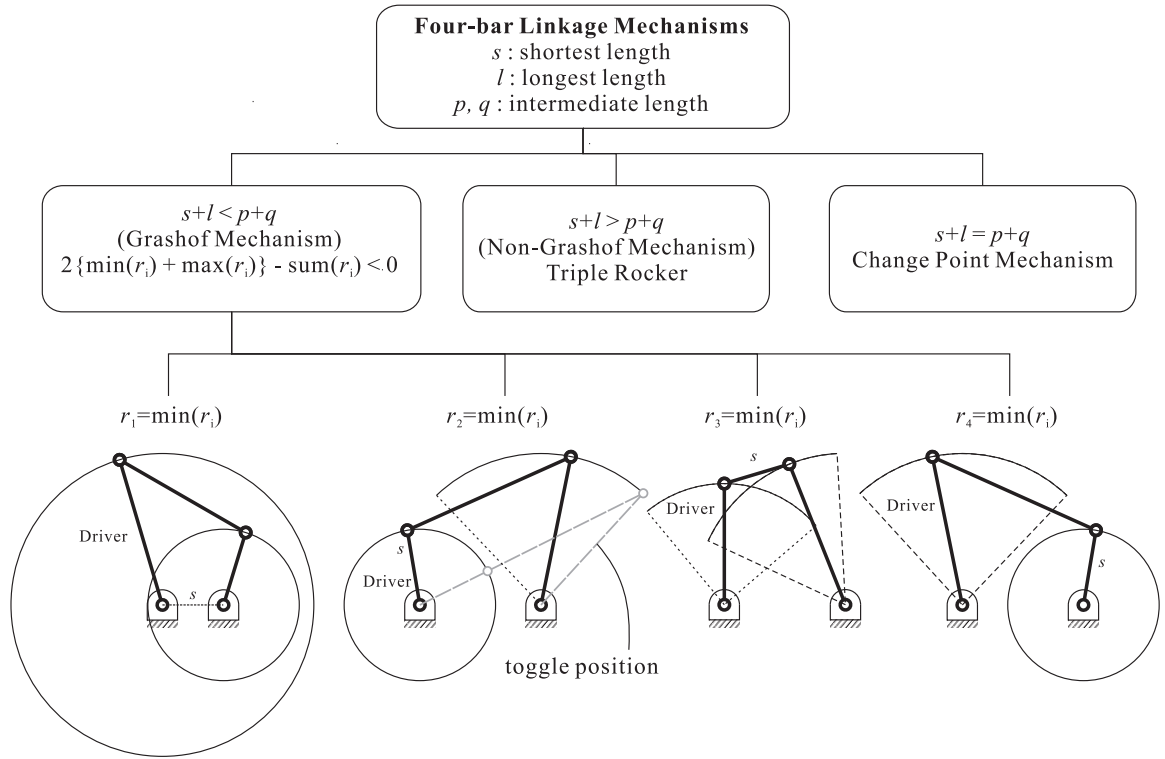


**Figure 4.3** Classification of four-bar linkage mechanisms.

where  $s$  and  $l$  are the shortest and longest links respectively, and  $p$  and  $q$  are the lengths of the other two links. The equality condition of Eqn. 4.7 is sometimes used for a change-point four-bar linkage mechanism. A non-Grashof mechanism satisfies

$$s + l > p + q. \quad (4.8)$$

Jensen et al [39] discussed the requirements for bistable behaviors of Grashof, Non-Grashof, and change-point mechanisms independently.

Grashof mechanisms can be divided into four subtypes as shown in the Fig. 4.3. In the figure, a toggle position occurs when the driver and coupler are lined up. One of the toggle positions are depicted in the figure. The condition lining up two adjacent links is essential to provide an unstable state in a mechanism. This concept is discussed later in this section.

It is not within the scope of this study to investigate all types of four-bar linkage mech-



anisms. Instead, the study in this section is limited to consideration of two types of Grashof mechanisms, and the idea can be extended to design bistable compliant mechanisms. To utilize one full revolution of the input link as the design range of two bistable configurations, and to reduce the difficulty of handling the immovable configuration, the first two types (the left two in Fig. 4.3) of Grashof mechanisms are used. The two types are

- Type 1.* A crank-crank mechanism which is obtained when the shortest link is the ground link, and
- Type 2.* A crank-rocker mechanism which is obtained when the shortest link is the input link.

These two Grashof mechanisms with crank inputs have two circuits but cannot reach immovable configuration. The circuit with the positive geometric inversion [22] is only considered in the analysis in this section.

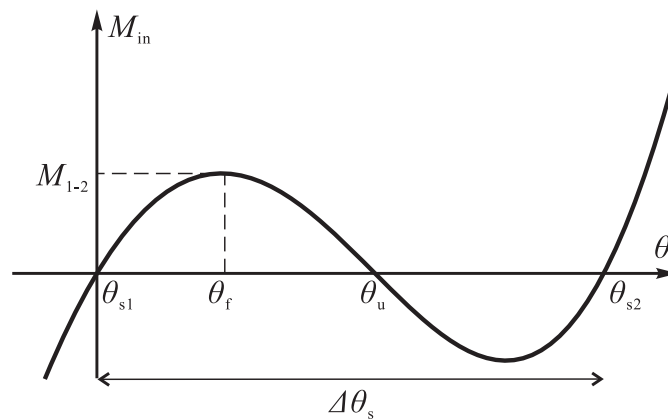


**Figure 4.4** Load-displacement curve of a typical bistable four-bar linkage mechanism.

Fig. 4.4 shows a desired load-displacement response of *Type 1* and *Type 2* Grashof mechanisms. The horizontal axis in the curve represents the rotation of  $\theta_2$  and the vertical axis indicates the input moment to  $r_2$ . The design requirements are

$$\begin{aligned}
&\text{the initial stable position : } \theta_s = \theta_{s1}, \\
&\text{the second stable position : } \theta_s = \theta_{s2} = \theta_{s1} + \Delta\theta_s, \\
&\text{the actuation load : } M_{in} = M_{1-2}.
\end{aligned} \tag{4.9}$$

where,  $\Delta\theta_s$  is defined as the rotation angle between the stable equilibria and the design variables are

$$\begin{aligned}
&\text{the length of each link : } r_i, \\
&\text{the spring constant of each torsional spring : } k_j.
\end{aligned}$$

To obtain a bistable behavior, the necessary and sufficient conditions must be satisfied. The necessary condition can be satisfied if the input load at the two stable positions,  $\theta_{s1}$  and  $\theta_{s2}$ , is zero. The sufficient condition can be satisfied if the slope at the unstable position,  $\theta_u$ , is negative. Alternatively, a positive load input at  $\theta_f$  can satisfy the sufficient condition if  $\theta_f$  is located between  $\theta_{s1}$  and  $\theta_u$ . Based on the design requirement and variables, the optimization problem to obtain the desired bistable behavior is formulated as

$$\begin{aligned}
&\text{Minimize : } f(r_i, k_i) = \omega_1 \cdot f_1 + \omega_2 \cdot f_2 + \omega_3 \cdot f_3 \\
&\text{subject to : } 1 < r_i < \infty \\
&\qquad\qquad\qquad 0 < k_i < \infty.
\end{aligned} \tag{4.10}$$

where  $\omega_i$  are the weighting factors and

$$\begin{aligned}
f_1 &= \{M_{in}(\theta_u)\}^2 + \{M_{in}(\theta_{s2})\}^2 + \{M_{in}(\theta_f) - M_{1-2}\}^2 \\
f_2 &= \sum r_i \\
f_3 &= \sum k_i.
\end{aligned} \tag{4.11}$$

where  $\theta_u$  is an angle at an unstable state, and  $\theta_f$  is an angle at the load-threshold. The first and the second terms in  $f_1$  represent the necessary conditions at stable and unstable positions of the potential energy. The last term in  $f_1$  represents two conditions; the sufficient condition of the local minima of the potential energy and the desired load-threshold.

The design requirements and the initial values of two design examples are listed in Table 4.1.

**Table 4.1** Design requirements and initial values of two design problems for bistable four-bar linkage mechanisms

Case	$\theta_{s1}$	$\theta_{s2}$	$M_{1-2}$	$\omega_i$	initial $r_i$	initial $k_i$
Case 1	30°	60°	10	[1,0.01,0.01]	[4 1 5 6]	[1 3 2 1]
Case 2	10°	20°	10	[1,0.01,0.01]	[4 1 5 6]	[1 3 2 1]

The two optimal solutions for each bistable four-bar linkage mechanism are shown in Fig. 4.5 and 4.6. The thicker links represent the initial configuration and the thinner links indicate the second stable position. Fig. 4.5 (a) shows two stable configurations of the *Type I* mechanism for Case 1. In the figure, the torsional spring with the largest spring constant,  $k_2$ , is located on the opposite side of the shortest link,  $r_1$ . The spring with the second largest spring constant,  $k_4$ , is located at the opposite joint from  $k_2$ . The other two spring constants are zeros. Even though the configurations are different, this condition is true for all of the mechanisms in Fig. 4.5 and 4.6. Note that the largest spring constant is much greater than the second largest spring constant. The ratio of the two spring constant is discussed in the next subsection.

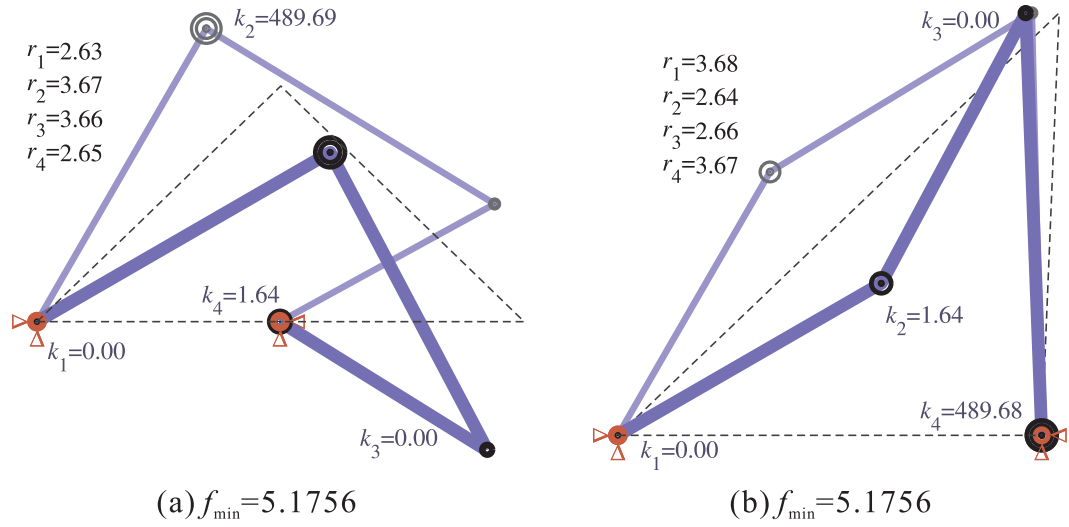


**Figure 4.5** Two optimal solutions of Case 1: (a) *Type 1* and (b) *Type 2*

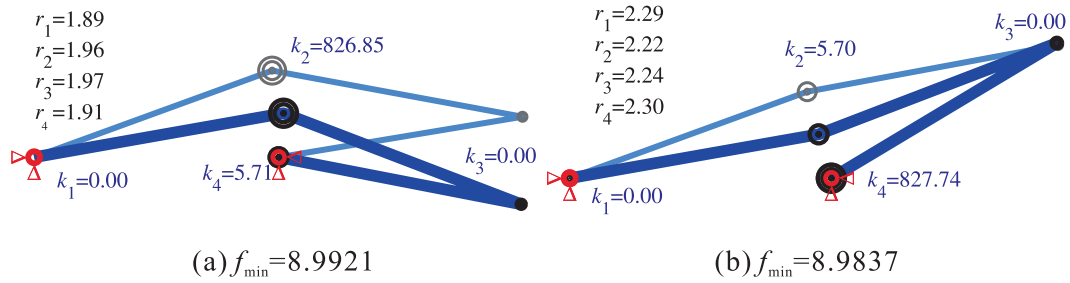


**Figure 4.6** Two optimal solutions of Case 2: (a) *Type 1* and (b) *Type 2*

The unstable equilibrium configuration should be between the initial and the second stable equilibria. Therefore, at the unstable equilibrium,  $r_1$  and  $r_4$  are close to being in line for Fig. 4.5(a) and 4.6(a); and the mechanisms are close to their toggle positions in Fig. 4.5(b) and 4.6(b). The dotted lines in Fig. 4.5(a) and (b) indicate the positions when the two adjacent links are in line. Now, suppose the  $r_2$  in Fig. 4.5(a) is a ground link and  $r_1$  is a moving link, this is known as a kinematic inversion [22]. Performing this kinematic inversion results in the mechanism shown in Fig. 4.5(b). This is true for the mechanism shown in Fig. 4.6 as well. Therefore, based on the optimal geometries and kinematic inversion, we can conclude the following.

A four-bar linkage mechanism *can* be *bistable* if its two adjacent links, which can be in line, include a torsional spring,  $k_s$ , and the other torsional spring,  $k_l$ , which is much stiffer than  $k_s$ , is located at the opposite joint from  $k_s$ .

This is the necessary condition for a bistable four-bar linkage mechanism. Based on the necessary condition, all possible bistable four-bar linkage mechanisms can be obtained; they are listed in Table 4.2.

As discussed before, all bistable Grashof four-bar linkage mechanisms are similar and can be obtained through either kinematic inversion or mirroring from any one of the classes in Table 4.2. The four-bar linkage mechanisms in Table 4.2 have a spring that has the largest spring constant. The other spring which has smaller spring constant is located at the opposite joint of the spring.

#### 4.4.2 Bistability of Slider-crank Mechanisms

The optimal designs in the previous subsection show that two springs are located at two opposite joints in a bistable four-bar linkage mechanism. One of them has much larger stiffness than the other. In this subsection, the optimal results are verified by introducing a slider-crank mechanism.

A slider-crank mechanism is a special type of four-bar linkage mechanisms obtained by making the follower link infinite in length. Fig. 4.7(a) shows the initial configuration of a slider-crank mechanism in its toggle position. In the figure,  $l_1$  and  $l_2$  are the lengths of the two links.  $k_\theta$  is the spring constant of the torsional spring connecting the two links.  $k_\delta$  is the spring constant of the translational spring located at the end of  $l_2$ . The load,  $F_1$  is applied to the end of the spring,  $k_\delta$ , and the displacement at the loading point is defined as  $\delta_1$ . Since Fig. 4.7(a) represents the initial configuration, the potential energy stored in the two springs must be zero at that point. When the load,  $F_1$ , is greater than the critical load, the mechanism will turn into one of its buckled configurations (Fig. 4.7(b)) with the

**Table 4.2** Classification of bistable Grashof four-bar linkage mechanisms.

	Initial (1st stable) configuration	2nd stable configuration	$\theta_{s1}$	$\Delta\theta_s$
Positive $\Delta\theta_s$			$0 < \theta_{s1} < \pi/2$	$0 < \Delta\theta_s < \pi - \theta_{s1}$
			$0 < \theta_{s1} < \pi$	$0 < \Delta\theta_s < \pi$
			$0 < \theta_{s1} < \pi/2$	$0 < \Delta\theta_s < \pi - \theta_{s1}$
Negative $\Delta\theta_s$			$0 < \theta_{s1} < \pi$	$-\theta_{s1} < \Delta\theta_s < 0$
			$\pi < \theta_{s1} < 2\pi$	$-\pi < \Delta\theta_s < 0$
			$0 < \theta_{s1} < \pi$	$-\theta_{s1} < \Delta\theta_s < 0$

⊙ Location of the spring with the largest value of spring constant

displacement at  $\delta_1 = \Delta_0$ .

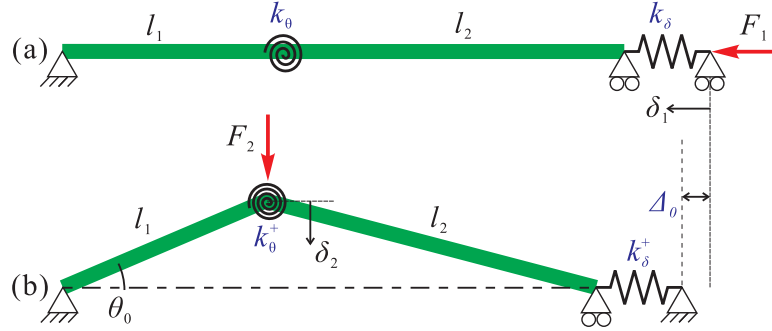


**Figure 4.7** A slider-crank mechanism with two springs: (a) initial configuration and (b) buckled configuration.

Assuming that the loading point is fixed at  $\delta_1 = \Delta_0$ , the potential energy stored in the mechanism at the configuration shown in Fig. 4.7(b) is no longer zero. The potential energy is stored in the two springs,  $k_\theta^+$  and  $k_\delta^+$ . The potential energy and the work done by  $F_1$  can be calculated as the following equation. Note that the same length,  $l$ , is used for the lengths,  $l_1$  and  $l_2$ , to simplify the problem.

$$\begin{aligned}
 U &= 2k_\theta\theta^2 + \frac{1}{2}k_\delta(2l - 2l\cos\theta - \delta_1)^2 \\
 W &= F_1\delta_1.
 \end{aligned}
 \tag{4.12}$$

where  $l = l_1 = l_2$ .

The total potential energy can be obtained by adding the potential energy stored in the springs and the potential energy of the force.

$$PE = U - W.
 \tag{4.13}$$

Taking the first derivative with respect to  $\theta$  and  $\delta_1$  yields

$$\begin{aligned}
\frac{\partial PE}{\partial \theta} &= 4k_{\theta}\theta + 2k_{\delta}(2l - 2l \cos \theta - \delta_1)l \sin \theta \\
\frac{\partial PE}{\partial \delta_1} &= -k_{\delta}(2l - 2l \cos \theta - \delta_1) - F_1.
\end{aligned} \tag{4.14}$$

The equilibrium position is obtained by setting Eqn.(4.14) equal to zero. There can be multiple solutions in this problem. Since we are looking for unstable state of the system at  $\theta = 0$ , the equilibrium of the mechanism is

$$\begin{aligned}
\theta &= 0 \\
F_1 &= k_{\delta}\delta_1.
\end{aligned} \tag{4.15}$$

To identify the critical condition to have bistable behavior, Hessian,  $\mathbf{H}$ , of the potential energy is calculated as follows.

$$\mathbf{H} = \begin{bmatrix} 4k_{\theta} + 4k_{\delta}l^2 \sin^2 \theta + 2k_{\delta}(2l - 2l \cos \theta - \delta_1)l \cos \theta & -2k_{\delta}l \sin \theta \\ -2k_{\delta}l \sin \theta & k_{\delta} \end{bmatrix}. \tag{4.16}$$

where Hessian is defined as

$$\mathbf{H} = \begin{bmatrix} \frac{\partial^2 PE}{\partial \theta^2} & \frac{\partial^2 PE}{\partial \theta \partial \delta_1} \\ \frac{\partial^2 PE}{\partial \delta_1 \partial \theta} & \frac{\partial^2 PE}{\partial \delta_1^2} \end{bmatrix}. \tag{4.17}$$

Eqn. 4.16 must be negative definite to make the system unstable. The determinant of the Hessian is

$$-(-4k_{\theta} - 4k_{\delta}l^2 \sin^2 \theta - 2k_{\delta}(2l - 2l \cos \theta - \delta_1)l \cos \theta)k_{\delta} - 4k_{\delta}^2l^2 \sin^2 \theta. \tag{4.18}$$



Eqn.(4.18) must be zero at the critical condition. Substituting the equilibrium (Eqn.(4.15)) conditions into the above equation yields

$$\frac{k_{\theta}}{k_{\delta}} = \frac{l}{2}\Delta_0. \quad (4.19)$$

where  $\delta_1$  is replaced with  $\Delta_0$ . This is the critical condition to have bistability at  $\delta_1 = \Delta_0$ . In order to ensure bistable behavior,

$$\frac{k_{\theta}}{k_{\delta}} < \frac{l}{2}\Delta_0. \quad (4.20)$$

The *stiffness ratio*,  $k_{\theta}/k_{\delta}$ , is an important parameter to ensure bistability.

If the force,  $F_2$ , is applied to the joint as shown in Fig. 4.7(b), the mechanisms that satisfy the above condition must provide bistability. The second stable configuration must be symmetric to the configuration shown in Fig. 4.7(b). One can identify the bistability from the load-displacement ( $F_2$  vs.  $\delta_2$ ) curve. The load-displacement curves of Fig. 4.7(b) with various stiffness ratio,  $k_{\theta}/k_{\delta}$ , are shown in the second column of Table 4.3. Here,  $\Delta_0 = 1$  and  $l = 8$  are used to obtain the curves. As shown in the table, the bistable behavior ( $F_2$  vs.  $\delta_2$ ) can be shown when  $k_{\theta}/k_{\delta} < 4.0$ .

Fig. 4.8 shows the same configuration as shown in Fig. 4.7(b). However, there is no potential energy stored in two springs at the position. Thus, the configuration shown in the Fig. 4.8 is the initial configuration with zero potential energy. If the force,  $F_3$ , is applied to the joint as shown in the figure, can the mechanism provide bistability?

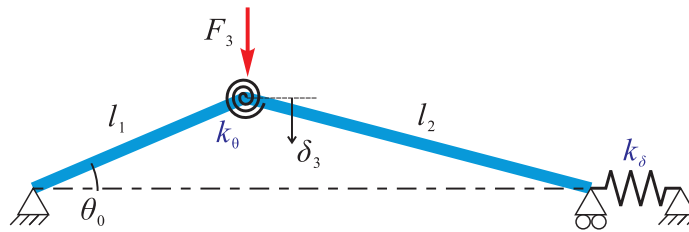
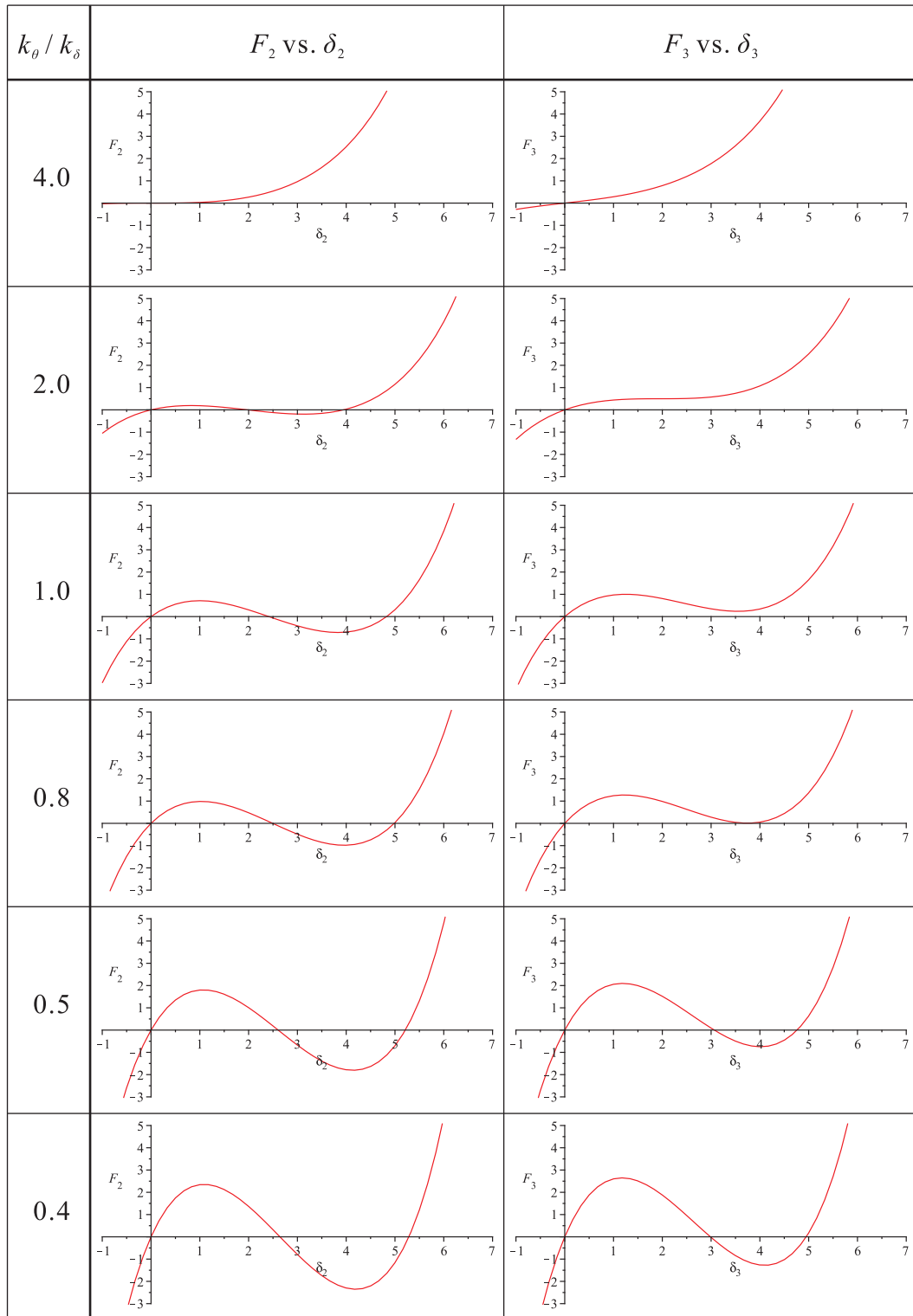


**Figure 4.8** Initial configuration of a slider-crank mechanism with two springs.

The right column of Table 4.3 shows the load-displacement ( $F_3$  vs.  $\delta_3$ ) curves of Fig. 4.8

**Table 4.3** Load-displacement curves for various stiffness ratio,  $k_\theta/k_\delta$ .



with various stiffness ratio,  $k_\theta/k_\delta$ . In this case, to have the bistability, the stiffness ratio must be smaller than 0.8. Therefore, to ensure the bistability of the mechanism shown in Fig. 4.8,

$$\frac{k_\theta}{k_\delta} \ll \frac{l}{2}\Delta_0. \quad (4.21)$$

Based on the analysis in this subsection, it is also possible to find the definition of the stiffness ratio for four-bar linkage mechanisms discussed in the previous subsection. A correlation between a four-bar linkage mechanism and a slider-crank mechanism can be obtained if the follower of the four-bar linkage mechanism is infinitely long. The corresponding stiffness ratio for the four-bar linkage mechanisms is  $k_s/k_l$ . The sufficient condition to ensure bistability of the four-bar linkage mechanisms is

$$\frac{k_s}{k_l} \ll 1. \quad (4.22)$$

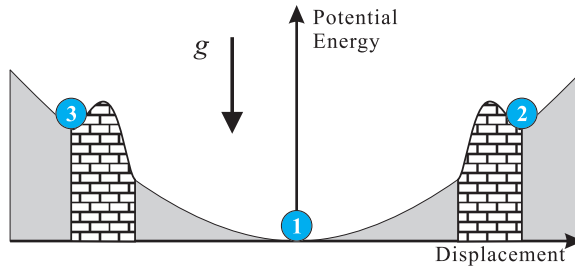
Eqn.(4.22) supports the optimal configurations of bistable four-bar linkage mechanisms obtained in the previous subsection. In each mechanism, the largest spring constant is much greater than the second largest spring constant in Fig. 4.5 and 4.6.

### 4.4.3 Tristable Four-bar Linkage Mechanism

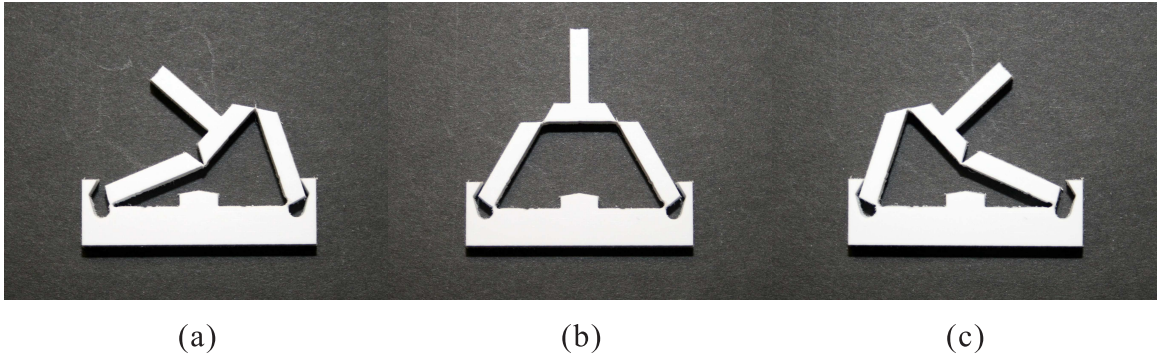
The third row of Table 4.2 has the largest spring constant at  $k_4$ . If the location of the largest spring constant can switch between  $k_1$  and  $k_4$ , the four-bar linkage mechanism can have tristable behavior. It is possible to use contact conditions for both springs. The contact conditions change the potential energy discretely, so that it can provide multistability as shown in Fig. 4.9.

Fig. 4.10 shows a tristable switch by applying the contact condition to  $k_1$  and  $k_4$ .

Fig. 4.10 (b) is the initial configuration of the tristable switch. Fig. 4.10 (a) is another stable configuration when  $k_4$  is active. Fig. 4.10 (c) is the other stable configuration with



**Figure 4.9** A multistable behavior by applying contact conditions.



**Figure 4.10** Tristable four-bar switching mechanism.

active  $k_1$ . This concept is also addressed in Chapter 5 to design a multistable switch using clamped-pinned beams.

## 4.5 Bistability of Buckled Configurations

The necessary condition for a four-bar linkage mechanism to have bistable behavior is that two adjacent links are lined up (e.g. a toggle position) in the feasible range of motion. The other two ends are free to rotate but the relative motion between the two ends is constrained by a spring with large stiffness.

There is a similarity between a toggle position of four-bar linkage mechanisms and a buckled shape of a beam. The relative motion between the two ends of a buckled clamped-clamped beam is zero (infinite stiffness) and the curvatures at the two clamped ends are infinite (no strain energy stored at the ends). The two buckled shapes of the clamped-clamped beam are symmetric and identical. Fig. 4.11 shows the two stable configurations

of the buckled beam.

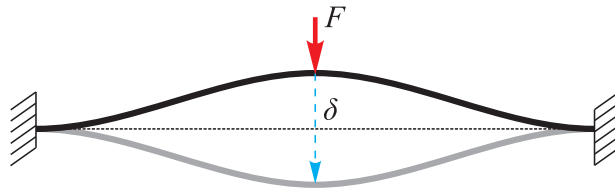


**Figure 4.11** Bistability of a buckled beam (an oil-canning problem).

In the figure, if a load-threshold,  $F$ , is applied at the center of the buckled beam, the second stable configuration can be obtained.

In this section, a buckled configuration is used as an initial configuration of a bistable compliant mechanism. A beam can be buckled by many different physical conditions. However, the load,  $F$ , cannot provide the buckling condition. The approach used to generate a buckling configuration from the load,  $F$ , is introduced in Fig. 4.12. Fig. 4.12 (a) shows the two desired stable positions of a buckled beam. In Fig. 4.12(b), the same load,  $F$ , is applied to a straight beam in the opposite direction to the original direction of the load. Then a static structural analysis is performed to find the static displacement of the beam (Fig. 4.12(c)). The displacement results are added to the original shape of the beam shown in (b). The load,  $F$ , on the updated geometry can provide internal forces to make the beam buckled as shown in Fig. 4.12(d). The internal forces are used to perform the buckling analysis for the initial shape. Finally, one of the buckled configurations will be used as the initial configuration (Fig. 4.12(e)).

### 4.5.1 Modal Strain Energy

Suppose a system has an unstable state, it should be bistable because an unstable state always exists between two stable states. In structural analysis, when a structure is unstable, it buckles. In other words, an unstable structure tends to deform to its stable status using its buckled shape. When an unstable structure is buckled with finite displacement, the strain energy at both stable states is the same and not zero (the dashed line in the Fig. 4.13).

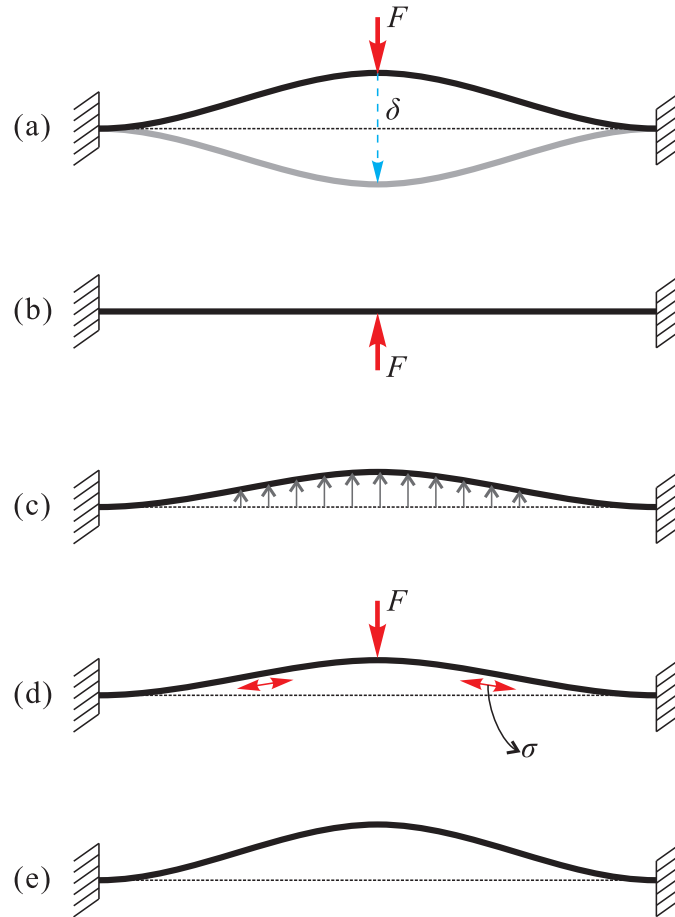


**Figure 4.12** Buckling analysis procedure to obtain buckled configurations. (a) desired buckled configuration, (b) applying load to the initial shape, (c) performing static analysis, (d) applying load to the deformed shape, (e) applying internal forces to the initial shape in order to determine the buckled configuration.

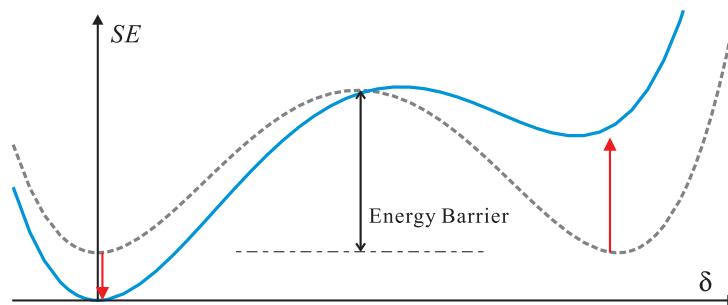


**Figure 4.13** Strain Energy change when one of the buckled configurations is used as an initially unstressed configuration.

When one of the buckled configurations is used as an initially unstressed configuration, the strain energy at the initial shape is zero and the strain energy at the other shape is increased (the solid line in the Fig. 4.13). If the strain energy at the second shape increases more than the energy barrier, the bistability will be lost. Losing bistability depends on the design parameters of the structure, such as thicknesses of the beams and locations of the points. Therefore the energy barrier (Fig. 4.13) between the two stable states must be maximized.

The idea of modal strain energy is that, by maximizing it, the energy barrier can be maximized. Additionally, no nonlinear static analysis is required to determine the magnitude of the energy barrier. The modal strain energy,  $V_M$ , is defined as

$$V_M = \bar{\mathbf{x}}_1^T \mathbf{K} \mathbf{v}. \quad (4.23)$$

where  $\bar{\mathbf{x}}_1^T$  is the first buckling mode,  $\mathbf{K}$  is the stiffness matrix of the structure, and  $\mathbf{v}$  is the displacement at the input node when a unit load input is applied. Fig. 4.14 shows the finite element formulations for the static analysis, the static analysis with a unit load, and the buckling analysis of a compliant structure.  $\mathbf{K}_G$  in Fig. 4.14(c) is the geometric stiffness matrix, and  $\lambda$  is the eigenvalue or the critical load factor of the input load,  $\mathbf{p}$ .

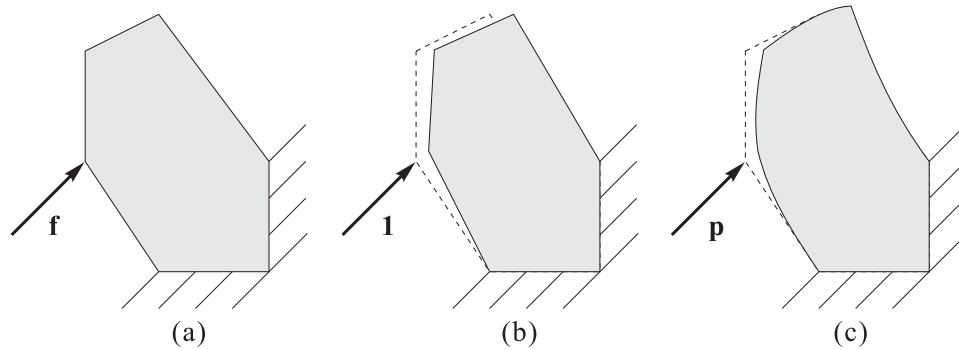


**Figure 4.14** (a) static analysis:  $\mathbf{K} \mathbf{u} = \mathbf{f}$ , (b) static analysis with unit load input:  $\mathbf{K} \mathbf{v} = \mathbf{1}$ , and (c) buckling analysis:  $(\mathbf{K} + \lambda_i \mathbf{K}_G) \bar{\mathbf{x}}_i = \lambda \mathbf{p}$

The topology optimization formulation can be posed as follows:

$$\begin{aligned}
&\text{Maximize} && V_M = \bar{\mathbf{x}}_1^T \mathbf{K} \mathbf{v} && (4.24) \\
&\text{subject to} && t_{j\min} \leq t_j \leq t_{j\max} \\
&&& g = \text{Volume}/V_{\max} - 1 \leq 0.
\end{aligned}$$

The variable  $t_j$  represents cross-sectional thickness of each line element. The line element contains more than two beam elements. The total volume constraint, expressed by  $g$ , is applied to maintain a specified total volume fraction of the mechanism.

## 4.5.2 Finite Element Model

In order to synthesize topology of a bistable compliant mechanism based on the objective function in Eqn.(4.25), a finite element method is applied to perform the buckling analysis. The buckling analysis model includes rigid bodies and the analysis step described in Fig. 4.12 is used. For the buckling analysis, unlike the static analysis, there must be at least two elements to represent a beam. Because the shape function of the beam element is formulated as a third order polynomial, it cannot represent the buckling modes. Buckling modes are usually expressed in sinusoidal functions and require at least a fifth order polynomial to represent the modes. The Taylor series expansions of the sinusoidal functions,  $\sin x$  and  $\cos x$ , are following.

$$\begin{aligned}
\sin x &= x - \frac{x^3}{3!} + \frac{x^5}{5!} - \dots, \\
\cos x &= 1 - \frac{x^2}{2!} + \frac{x^4}{4!} - \dots
\end{aligned} \tag{4.25}$$

Using two elements per beam can provide the sinusoidal function effectively without using higher order polynomials.



## 2-D Beam Element

Derivation for element matrices for 2-D beam element can be found in many textbooks on FEA. This section summarizes the matrices related to the research based on the Scattering method [18].

The model of a beam element is shown in Fig. 4.15.

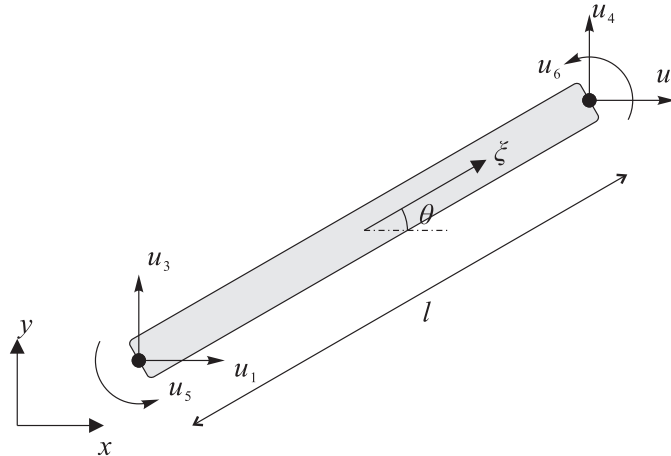


**Figure 4.15** 2-D beam element in the  $x - y$  plane.

The element displacement vector can be expressed as

$$\mathbf{u}_e = \left\{ u_1 \quad u_2 \quad u_3 \quad u_4 \quad u_5 \quad u_6 \right\}^T \quad (4.26)$$

The total displacement vector is

$$\mathbf{U} = \sum_{\text{All}} \mathbf{u}_e \quad (4.27)$$

The elemental stiffness is shown in the following equation.

$$\mathbf{K}_e = \frac{E}{l} \begin{bmatrix} A & -A & 0 & 0 & 0 & 0 \\ & A & 0 & 0 & 0 & 0 \\ & & 12\frac{I}{l^2} & -12\frac{I}{l^2} & 6\frac{I}{l} & 6\frac{I}{l} \\ & & & 12\frac{I}{l^2} & -6\frac{I}{l} & -6\frac{I}{l} \\ & Sym & & & 4I & 2I \\ & & & & & 4I \end{bmatrix}, \quad (4.28)$$

where  $A = bh$ ,  $\frac{bh^3}{12}$ ,  $E$  is an elastic modulus, and  $l$  is the length of an element.

In order to calculate the global stiffness matrix, the elemental coordinates must be transformed to the global coordinates. This can be done by using the transformation matrix.

$$\mathbf{T}_e = \begin{bmatrix} \cos \theta & 0 & \sin \theta & 0 & 0 & 0 \\ 0 & \cos \theta & 0 & \sin \theta & 0 & 0 \\ -\sin \theta & 0 & \cos \theta & 0 & 0 & 0 \\ 0 & -\sin \theta & 0 & \cos \theta & 0 & 0 \\ 0 & 0 & 0 & 0 & 1 & 0 \\ 0 & 0 & 0 & 0 & 0 & 1 \end{bmatrix}. \quad (4.29)$$

The global stiffness matrix can be obtained by

$$\mathbf{K} = \sum_{All} \text{sct} (\mathbf{T}_e^T \mathbf{K}_e \mathbf{T}_e) \quad (4.30)$$

where the function,  $\text{sct}$ , is the scattering function[18].

## 2-D Rigid Element (MPC)

A multipoint constraint (MPC) is a linear equation relating displacement degrees of freedom [73]. Using MPC, it is possible to model a rigid element between two node points.

Consider the rigid element that connects two points as shown in Fig. 4.16.

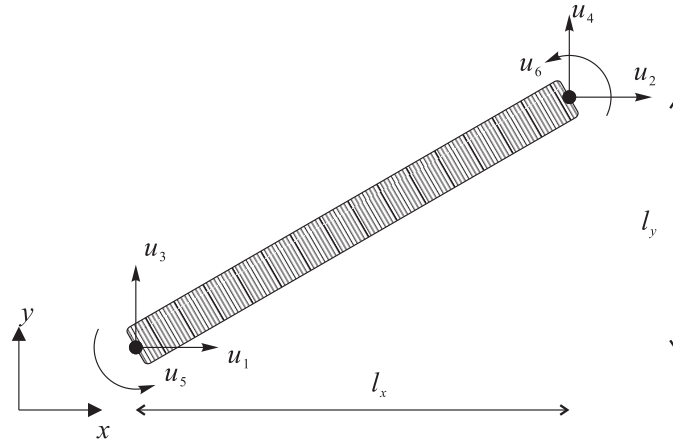


**Figure 4.16** Rigid member (MPC) in the  $x-y$  plane.

The following kinematic relations can be obtained based on the assumption of small rotation of the rigid element.

$$u_2 = u_1 - l_y \cdot u_5 \quad (4.31)$$

$$u_4 = u_3 + l_x \cdot u_5$$

$$u_6 = u_5$$

where  $l_x$  and  $l_y$  represent the distance between the two points in the  $x$  and  $y$  directions respectively.

The MPC relations can be expressed as the following matrix and equation.

$$\mathbf{R}_e = \begin{bmatrix} 1 & -1 & 0 & 0 & -l_y & 0 \\ 0 & 0 & 1 & -1 & l_x & 0 \\ 0 & 0 & 0 & 0 & 1 & -1 \end{bmatrix} \quad (4.32)$$

$$\mathbf{R}_e \mathbf{u} = \mathbf{0} \quad (4.33)$$

## Buckling Analysis

In general, the objective of a linear buckling problem is to obtain a load scale factor,  $\lambda$ , such that the following equation is satisfied.

$$(\mathbf{K} + \lambda_i \mathbf{K}_G) \bar{\mathbf{x}}_i = \lambda \mathbf{p}, \quad (4.34)$$

where  $\mathbf{K}_G$  is called a geometric stiffness matrix and is obtained by

$$\mathbf{K}_G = \sum_{\text{All}} \text{sct} (\mathbf{T}_e^T \mathbf{G}_e \mathbf{T}_e), \quad (4.35)$$

where  $\mathbf{G}_e$  is the elemental geometric stiffness matrix.

The elemental geometric stiffness matrix can be calculated as

$$\mathbf{G}_e = F_e \begin{bmatrix} 0 & 0 & 0 & 0 & 0 & 0 \\ 0 & 0 & 0 & 0 & 0 & 0 \\ & & \frac{6}{5l} & -\frac{6}{5l} & \frac{1}{10} & \frac{1}{10} \\ & & & \frac{6}{5l} & -\frac{1}{10} & -\frac{1}{10} \\ \text{Sym} & & & & \frac{2}{15}l & -\frac{l}{30} \\ & & & & & \frac{2}{15}l \end{bmatrix} \quad (4.36)$$

where  $F_e$  is an internal load applied to a beam element. It can be obtained from a static analysis.

In this subsection, the necessary formulations for 2-D beam elements, rigid beam elements, and buckling analysis are explained. Based on the formulations, Eqn.(4.25) is used to obtain topologies of bistable compliant mechanisms in the following subsection.

### 4.5.3 Topology Synthesis Using Buckling Configurations

The goal of topology synthesis for bistable compliant mechanisms is to identify the best possible topology that can provide bistable behavior. The work presented in this subsection

is based on the early stage of the development of topology synthesis using the buckling configuration.

Two examples, a rotational and translational bistable compliant mechanism, are presented here. To perform the topology synthesis, design domains and desired directions of the bistable behaviors must be established. Fig. 4.17 shows the design domains for the two problems.

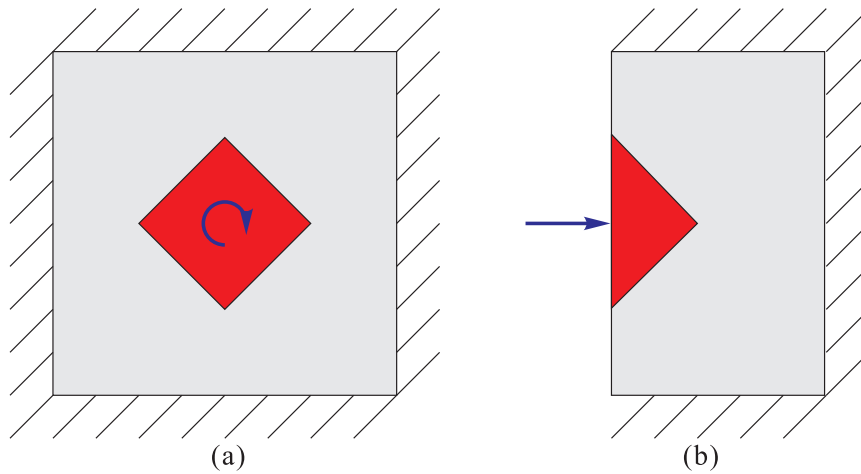


**Figure 4.17** Bistable compliant mechanisms design: (a) rotational bistable compliant mechanism, and (b) translational bistable compliant mechanism.

The design domain shown in Fig. 4.17 (a) is for a rotational bistable compliant mechanism. The four boundaries of the design domain are fixed. The solid square at the center represents a rigid area where the input torque is applied. Fig. 4.17 (b) shows the design domain of a translational bistable compliant mechanism. The top, bottom, and right sides of the domain have fixed boundary conditions. The solid triangle on the left side of the domain is the rigid member where the input load is applied.

### **Rotational and Translational Bistable Compliant Mechanism Design**

Once the design domain is defined, it is discretized using beam elements. Since the design domain shown in Fig. 4.17 (a) is cyclic symmetric, only the right-top portion of the design domain is discretized with an additional boundary condition at the center. Also the upper

half of Fig. 4.17 (a) is considered to be discretized. Fig. 4.18 shows a reduced design domains of the rotational and translational cases.

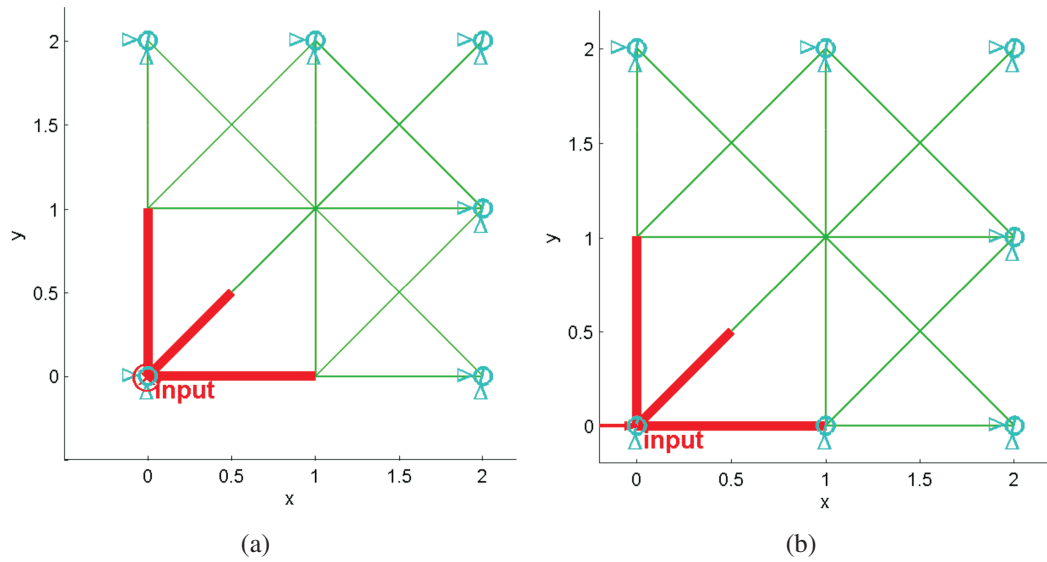


**Figure 4.18** Design domain discretization: (a) the right-top corner of the design domain in Fig. 4.17 (a), and (b) the upper half of the design domain in Fig. 4.17 (b)

A  $2 \times 2$  fixed-node modular ground structure is used for each discretization. There are 28 lines in the ground structure. However because each line must have at least two beam elements to perform the buckling analysis, the total number of beam elements used in the discretization is 56. The number of design variables is still 28 because the two elements in each line have the same cross section. In the specific cases shown in Fig. 4.18, some of the lines that do not affect the final design are removed (i.e., the lines inside the rigid area, and the lines on the fixed boundary). There are now 19 design variables in each discretized design domain.

Matlab, a commercial mathematical software package, is used to solve the optimization problem of Eqn.4.25. It is possible to use a gradient-based optimization since the design variables (thicknesses) are continuous. Sequential quadratic programming (SQP) is used for the gradient-based optimization algorithm and finite-difference approximation is applied to calculate the gradients of the objective function and constraint. Alternatively,

sensitivity analysis of the buckling modes can be performed using the equations in Appendix E to provide the gradients to the algorithm.

Using this framework, a finite element analysis code was developed in the Matlab environment. The buckling analysis was performed by following the steps described in Fig. 4.12. Fig. 4.19 shows the optimal topology of the problem shown in Fig.4.18. Fig. 4.20 shows the final topologies based on the optimal topologies shown in Fig. 4.19.

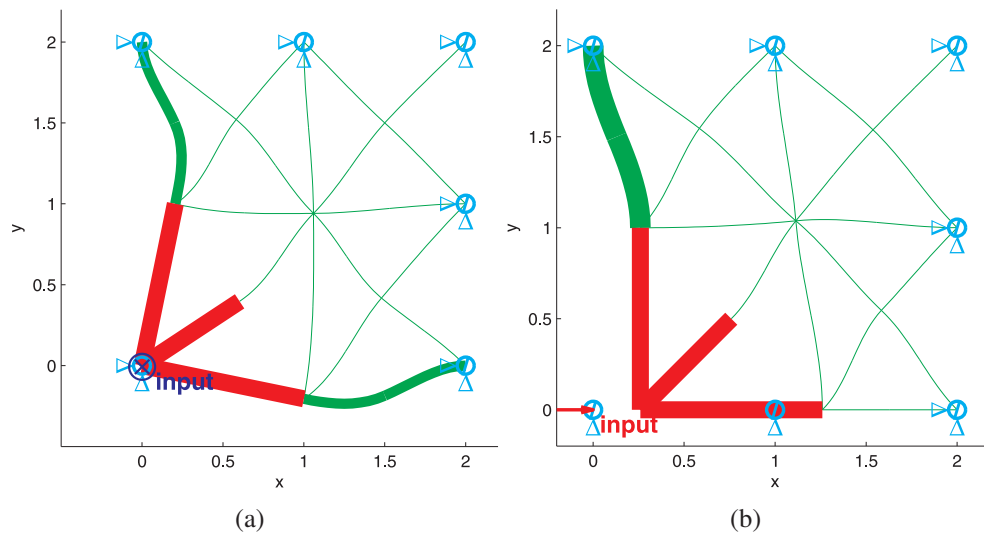


**Figure 4.19** The optimal topology of the right-top corner of a bistable compliant mechanism (SQP).

The genetic algorithm (GA) is one of the most commonly used methods for discrete optimization to find the optimal topology in compliant mechanism design. To use a GA for the problem in Fig.4.18, two discrete values are used for the thickness of each beam element. By using two values, we can avoid encountering difficulties with the connectivity of the structure. Also, the volume constraint in Eqn.4.25 is not applied. Some of the results from the GA for the two design problems are shown in Fig. 4.21 and 4.22.

As shown in the above examples of rotational bistable compliant mechanisms, a buckled mode of the beam connecting the rigid area with a pin joint at the center and a fixed boundary provides bistability. Fig. 4.23 shows a simple bistable latching mechanisms using this buckled configuration. The initial configuration is used as a closed position of the

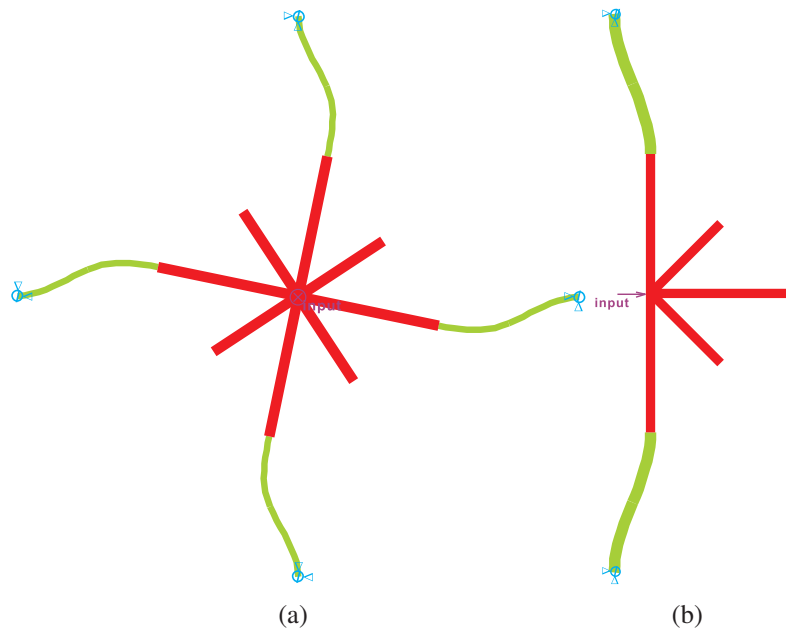


**Figure 4.20** The optimal topology of a rotational bistable compliant mechanism.

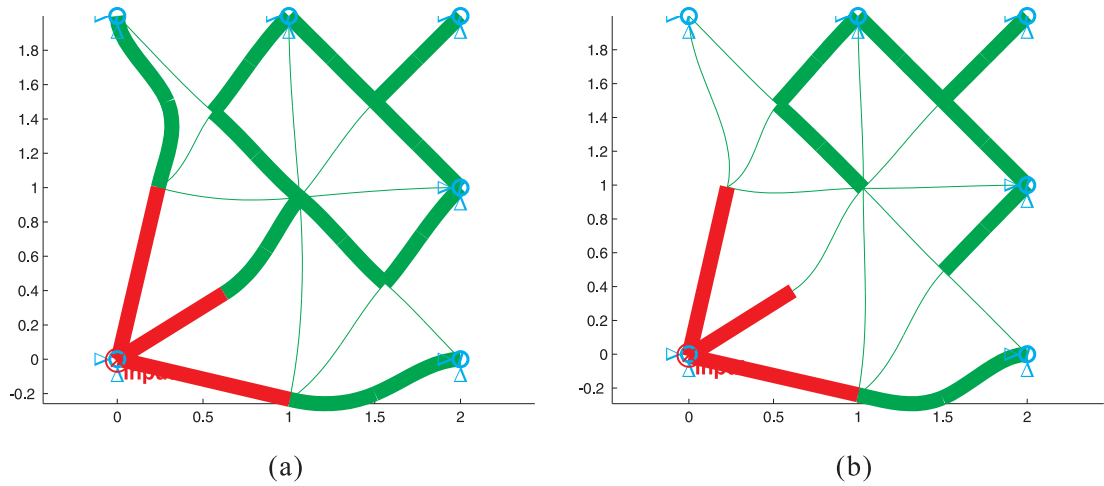


**Figure 4.21** The optimal topology of the right-top corner of a rotational bistable compliant mechanism (GA): (a)  $V_M = 0.23461$  (b)  $V_M = 0.22842$ .



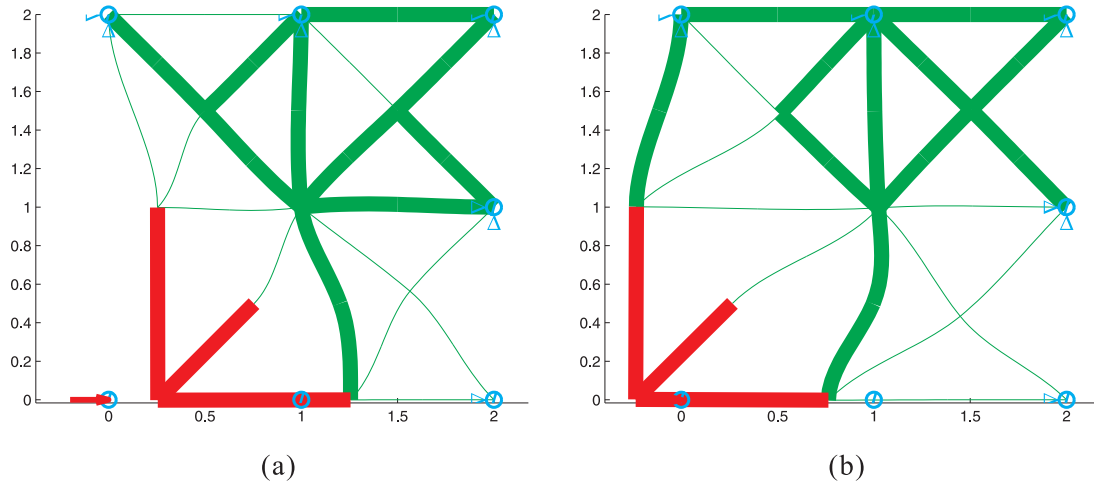
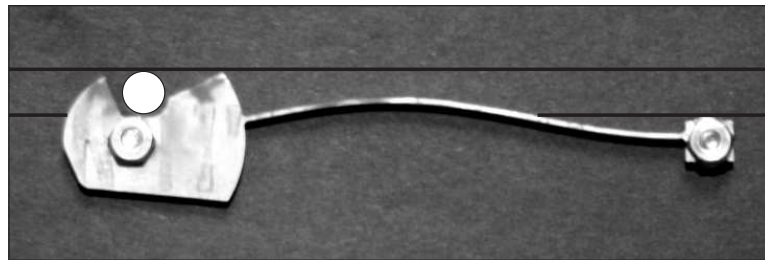
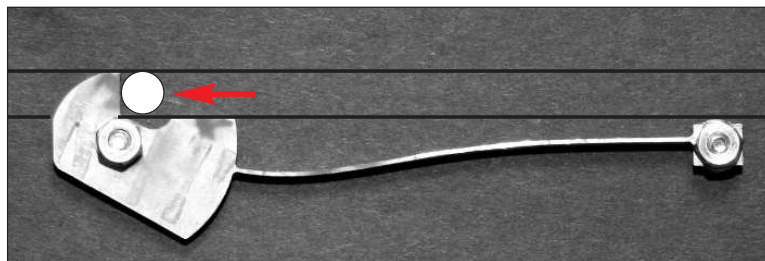


**Figure 4.22** The optimal topology of the right-top corner of a translational bistable compliant mechanism (GA): (a)  $V_M = 0.25522$  (b)  $V_M = 0.23594$ .

latching mechanism (top) and the latch is in the open position when the mechanism has the second stable state (bottom). The arrow in Fig. 4.23(b) indicates the direction of the load applied to the rigid body of the mechanism to have the closed position.



(a) the initial stable (close) configuration



(b) the second stable (open) configuration

**Figure 4.23** A rotational bistable compliant mechanism: The initial stable and the second stable configurations [ME551 design project: a bistable trunk latch].

Based on the result shown in Fig. 4.22 (b), a translational bistable compliant mechanism was fabricated by using waterjet machining. The prototype is made of Homopolymer Polypropylene. The two stable configurations are shown in Fig. 4.24.

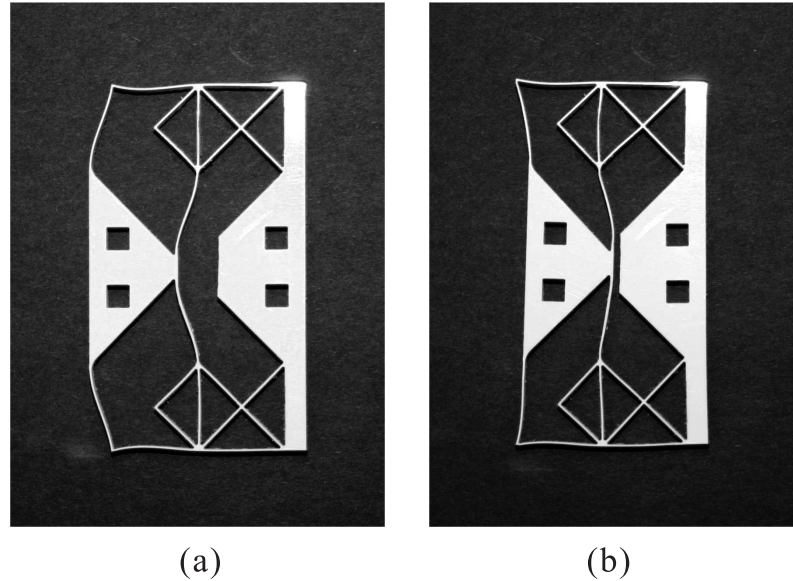


**Figure 4.24** A translational bistable compliant mechanism: (a) the initial stable configuration, and (b) the second stable configuration.

#### 4.5.4 Effect of Imperfections

An unstable system can be sensitive to the imperfections in manufacturing processes, operating conditions, boundary conditions, and even material properties. A system with more than one stable state always encounters an unstable state because the unstable status must exist between two stable states.

In order to design multistable compliant mechanisms, nonlinear finite element analysis without considering imperfections is not safe to estimate the actual behavior because the effect of the imperfections is sometimes very critical. The effect of imperfections can (1) change the unstable behavior, (2) shift/remove the stable position, and (3) reduce the actuation loads.

There are several methods to apply imperfect conditions to finite element models in-

cluding the followings: (1) applying numerical imperfections, (2) implementing physical imperfections, (3) adding buckling modes. Numerical imperfections can be applied to a symmetric structure by meshing it asymmetrically. If the imperfection is already known (e.g. imperfection due to the manufacturing tolerances at specific locations) it can be added to the original model by adjusting some of the nodal locations. Utilizing buckling modes as imperfect geometry is also commonly used for imperfection analysis. Fig. 4.25 shows how buckling modes can be added to the original geometry.

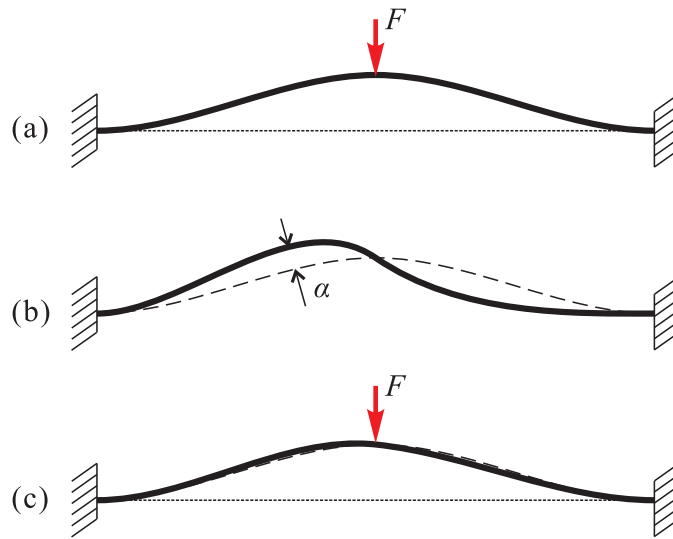


**Figure 4.25** Implementing buckling modes to the original geometry: (a) preparing nonlinear analysis to obtain the bistable behavior of a perfect geometry, (b) solving for linear buckling modes, (c) accumulating obtained modes to the original geometry.

Fig. 4.25(a) shows the original bistable problem with perfect geometry. By performing a linear buckling analysis, a number of buckling modes can be obtained (e.g. Fig. 4.25(b)). The buckling modes are added to the original perfect geometry based on the following equation.

$$\mathbf{x}_{\text{update}} = \mathbf{x}_0 + \sum \omega_i \bar{\mathbf{x}}_i. \quad (4.37)$$

where  $\mathbf{x}_0$  and  $\mathbf{x}_{\text{update}}$  are the original and updated geometries respectively.  $\bar{\mathbf{x}}_i$  and  $\omega_i$  are  $i^{\text{th}}$  buckling mode and the corresponding weighting value respectively. In general, the first

buckling mode is critical and it can adequately represent the general imperfection. The imperfection parameter,  $\alpha$ , in Fig. 4.25 (b) is usually smaller than the thickness of the beam (less than 1%). If the maximum displacement of the first buckling mode is defined as  $x_{1max}$ , the weighting value for the first mode is

$$\omega_1 = \alpha/x_{1max}. \quad (4.38)$$

By solving the problem with the same load/boundary conditions shown in Fig. 4.25 (a) and the updated geometry in Fig. 4.26 (c), it is possible to obtain nonlinear behavior considering imperfections.

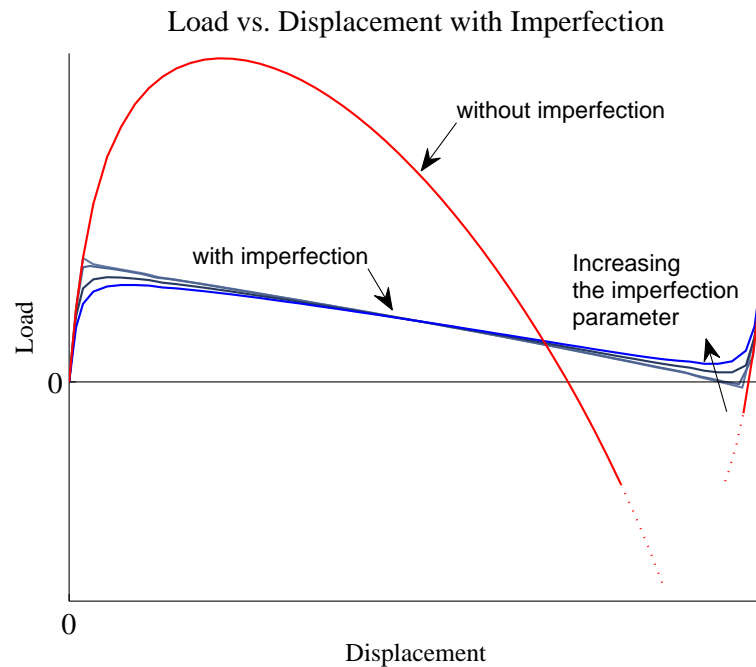


**Figure 4.26** Load-displacement curves with and without imperfections.

Fig. 4.26 shows how a bistability can be lost due to imperfection. The load-displacement curve with perfect geometry has much greater actuation load than the one with the imperfect condition. If the imperfection parameter,  $\alpha$ , is increased, it is possible to lose the bistability because the second stable position can disappear as shown in Fig. 4.26. Even though Fig. 4.26 is an extreme example, the imperfection analysis must be performed to

design bistable and multistable compliant mechanisms. However, imperfection analysis is not easy to implement with gradient-based optimization problems because of the difficulty obtaining the gradients of the objective and constraint functions with imperfections.

Therefore, it is desirable to design bistable compliant mechanisms that are less sensitive to imperfections. A design method for robust bistable compliant mechanisms that are not sensitive to imperfection is introduced in the following chapter.

## 4.6 Conclusions

In this chapter, first, the bistability of conventional four-bar linkage mechanisms with torsional springs on each joint was presented. There are two active torsional springs, which have non-zero stiffness values, among the four springs on each joint. Two spring constants,  $k_s$  and  $k_l$ , are related to the necessary and sufficient conditions of bistable four-bar linkage mechanisms. A slider-crank mechanism with two springs was also investigated as a special type of a bistable four-bar linkage mechanism. The necessary and sufficient conditions show how their unstable positions are related to the buckling modes of compliant structures. The similarity between the toggle position of the slider-crank mechanism and the buckling modes of the clamped-clamped beam shows that the first buckling mode of a compliant structure can be used to make it bistable.

The first buckling mode is used as the initially unstressed stable configuration of a bistable compliant mechanism. In order to apply the idea of utilizing the buckling mode to the topology synthesis, a modal strain energy formulation is introduced. Maximizing modal strain energy raises the energy barrier between two stable positions and, in turn, increases the possibility of having bistability.

A rotational and translational bistable compliant mechanisms are designed by maximizing the modal strain energy. Based on the results of the topology optimization, two prototypes were fabricated. These demonstrate that utilizing the first buckling modes can

provide bistability.

This methodology enables users to design a bistable compliant mechanism with desired behavior using a topology synthesis approach. However, normally, bistability that includes buckling behavior is very sensitive to imperfections in manufacturing processes, operation conditions, and boundary conditions. This is because the effect of imperfections can change the unstable behavior, shift/remove the stable position, and reduce the actuation loads. In the following chapter, a design method for robust bistable compliant mechanisms is introduced.

## Chapter 5

### **Robust Design of Bistable Compliant Mechanisms Using the Bistability of a Clamped-Pinned Beam**

The work presented in this chapter is the first step towards development of a method for synthesizing robust bistable mechanisms with distributed compliance. The bistability of a cantilever beam under various loading conditions is introduced by solving a large deformation problem. Through such analysis, it is possible to identify conditions under which a beam will exhibit bistable behavior that is not sensitive to imperfections arising from manufacturing errors or boundary conditions. A compliant mechanism, designed as a counterpart to the cantilever beam, will impose load-displacement conditions on the cantilever beam to obtain bistability.

#### **5.1 Introduction**

This research investigates a new approach to the design of bistable compliant mechanisms using the bistability of a clamped-free beam. Bistability plays an important role for a variety of applications since energy is applied only to move the mechanism from one stable position to another and no energy needs to be expended once a stable position is reached. The behavior of a bistable compliant mechanism, in general, is highly non-linear and relies on the buckling phenomenon. The buckling phenomenon involves instability of the structure, and the instability is usually triggered by local buckling. In other words, local buckling can dominantly produce bistability in an entire structure. The concept presented here is to use a single clamped-pinned beam to create local buckling resulting in a bistable

mechanism. Additionally, buckling is very sensitive to imperfections in manufacturing processes, operating conditions and boundary conditions. By utilizing the behavior of a simple clamped-free beam, a method is presented for designing bistable mechanisms that are robust against such imperfections

A solution for large deformation of a simple clamped-free beam is first obtained to study its bistable behavior under various loading conditions. If the load is greater than the critical buckling load, the beam can be deflected not only in the normal direction but also in a 'reverse-lateral' (RL) direction. The RL deformation will be a major topic of discussion in this chapter. First, an initially straight beam must be bent to a certain curvature under the action of the applied force. In the second loading condition, the partially bent beam is further loaded so that it buckles in the RL direction into a stable position. The magnitude and direction of the forces in both loading conditions that are conducive to bistability are thus determined. A compliant mechanism is then designed such that its output generates desired forces on the beam to deform it in the RL direction. We demonstrate that the RL deformation is less sensitive to the imperfections and ensures bistable behavior.

Using clamped-pinned beams, two design examples (translational and rotational cases) of bistable compliant mechanisms are presented. Results show very good correlation between the finite element analysis and experimental tests on prototypes.

## **5.2 Organization of This Chapter**

In the next section, bistability of a clamped-free beam is first introduced, and then an analytical solution is derived for the large deformation of the beam. Following this, a method for designing of a bistable mechanism using the clamped-free beam is discussed. Two case studies, (i) symmetrical and (ii) asymmetrical bistable mechanisms, are introduced, and the analytical results are compared to the experimental tests and FEA results.



## 5.3 Bistability of a Clamped-Free Beam

### 5.3.1 Reverse-lateral Deformation

In general, a linear buckling analysis is performed to identify the stability of a structure. The first buckling mode and corresponding critical load represent the unstable state of the structure. Unlike the linear buckling analysis, the buckled status in a nonlinear analysis represents the stable status of a structure under given boundary and loading conditions. For example, the straight beam described in Fig. 5.1(a) has the buckled configuration,  $A_1$  or  $B_1$ , once a critical buckling load,  $P_{cr}$ , is applied in the axial direction at the free-end of the beam. These configurations are identical and symmetrical to each other. Either of the two configurations corresponds to the stable status of the beam under the given boundary and loading conditions. The buckling direction,  $A_1$  or  $B_1$ , usually depends on imperfections, such as disturbances to the off-loading direction, defects in the structure, tolerance errors in manufacturing, or imperfect boundary conditions. The buckled status retains the similarity to the linear buckling in terms of its mode shapes. Note that the first linear buckling mode represents stable equilibrium for a large deformation, while higher order buckling modes do not.

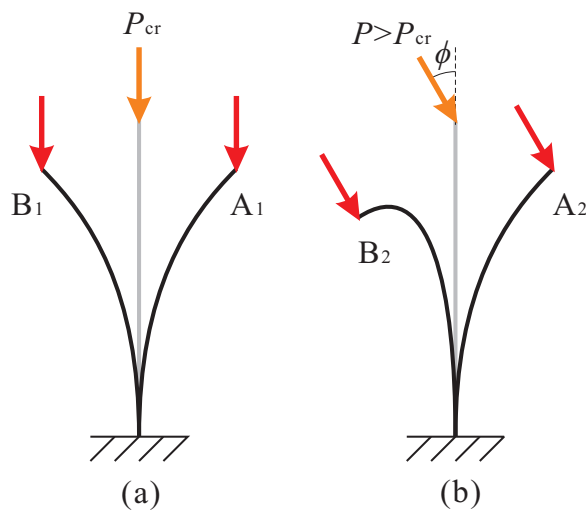


**Figure 5.1** Two stable stages of a beam with a force applied at the tip.

If a force with an angle,  $\phi$ , is applied to the free end of the beam, the bistability of this condition differs somewhat compared to the axial loading condition. Fig. 5.1(b) describes the two stable configurations of the loading (these are not buckled cases). Configuration  $A_2$  shows a normal static deformation, and configuration  $B_2$  shows the reverse-lateral (RL) deformation of  $A_2$ . These configurations are uniquely defined by the vector  $P$ . Configuration  $B_2$  satisfies the static equilibrium of the given condition, but it can only be reached with additional history of the loading or boundary condition, such as the initial load, displacement, or the velocity at the free end. Since the two configurations are unique and stable, any configuration between these two is not stable. Therefore, any position of the free end, other than these two positions, indicates instability. The reverse lateral deformation is useful in the design of bistable mechanisms as will be shown in the following sections.

### 5.3.2 Solution for a Clamped-free Beam with a Reverse-lateral Deformation

In large deformation problems with cantilever beams under various loading conditions, the axial load is scaled to solve bending problems [32, 15, 50]. However, in this section, a large deformation solution for an RL deformation is derived by scaling vertical directional loads.

An RL deformation of an initially straight cantilever beam with the length  $l$  is shown in Fig. 5.2. A load  $P$  is applied to the free end. This load can be described as a combination of  $P_x$  and  $P_y$ ,

$$\begin{aligned} P_x &= P \cos(\phi) = F, \\ P_y &= P \sin(\phi) = nF. \end{aligned} \tag{5.1}$$

where  $n = \tan \phi$ . The magnitude of  $P$  can be calculated as  $F\sqrt{1+n^2}$

In the figure,  $a$  and  $b$  are defined as the  $x$  distance from the  $y$ -axis and the  $y$  distance from the  $x$ -axis to the end of the beam respectively. The notation  $s$  indicates the tangential distance along the deformed beam, and  $d$  is the distance from the initial to the final position

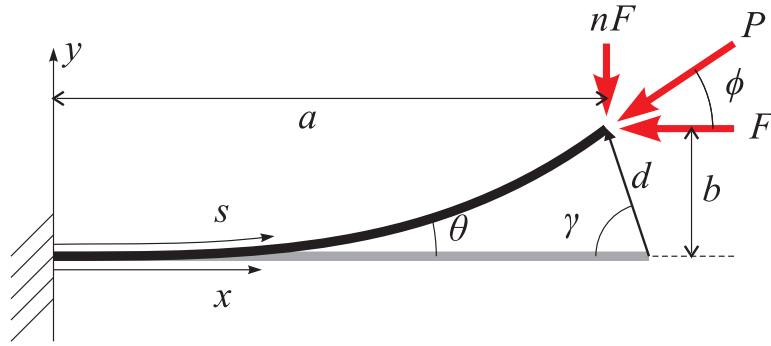


**Figure 5.2** Problem definition of a reverse-lateral deformation.

of the beam end.  $\theta$  is the angle between the slope and the  $x$ -axis along the beam, and  $\theta_e$  is the value of the angle,  $\theta$ , at the end of the beam.

When a cantilever beam has an RL deformation, a strict relationship between  $\theta_e$  and  $n$  can be found. Fig. 5.3(a) shows an unstable equilibrium status of an RL deformation. The load  $P$  is pointing to the clamped end of the beam. Therefore, there is no reaction moment at the clamped end. This condition is identical to the buckling condition of a pinned-pinned beam, and  $\theta_e$  can be calculated as  $2 \tan^{-1}(n)$ . Once the position of the load is lower than the unstable equilibrium position (i.e., Fig. 5.3(a)) as shown in Fig. 5.3(b), the direction of the moment at the clamped end becomes opposite to the stable direction and the deformed shape no longer has the first buckling mode. The structure is unstable and will find the other stable position, as described in Fig. 5.1(b)  $A_2$ . Additionally,  $\theta_e$  cannot be greater than or equal to the loading direction as shown in Fig. 5.3(c). The corresponding  $\theta_e$  is the maximum and can be obtained as  $\pi + \tan^{-1}(n)$ . Therefore, the following condition is always true for the RL deformation:

$$2 \tan^{-1}(n) < \theta_e < \pi + \tan^{-1}(n). \quad (5.2)$$

Similar to the normal deformation shown in Fig. 5.1(b)  $A_2$ , using an elliptic integral solution [32], with the assumption that the beam is linearly elastic and inextensible, the deflection of the free end in the aforementioned problem can be obtained. Note that Eqn. (5.2)

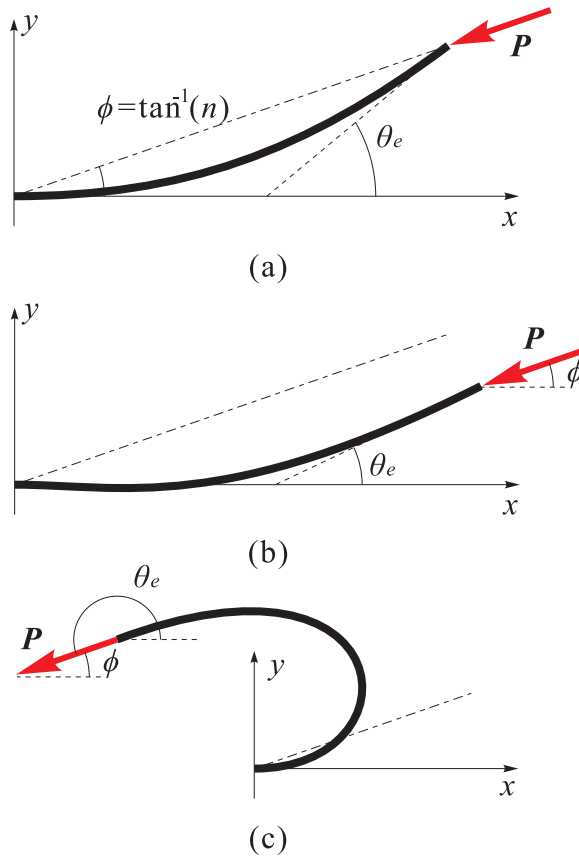


**Figure 5.3** Illustration of the relationship between  $\theta_e$  and  $n$ .

should be applied to the entire procedure of this analysis. The moment along the deformed beam is given by

$$M(s) = -nF(a - x(s)) + F(b - y(s)). \quad (5.3)$$

The curvature,  $\kappa$ , is defined as the rate of change of the slope angle of the curve with respect to distance along the curve.  $\kappa$  can be obtained using the following relationship of the Bernoulli-Euler equation, which states that the curvature is proportional to the bending moment:

$$\kappa = \frac{d\theta}{ds} = \frac{M}{EI} \quad (5.4)$$

Given that the above relationship is available in many solid mechanics textbooks [19, 11], it is not discussed in detail here. Substituting Eqn. (5.3) into Eqn. (5.4), and differentiating with respect to  $s$  results in

$$\frac{d\kappa}{ds} = \frac{F}{EI} \left( -\frac{dy}{ds} + n\frac{dx}{ds} \right). \quad (5.5)$$

Using Eqn. (5.4) and applying the chain rule of differentiation, the left side of Eqn. (5.5) can be written as

$$\begin{aligned} \text{Left side of Eqn. (5.5)} &= \\ \frac{d\kappa}{ds} &= \frac{d^2\theta}{ds^2} = \frac{d}{ds} \frac{d\theta}{ds} = \frac{d}{d\theta} \left( \frac{d\theta}{ds} \right) \frac{d\theta}{ds} = \frac{d\kappa}{d\theta} \kappa = \frac{d}{d\theta} \frac{\kappa^2}{2} \end{aligned}$$

The relationships between  $x$  and  $y$ , and  $\theta$  and  $s$  are given by the differential equations  $dx/ds = \cos \theta$  and  $dy/ds = \sin \theta$  respectively. These relationships are always true given that  $dx$ ,  $dy$ , and  $ds$  are infinitesimal. Substituting these relationships into the right side of the equation results in

$$\begin{aligned} \text{Right side of Eqn. (5.5)} &= \\ \frac{F}{EI} \left( -\frac{dy}{ds} + n\frac{dx}{ds} \right) &= \frac{F}{EI} (-\sin \theta + n \cos \theta) \end{aligned}$$

At this point, by substituting the left and right sides, Eqn. (5.5) can be rewritten and rearranged as

$$\frac{d}{d\theta} \left( \frac{\kappa^2}{2} \right) = \frac{F}{EI} (n \cos \theta - \sin \theta). \quad (5.6)$$

Integrating Eqn. (5.6) with respect to  $\theta$  yields

$$\begin{aligned}
\frac{\kappa^2}{2} &= \frac{F}{EI} \int (n \cos \theta - \sin \theta) d\theta \\
&= \frac{F}{EI} (n \sin \theta + \cos \theta) + C_e,
\end{aligned} \tag{5.7}$$

where  $C_e$  is a constant in the integration, i.e., it can be found by applying the condition at the end of the beam. Given the curvature at the end of the beam is zero and setting the slope angle at the end as  $\theta_e$ ,  $C_e$  can be obtained as

$$C_e = -\frac{F}{EI} (n \sin \theta_e + \cos \theta_e). \tag{5.8}$$

Substituting Eqn. (5.8) into Eqn. (5.7) and solving for  $\kappa$  yields

$$\begin{aligned}
\kappa &= \sqrt{2 \frac{F}{EI} (n \sin \theta + \cos \theta - n \sin \theta_e - \cos \theta_e)} \\
&= \sqrt{2} \frac{\alpha}{L} \sqrt{n \sin \theta + \cos \theta - n \sin \theta_e - \cos \theta_e} = \frac{d\theta}{ds},
\end{aligned} \tag{5.9}$$

where  $\alpha^2 = \frac{FL^2}{EI}$  is the dimensionless form of the input force,  $F$ .

Reorganizing the equation for  $\alpha$  yields

$$\sqrt{2} \frac{\alpha}{L} \int_0^L ds = \int_0^{\theta_e} \frac{d\theta}{\sqrt{n \sin \theta + \cos \theta - n \sin \theta_e - \cos \theta_e}}. \tag{5.10}$$

Solving for  $\alpha$  yields

$$\alpha = \frac{1}{\sqrt{2}} \int_0^{\theta_e} \frac{d\theta}{\sqrt{n \sin \theta + \cos \theta - n \sin \theta_e - \cos \theta_e}}. \tag{5.11}$$

Substituting the relationships between  $x$  and  $y$ , and  $\theta$  to Eqn. (5.9) results in

$$\begin{aligned}
\kappa &= \frac{d\theta}{dx} \cos \theta \\
&= \sqrt{2} \frac{\alpha}{L} \sqrt{n \sin \theta + \cos \theta - n \sin \theta_e - \cos \theta_e},
\end{aligned} \tag{5.12}$$

and

$$\begin{aligned}
\kappa &= \frac{d\theta}{dy} \sin \theta \\
&= \sqrt{2} \frac{\alpha}{L} \sqrt{n \sin \theta + \cos \theta - n \sin \theta_e - \cos \theta_e}.
\end{aligned} \tag{5.13}$$

Rearranging these equations yields

$$\frac{a}{L} = \frac{1}{\sqrt{2}\alpha} \int_0^{\theta_e} \frac{\cos \theta d\theta}{\sqrt{n \sin \theta + \cos \theta - n \sin \theta_e - \cos \theta_e}}, \tag{5.14}$$

and

$$\frac{b}{L} = \frac{1}{\sqrt{2}\alpha} \int_0^{\theta_e} \frac{\sin \theta d\theta}{\sqrt{n \sin \theta + \cos \theta - n \sin \theta_e - \cos \theta_e}}. \tag{5.15}$$

Eqn. (5.14) and (5.15) show the dimensionless displacements of the beam end. These dimensionless displacements and loads are not geometry or material dependent. Numerical integration using Gaussian quadrature is used to solve Eqn. (5.11), (5.14) and (5.15) numerically. Alternatively, these integrals can be solved using the elliptic integral tables [17] (See Appendix D for these equations).

In Fig. 5.4(a) and (b), the dimensionless variables for the horizontal and the vertical displacement are plotted. The lines in the plots are the response curves when  $n$  varies from  $-2.0$  to  $2.0$ . Since  $n = \tan \phi$  is monotonic and odd function for  $-\pi/2 < \phi < \pi/2$ , the signs of  $n$  and  $\phi$  must be same. Negative  $n$  indicates that normal deformations ( $\phi < 0$ ) occur, and positive  $n$  is for RL deformations ( $\phi > 0$ ). When  $n = 0$ , only axial load is applied

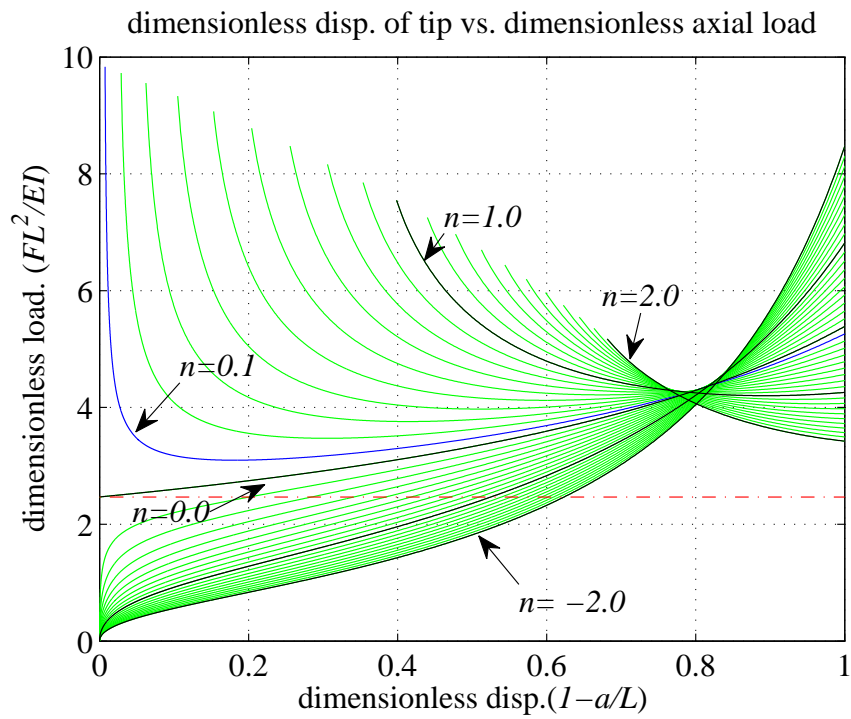
to the clamped-free beam ( $\phi = 0$ ). If  $n$  is smaller than zero, the response curves start from the origin of the coordinates and increase monotonically. In the case of a positive  $n$  value, the curves are convex functions and do not start from a zero displacement or zero load. These convex curves have dimensionless loads of minimum values, and the minimum values are the required loads for the given loading angle,  $n$ , to have the RL deformations. It is conceivable that the minimum load for  $n = 0$  is equal to the linear buckling or critical load of the beam (Fig. 5.4). Since the linear buckling load for this system is  $F_{cr} = \pi^2 EI/4L^2$ , the critical dimensionless load is  $\alpha^2 = \pi^2/4 \approx 2.47$ . This is the minimum load required to trigger any RL deformation.

Fig. 5.5 shows the minimum required loads to activate RL deformations for various values of  $n$ . These loads are only available for positive  $n$  values. It is important to note that the dimensionless load in the figure is for the load  $F$  and not for  $P$ .  $P$  can be calculated using Eqn. (5.1) once  $F$  is known.

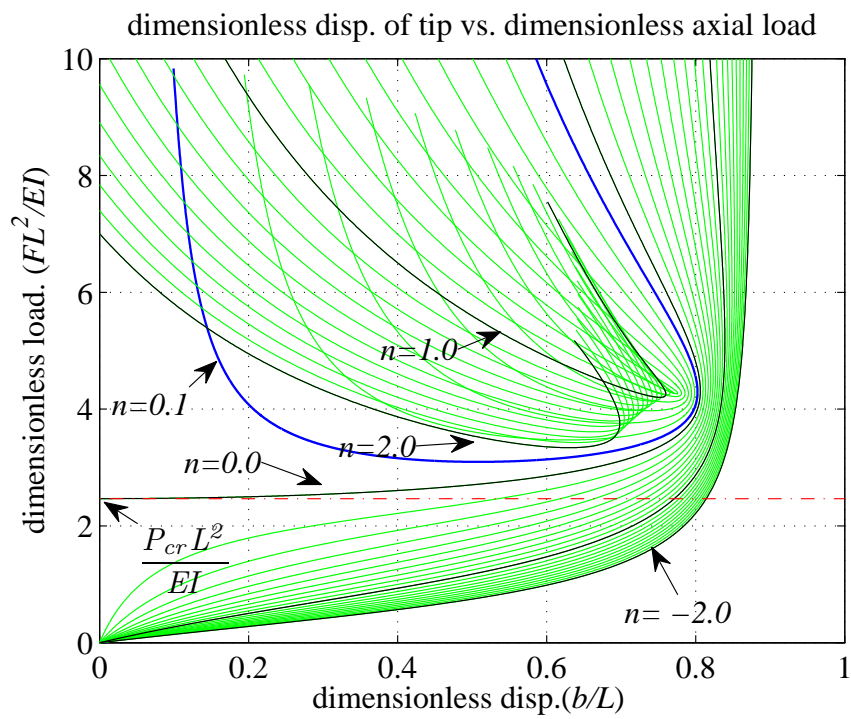
Unlike the normal deformation in which the starting points are always the same, the RL deformation has a different deflection path. Combining the results of Fig. 5.4(a) and (b) produces the deflection paths at the end of the beam. Fig. 5.6 shows these paths for various values of  $n$ . The normal ( $n < 0.0$ ) and the RL ( $n > 0.0$ ) deformations are compared in Fig. 5.6(a) and (b) respectively. The starting points of the normal deformation are identical at the point  $[x/L = 1, y/L = 0]$  and are spread out once  $\theta_e$  increases. In contrast, the RL deformation path has a unique starting point ( $\circ$ ) for each value of  $n$ . It also has a unique initial point ( $\star$ ) for the minimum load. For a more specific representation of the deformation, we can look at  $n = -1.0$  and  $1.0$  (Fig. 5.7). In Fig. 4.1(b), the initial point is located in the middle of the deflection path. Once  $P$  increases without changing its direction, the beam end will move along the deflection path by decreasing its  $x/L$  value. It may be able to follow its positive  $x/L$  direction, if there is a displacement condition forcing this direction.

There are two factors that should be noted from the figures: the maximum stresses and





(a)



(b)

**Figure 5.4** Dimensionless displacement of the free-end vs. dimensionless load for the loading direction,  $n = 0.0 \cdots 1.2$ .

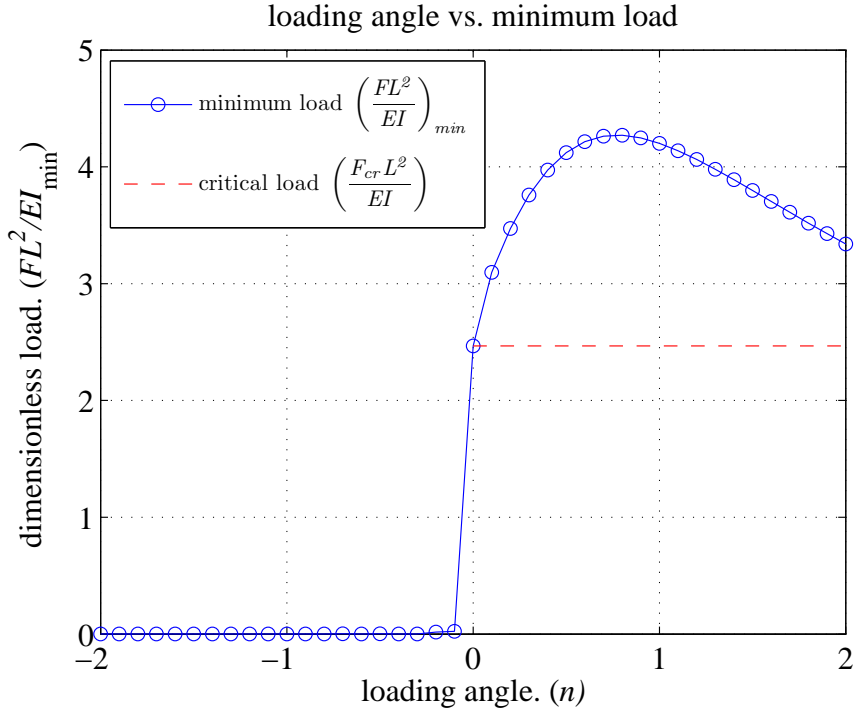
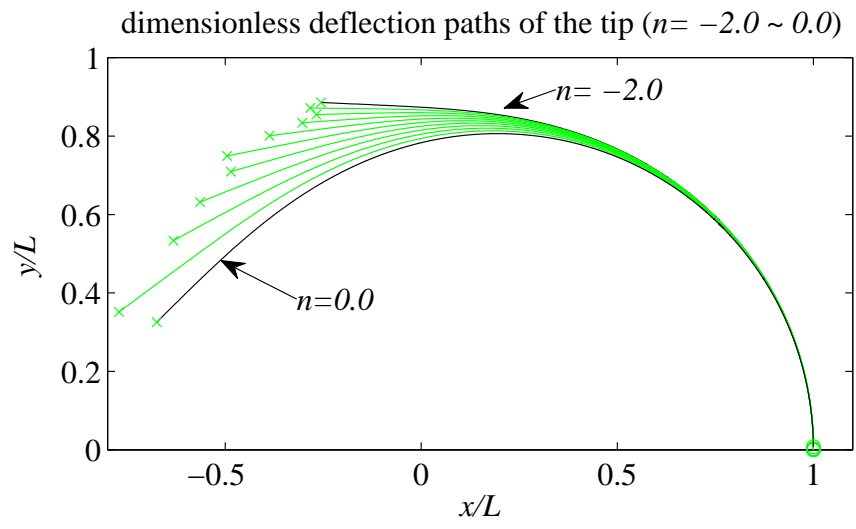
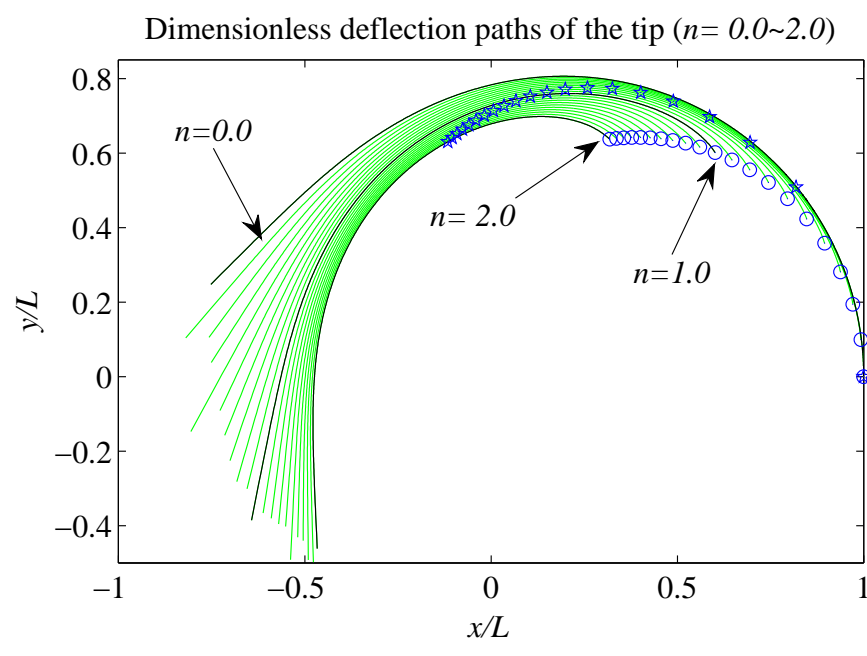


**Figure 5.5** Minimum dimensionless load for the loading direction,  $n = -2.0 \dots 2.0$ .

the recovery energy. Since the moment arm for a negative  $n$  value is greater than that for a positive  $n$  value, the maximum stress at the fixed end is smaller with a positive  $n$ . With a negative  $n$  value, the maximum stress always occurs at the clamped end. With a positive  $n$  value, the maximum stress occurs where the maximum curvature is located. If the same minimum loads  $P$  (Fig. 5.7) are applied to the cases with  $n = -1$  and 1, the stress at the fixed end of the case with positive  $n$  is always smaller than the stress for negative  $n$ . To recover to the original shape by following the paths, the applied force for a negative  $n$  value decreases. However, the applied force for the RL deformation increases dramatically. Fig. 4.1(a) and (b) show this graphically. The slopes for positive  $n$  values are stiff and require large loads when the displacement becomes zero. This implies that there is a potential energy barrier to go over. And the smaller the positive value  $n$  is, the stiffer the slope becomes. This implies that the bistability of the RL deformation is robust. On the other hand, the slopes for the negative  $n$  values are decreased gradually without any barrier on the load input.



(a)



(b)

**Figure 5.6** Feasible deflection paths of the free-end for the loading direction: (a)  $n = -2.0 \cdots 0.0$ , (b)  $n = 0.0 \cdots 2.0$ .

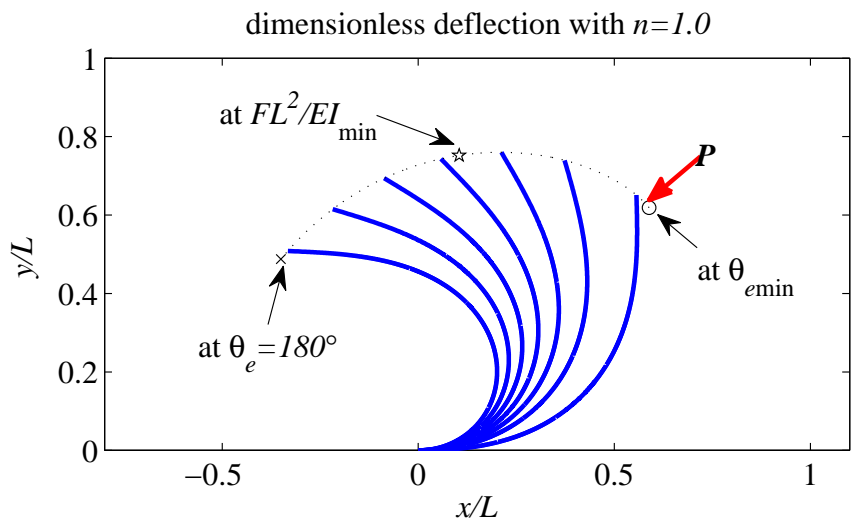
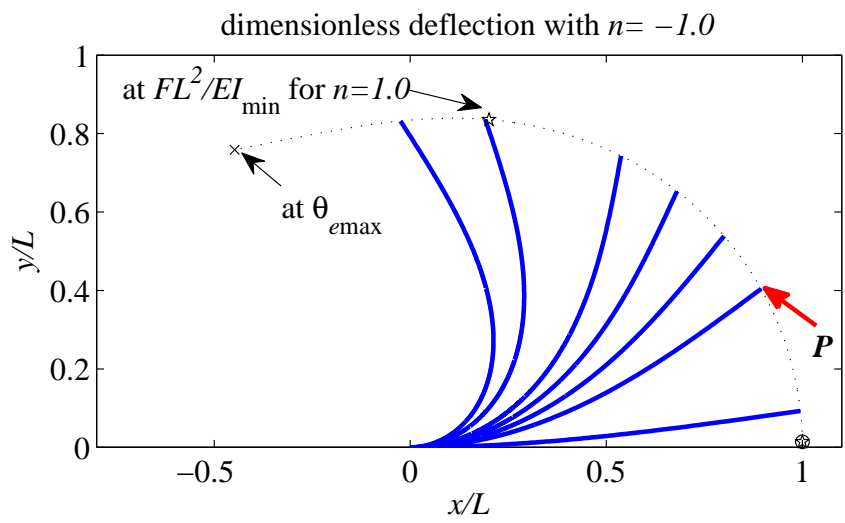


**Figure 5.7** Deflected shapes for (a)  $n = -1.0$  and (b)  $n = 1.0$ .

If a load  $P$  is applied with an angle of  $45^\circ$ , up to the minimum loading, there is a unique solution for the deformation. When the load is greater than the minimum load, there are multiple solutions. The combined solution for  $n = -1.0$  and  $1.0$  illustrates (Fig. 5.8) the range of feasible solutions is divided into the two regions of unique and multiple-solution regions.

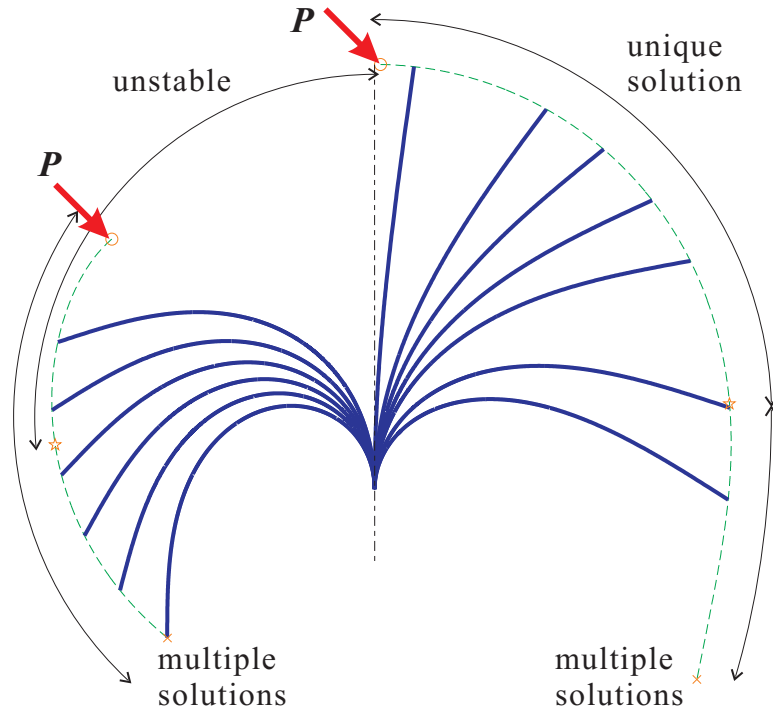


**Figure 5.8** Feasible range of the deflection when load  $P$  applied with an angle of  $45^\circ$ .

## 5.4 Design of Bistability Using a Clamped-Pinned Beam

The RL deformation of a cantilever beam can be used to design bistable mechanisms by applying a pin joint at the end because the pin joint does not provide a moment to the end of the beam. Fig. 5.9(a) shows a clamped beam and an undefined mechanism that are labeled  $A$  and  $B$  respectively. These two bodies are pin-jointed to each other. Body  $B$  has input and output nodes.

To achieve bistability in the entire mechanism, the deformed position and the reaction

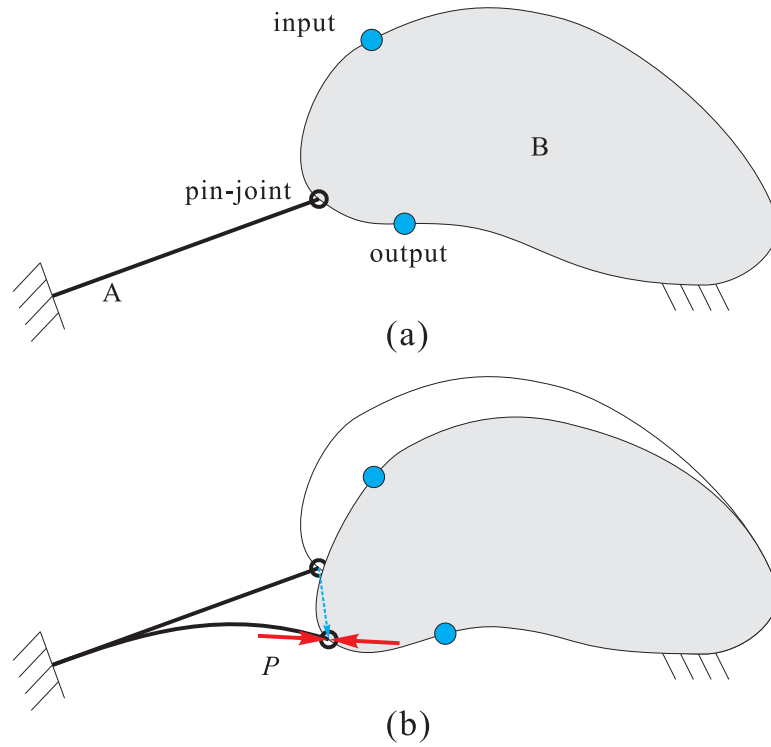


**Figure 5.9** Conceptual drawing of a bistable compliant mechanism with a clamped-pinned beam.

force at the pin-joint of Body  $B$  must satisfy the RL condition of Beam  $A$ . The displacements at the joint should be identical and the reaction loads should be equal and opposite. The topology design of Body  $B$  is not discussed in this chapter. It can be designed using topology optimization with nonlinear analysis [44].

To utilize the RL deformation to generate bistabilities, it is necessary to define the second stable configuration. In this section, the deformation vector of the end of the beam is chosen. To describe the vector, the dimensionless parameters  $d$  and  $\gamma$  are used. These two parameters are illustrated in Fig. 5.2 and can be calculated respectively, using the following two equations:

$$\frac{d}{L} = \sqrt{\left(1 - \frac{a}{L}\right)^2 + \left(\frac{b}{L}\right)^2}, \quad (5.16)$$

and

$$\gamma = \frac{\pi}{2} - \tan^{-1} \left( \frac{1 - a/L}{b/L} \right). \quad (5.17)$$

Fig. 5.10 shows the relationship between these two parameters for various values of  $n$ . These curves are plotted based on the fact that the  $\theta_e$  is greater than the minimum values (Eqn. (5.2)) and is smaller than  $\pi$ . Once  $n$  and  $\gamma$  are determined,  $d/L$  can be graphically found using the figure.

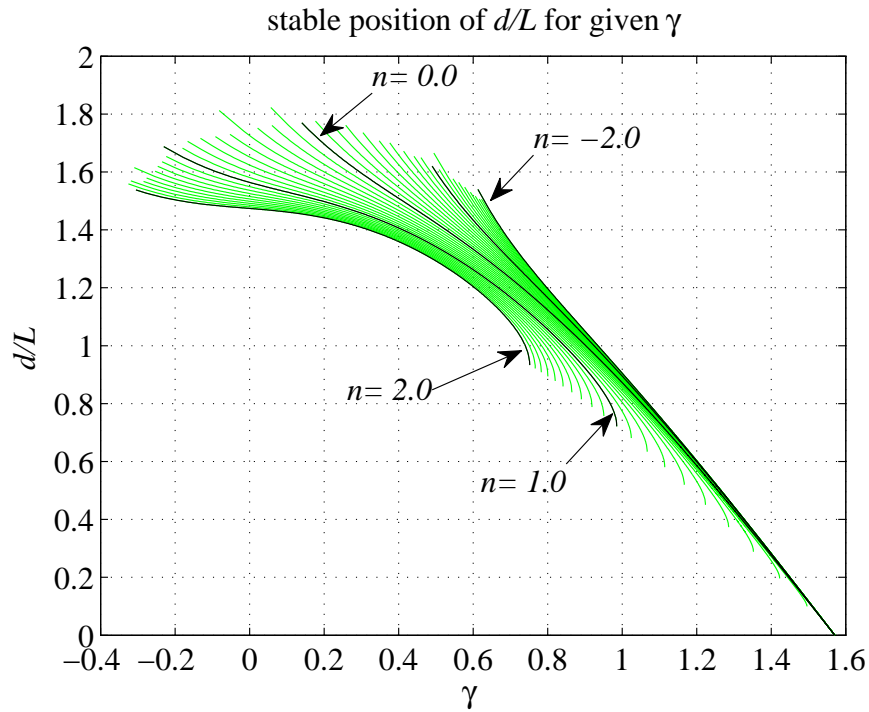


**Figure 5.10** Relationship between  $\gamma$  and  $d/L$  for various values of  $n$ .

### 5.4.1 Design of Bistability Using Two RL Deformations

In certain cases,  $n$  and  $\gamma$  have a relationship. For example, if two identical clamped-pinned beams are used and connecting using a living hinge (Fig. 5.11), there are symmetrical RL

deformations, and the relationship is

$$n = C \cot \gamma. \quad (5.18)$$

with  $C = 1$ . The positive constant  $C$  varies once an asymmetrical condition is applied.

Both stable configurations of the symmetric case are depicted in Fig. 5.11. Applying Eqn. (5.18) to Fig. 5.10 produces a bijective relationship between  $d/L$  and  $\gamma$ . This relationship is exact for the symmetric condition and plotted in Fig. 5.12. This relationship does not depend on any properties related to cross-section and material properties.

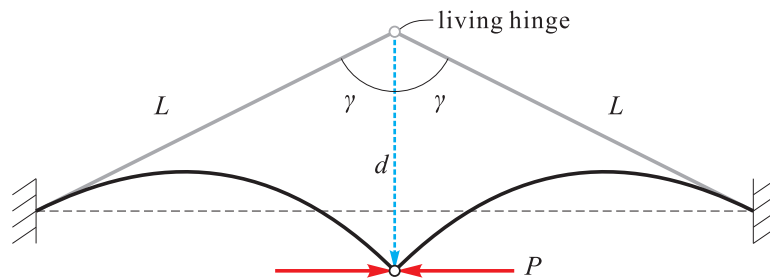


**Figure 5.11** Both stable configurations of a symmetrical bistable mechanism.

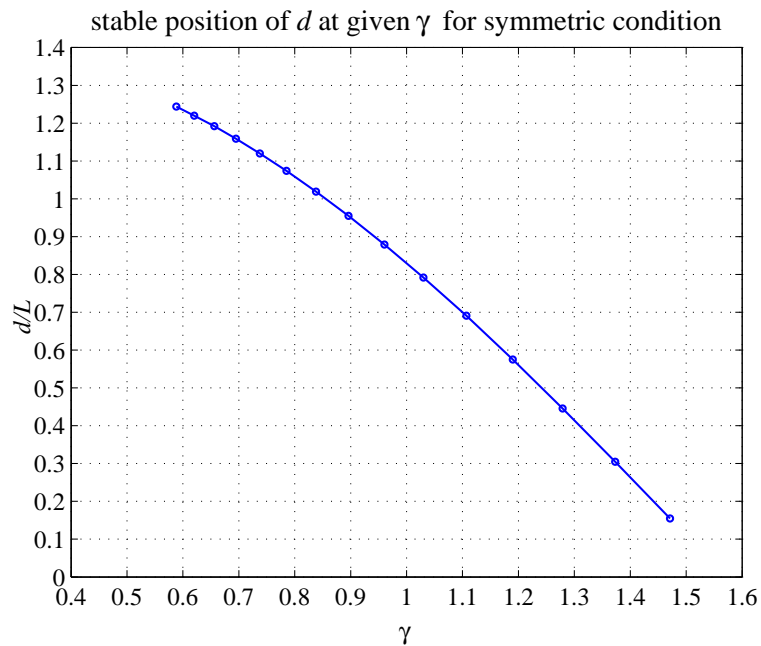


**Figure 5.12** Relationship between  $\gamma$  and  $d/L$  for a symmetrical condition.



It is important to note that utilizing the two identical RL deformations in Fig. 5.11 is more robust to provide bistable behavior than utilizing the first buckling mode of a clamped-clamped beam shown in Fig. 4.25 (a). The essential factor producing the robustness is the small stiffness of living hinge at the center. The torsional stiffness of the living hinge is much less than bending stiffness of the two beams and provide sufficient condition (Eqn.(4.21)) to ensure bistability as discussed in Chapter 4. As shown in Table 4.3, minimizing the torsional stiffness of the living hinge,  $k_\theta$ , is desired to ensure the bistability. Maximizing the translational stiffness,  $k_\delta$ , is satisfied by fixing the ends of the two beams in Fig. 5.11.

Table 5.1 presents analytical and experimental results of four cases that were uniquely defined by their included angles of  $\Gamma$ , where  $\Gamma = 2\gamma$ . The results are in good agreement with error of less than 5%. The material used in the tests is Nylon66. The results of the finite element analysis for the four cases are shown as the load-displacement responses in Fig. 5.13

**Table 5.1** Comparison of the results from Fig. 5.12 and experimental tests for various values of the included angle,  $\Gamma$ .

Desired $d/L$ (Fig. 5.12)	$\gamma$ [rad]	$n$ Eqn. (5.18)	$\Gamma = 2\gamma$ [degree]	$d/L$ (experiment)
0.27	1.40	0.17	160°	0.25
0.50	1.22	0.37	140°	0.48
0.81	1.05	0.57	120°	0.77
1.05	0.83	0.91	95°	1.05

Fig. 5.14 shows prototypes of the four cases in their initial and second stable configurations. These prototypes are made of Homopolymer Polypropylene which has greater material nonlinearity than Nylon66. Therefore the second stable positions are slightly larger than the values shown in Table 5.1.

For the case with asymmetrical RL deformation shown in Fig. 5.15, the following two relationships need to be satisfied in the global coordinates:

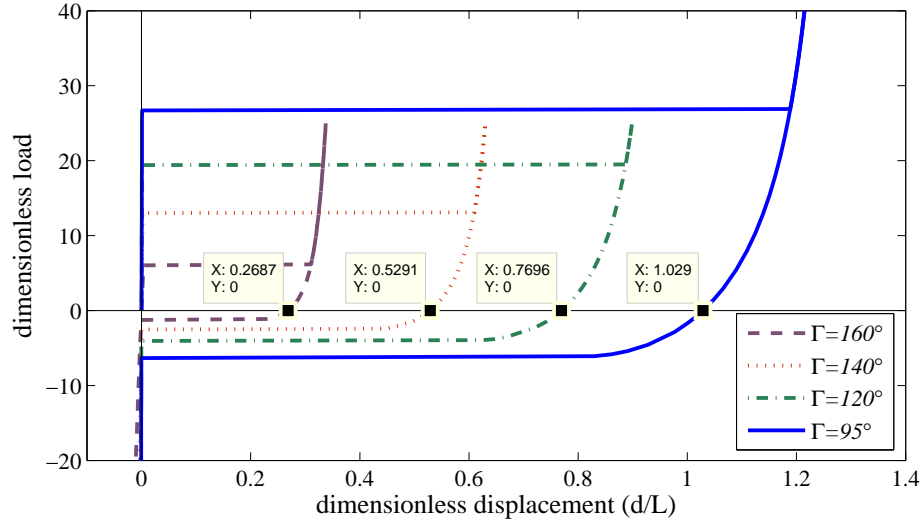


**Figure 5.13** Load-displacement plots for four symmetric problems [ANSYS]

$$\begin{aligned}\vec{P}_A &= -\vec{P}_B \\ \vec{d}_A &= \vec{d}_B\end{aligned}\quad (5.19)$$

It may be convenient to use an approximated solution since it is not easy to obtain the directions,  $n$ , of the reaction forces,  $P$ , at the pin-joint intuitively. The relationship in Fig. 5.12 can be used to solve asymmetric problems because the constant  $C$  in Eqn. (5.18) for one body is less than 1 and the value for the other body is greater than 1, and the average  $C$  for both beams will be close to the value 1. A linear trend line for Fig. 5.12 was selected to solve this problem. The approximated relationship is

$$d_i = -1.1372\gamma_i L_i + 1.9183L_i \quad (i = A, B) \quad (5.20)$$

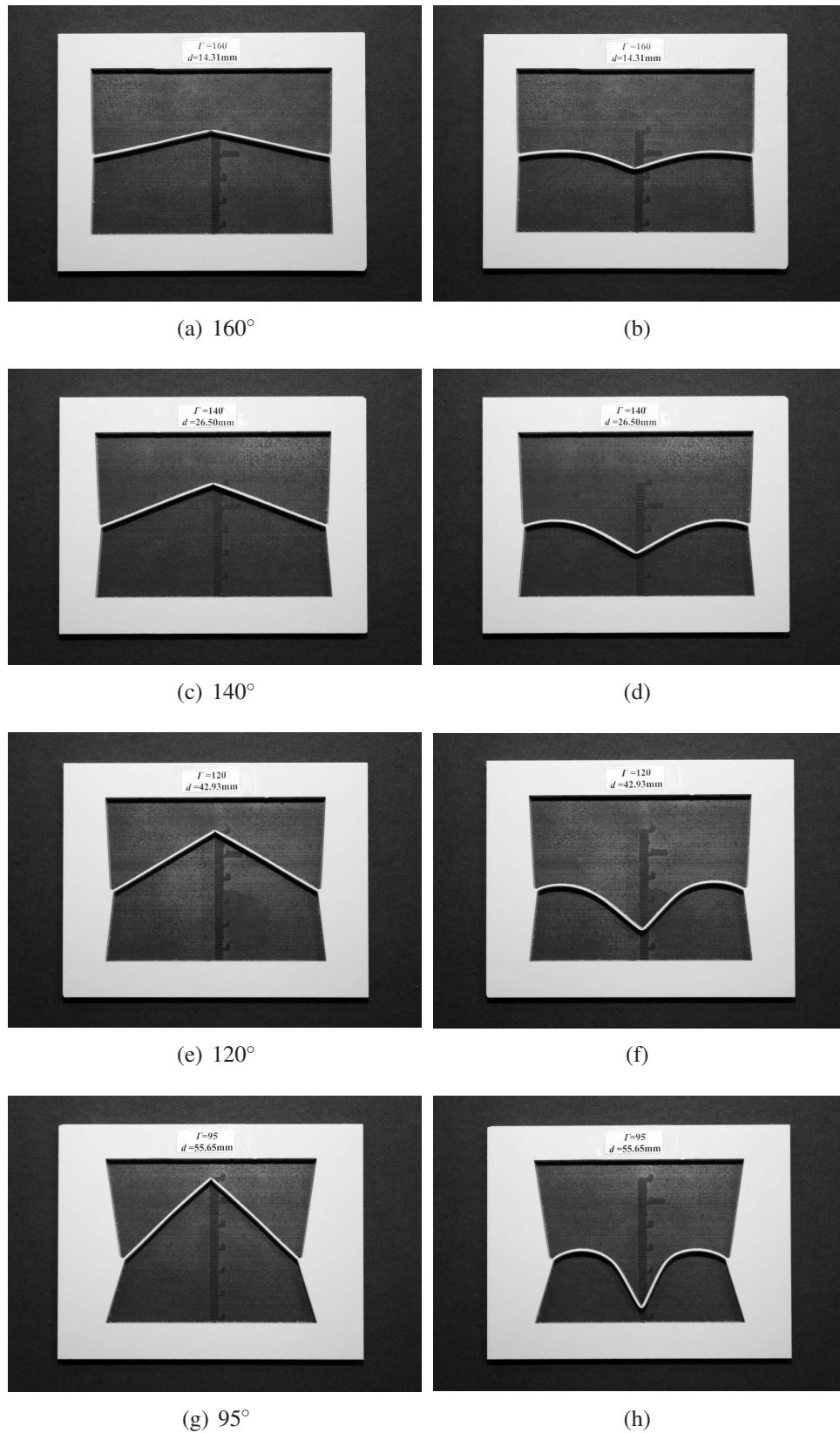


**Figure 5.14** Bistable mechanisms using symmetric RL deformed beams. = (a)  $160^\circ$ , (b)  $140^\circ$ , (c)  $120^\circ$ , and (d)  $95^\circ$ .

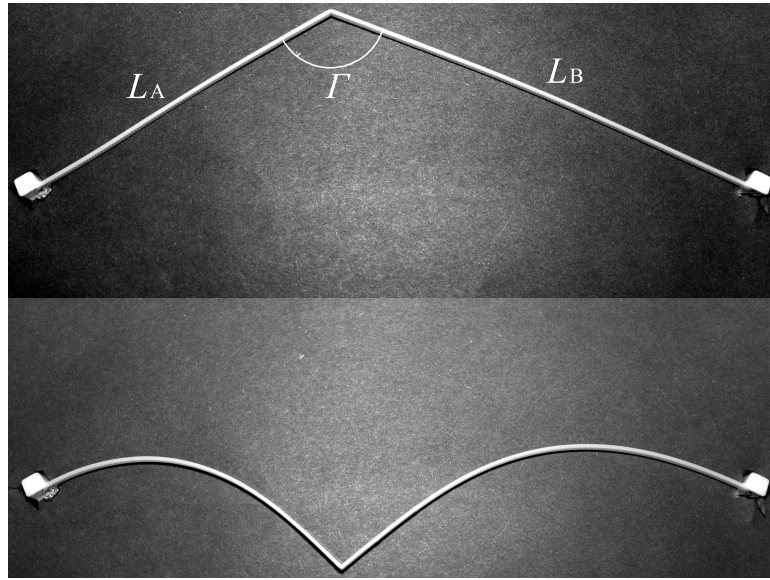


**Figure 5.15** Two stable configurations of an asymmetric bistable mechanism.

The following dimensions are used to estimate the displacement of the pin-joint.

$$\begin{aligned}
 L_A &= 4.538[\text{in}] \\
 L_B &= 6.034[\text{in}] \\
 \Gamma &= \gamma_A + \gamma_B = 127^\circ = 2.22[\text{rad}]
 \end{aligned}
 \tag{5.21}$$

Substituting these values into Eqn. (5.20) to solve for  $d$  yields

$$d = d_A = d_B = 3.40[\text{in}]. \tag{5.22}$$

The dimensionless displacement  $d/L$  for the beam, A, is

$$d_A/L_A = 0.749. \tag{5.23}$$

Our results were confirmed using a FEA tool, ANSYS, and experimental tests. The deformed configuration and the load-displacement curve are shown in Fig. 5.16. The result showed  $d_A/L_A = 0.770$  which correlated well with the value attained from experimental testing, 0.766. These values show that the estimated displacement is within an error range

of 2 ~ 3%. Alternatively, this problem can be solved using an optimization algorithm.

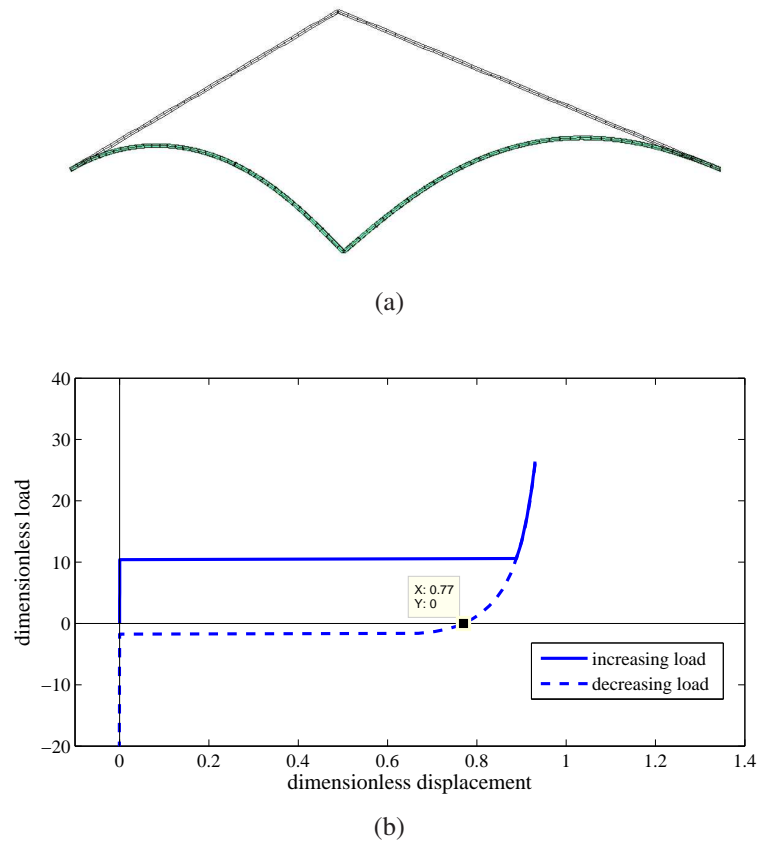


**Figure 5.16** (a) Deformed result of an asymmetrical problem, and (b) load-displacement curve for the asymmetrical example.

So far, bistable behaviors that produce translational motions are discussed in terms of the vector  $\mathbf{d}$  shown in Fig. 5.2. In the next subsection, a rotational bistable compliant mechanism is designed using the RL deformation.

## 5.4.2 Design of a Rotational Bistable Compliant Mechanism Using RL Deformation

A rotational bistable compliant mechanism can be designed by arranging the RL deformations cyclic-symmetrically. Instead of using a flexible beam as the counterpart of RL deformation, in this case, a rigid body is used. For example, a circular rigid body can be

the counterpart of the RL deformation, and another annular rigid body can work as a fixed boundary of the beam. The relative rotation of the two rigid bodies can provide bistability. A 90 degree section of a rotational bistable compliant mechanism is shown in Fig. 5.17.

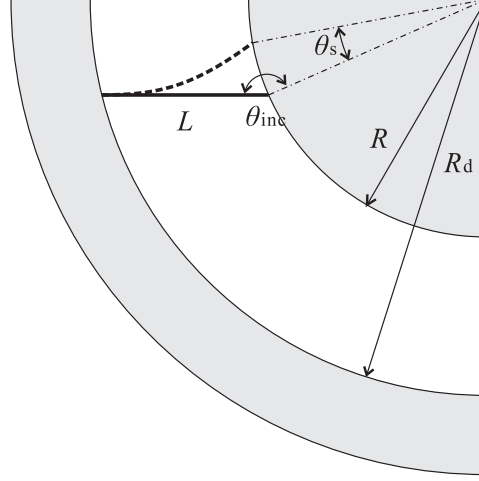


**Figure 5.17** Rotational bistable compliant mechanism design

In the figure,  $\theta_s$  is defined as the angle between the two stable positions, and  $\theta_{inc}$  is the included angle between the initial configuration of the RL beam and the line that connects the end of the beam and the center of the rigid circle.  $L$ ,  $R$ , and  $R_d$  are the length of the RL beam, the radius of the rigid circle, and the radius of the inner bound of the annular rigid body respectively.

In this case, Eqn. (5.16) and (5.17) are still true, and the relationship between  $n$  and  $\gamma$  is described as

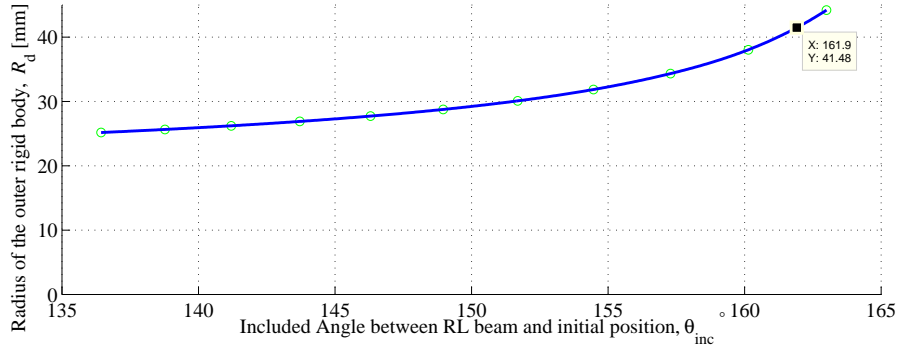
$$n = \arctan \left( \gamma + \frac{\theta_s}{2} - \frac{\pi}{2} \right). \quad (5.24)$$

In the rotational bistable compliant mechanism design, since  $\gamma$  and  $d$  in Fig. 5.2 are not directly related to the design, other design variables are used. For example, if  $\theta_s$  and  $R$  are given as

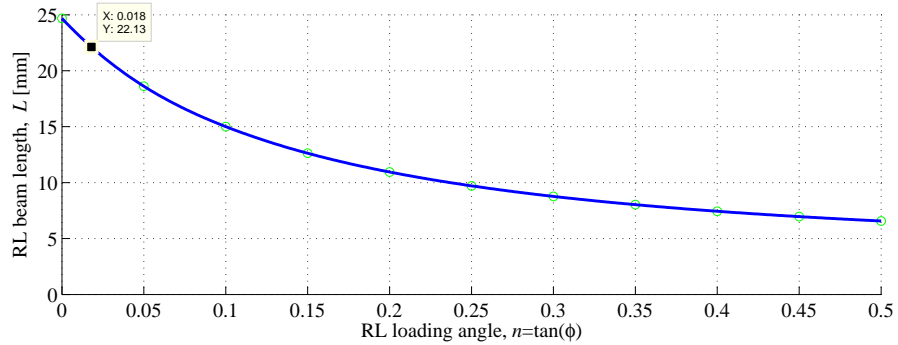
$$\theta_s = 17^\circ$$

$$R = 20[\text{mm}],$$

the relationship between  $R_d$  and  $\theta_{\text{inc}}$  can be obtained by using Fig. 5.18(a). The curves in Fig. 5.18(a) and (b) are unique to the given values of  $\theta_s$  and  $R$ . Since, Fig. 5.18(a) and (b) are dependent on each other, selecting a point on the curve in Fig. 5.18(a) will fix the equivalent point on the curve in Fig. 5.18(b). For example, if  $\theta_{\text{inc}} = 162^\circ$  is selected, the  $R_d$  is fixed at 41.5[mm] and the corresponding RL beam is defined by the length,  $L = 22.13[\text{mm}]$ , and the angle,  $n = 0.018$ , as shown in Fig. 5.18(b).



(a)



(b)

**Figure 5.18** (a)The relationship between  $R_d$  and  $\theta_{\text{inc}}$ , and (b) the relationship between  $L$  and  $n$  when  $\theta_s = 17^\circ$  and  $R = 20[\text{mm}]$ .

The stress distribution along the beam at the second stable configuration can be obtained by summing the stress due to the moment and force at the cross section as the following

equations. Note a rectangular uniform cross section along the beam is used.

$$\sigma(s) = \underbrace{\frac{Eh}{2}\kappa(s)}_{\text{stress due to moment}} + \underbrace{\frac{E\alpha^2 h^2}{12L^2}\cos(\theta(s))}_{\text{stress due to force}}, \quad (5.25)$$

where  $E$  and  $h$  are Young's modulus and the in-plane thickness of the beam respectively. All other variables,  $\kappa(s)$ ,  $\alpha$ , and  $\theta(s)$ , can be calculated once  $L$  and  $n$  are selected from Fig. 5.18(b).

Fig. 5.19 shows a prototype of the rotational bistable compliant mechanism based on the example shown in Fig. 5.18. Fig. 5.19(a) and (b) display the initial and the second stable configurations respectively. The angle between the two stable positions is slightly ( $< 1^\circ$ ) greater than  $17^\circ$  due to the nonlinear material properties of Homopolymer Polypropylene.

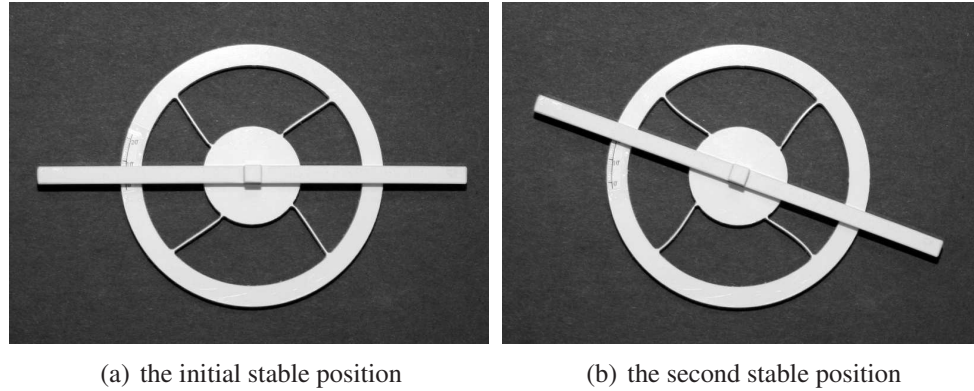


**Figure 5.19** A rotational bistable compliant mechanism using RL deformed beams.

A tool to design rotational bistable compliant mechanisms using RL deformations is developed based on the design approach covered in this subsection. A user can specify the design requirements, such as  $\theta_s$  and  $R$ , as the inputs of the design tool. Once the value  $n$  is selected by the user, the other dimensions,  $L$ ,  $R_d$ , and  $\theta_{inc}$ , can be obtained as design outputs of the design tool. From the obtained dimensions, stress information along the RL deformed beam can be evaluated and plotted. This tool is developed in the Matlab environment. The GUI of the design tool is shown in Fig. 5.20 with an example problem.



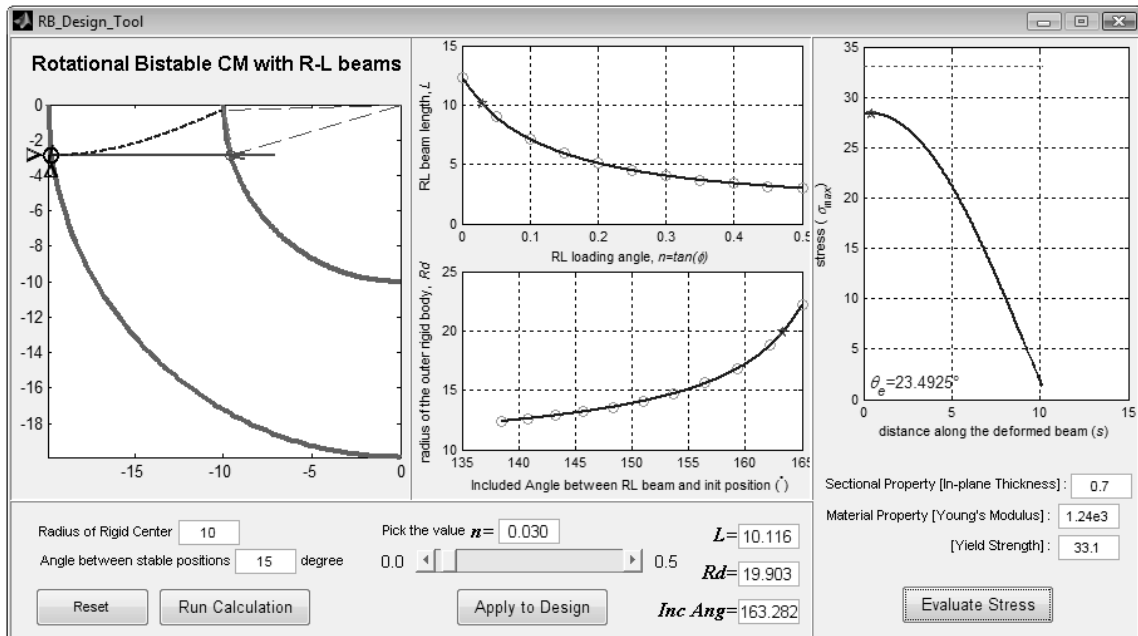


**Figure 5.20** A rotational bistable compliant mechanism design tool.

The design tool shown in Fig. 5.20 has three panels. The axis in the left panel provides the 90 degree section of the final design of the rotational bistable compliant mechanism. The larger and the smaller circles represent the annular and circular rigid bodies respectively. The RL beam and its deformed shape are shown as a straight solid line and curved broken line respectively. The initial and the second stable positions are shown on the circular rigid body. The two curves in the center panel provide for users to select the value of  $n$ . Once the value,  $n$ , is chosen, the other dimensions,  $L$ ,  $R_d$ , and  $\theta_{inc}$ , are automatically determined. Once the initial design is finalized, users can estimate the stress distribution along the deformable members in the rotational bistable compliant mechanism by using the right panel of the tool. In the procedure, users must provide the sectional and material properties. Note that the maximum stress during the operation can be higher than the maximum shown in the panel.

Design of bistable compliant mechanisms using RL deformations has been discussed in this section. In the following subsection, multistable compliant mechanisms that have

more than two stable states are designed using RL deformations

### 5.4.3 Design of Tristable Compliant Mechanisms Using RL Deformation

By applying the same concept used to design the tristable switch in Chapter 4 (Fig. 4.10), it is possible to utilize contact conditions to generate tristability using RL deformations. Fig. 5.21 shows a tristable switch that contains two RL beams. Fig. 5.13 (b) is the initial state, and Fig. 5.13 (a) and (c) are the other two stable configurations. In each stable state shown in (a) and (c), only one beam is in its active position of RL deformation. The other beam is inactive and stays with its initial shape that is constrained by the contact condition applied to the beam. Using the contact condition, the instant center of the rigid body is fixed. Therefore the tristable switch can be designed using the same approach applied to design a rotational bistable compliant mechanism discussed in the previous subsection. It is also possible to use the design tool introduced in the previous subsection.

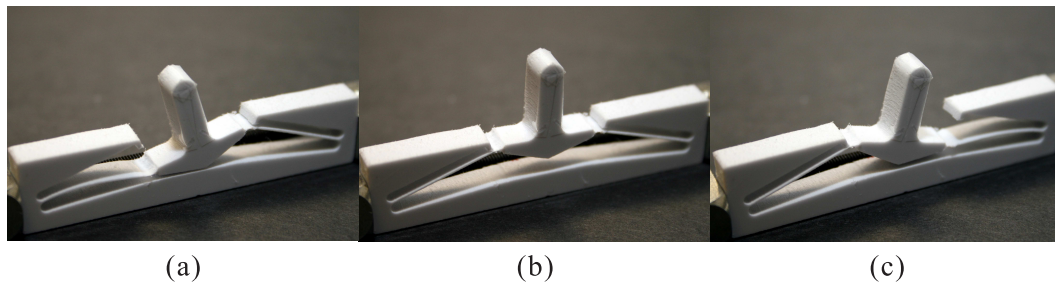


**Figure 5.21** A tristable compliant switching mechanism.

A multistable compliant mechanism can be designed by combining multiple bistable compliant mechanisms in series [62]. A series combination of the two bistable mechanisms produces up to four stable equilibria. When the two bistable compliant mechanisms are identical, it is possible to design a tristable compliant mechanism because the two stable equilibria among the four are overlapped. Three stable configurations of a series combination of two identical rotational bistable compliant mechanism are shown in Fig. 5.22.

Further details to synthesize multistable compliant mechanisms are discussed in Chapter 6.

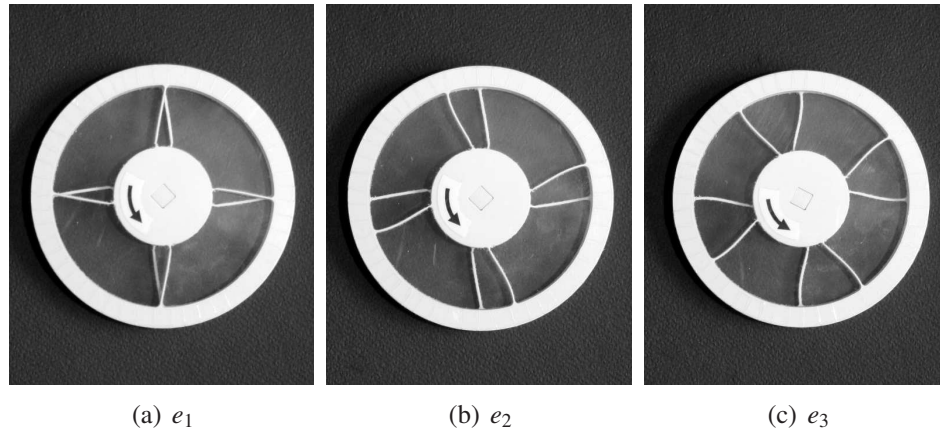


**Figure 5.22** A multistable rotational compliant mechanism using RL deformed beams.

## 5.5 Conclusions

In this chapter, the use of the bistability of a clamped-free beam to design bistable compliant mechanisms has been discussed. A reverse lateral (RL) deformation has been introduced to describe the bistability of the beam with various directions of loading. An analytical solution for a large amount of deformation in the beam has been obtained using numerical and elliptic integrations. The solution has been provided as several response plots. This study has also shown that an RL deformation is less sensitive to imperfections, such as disturbances to the off-loading direction, defects in the structure, tolerance errors in manufacturing, or imperfect boundary conditions, compared to a normal deformation.

The large deformation solution of the clamped-free beam has been applied as a required behavior for the clamped-pinned beam in the design of bistable compliant mechanisms. In case studies, two design examples were presented: a translational and rotational bistable compliant mechanisms. The exact solution was used to evaluate symmetrical translational bistable compliant mechanisms. Additionally, linear approximation was applied to calculate an asymmetrical bistable compliant mechanism. Here, for translational bistable

compliant mechanisms, only an exact solution for a symmetrical case with two RL deformations has been provided. The exact solution for the asymmetrical case with additional design variables of the ratio ( $l_B/l_A$ ) can provide a convenient mode of design. However, an approximate solution for an asymmetrical case shows sufficient accuracy. Its accuracy can be reduced once the ratio of the lengths of the beams becomes very small or large. A design approach for rotational bistable compliant mechanisms with RL deformations has been explained. A design tool for rotational bistable compliant mechanisms has been used. The results of experimental tests and finite element analysis are found to be in good agreement with the analytical solutions.

The design approaches introduced in this chapter enables the user to (i) design bistable translational compliant mechanisms with two RL deformations by utilizing provided plots and (ii) design rotational compliant mechanisms with rigid bodies as the counterparts of the RL deformation. Either a single beam or a rigid body is used as a counterpart for the RL deformed beam to provide bistability; In fact the counterpart can be another compliant mechanism that can generate the same reaction force to the RL deformed beam to ensure bistability.

## Chapter 6

### Synthesis of Multistable Compliant Mechanisms (MSCM)

#### 6.1 Introduction

In this chapter, a mathematical approach to synthesize multistable compliant mechanisms (MSCM) by combining multiple bistable equilibrium mechanisms is presented. The behavior of a bistable compliant mechanism, in general, is highly nonlinear. Using combinations of such nonlinearities to capture the behavior of multistable (more than two stable positions) compliant mechanisms can be quite challenging. So far, no definitive method has been developed to overcome this difficulty. To determine multistable behavior, a simplified mathematical scheme capturing the essential parameters of bistability, such as the load-thresholds that cause the jump to the next stable position, is introduced in this chapter. More specifically, various types of bistabilities are identified and categorized by characterizing the essential elements of their complicated deformation pattern. This mathematical simplification enables designers to characterize bistable mechanisms by using piecewise lower-order polynomials and, in turn, synthesize multistable mechanisms.

Three case studies involving combinations of two, three, and four bistable behaviors are presented for the purpose of generating multistable mechanisms with up to 16 stable positions. The methodology of combining multiple bistable behaviors enables designers to design a compliant mechanism with a desired number of stable positions. A design example of a rotational quadristable compliant mechanism consisting of two bistable sub-mechanisms is presented to demonstrate the effectiveness of the approach.

## 6.2 Organization of This Chapter

In the next section, nonlinear behavior of MSCMs is discussed. In the following section, a simplified model by using mathematical expressions is introduced. Then, a method of synthesizing multistability from multiple bistabilities is described. Following this, three case studies that involve a combination of two, three, and four bistable behaviors to generate multistable behaviors are discussed. Finally, to demonstrate the synthesis methodology, a rotational multistable compliant mechanism is designed.

## 6.3 Understanding the Characteristics of MSCMs

### 6.3.1 Understanding the Characteristics of MSCMs<sup>1</sup>

A multistable system is a system with more than two stable equilibrium states. Its stable positions correspond to the local minima of the potential energy curve of the system. This is analogous to the ‘*ball on the hill*’, as shown in Fig. 6.1. The potential energy of the ball depends on its position on the hill and hence on  $x$ . The potential energy is

$$U(x) = mgh(x), \quad (6.1)$$

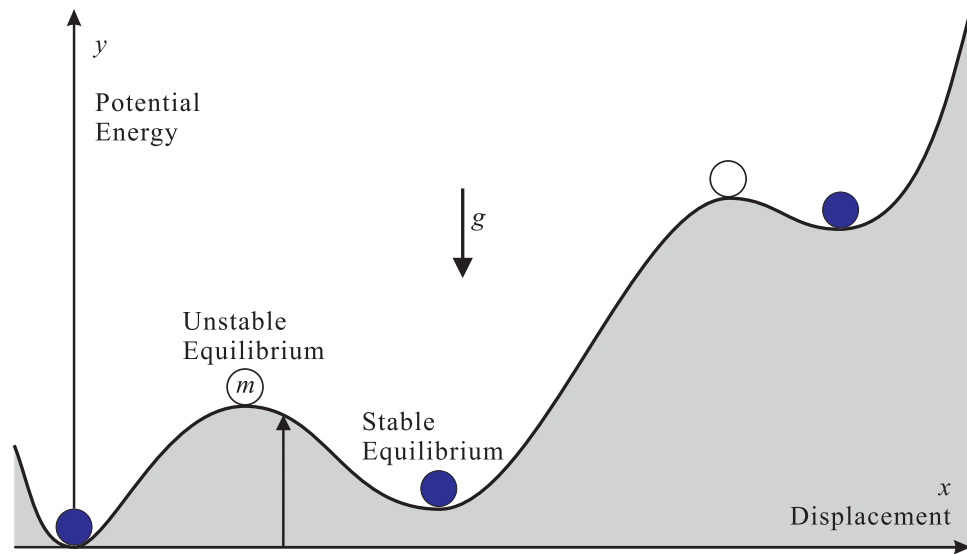
where  $m$  is the mass of the ball,  $g$  is the acceleration of gravity and  $y = h(x)$  is the equation that defines the height of the hill at  $x$ . Thus, the equilibrium positions are located where  $\partial h(x)/\partial x = 0$ . Hence,

$$\frac{\partial U}{\partial x} = mg \frac{\partial h}{\partial x} = 0. \quad (6.2)$$

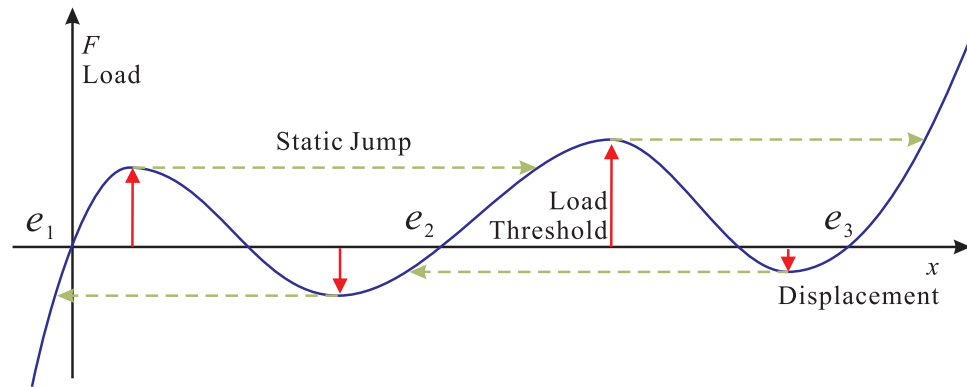
The stable positions (solid balls) are located at the local minima of the hill, i.e., locations

---

<sup>1</sup>Some of the explanations in this section are based on the explanations in Section 4.3.



(a) Potential energy



(b) Load-displacement

**Figure 6.1** Potential energy and load-displacement curves of a multistable system.

where

$$\frac{\partial^2 U}{\partial x^2} = mg \frac{\partial^2 h}{\partial x^2} > 0. \quad (6.3)$$

The gravitational force,  $F_g$ , acting upon the ball can be regarded as the action of the gravitational field that is present at the location of the ball. Because the gravitational force is in the potential field, it is a conservative force equal and opposite to the gradient of a

potential. The gravitational force is expressed as follows:

$$F_g = -\frac{\partial U}{\partial h} = -mg \quad (6.4)$$

By ignoring the friction on the surface, the external force applied to the ball to hold the stable position can be obtained by Eqn. (6.2).

$$F_{\text{external}} = -F_g \frac{\partial h}{\partial x} = \frac{\partial U}{\partial h} \frac{\partial h}{\partial x} = 0. \quad (6.5)$$

Its derivative at stable positions can be obtained by Eqn. (6.3). Hence,

$$\frac{\partial F_{\text{external}}}{\partial x} = \frac{\partial^2 U}{\partial x^2} > 0. \quad (6.6)$$

The first equality condition of Eqn. (6.4) is generally true for all conservative forces. Additionally, Eqn. (6.5) and (6.6) are required conditions to the local minima of the potential energy due to the conservative forces. These conditions must also be satisfied for a spring force,  $F_s$ , because it is a conservative force. Since external load applied to a spring is equal and opposite to the spring force, the following equations can be derived for stable equilibria of the spring:

$$\begin{aligned} F_{\text{external}} &= -F_s = \frac{\partial U}{\partial x} = 0 \\ \frac{\partial}{\partial x} F_{\text{external}} &= -\frac{\partial F_s}{\partial x} = \frac{\partial^2 U}{\partial x^2} > 0. \end{aligned} \quad (6.7)$$

The equilibria,  $e_1$ ,  $e_2$  and  $e_3$ , in Fig. 6.1(b) satisfy the conditions described in Eqn. (6.8). Therefore, load-displacement responses can be used to identify stable equilibria, which are located where the load input is zero and the slope is positive. In other words, each stable configuration of the system is defined when its potential energy is at one of its local minima (potential energy curve), or the stiffness of the system is positive without any external load



input (load-displacement curve).

The characteristics of multistable systems can be described by the potential energy curve and the load-displacement curve. The characteristics can be characterized by three attributes: the number of stable configurations (e.g., position and shape), the mechanical properties at the configurations (e.g., stiffness and natural frequency), and the correlations between the stable equilibria (e.g., actuation load, static jump, energy barrier, and energy change between two stable equilibria). Here, the actuation load is defined as a load-threshold that causes the jump from one stable position to the next; it can be identified with the aid of a load-displacement curve (Fig. 6.1(b)). Some of the characteristics, such as the stable position and actuation load, become design requirements.

### **6.3.2 Nonlinear Behavior of MSCM**

In general, multistability requires snap-through behaviors to reach different stable configurations. Snap-through behaviors normally cause large displacements and large rotations, which require geometric nonlinear analysis. This requirement is true for any mechanism, rigid or compliant. Nonlinear problems cannot be solved in a single step and require iterative algorithms such as the Newton-Raphson method or a modified Newton-Raphson method. However, in some nonlinear buckling problems, such methods cannot be used by themselves because the tangent stiffness matrix may become singular and cause convergence difficulties. Such nonlinear buckling analyses are required when the structure either collapses completely or snaps-through to another stable configuration. For such situations, an alternative iteration method is required.

Path following, load-control and displacement-control methods can be used for collapse or snap-through behavior. An example of a bistable mechanism is shown in Fig. 6.2. A partially rigid and partially flexible curved beam with pinned-fixed boundary conditions is illustrated in the figure. A buckled configuration of the straight beam is utilized to find the initial curvature of the flexible member. When the moment is applied at the pinned end, the

other stable configuration is reached by means of snap-through behavior.

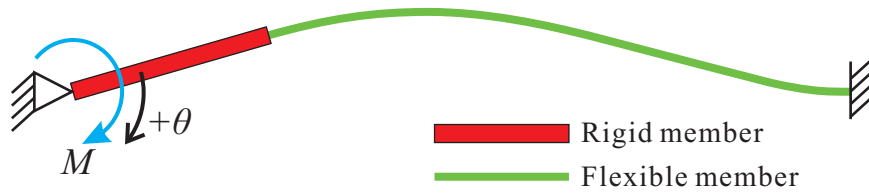


**Figure 6.2** A simple bistable compliant mechanism.

Of the three methods, the load-control method is the most appropriate for our problem since it provides the simplest response curve. Fig. 6.3 shows the load-displacement curves of the problem described in Fig. 6.2. Fig. 6.3(a) is obtained with a path-following method, such as Arc-length or Riks method [8, 4]. The complicated curve representing the post-buckling behavior may not depict a real situation. Fig. 6.3(b) shows the same response curve obtained with the displacement-control method. Fig. 6.3(b) is obtained by increasing and decreasing the displacement monotonically. The displacement-control method reduces the complexity but does not eliminate negative slopes. On the other hand, the load-control method captures the essential characteristics, as shown in Fig. 6.3(c), stripping away the unnecessary complexity including the negative slopes of Fig. 6.3(a) and (b). Fig. 6.3(c) is obtained by gradually increasing the input load to the maximum positive load and then decreasing it to the minimum negative. There are several advantages of the load-control method: the response curve is always either stable or marginally stable (zero or positive slope) during the nonlinear analysis, and the complicated post-buckling behavior is eliminated without affecting the key parameters such as the stable positions and actuation loads. In the rest of the chapter, the load-control method is used for nonlinear finite element analysis.

An example of load-displacement curves for an MSCM with four stable equilibria is illustrated in Fig. 6.4. In general, a multistable compliant mechanism with  $n$ -stable equilibria has the following representative characteristics:  $n$  equilibrium positions,  $e_i$ , and  $2(n - 1)$  actuation loads,  $F_{i-j}$ , which are the required loads to jump from  $e_i$  to  $e_j$ . Each stable equi-

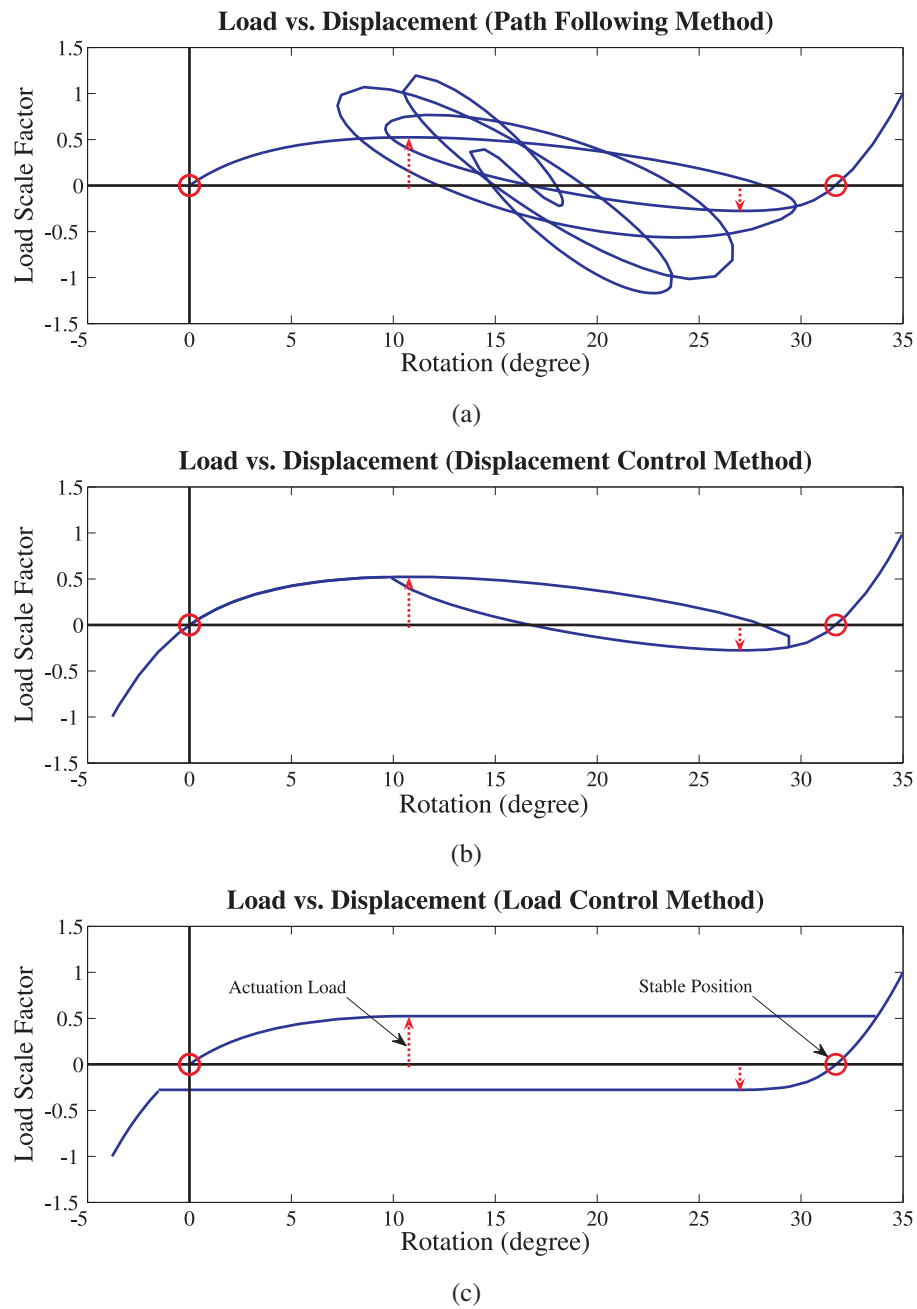


**Figure 6.3** Load-displacement curves of : (a) solved using path following method, (b) solved using displacement-control method, and (c) solved using load-control method. (ABAQUS).

librium,  $e_i$ , is circled in the figure. The six dotted arrows parallel to the load ( $F$ ) axis represent load-thresholds (actuation loads). When the load reaches the load-thresholds, there will be a sudden displacement or static jump. There are six corresponding static jumps depicted by the dotted arrows parallel to the displacement ( $x$ ) axis. Note that the complicated post-buckling behavior is not shown in the figure.

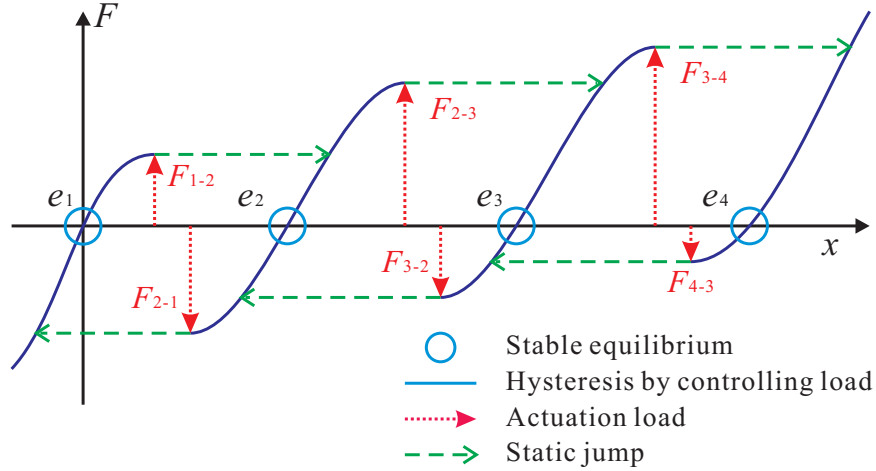


**Figure 6.4** Illustration of the nonlinear behavior of a multistable compliant mechanism with four stable equilibria.

### 6.3.3 Simplified Mathematical Expression of Bistable Behavior

To represent the essential parameters such as stable positions and actuation loads, the bistable behavior is mathematically expressed with an approximated piecewise-continuous function,  $F(\delta)$ , which is described in Eqn. (6.8). The piecewise-continuous function is plotted in Fig. 6.5. The sub-functions,  $f_1(\delta)$ ,  $f_2(\delta)$  and  $f_3(\delta)$ , which are required to satisfy the matching conditions in Eqn. (6.10), represent the key parameters of the bistable behavior. The parameters  $A$  and  $B$  in Eqn. (6.8) denote the displacements where the static jumps start. The sub-functions  $f_1(\delta)$  and  $f_3(\delta)$  represent the stable intervals and are third-order polynomials. The sub-function  $f_2(\delta)$  between the two stable intervals represents the unstable region and is a fourth-order polynomial. The input load at the initial ( $\delta = 0$ ) equilibrium and the second ( $\delta = \beta$ ) stable equilibrium must be zero, and the slope at the

displacement where the static jump starts must be zero. Additionally, the function must satisfy the prescribed value of the actuation load as follows:

$$F(\delta) = \begin{cases} f_1(\delta) & \delta < \mathbf{A} \\ f_2(\delta) & \mathbf{A} \leq \delta < \mathbf{B} \\ f_3(\delta) & \mathbf{B} \leq \delta \end{cases} . \quad (6.8)$$

$$\begin{aligned} F(0) &= F(\beta) = 0, \\ \left. \frac{\partial F}{\partial \delta} \right|_{\delta=\mathbf{A}} &= \left. \frac{\partial F}{\partial \delta} \right|_{\delta=\mathbf{B}} = 0, \\ F(\mathbf{A}) &= F_{1-2}, \text{ and } F(\mathbf{B}) = F_{2-1}. \end{aligned} \quad (6.9)$$

Fig. 6.5 depicts an example of the approximated function,  $F(\delta)$ , of the bistable behavior shown in Fig. 6.3(a). It is important to note that  $f_2(\delta)$  in Fig. 6.4 is not meant to capture the post-buckling behavior of Fig. 6.3(a) but, instead, represents the instability between the stable intervals. Most of the bistable behaviors can be simplified with such piecewise-continuous functions. Furthermore, some simple bistability can be expressed as a single third-order polynomial.

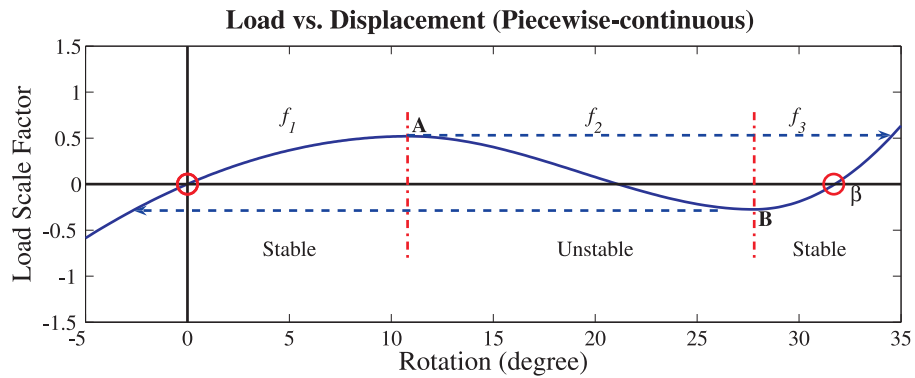


**Figure 6.5** Piecewise-continuous function representing the key parameters (stable positions and actuation loads).

## 6.4 Combining Multiple Bistable Behaviors in Series

There are two ways to combine bistabilities: parallel and series combinations. A parallel combination of bistable behaviors changes the existing key parameters and helps designers synthesize new bistable mechanisms from existing bistable compliant mechanisms. To generate multistability from existing bistable compliant mechanisms, bistable behaviors are combined in series.

To show how the concept of combining bistable systems can synthesize multistability, the simplified mathematical expressions of bistable behavior were introduced in the previous section. The approach simplifies the complicated structural bistabilities into simple representation that enables easy verification of the desired multistability.

To begin, two translational 1-D bistable systems, which are shown in Fig. 6.6(a) and (b), are defined. The second stable equilibrium position is at  $\beta_1$  in one system and at  $\beta_2$  in the other system. The forces,  $F_i$ , and the displacements,  $\delta_i$ , are parallel to the intended direction of motion of each bistable system. The two bistable systems are combined in series to form the multistable system shown in Fig. 6.6(c). This combination can be accomplished by applying a rigid connector between the bistable systems. Note that if  $n$  bistable behaviors are combined in series, up to  $2^n$  stable positions can be obtained. This phenomenon is explained in the following section.

Two third-order polynomials are used to express the bistabilities. The two bistable systems are called as BES1 and BES2, and their mathematical expressions are as follows:

$$\begin{aligned} \text{BES1 : } F_1(\delta_1) &= K_1 \delta_1 (\delta_1 - \alpha_1) (\delta_1 - \beta_1) \\ \text{BES2 : } F_2(\delta_2) &= K_2 \delta_2 (\delta_2 - \alpha_2) (\delta_2 - \beta_2). \end{aligned} \quad (6.10)$$

where  $\alpha_i$  and  $\beta_i$  are the unstable and stable equilibrium positions of each bistable system respectively, and the  $K_i$  values are constants proportional to the actuation loads,  $F_i$ .

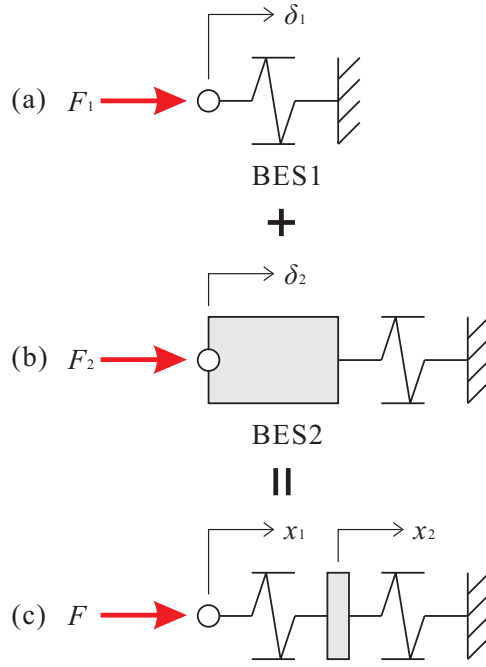


**Figure 6.6** (a)(b)Two bistable systems and (c) a combined multistable system.

The potential energy,  $U_i$ , stored in each bistable system is the total recoverable mechanical energy and can be written as

$$U_i = - \int \vec{F}_s \cdot d\vec{\delta}_i = \int \vec{F}_i \cdot d\vec{\delta}_i. \quad (6.11)$$

The total potential energy,  $U_{tot}$ , can be obtained by

$$U_{tot} = U_1(\delta_1) + U_2(\delta_2) = U_1(x_1 - x_2) + U_2(x_2), \quad (6.12)$$

where  $U_{tot}$  has four ( $= 2^2$ ) local minima, as expected, at

$$(x_1, x_2)_{\min} = (0, 0), (\beta_1, 0), (\beta_2, \beta_2), (\beta_1 + \beta_2, \beta_2). \quad (6.13)$$

Because the only controllable coordinate is  $x_1$ , the corresponding  $x_2$  depends on the potential energy path. Hence, the accessibilities of the four local minima are path-dependent. The accessibilities are discussed in detail in the following case studies.

### 6.4.1 Combining Bistable Behaviors with Different Actuation Loads

For two bistable systems connected in series, four distinct types of combination are possible on account of the magnitudes of the actuation loads of the increasing and decreasing load steps. The four types of bistability combinations are defined as

$$\beta_1 > \beta_2 \left\{ \begin{array}{l} |F_{ac1_A}| < |F_{ac2_A}| \\ |F_{ac2_A}| < |F_{ac1_A}| \end{array} \right\} \left\{ \begin{array}{l} |F_{ac1_D}| < |F_{ac2_D}| : \text{TYPE}_{12}^{12} \\ |F_{ac2_D}| < |F_{ac1_D}| : \text{TYPE}_{21}^{12} \\ |F_{ac1_D}| < |F_{ac2_D}| : \text{TYPE}_{12}^{21} \\ |F_{ac2_D}| < |F_{ac1_D}| : \text{TYPE}_{21}^{21} \end{array} \right.$$

where  $\beta_i$  and  $F_{aci}$  are illustrated in Fig. 6.7 and explained in Table 6.1. For convenience, the bistable behavior with the larger interval between the two stable equilibria is defined as BES1.

**Table 6.1** Actuation loads and equilibrium positions defined in two bistable systems.

Bistable System	Actuation Load of Increasing Load Step	Actuation Load of Decreasing Load Step	Unstable Equilibrium	2nd Stable Equilibrium
BES1	$F_{ac1_A}$	$F_{ac1_D}$	$\alpha_1$	$\beta_1$
BES2	$F_{ac2_A}$	$F_{ac2_D}$	$\alpha_2$	$\beta_2$

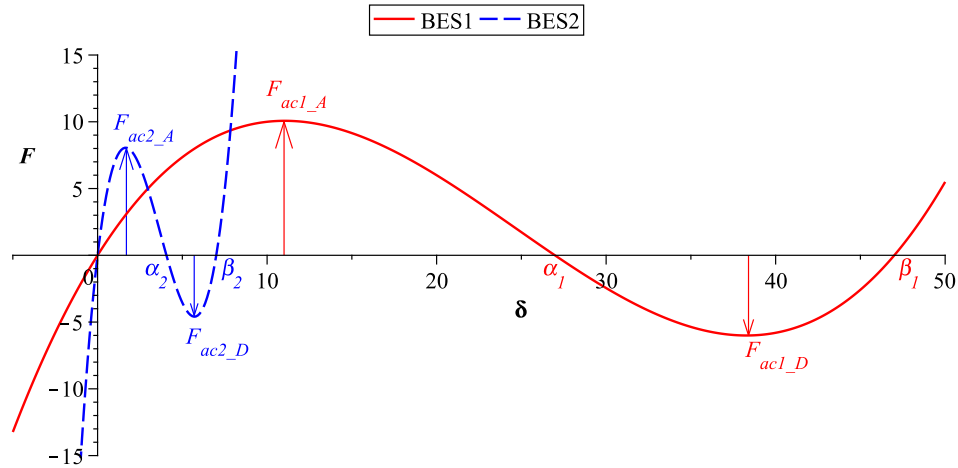


**Figure 6.7** Load-displacement curves of two bistable behaviors ( $\text{TYPE}_{21}^{21}$ ).



The integers next to **TYPE** symbolize the bistable behaviors. The bistable behavior with the largest  $\beta$  is set as integer 1 or BES1. The superscript and subscript represent the increasing and decreasing load steps respectively. The sequence of integers corresponds to the ascending order of the magnitude of the actuation loads. For example, **TYPE**<sub>312</sub><sup>213</sup> consists of three bistable behaviors and their actuation loads have the following relation:

$$\beta_1 > \beta_2 > \beta_3$$

$$|F_{ac2_A}| < |F_{ac1_A}| < |F_{ac3_A}| \& |F_{ac3_D}| < |F_{ac1_D}| < |F_{ac2_D}|$$

Again, the bistable behavior with the largest interval,  $\beta_1$ , is set as BES1 and the smallest,  $\beta_3$ , is set as BES3. Thus far, only the inequality conditions of actuation loads are considered. When multiple bistable mechanisms are combined to have the same actuation load, the inequality conditions may still apply. The details are discussed in Appendix A.

## 6.4.2 Numerical Procedure to Determine the Combined Multistable Behavior

The following case study illustrates the multistabilities of **TYPE**<sub>21</sub><sup>21</sup>. Load-displacement plots for the bistabilities are obtained by using Eqn. (6.10) or (6.11)). Potential energy contour plots (for example, Fig. 6.8) are generated by combining the potential energy functions of the two bistable systems (Eqn. (6.11) or (6.12))). The path on the potential energy contour can be calculated by the following procedure:

- Step 1.* Set the iteration number,  $i = 0$ , total number of increment,  $n$ , and the maximum displacement of  $x_1, x_1^n$ . Specify the displacement increment as  $\Delta x_1 = x_1^n/n$ .
- Step 2.* Set the starting point at  $(x_1^0, x_2^0) = (0, 0)$  which is the initial stable position.
- Step 3.* Set  $i = i + 1$ , and  $x_1^i = x_1^{i-1} + \Delta x_1$ .
- Step 4.* Evaluate the initial point,  $x_0^i = (x_1^{i-1}, x_2^{i-1})$ , for the optimization problem defined

in *Step 5*.

*Step 5*. Define the unconstrained optimization problem of

Minimize :  $f_i = U_{tot}(x_1, x_2)$  at  $x_1 = x_1^i$ ,

and solve for  $x_{2min}$ .

*Step 6*. Update the initial value,  $x_2^i = x_{2min}$ .

*Step 7*. If  $i < n$ , then go to *Step 3*. Otherwise continue.

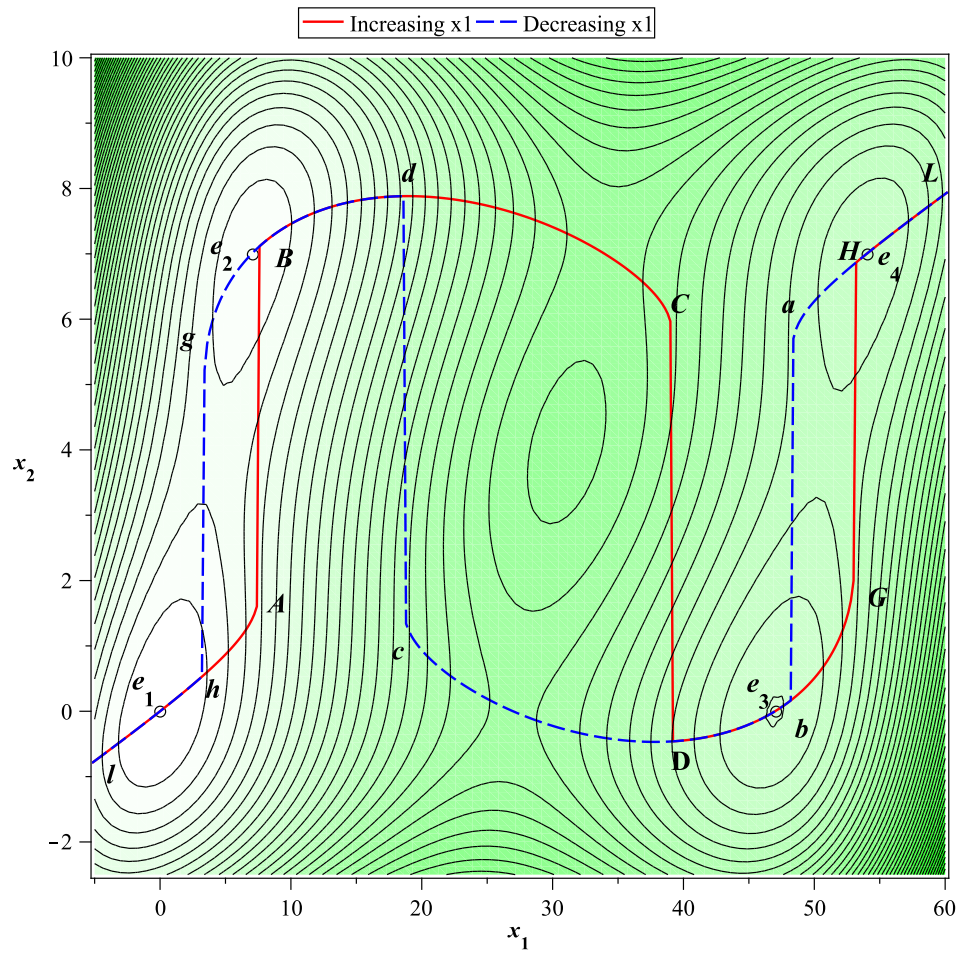
*Step 8*. Plot  $x_0^i$  for  $i = 0 \dots n$ .

The load-displacement curve of the combined multistability with the displacement-control method is obtained from the potential energy path, and then it is converted to a load-displacement curve with the load-control method.

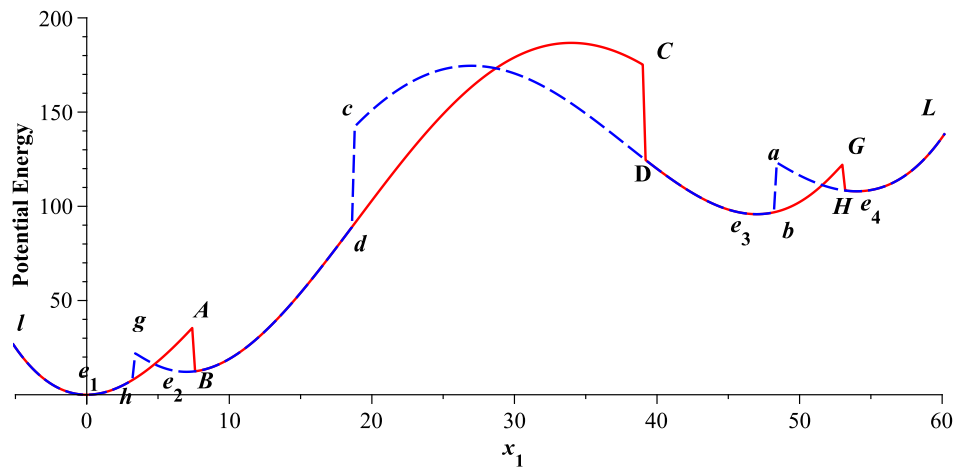
Maple™, a commercial mathematics software package, is used to solve and visualize the results of the problems. The optimization package included in the software is used to obtain the potential energy paths. A sequential quadratic programming (SQP) algorithm is used for the unconstrained nonlinear programs.

## 6.5 Case Study 1: Combining Two Bistable Behaviors

In this section, we present a case study of combining two bistable behaviors. The system illustrated in Fig. 6.6(c) is used for the analysis. In **TYPE<sub>21</sub><sup>21</sup>**, the actuation loads for both the increasing and decreasing displacement steps of one system, BES1, is greater than the actuation loads for the other system, BES2. Fig. 6.7 depicts the behaviors of **TYPE<sub>21</sub><sup>21</sup>**. Using the global coordinate systems, the total potential energy is calculated with Eqn. (6.11) and (6.12), and the corresponding contour plot is shown in Fig. 6.8(a). There are four local minima at the points,  $e_1$ ,  $e_2$ ,  $e_3$ , and  $e_4$ , as shown in the figure. The potential energy paths, which are obtained by using the optimization procedure described in the previous section, are plotted on the contour plot. When  $x_1$  increases monotonically, the potential energy



(a)



(b)

**Figure 6.8** Potential energy contour plot and potential energy (PE) path for **TYPE<sub>21</sub><sup>21</sup>**. (b) represents the two axes ( $x_1$  and PE) isolated from the normal three axes, i.e. ( $x_1, x_2, PE$ ). The vertical lines, in (b) correspond to the jumps of  $x_2$  in (a).

stays on the route of  $e_1 \rightarrow A \rightarrow B \rightarrow C \rightarrow D \rightarrow e_3 \rightarrow G \rightarrow H \rightarrow L$ . When  $x_1$  decreases, potential energy follows a different route of  $e_4 \rightarrow a \rightarrow b \rightarrow c \rightarrow d \rightarrow e_2 \rightarrow g \rightarrow h \rightarrow l$ . The straight lines parallel to the  $x_2$ -axis represent various static jumps of  $x_2$ . Fig. 6.8(b) represents the two axes ( $x_1$  and Potential Energy) isolated from the normal three axes, i.e. ( $x_1, x_2, \text{Potential Energy}$ ). The vertical lines, in Fig. 6.8(b) represent the jumps of  $x_2$  in Fig. 6.8(a).

Fig. 6.9 illustrates the behaviors of the MSCM. The solid square at the right-hand side represents the current location of  $x_2$ , whereas the other square represents  $x_1$  as it steadily (or monotonically) increases. The behavior follows the solid line in Fig. 6.8(a). Fig. 6.9(A–H) shows the three static jumps of  $x_2$  in the contour plot. The first jump is from left to right (A–B); the second jump is from right to left (C–D); and the third jump is from left to right again (G–H). The jump to the left indicates that there is a negative load applied to  $x_2$ . This jump occurs when the magnitude of  $F_{ac1D}$  is greater than the magnitude of  $F_{ac2D}$ . The displacements of  $x_1$  when  $x_2$  jumps are approximated since the negative slopes of the load-displacement curve are simplified. If we rely solely on the positive slopes to obtain the load-displacement curve of the load-control method, the approximation does not affect the response.

Two load-displacement curves for the combined multistable system are obtained (Fig. 6.10). Fig. 6.10(a) is plotted by assuming that the displacement at the input node,  $x_1$ , is controlled (Displacement-control). The curve in Fig. 6.10(b) can be obtained by assuming that the input load is repeatedly increased and decreased (or relaxed) in several different ways to find all possible stable equilibria in the system (Load-control). The load-displacement behavior obtained by the load-control method can also be obtained by taking the positive slopes of Fig. 6.10(a) and setting the negative slopes to zero. This response follows some parts of the paths that are traced in Fig. 6.18(a) because the static jumps occur simultaneously for both  $x_1$  and  $x_2$  even though  $\delta_1$  and  $\delta_2$  jump independently.

In the Fig. 6.10(b), when the load increases from the initial stable equilibrium,  $e_1, x_1$

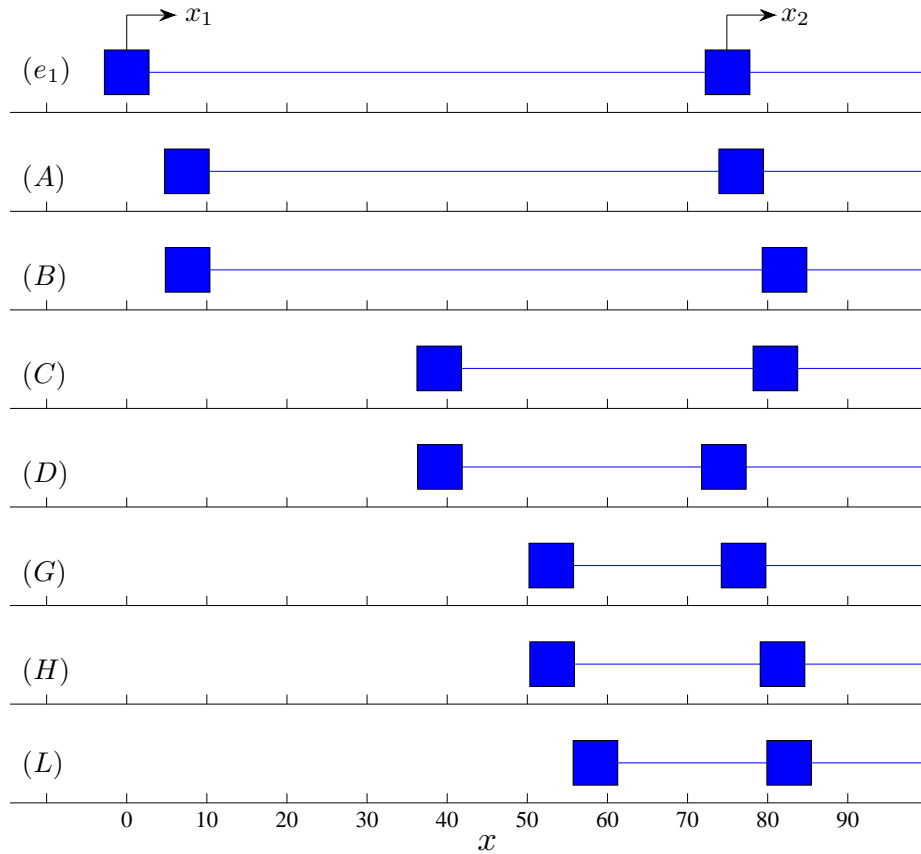


**Figure 6.9** Deformed configurations of  $BES1(x_1)$  and  $BES2(x_2)$  of  $TYPE_{21}^{21}$  when  $x_1$  increases steadily.

can go up to  $A$ . A further increase in the load causes a static jump of  $x_1$  in the system from  $A$  to  $A'$ . If the load decreases from point  $A'$ , the second stable equilibrium,  $e_2$ , can be obtained. Conversely, if the load is continuously increased from point  $A'$ ,  $x_1$  reaches  $d$  and then jumps to  $d'$ . If the load is reduced at this point, the fourth stable equilibrium,  $e_4$ , can be reached. If the load is decreased,  $x_1$  reaches  $a$  and then jumps to  $a'$ . Further reduction makes  $x_1$  arrive at  $D$  and then jump to  $D'$ . If the load at  $a'$  is increased, the third stable equilibrium,  $e_3$ , can be located. Alternatively, Fig. 6.10(b) can be obtained by using the load equilibrium of the system and solving the optimization. The disadvantage of this approach is that the problem must be solved iteratively to obtain all accessible stable equilibria. A summary table is provided at the end of this section for the load-displacement

curves of all four types of combination defined in the previous section.

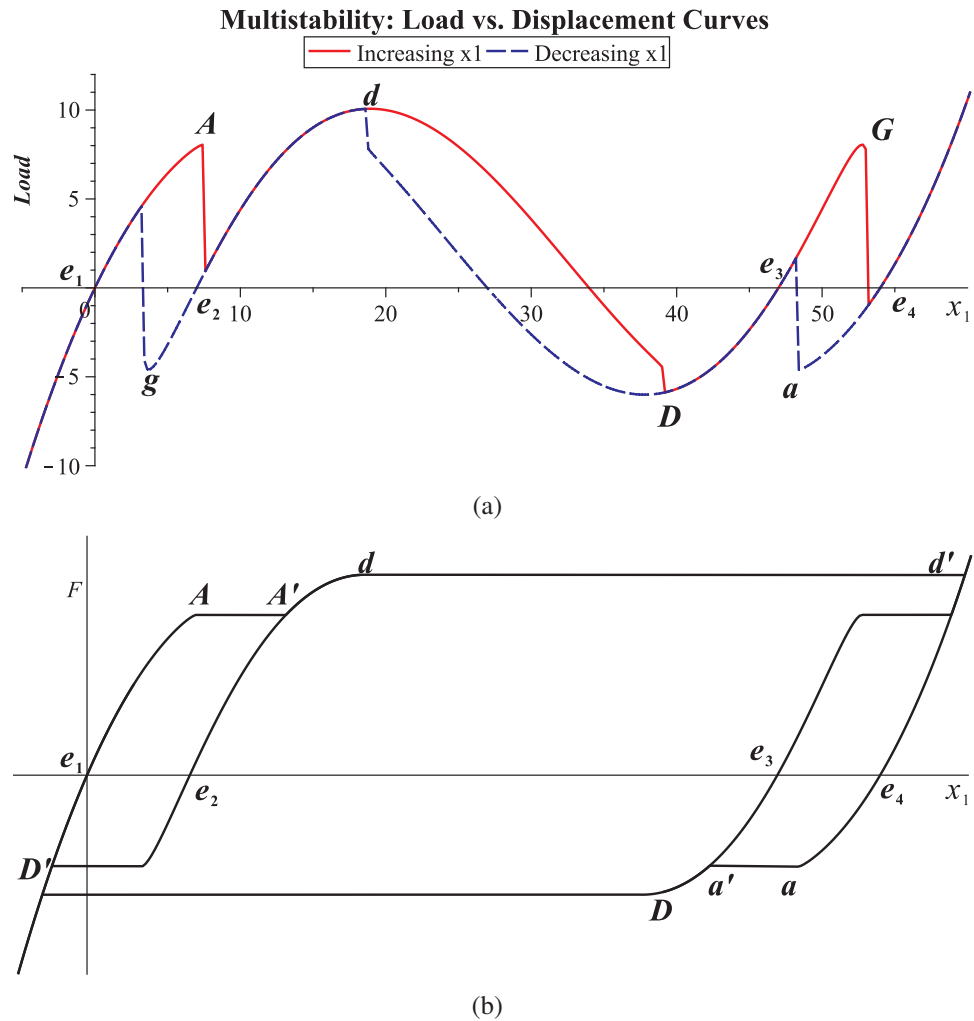


**Figure 6.10** Load-displacement curves of the combined multistability: (a) displacement control and (b) load control.

All four local minima appear in **TYPE<sub>12</sub><sup>12</sup>** and **TYPE<sub>21</sub><sup>21</sup>**. However, in some cases, not all the local minima can be reached. As shown in the potential energy contour plots in Fig. 6.11, only three of the four stable equilibria can be reached in **TYPE<sub>12</sub><sup>21</sup>** and **TYPE<sub>21</sub><sup>12</sup>**. Thus, **TYPE<sub>12</sub><sup>12</sup>** and **TYPE<sub>21</sub><sup>21</sup>** are suitable for designing quadristable systems through the combination of two bistable behaviors. On the other hand, **TYPE<sub>12</sub><sup>21</sup>** and **TYPE<sub>21</sub><sup>12</sup>** are suitable for generating tristable systems.

Table 6.2 summarizes the multistable behaviors of all four types. This table can also be

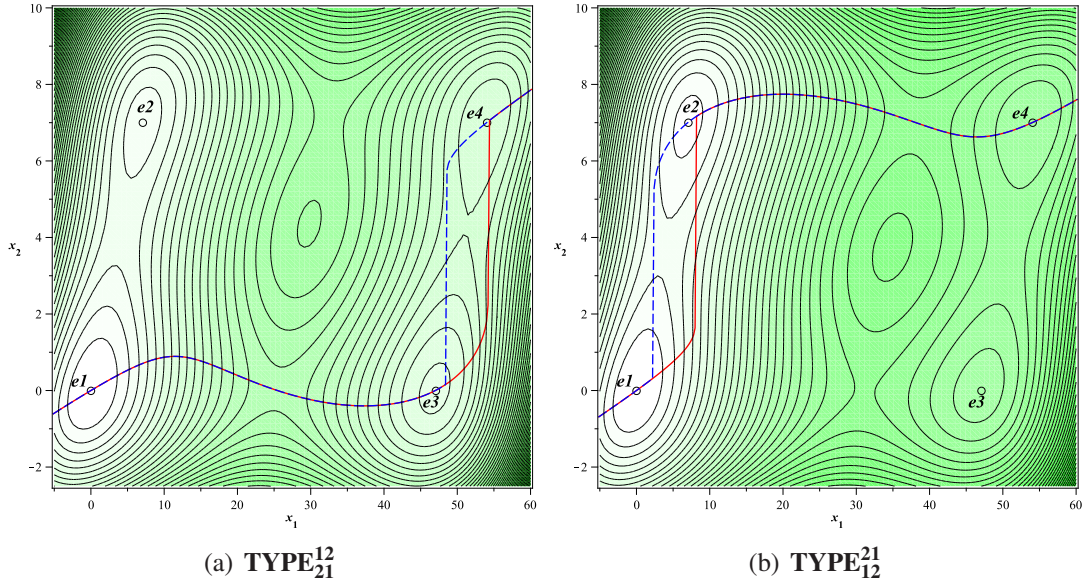


**Figure 6.11** Potential energy contour plot and potential energy path for **TYPE<sub>21</sub><sup>12</sup>** and **TYPE<sub>12</sub><sup>21</sup>**.

used to combine more than two bistable behaviors as described in the following case study.

## 6.6 Case Study 2: Combining Three Bistable Behaviors

In this case study, three bistable behaviors are combined to synthesize a multistable system with five stable equilibria. A schematic drawing of the combined translational multistable system is illustrated in Fig. 6.12. Third-order polynomials are used to represent the bistable behaviors and are plotted in Fig. 6.13. This combination is **TYPE<sub>312</sub><sup>231</sup>**.

$$\beta_1 > \beta_2 > \beta_3$$

$$|F_{ac2A}| < |F_{ac3A}| < |F_{ac1A}| \& |F_{ac3D}| < |F_{ac1D}| < |F_{ac2D}|$$

Because the combined system has three degrees of freedom, the potential energy contour plot cannot be visualized. However, the procedure described in the previous section enables us to generate the potential energy vs. displacement curve can be gener-

**Table 6.2** Summary table for the combination of two bistable behaviors in series ( $n = 2$ ).

TYPE		Load-displacement	Number of Stable Equilibria
12 12	$ F_{ac1A}  <  F_{ac2A} $ $ F_{ac1D}  <  F_{ac2D} $		4
12 21	$ F_{ac1A}  <  F_{ac2A} $ $ F_{ac2D}  <  F_{ac1D} $		3
21 12	$ F_{ac2A}  <  F_{ac1A} $ $ F_{ac1D}  <  F_{ac2D} $		3
21 21	$ F_{ac2A}  <  F_{ac1A} $ $ F_{ac2D}  <  F_{ac1D} $		4

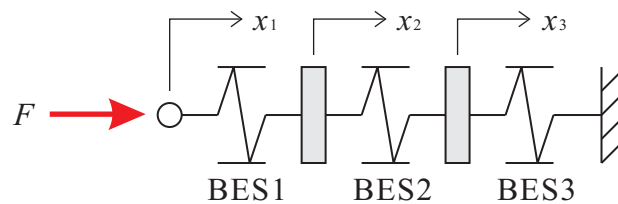


**Figure 6.12** Combined multistable system consisting of three bistable systems.

ated (Fig. 6.14). The corresponding load-displacement curve in Fig. 6.15 shows that there are five accessible stable equilibria (5 solid circles). In general, the combination of three bistable mechanisms in series can produce up to eight ( $= 2^3$ ) stable equilibria, though three ( $= 8 - 5$ ) of the stable equilibria are not reachable in this combination as illustrated by the three dotted circles.

The potential energy curve is obtained by using the optimization procedure described earlier, and the load-displacement curve can be calculated from the potential energy curve. Alternatively, it is possible to obtain an approximated shape of the load-displacement curve by using Table 6.2. The details are explained Appendix B.



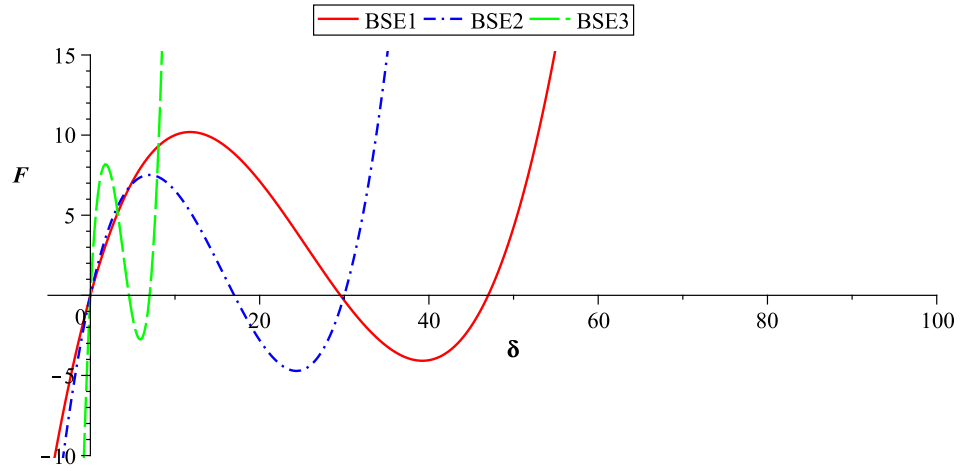


**Figure 6.13** Load-displacement curves of three different bistable behaviors ( $\text{TYPE}_{312}^{231}$ ).

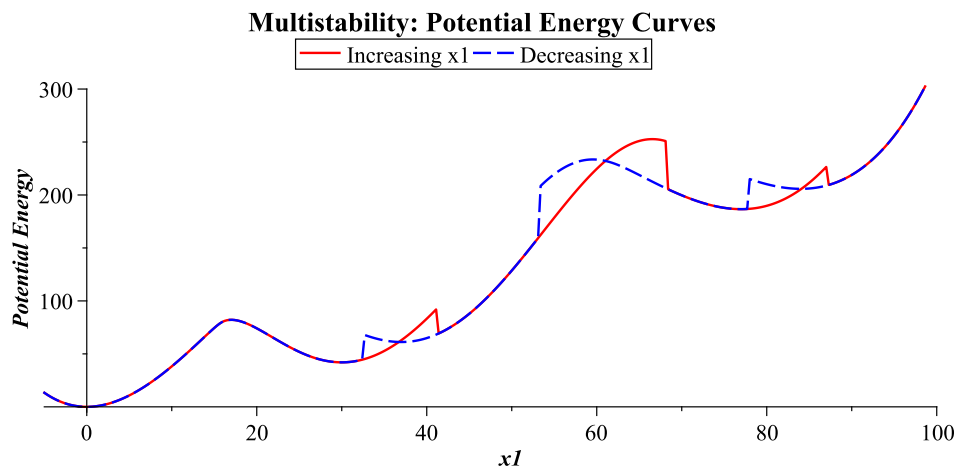


**Figure 6.14** Potential Energy vs. displacement curve of combined multistable system behaviors ( $\text{TYPE}_{312}^{231}$ ).

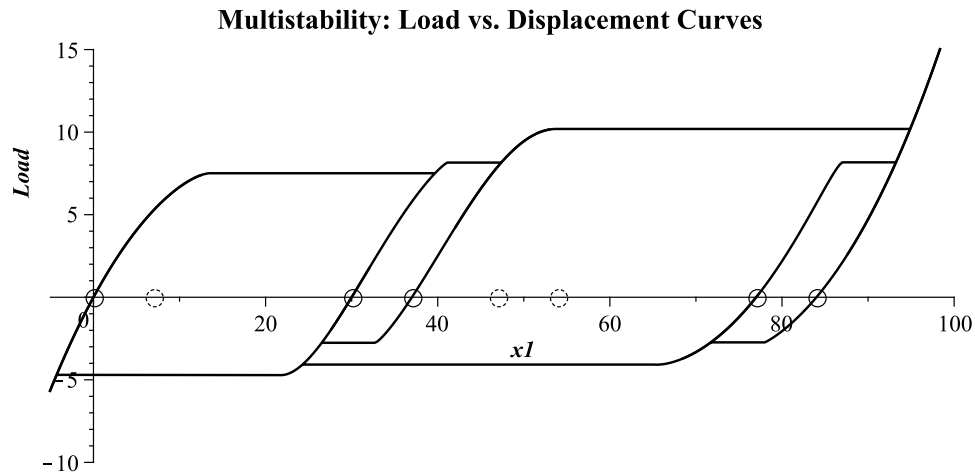


**Figure 6.15** Load-Displacement curve of the combined multistability with controlling the load behaviors (**TYPE**<sub>312</sub><sup>231</sup>).

All 36 types of combinations of the three bistable behaviors ( $n = 3$ ) are summarized in Appendix C. The load-displacement behavior and the total number of stable equilibria for each type are provided. Table 6.3 shows the number of stable equilibria in a matrix form. Since the matrix is symmetric, the superscript and subscript need not be specified. As shown in the table, when the orders of the superscript and subscript are identical, the combined system has the maximum number of stable equilibria ( $2^n = 8$ ). On the other hand, when the orders of the superscript and subscript are in an opposite order, only the minimum number ( $n + 1 = 4$ ) of stable positions can be realized. All other types exhibit between five and seven accessible stable equilibria. This outcome is always true for all other cases including combinations of more than three bistable behaviors and combinations of two bistable behaviors.

## 6.7 Case Study 3: Combining Four Bistable Behaviors

In this case study, four bistable behaviors ( $n = 4$ ) are combined to synthesize a multistable system with 16 stable equilibria. Piecewise continuous functions, which are used to represent the bistable behaviors, are plotted in Fig. 6.16. The multistable system satisfies the

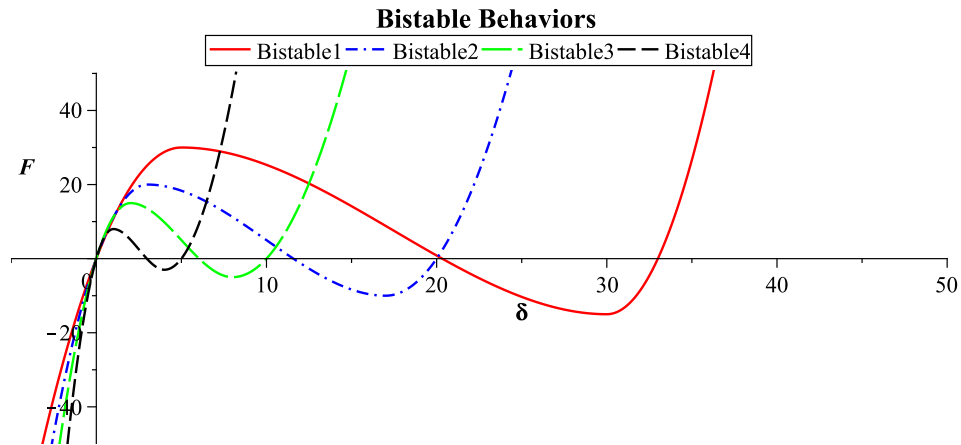
**Table 6.3** Matrix for number of stable equilibria for combinations of three bistable mechanisms.

TYPE	123	132	213	231	312	321
123	8	6	6	5	5	4
132	6	8	5	4	7	5
213	6	5	8	6	4	5
231	5	4	6	8	5	6
312	5	7	4	5	8	6
321	4	5	5	6	6	8

following conditions and its combination is **TYPE**<sub>4321</sub><sup>4321</sup>.

$$\beta_1 > \beta_2 > \beta_3 > \beta_4$$

$$|F_{ac4_A}| < |F_{ac3_A}| < |F_{ac2_A}| < |F_{ac1_A}| \& |F_{ac4_D}| < |F_{ac3_D}| < |F_{ac2_D}| < |F_{ac1_D}|$$

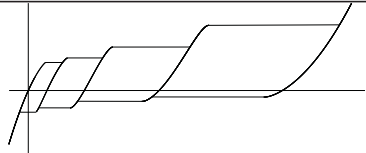
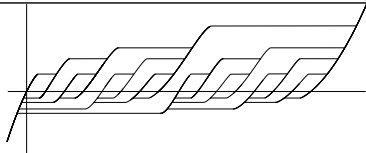


**Figure 6.16** Load-displacement curves of four bistable behaviors.

Since the superscript and the subscript of the **TYPE** are in the same order, the maximum number ( $2^n = 16$ ) of stable equilibria is expected in this type. The combined load-displacement curve is plotted in Table 6.4. Since there are too many combinations to be listed, only combinations with minimum ( $n + 1 = 5$ ) and maximum ( $2^n = 16$ ) numbers of

stable equilibria are listed in the table.

**Table 6.4** Summary table for the combination of two bistable behaviors in series ( $n = 4$ ).

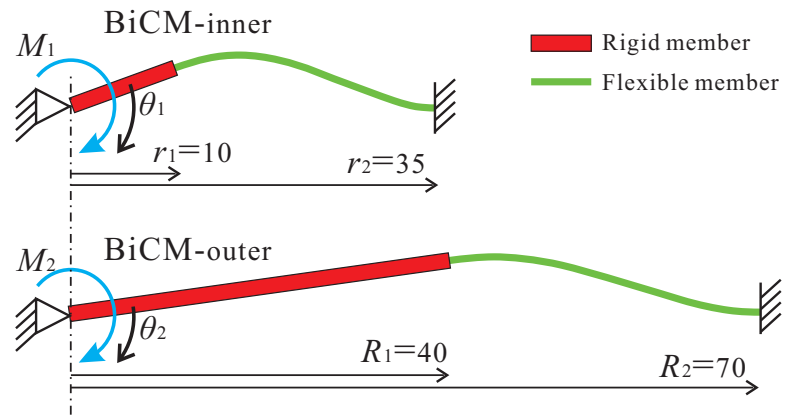
TYPE	Load-displacement	Number of Stable Equilibria
4321 1234		5
⋮	574 more types	5~16
4321 4321		16

## 6.8 Example: Quadrizable Equilibrium Rotational Compliant Mechanism

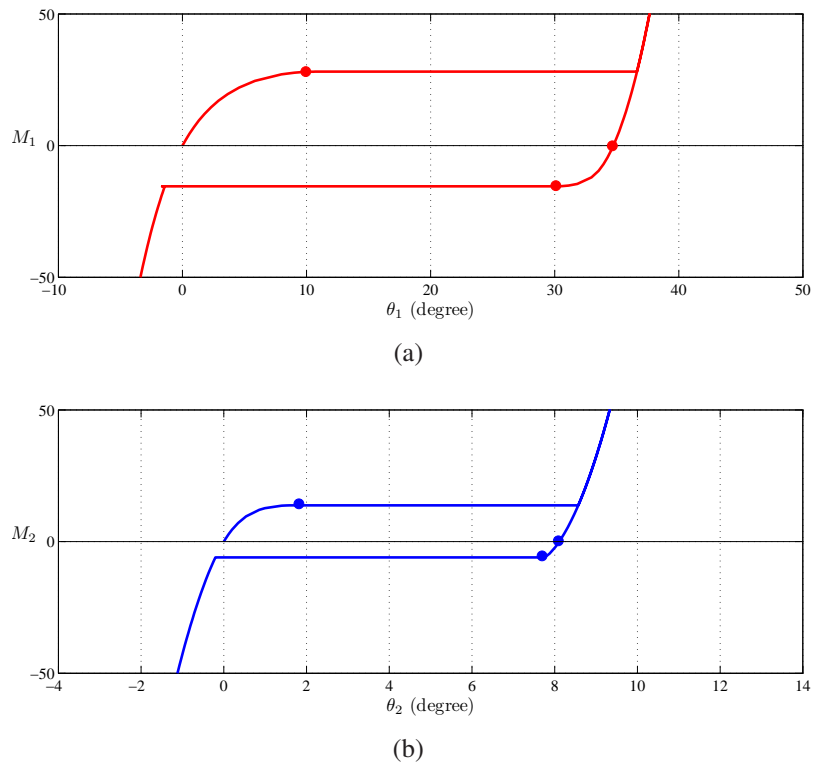
The goal of this example is to combine two bistable rotational compliant mechanisms to synthesize a multistable mechanism with four stable equilibrium positions. Additionally, the results of a nonlinear structural analysis will be compared to the results of the mathematical approach described in the previous section.

Fig. 6.17 shows two rotational compliant mechanisms, BiCM-inner and BiCM-outer, whose initial shapes are the stress-free buckled configurations of straight beams. In the same sense that BES1 is combined into the rigid body of BES2 in Fig. 6.6, BiCM-inner is substituted for the rigid portion of BiCM-outer to produce the multistability. The two bistable behaviors are plotted in Fig. 6.18. The plots are obtained with the load-control method.

Unlike the translation mechanisms in Fig. 6.6, the combined rotational compliant mechanism is not easily visualized with two rigid-flexible beams. By applying a cyclic symmet-



**Figure 6.17** Two bistable compliant mechanisms of different dimensions (size and proportion)



**Figure 6.18** Load-displacement curves for the bistable compliant mechanisms. (a) BiCM-inner, and (b) BiCM-outer. Key parameters are marked as circles. (ABAQUS)

ric condition, however, the combined mechanism can be formed. Fig. 6.19 shows a cyclic symmetric model of the combined rotational MSCM.

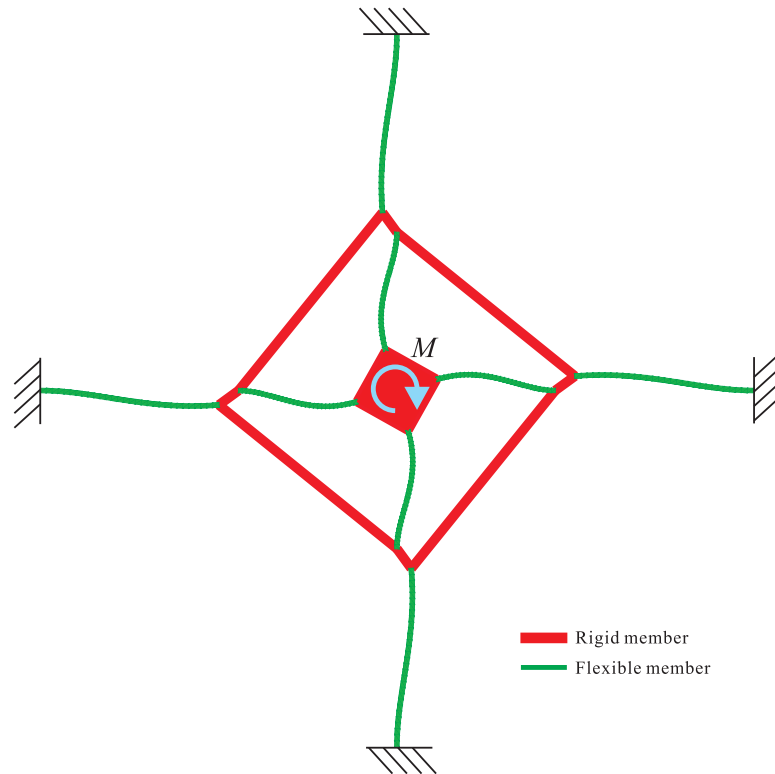


**Figure 6.19** Combined multistable equilibrium rotational compliant mechanism with four stable equilibria.

The simplified mathematical expressions of the two bistable behaviors can be obtained by using the matching condition described in Eqn. (6.10). The piecewise-continuous functions that satisfy the key parameters in Fig. 6.18 are

$$\begin{aligned}
 M_1 &= \begin{cases} 5.20\theta_1 - 0.26\theta_1^2 & \theta_1 < 10 \\ -16.0 + 9.45\theta_1 - 0.63\theta_1^2 + 0.01\theta_1^3 & 10 \leq \theta_1 < 30 \\ 560.0 - 38.40\theta_1 + 0.64\theta_1^2 & 30 \leq \theta_1 \end{cases} \\
 M_2 &= \begin{cases} 15.0\theta_2 - 3.75\theta_2^2 & \theta_2 < 2.0 \\ 3.17 + 12.98\theta_2 - 4.11\theta_2^2 + 0.29\theta_2^3 & 2.0 \leq \theta_2 < 7.5 \\ 1024.16 - 275.51\theta_2 + 18.37\theta_2^2 & 7.5 \leq \theta_2 \end{cases} \quad (6.14)
 \end{aligned}$$

where  $\theta_1$  and  $\theta_2$  are defined in Fig. 6.17. The two functions are plotted in Fig. 6.20(a).

From Eqn. (6.11) and (6.12), the total potential energy can be calculated. The potential energy path is obtained by using the procedure described in the previous section. Fig. 6.20(b) shows the multistable behavior of the combined compliant mechanism. Non-linear structural analysis of the combined system is performed with the aid of ABAQUS, which is a commercial finite element analysis software package. Due to the snap-through behaviors, the design of the combination is evaluated by using hybrid beam elements (B31H), which allows us to handle slender beams, the axial stiffness of which is very large compared to the bending stiffness [5]. In order to apply the load-control method, STABILIZE option is activated. This option helps the solver to continue with the solution even when the tangential stiffness matrix becomes singular [4].

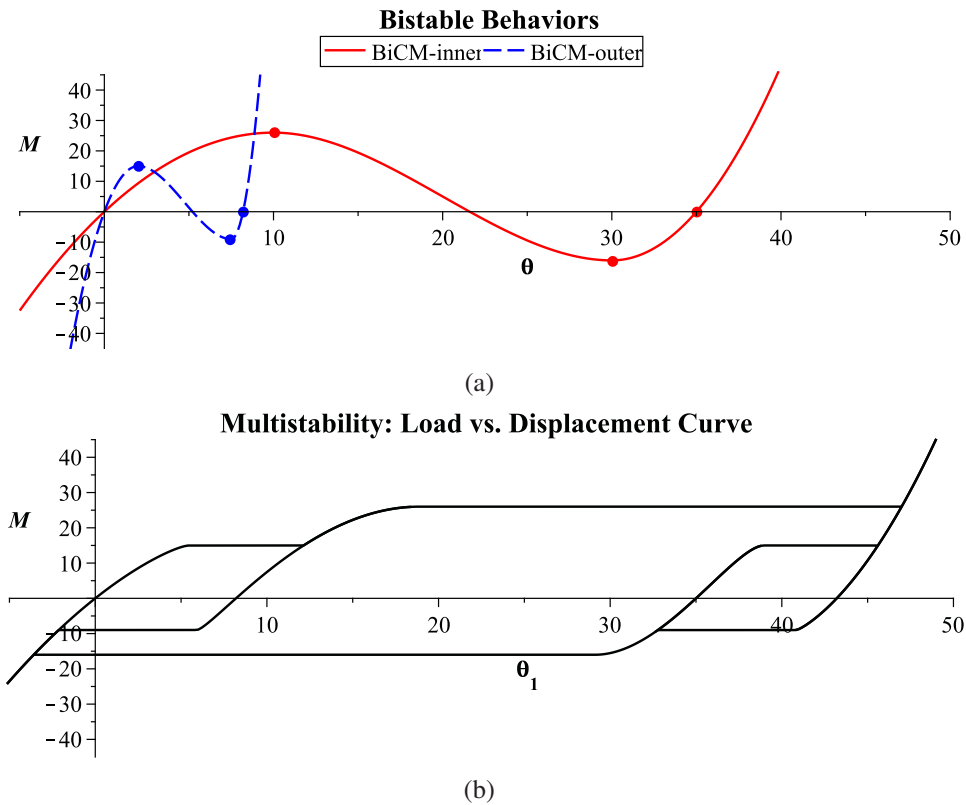


**Figure 6.20** (a) Simplified mathematical functions of the two bistable behaviors, and (b) the combined results from Maple software.

The multistable hysteresis of the combined compliant mechanism is plotted in Fig. 6.21 and its stable configurations are shown in Fig. 6.22. All the key parameters are matched to the curve from a mathematical approach. Hence, for an evaluation of the combined multistable compliant mechanism, it is not necessary to perform nonlinear structural analysis. The mathematical approach offers an efficient evaluation and is less cumbersome because of the nonlinear analysis that is needed to synthesize multistable compliant mechanisms.

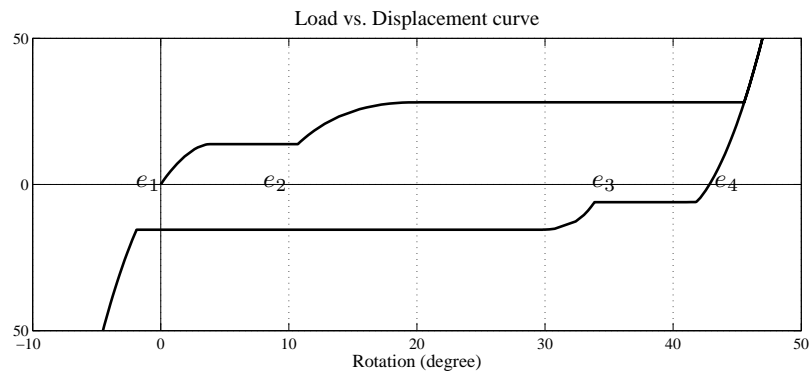


**Figure 6.21** Load-displacement curves for the combined multistable compliant mechanism using nonlinear analysis (ABAQUS).

## 6.9 Design of Tristable and Quadrastable Compliant Mechanisms by Combining Two Bistable Compliant Mechanisms

To verify the multistabilities of combined bistable behaviors in series, two rotational bistable compliant mechanisms are designed and manufactured. Among the four combination types of two bistable behaviors, **TYPE<sub>21</sub><sup>21</sup>** and **TYPE<sub>12</sub><sup>21</sup>** are demonstrated in this section.



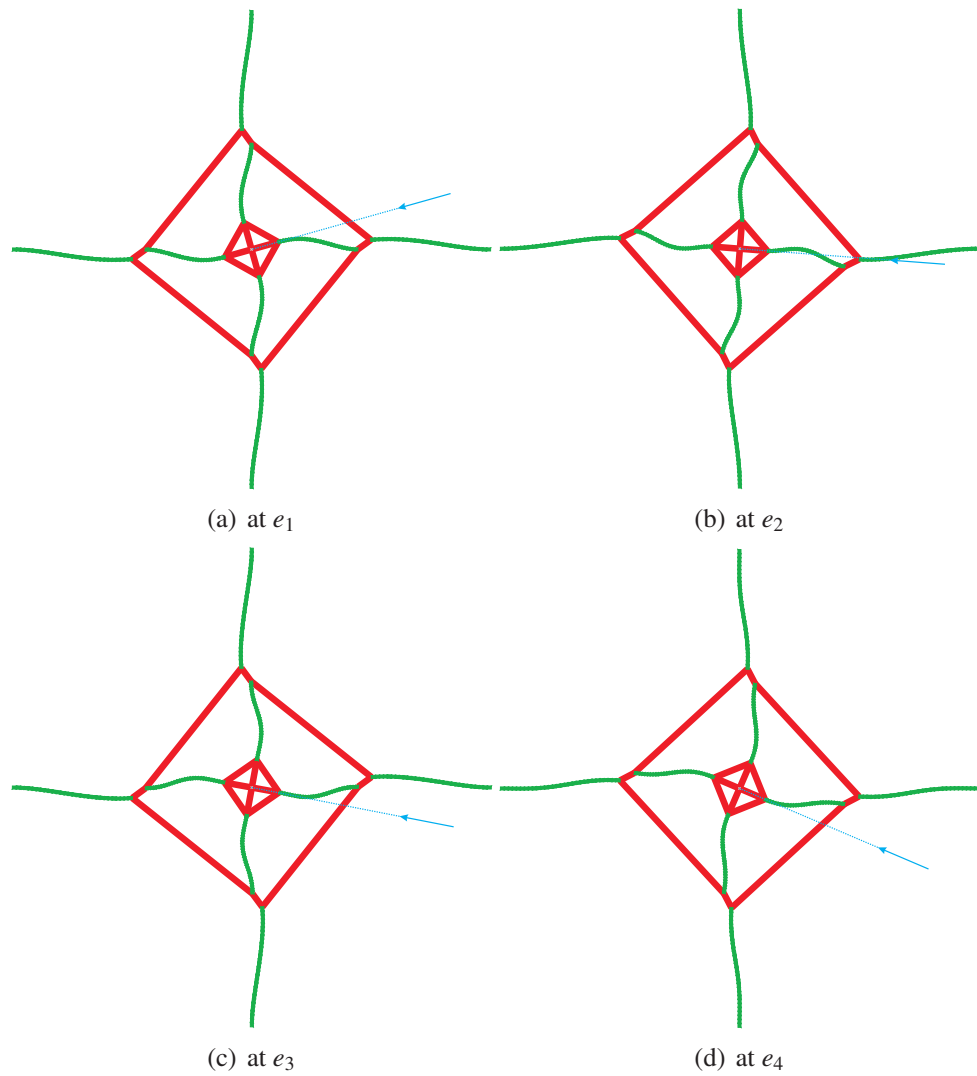


**Figure 6.22** Four stable configurations of the rotational multistable compliant mechanism.

### 6.9.1 Experimental Verification of the Two Combination Types, $\text{TYPE}_{21}^{21}$ and $\text{TYPE}_{12}^{21}$

Combining two bistable behaviors generates up to four stable positions.  $\text{TYPE}_{12}^{21}$  and  $\text{TYPE}_{21}^{21}$  have three and four active stable configurations respectively. The conditions of  $\text{TYPE}_{12}^{21}$  and  $\text{TYPE}_{21}^{21}$  are described in the third and fourth rows of Table 6.2.  $F_{ac1A}$  and  $F_{ac1D}$  are the actuation loads of increasing and decreasing load steps respectively, for BES1 which has the largest interval between the two stable equilibria.  $F_{ac2A}$  and  $F_{ac2D}$  are the actuation loads of increasing and decreasing load steps for BES2. The combination  $\text{TYPE}_{21}^{21}$  has greater actuation loads of BES1 for both increasing and decreasing load steps. The actuation load of BES1 for increasing load step in  $\text{TYPE}_{12}^{21}$  is greater than the load of BES2, and the actuation load of BES2 for decreasing load step is greater than the load of BES1. The combined load-displacement responses are illustrated in Table 6.2. Note that the third stable position of  $\text{TYPE}_{12}^{21}$  is not active.

Two rotational bistable compliant mechanisms are designed using the first buckling mode of a pinned-clamped partially rigid and partially flexible beam. The buckled configuration is shown in Fig. 6.2. Instead of using a single beam with a pin joint at one end, by introducing cyclic symmetric condition of four repeated beams, the pinned end is able to be removed. Two rotational bistable compliant mechanisms can be combined in either the in-plane (single layer) or out-of-plane (multilayer) direction. In order to demonstrate the two types of combination,  $\text{TYPE}_{12}^{21}$  and  $\text{TYPE}_{21}^{21}$ , using two bistable mechanisms, the multilayer combination is used in this report. The disadvantage of the multilayer combination is that more than one part is necessary. The single layer combination can be manufactured monolithically but it increases the in-plane size. An example of the single layer combination is shown in Fig. 6.40 at the end of this chapter.

One of the two rotational bistable compliant mechanisms is shown in Fig. 6.23. There are four flexible beams and two rigid bodies. One of the rigid bodies will be connected to

the other rotational bistable compliant mechanism.

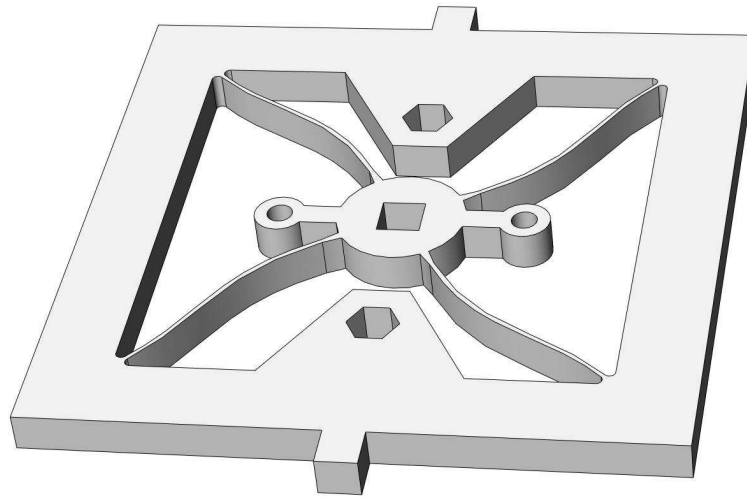


**Figure 6.23** Rotational bistable compliant mechanism.

The prototypes shown in this chapter are made of homopolymer polypropylene and fabricated by waterjet machining.

## 6.9.2 Digitizing Multistable Behaviors

To describe the individual behaviors of the bistable mechanisms composing the combined multistable mechanism, digitizing multistable behaviors is introduced. Digitizing multistability can be done by utilizing the binary property of bistable behaviors.

### Digitizing Bistability

Since a bistable system has only two stable equilibria, it is possible to use binary number to describe its current state. Because the displacement and the potential energy at the initial stable position is zero, the corresponding binary number of the initial stable position is defined as 0. And the other stable position can be described as a binary number, 1. Note that a bistable system is active when its current status is defined as 1. Table 6.5 shows the summary of digitizing bistability using binary numbers.

**Table 6.5** Digitizing bistability.

Stable Position	BES
Initial Stable Position	0
Second Stable Position	1

### Digitizing Multistability

Each stable position of a multistable system has a unique binary number. Thus, it is possible to identify active and inactive bistable systems. For example, if the current stable position of a multistable system has  $\{1011\}$ , the second bistable system is not active and all other bistable systems are active. Table 6.6 shows how the system can be digitized using the binary numbers. Digitizing multistability is also useful to identify the number of bistable systems in the combined multistable system. In the example in Table 6.6, there are four bistable systems since four binary numbers are used to describe current status.

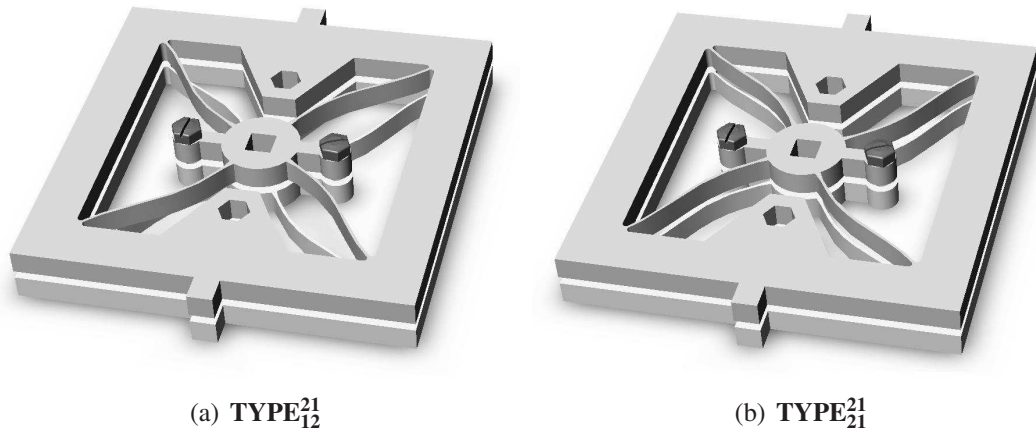
**Table 6.6** An example of digitizing multistability: 1011.

Stable Position	BES1	BES2	BES3	BES4
Initial Stable Position	0	0	0	0
Second Stable Position	1	1	1	1

### 6.9.3 Combining Two Rotational Bistable Compliant Mechanisms

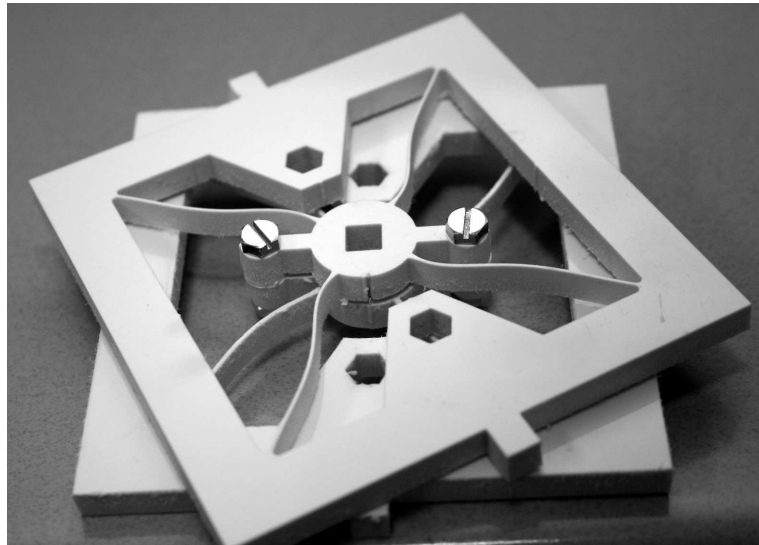
Two different combination types can be produced by stacking and bolting the two rotational bistable compliant mechanisms together. By matching the opposite faces of the two mechanisms together,  $\text{TYPE}_{21}^{21}$  can be produced.  $\text{TYPE}_{12}^{21}$  can be made by setting the two mechanisms to face the same direction. The two combination types are illustrated in Fig. 6.24. BES1 is at the bottom and BES2 is at the top.

Fig. 6.25 shows the prototype made of two polypropylene bistable mechanisms. The configuration shown in the figure has BES1 with the initial stable status at the bottom



**Figure 6.24** Two combinations of the rotational bistable compliant mechanisms.

and BES2 with the second stable status at the top. Therefore, BES2 is active and the configuration in the figure can be digitized as  $\{01\}$ .



**Figure 6.25** Combining two bistable compliant mechanisms in series:  $\{01\}$

### Combination $\text{TYPE}_{21}^{21}$

The combination  $\text{TYPE}_{21}^{21}$  is depicted in Fig. 6.24(a). It has the following relations between the two bistabilities.

$$|F_{ac2_A}| < |F_{ac1_A}|$$

$$|F_{ac2_D}| < |F_{ac1_D}|$$

Both actuation loads for increasing and decreasing displacements of BES1 are greater than the actuation loads for BES2. The load-displacement behaviors of the two bistable compliant mechanisms are shown in Fig. 6.26. In the figure, approximated piecewise continuous functions are used to represent the bistable behaviors.

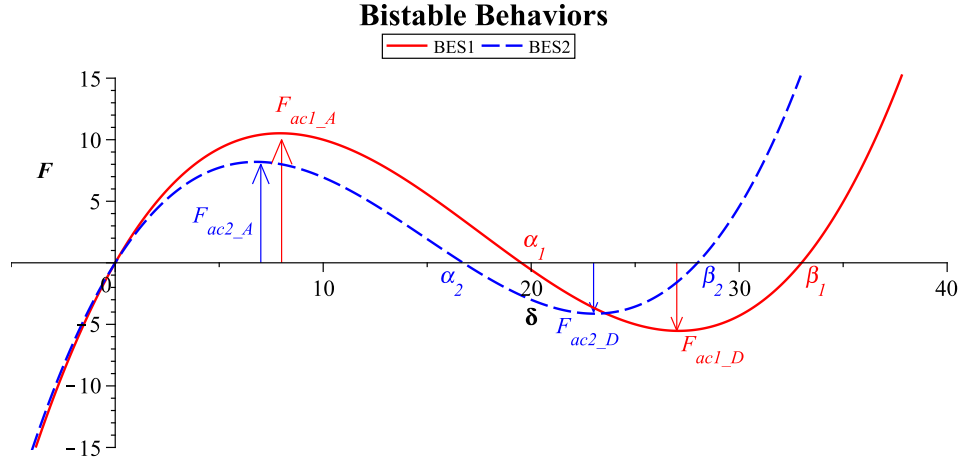


**Figure 6.26** Load-displacement responses of the two bistable mechanisms.

Based on the approximated piecewise continuous functions, the potential energy stored in the multistable compliant mechanisms is obtained and plotted in Fig. 6.27. The equilibrium routes are shown in the contour plot. All four local minima of the potential energy can be identified by the potential energy curve in Fig. 6.28.

The load-displacement relation can be obtained by differentiating the potential energy curve with respect to the displacement. The load-displacement response using the load control method is depicted in Fig. 6.29. If the input load is increased gradually, the second stable position,  $e_2$ , can be obtained. The fourth stable position,  $e_4$ , can be reached if the load is increased further. If the input load is decreased from the stable position at  $e_4$ , one can find the third stable position,  $e_3$ . The initial stable position,  $e_1$ , can be obtained by

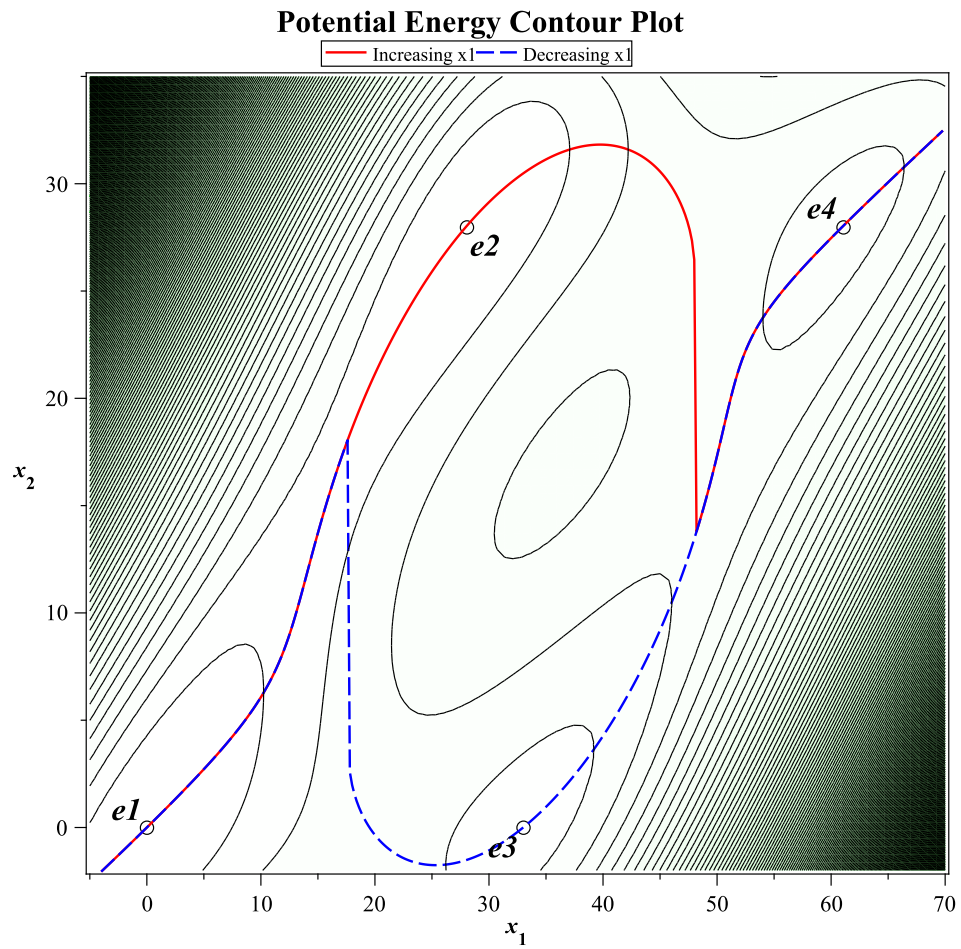


**Figure 6.27** Potential energy contour plot and the equilibrium paths of the combined multistable mechanism,  $\text{TYPE}_{21}^{21}$ .

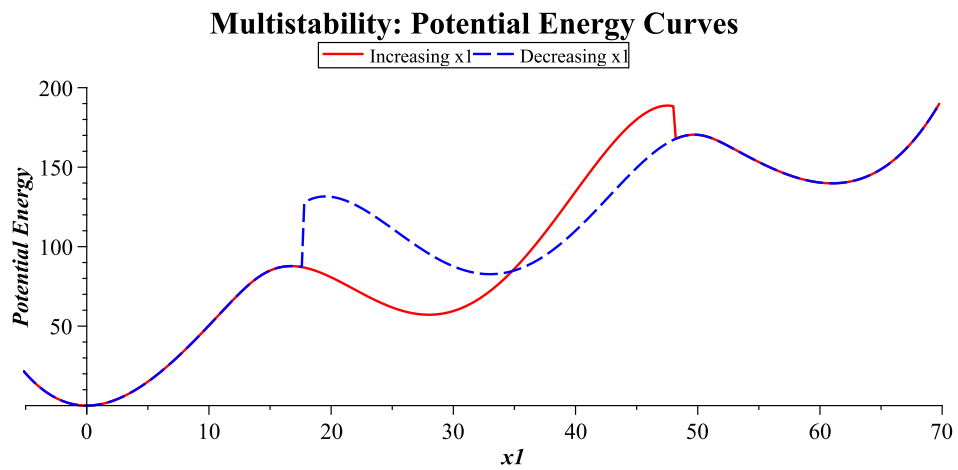


**Figure 6.28** Potential energy curve of the combined multistable mechanism,  $\text{TYPE}_{21}^{21}$ .

decreasing the load again.

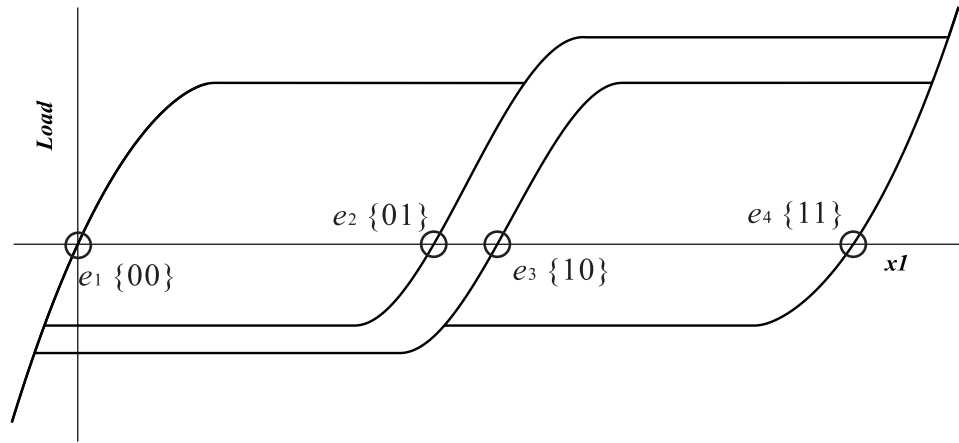


**Figure 6.29** Load-displacement behavior of the combined multistable mechanism,  $\text{TYPE}_{21}^{21}$ , using the load-control method.

Each stable configuration of the multistable compliant mechanism is shown in Fig. 6.30. The initially stable position,  $e_1$ , is located at  $0^\circ$ . The second stable position,  $e_2$ , is located at  $28^\circ$  and only BES2 is active. BES1 is active when the multistable mechanism is in its third stable position and the angle is  $33^\circ$ . At  $e_4$ , both BESs are active and the fourth stable position is at  $61^\circ$ .

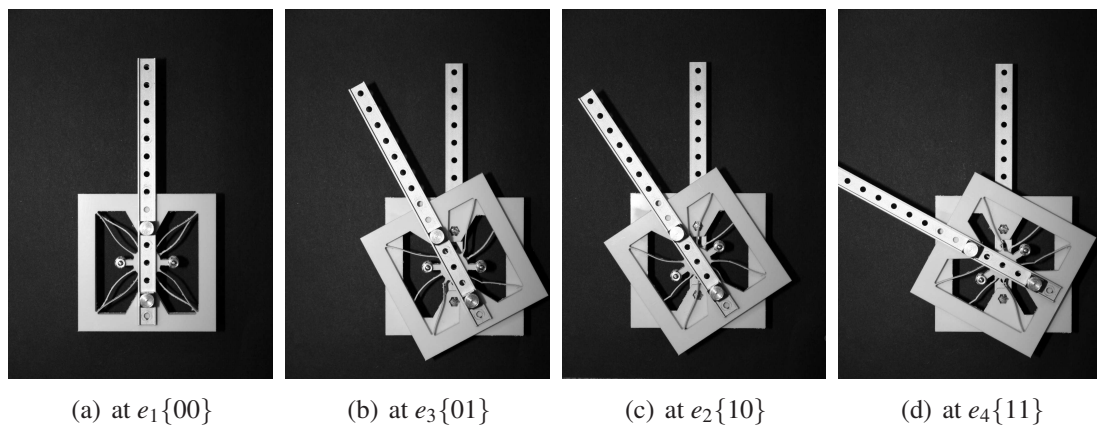


**Figure 6.30** Four stable configuration of the combined multistable mechanism,  $\text{TYPE}_{21}^{21}$ : (a)  $0^\circ$ , (b)  $28^\circ$ , (c)  $33^\circ$ , and (d)  $61^\circ$ .



### Combination TYPE<sub>12</sub><sup>21</sup>

The combination TYPE<sub>12</sub><sup>21</sup> is depicted in Fig. 6.24(b). It has the following relations between the two bistabilities.

$$|F_{ac2_A}| < |F_{ac1_A}|$$

$$|F_{ac1_D}| < |F_{ac2_D}|$$

The actuation load for increasing displacement of BES1 is greater than the actuation load for increasing displacement of BES2. For decreasing displacement, the actuation load for BES2 is greater than the one for BES1. The two bistable behaviors are shown in Fig. 6.31. Note that the direction of the displacement of BES2 is opposite to the direction of the displacement of BES1 in this case.

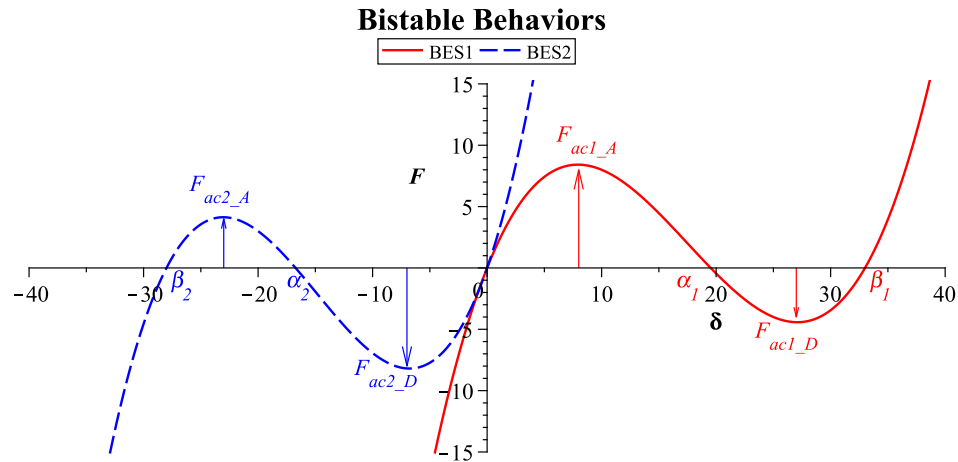


**Figure 6.31** Load-displacement responses of the two bistable mechanisms.

The potential energy curve of the combined system has three local minima as shown in Fig. 6.32 so there are three active stable positions. The initial position of this combination is located between the other two stable positions since BES2 has the opposite behavior.

Fig. 6.33 shows the potential energy contour plot and the equilibrium routes of the combined system. The three stable positions,  $e_1$ ,  $e_2$  and  $e_4$ , are located on the equilibrium routes. There is, however, another local minimum that does not exist in the potential energy

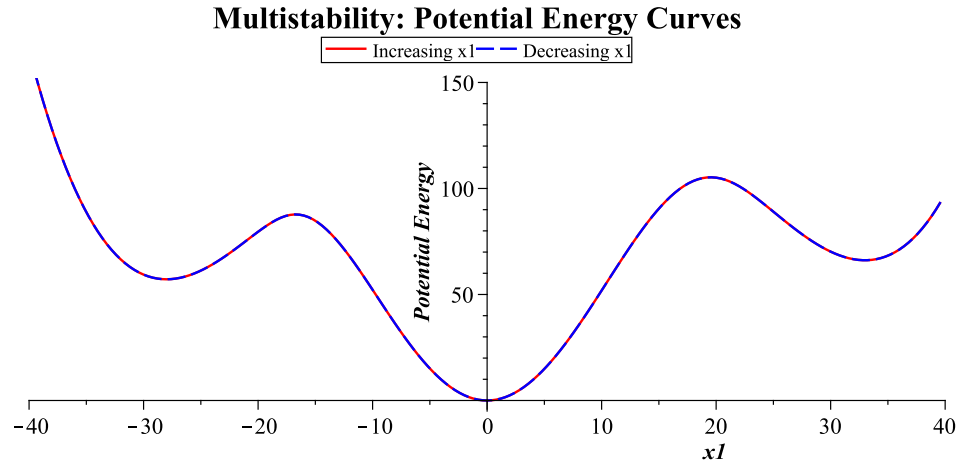


**Figure 6.32** Potential energy curve of the combined multistable mechanism, **TYPE<sub>12</sub><sup>21</sup>**.

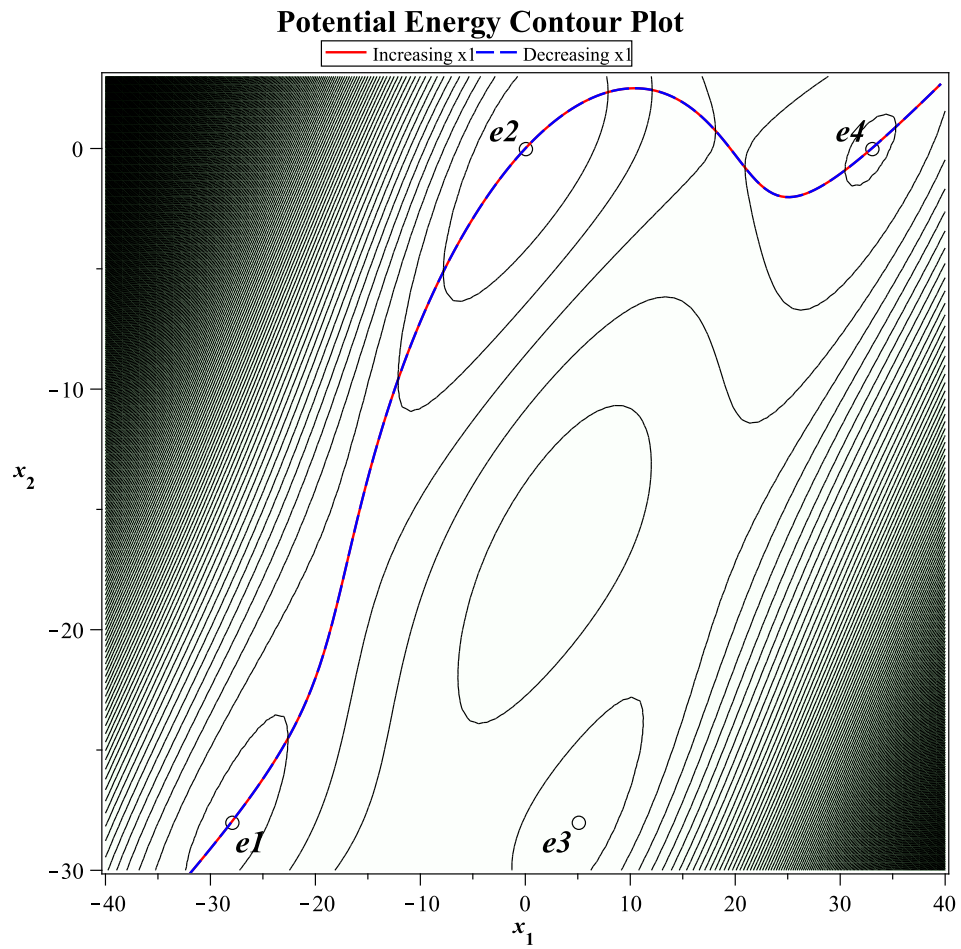
curve in Fig. 6.32. The local minimum,  $(e_3)$ , is a hidden stable equilibrium of the system. The parentheses indicate that the local minimum is hidden. The hidden stable position can be accessed when the two bistable compliant mechanisms are active simultaneously.

Fig. 6.34 shows the load-displacement curve of **TYPE<sub>12</sub><sup>21</sup>**. The load axis is located between the two stable equilibria,  $e_1$  and  $e_4$ . It has both negative and positive stable positions. The hidden stable position cannot be reached by applying an input load to the system. The only way to reach the position is applying a load to the connected rigid bodies between the two rotational bistable compliant mechanisms. Fig. 6.35 shows the three stable configurations and the hidden stable configuration.

#### 6.9.4 Combining Four Bistable Compliant Mechanisms

In this section, four bistable compliant mechanisms are combined in series and demonstrated. The same two **TYPE<sub>21</sub><sup>21</sup>** bistable systems are combined in series as shown in Fig. 6.36. Two bistable compliant mechanisms are connected rigidly.

Fig. 6.37 shows the initial stable position and the stable configuration with the maximum rotation angle. The maximum angle can be reached when all four bistable mechanisms are active. Therefore the binary numbers for the maximum rotation is  $\{1111\}$ .



**Figure 6.33** Potential energy contour plot and the equilibrium paths of the combined multistable mechanism,  $\text{TYPE}_{12}^{21}$ .

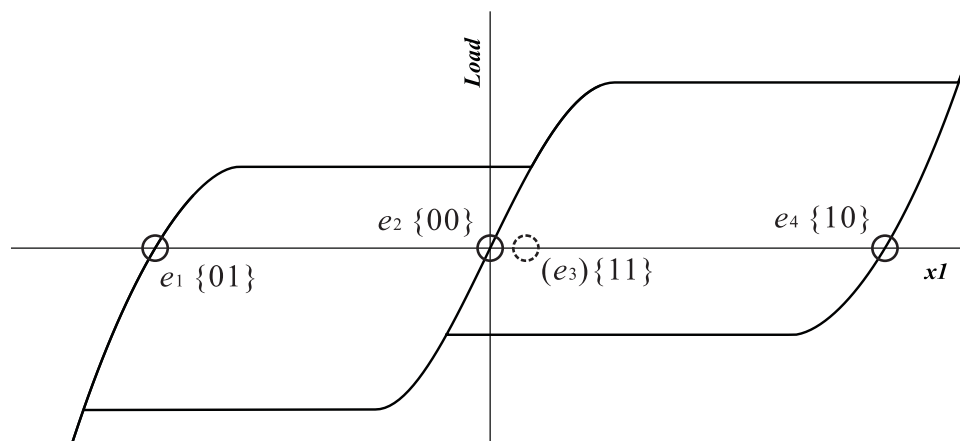


**Figure 6.34** Load-displacement behavior of the combined multistable mechanism,  $\text{TYPE}_{12}^{21}$ , using the load-control method.

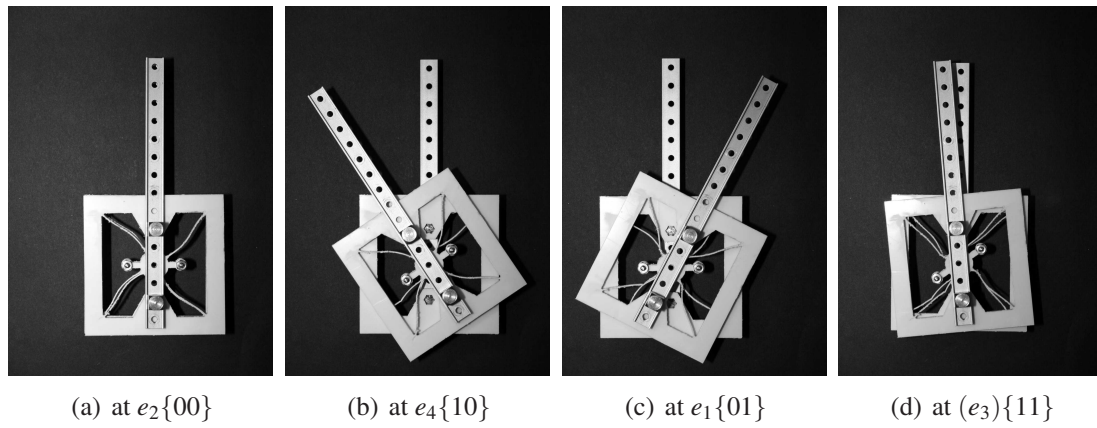


**Figure 6.35** Four stable configuration of the combined multistable mechanism, **TYPE<sub>12</sub><sup>21</sup>**: (a)  $0^\circ$ , (b)  $33^\circ$ , (c)  $-28^\circ$ , and (d)  $5^\circ$ .

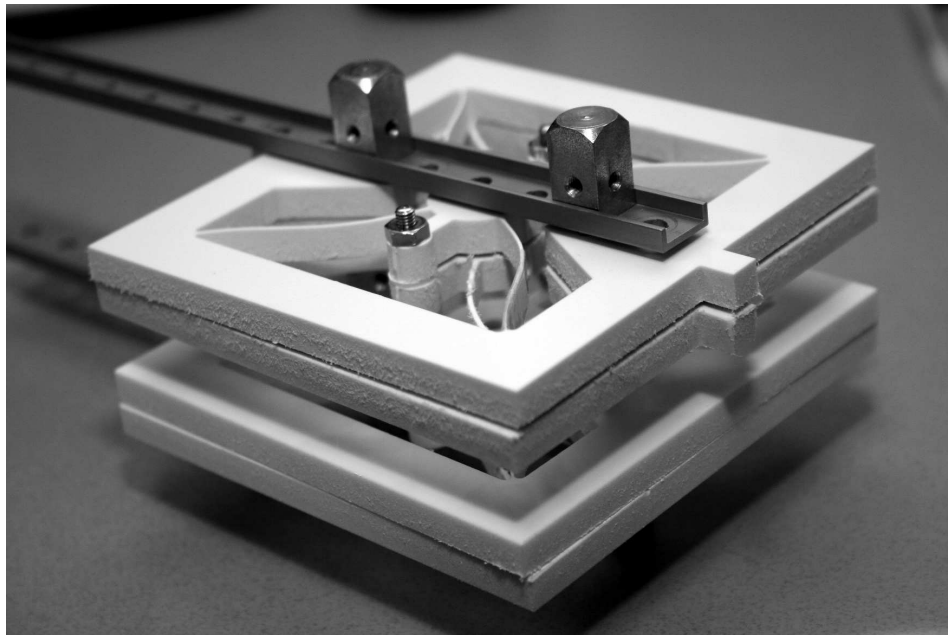


**Figure 6.36** Combining four bistable compliant mechanisms in series.

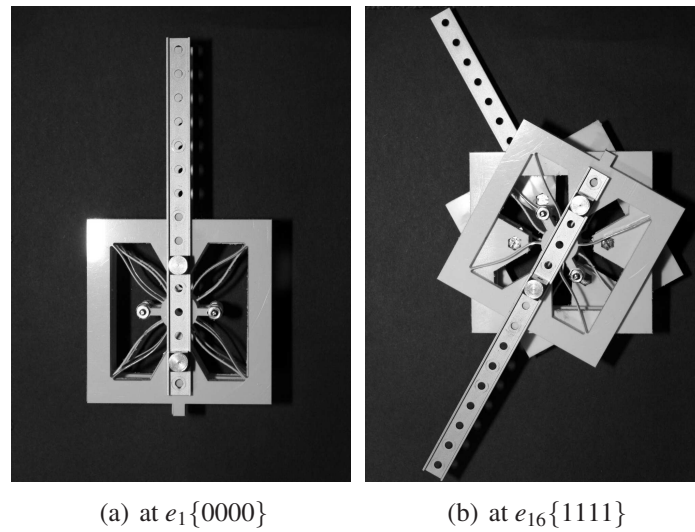


**Figure 6.37** Multistable compliant mechanisms using four bistable compliant mechanisms.

### 6.9.5 Combining Two Bistable Mechanisms Orthogonally

So far, combinations using two layers are considered. However, the direction of combination is not restricted when multiple layers are used. As mentioned earlier, two rotational bistable compliant mechanisms can be combined in either in-plane or out-of-plane directions. In this subsection, two other directions of combination are introduced: orthogonal and in-plane directions.

Combining bistable mechanisms in two orthogonal directions produces a biaxial multistable compliant mechanism. Fig. 6.38 shows the initial configuration of the combined compliant mechanism. The two bistabilities are orthogonal and activated independently. Therefore there are always four accessible stable configurations. Each stable configuration can be described using unique binary numbers. The initial stable configuration shown in Fig. 6.38 is  $\{00\}$ .

Fig. 6.39 shows three stable configurations of the combined biaxial multistable compliant mechanism. The two bistable degrees of freedom are depicted with a triad in the figure.

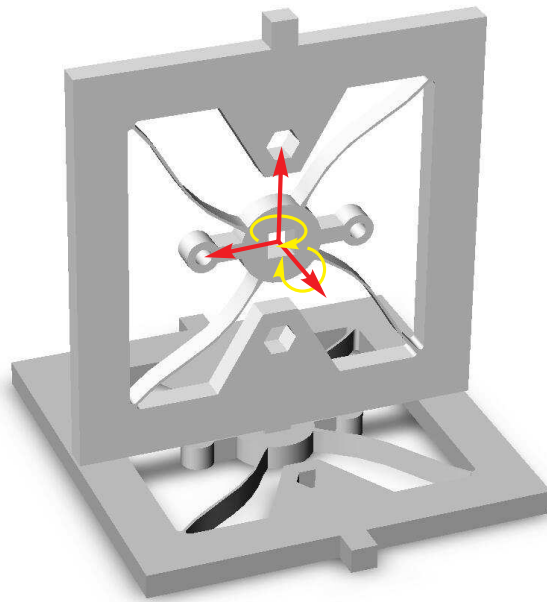
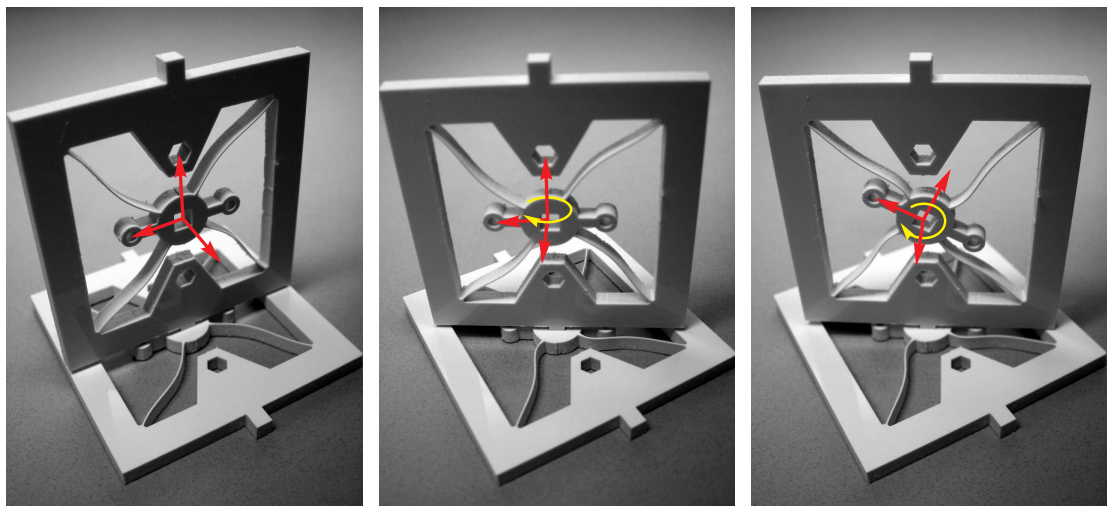


**Figure 6.38** Two axes rotational multi-bistable compliant mechanism.



(a) at  $e_1\{00\}$

(b) at  $e_2\{10\}$

(c) at  $e_3\{11\}$

**Figure 6.39** Biaxial rotational multistable mechanism.

Fig. 6.40 shows four stable configurations of a rotational quadristable compliant mechanism. The two rotational bistable compliant mechanisms are combined in the in-plane (single layer) direction. The main advantage of the single layer combination is that the multistable compliant mechanism can be manufactured as a single piece.

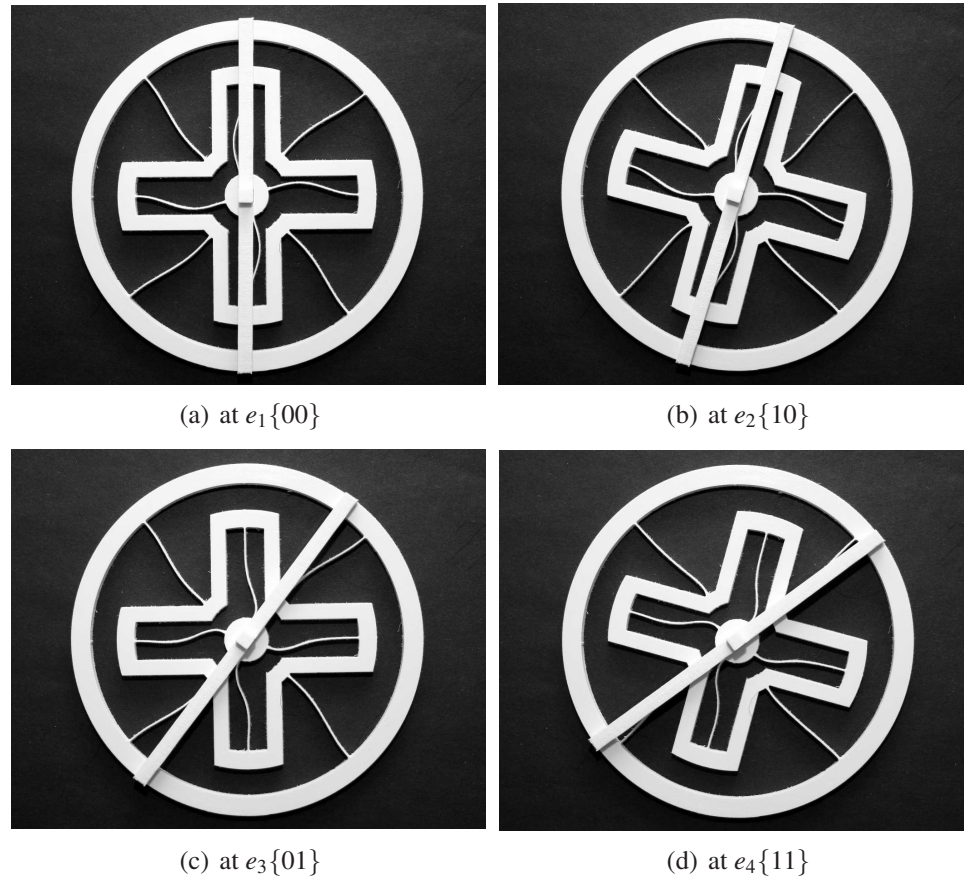


**Figure 6.40** Four stable configurations of the combined multistable mechanism,  $\text{TYPE}_{21}^{21}$ : (a)  $0^\circ$ , (b)  $-18^\circ$ , (c)  $-36^\circ$ , and (d)  $-54^\circ$ .

## 6.10 Conclusions

In this chapter, a mathematical approach of synthesizing multistability by combining multiple bistable mechanisms in series has been presented. The nonlinear behaviors of bistable compliant mechanisms are simplified to piecewise-continuous functions. The simplifica-

tion process eliminates the complicated post-buckling behavior of each bistable compliant mechanism. By controlling the input node of the combined mechanism, the potential energy path from the total potential energy of the system can be obtained.

The mathematical basis of the proposed design synthesis methodology focuses on shaping the load-displacement curves of the multistable systems so that the resultant curves appropriately match the desired properties. The example problems showed that the load-displacement curve obtained from the potential energy path can adequately represent the key parameters and the hysteresis of combined multistable compliant mechanisms. The methodology enables the user to (i) reflect the design requirements in a mathematical expression, (ii) decompose the problem into feasible sub-problems, (iii) synthesize the desired MSCM from a building block library (for example, Table 6.2 and Appendix C, and (iv) efficiently perform an evaluation without computationally intense nonlinear structural analysis.

In this chapter, only the actuation load and the stable positions have been considered as design requirements. If there is need for additional characteristics, such as the stiffness at a stable equilibrium position, higher order polynomials may be needed to represent the bistable behavior. Finally, to utilize the method described in this chapter as a generalized synthesis methodology of MSCMs, design methodologies for bistable compliant mechanisms are necessary. Design of bistable compliant mechanisms were discussed in Chapters 4 and 5.



## Chapter 7

### Design Examples

This chapter presents two design examples of multistable compliant mechanisms both of which demonstrate the utility of synthesis methodology described in the previous chapters: (i) utilizing RL deformation and (ii) utilizing buckling modes. The first design example is limited by size constraint, and the second example is governed by large loading conditions.

#### 7.1 Meso-scale Rotational Multistable Compliant Mechanisms

In this section, RL deformation is used to design a rotational multistable compliant mechanism. Since a RL deformed beam solution is based on Euler-Bernoulli beam theory, the behavior the beam is accurate when the beam is slender enough. It is recommended to use a beam with slenderness ratio,  $L/h$ , greater than 20, where  $L$  is the length of the beam and  $h$  is the thickness of the beam. This ratio is sometimes more critical than stress constraints in order to design bistable compliant mechanisms.

The scope of this case study is based on the following assumptions:

- i. A bistable compliant mechanism will be designed by using the design tool for RL deformation that is introduced in Chapter 5.
- ii. The actuation load is not considered in the design since it can be multiplied by the number of cyclic symmetric beams and is proportional to the out-of-plane thickness (scalability).

### 7.1.1 Design Specifications

Small size rotational multistable compliant mechanisms are very useful in many devices with doors, covers or lids. Such devices include notebook PCs, hand-held devices, and small size lockers. More than two stable positions are desired in these devices since their purpose is not only opening or closing but also adjusting the intermediate orientations.

In this case study, design specifications for a small size rotational multistable compliant mechanism are following.

- i. *Footprint of the mechanism* : Each bistable compliant mechanism will be designed in a  $1\text{cm} \times 1\text{cm}$  footprint. These are meso-scale devices whose sizes or lengths are usually greater than 100 micron and smaller than 1cm.
- ii. *Number of stable equilibria* : The maximum number of stable equilibria is four, so at least two bistable compliant mechanisms are required.
- iii. *Combination type* : All four stable equilibria are activated. Combination **TYPE<sub>21</sub><sup>21</sup>** will be used in this case study.
- iv. *Range of Motion* : Desired range of motion of a combined rotational multistable mechanism is 70 degrees. Two rotational bistable mechanisms with 30 degree and 40 degree between the two stable equilibria will be designed.
- v. *Materials* : Living hinges are be used in order to provide the function of pin-joints presented in RL deformations. In general, polypropylene is used in wide variety of applications with living hinges. Manufacturing processes of polypropylene can be achieved via extrusion or injection molding which are well suited for to mass productions.

Once the two rotational bistable compliant mechanisms are designed based on the above specifications, they will be combined using the method introduced in Chapter 6 in order to synthesize multistability. Since **TYPE<sub>21</sub><sup>21</sup>** is desired for combined multistable behavior, the fourth type (the last row) in Table 6.2 is used. **TYPE<sub>21</sub><sup>21</sup>** have the following relation:

$$\beta_1 > \beta_2$$

$$|F_{ac1_A}| > |F_{ac2_A}| \& |F_{ac1_D}| > |F_{ac2_D}|$$

where  $\beta_i$  and  $F_{aci}$  are illustrated in Fig. 6.7 and explained in Table 6.1.

The two rotational bistable compliant mechanisms are

- BES1: A rotational bistable mechanism that has a 40° angle between two stable equilibria, and
- BES2: A rotational bistable mechanism that has a 30° angle between two stable equilibria.

Note that the actuation loads for BES1 is greater than the actuation loads for BES2.

## 7.1.2 Design of Two Rotational Bistable Compliant Mechanisms

**BES2: A rotational bistable mechanism that has a 30° angle between two stable equilibria**

A design tool for rotational bistable compliant mechanisms has been developed based on the solution for RL deformations derived in Chap. 5. Fig. 7.2 shows the design tool displaying the current design problem. The variables shown in the design tool are defined in Fig. 5.13 and is repeated here in Fig. 7.1.

Two input values are required to use the design tool: an angle between two stable positions and a radius of the rigid circle. The angle between stable positions is 30°. The radius of the inner rigid circle is set as 2mm. Based on the input values, two curves,  $L$  vs.  $n$  and  $R_d$  vs.  $\theta_{inc}$ , can be obtained as shown in Fig. 7.2. Note that  $R_d$  must be less than 5mm since the footprint of the mechanism is defined as 1cm × 1cm. However, since the rotational bistable compliant mechanism requires an annular rigid body,  $R_d$  smaller than 4.5mm is used.  $L$  must be as long as possible to maximize slenderness. Now the value,  $n$ , must be chosen. Since increasing  $n$  yields decreasing  $L$ , smaller  $n$  is desired. However, decreasing  $n$  also causes increasing  $R_d$  which increases the size of the mechanism. In this

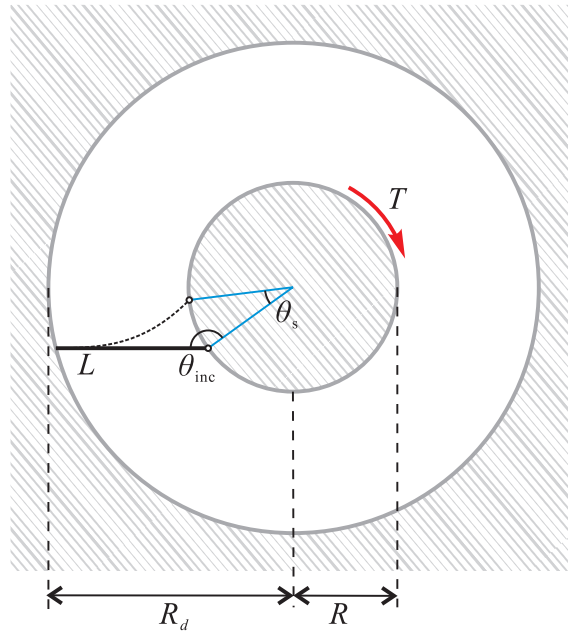


**Figure 7.1** A rotational bistable compliant mechanism using RL deformation.

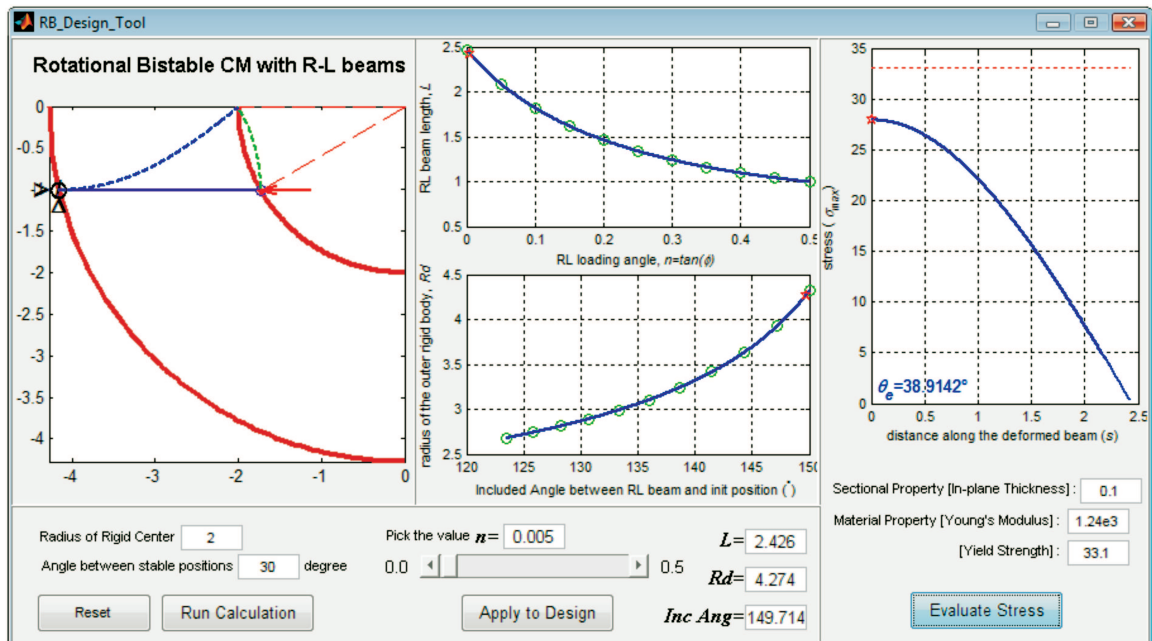


**Figure 7.2** Design and analysis results of Rotational Bistable CM Design Tool for BES2

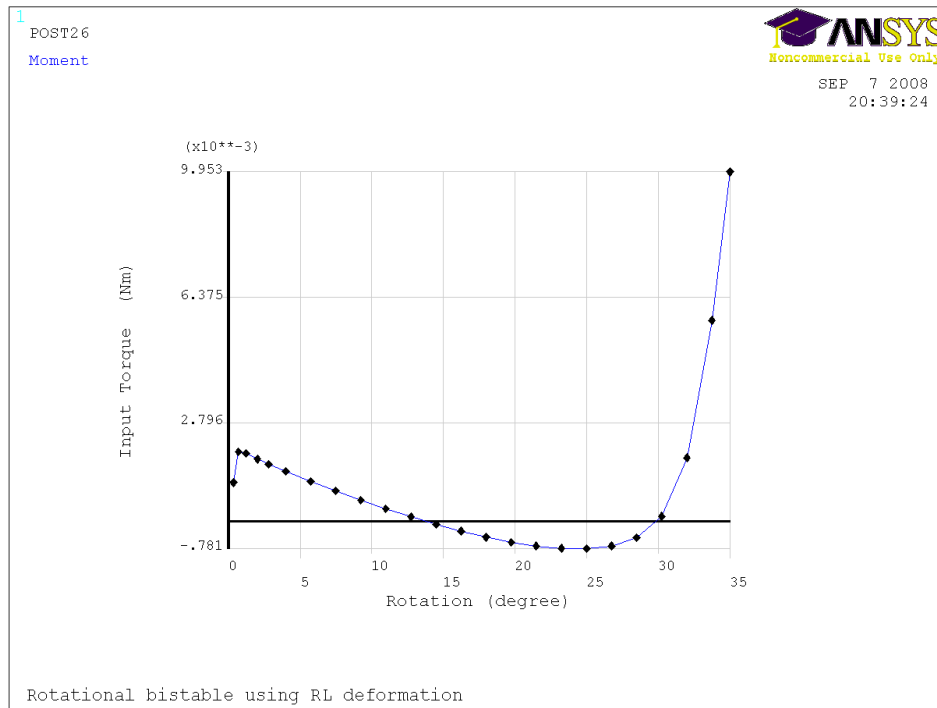
case, the following values are chosen.

$$\begin{aligned}n &= 0.005 \\L &= 2.426[mm] \\R_d &= 4.274[mm] \\\theta_{inc} &= 149.714^\circ\end{aligned}\tag{7.1}$$

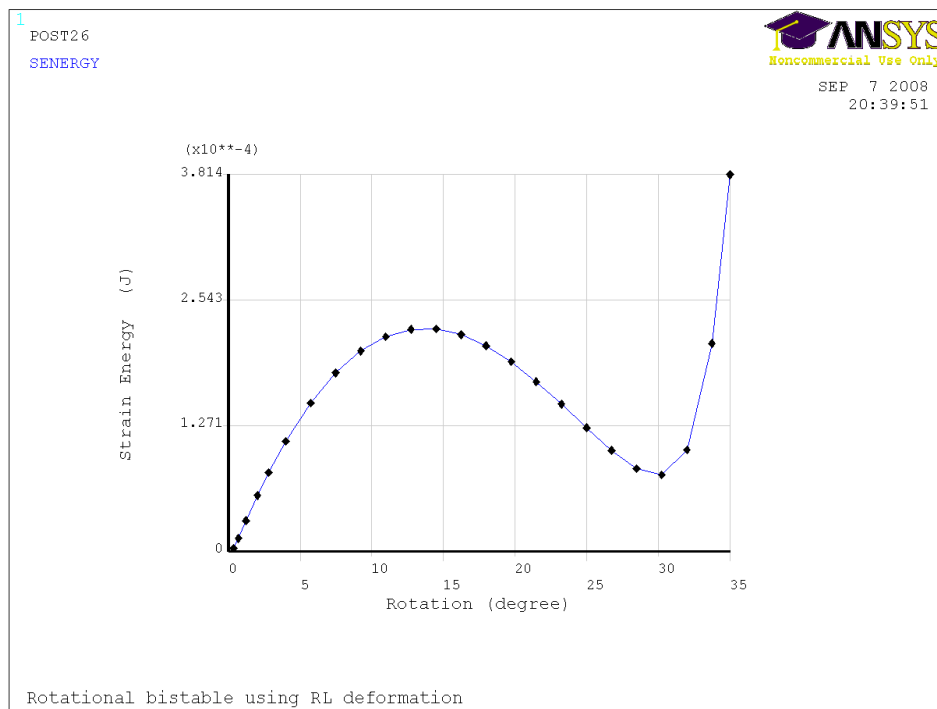
Based on the dimensions obtained, a 90 degree section of BES2 is displayed in Fig. 7.2. It shows the initial (solid line) and the second (dotted line) stable positions. So far, the thickness of the RL beam is not considered. To obtain the bistable behaviors at the final design, the RL beam must be a slender beam. The in-plane thickness,  $t$ , is selected based on the definition of slender beam ( $L/h > 20$ ). Manufacturing limitations must be considered in this process. In this problem,  $h=0.1\text{mm}$  is used.

Fig. 7.3 (a) and (b) show the load-displacement and strain energy plots of BES2 respectively. Nonlinear structural analysis was performed using a displacement control method. Note that a displacement control method is better than a load control method in this case since RL deformation is less sensitive to the imperfection and does not have complex nonlinear behaviors. Two stable configurations of the RL deformation with Von Mises stress are shown in Fig. 7.4. In the figure, meshed elements represent the RL beam of BES2, and the solid line represents the inner rigid circle. Note that clockwise rotation is the positive direction. As shown in the figure, the maximum stress (30MPa) along the beam closely matches the value obtained using the design tool.

The number of beams along the circle and the out-of-plane scale factor are determined based on the load requirement. Since BES2 requires smaller actuation loads than BES1, only three beams are placed cyclic symmetrically. The out-of-plane thickness is 6.35mm for both BES1 and BES2. Note that the input torque shown in Fig. 7.3(a) is shared by all



(a)



(b)

**Figure 7.3** Nonlinear FE analysis for **BES2** : (a) load-displacement response and (b) strain energy plot [Ansys].

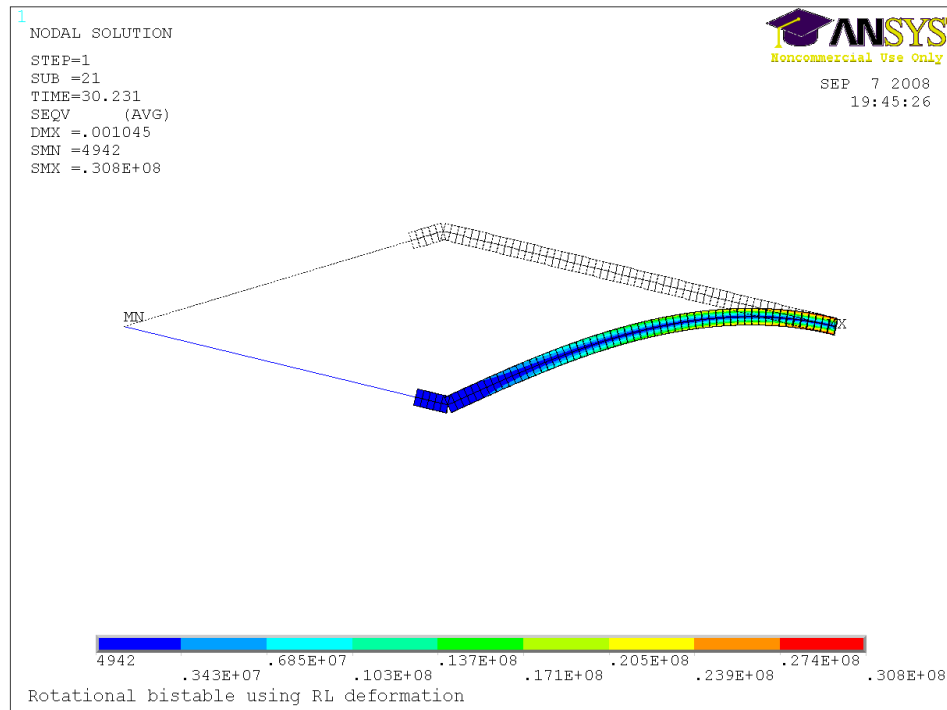


**Figure 7.4** Two stable positions of a RL beam of **BES2** and stress results.

three RL beams of BES2. The final design of the rotational bistable compliant mechanism with a  $30^\circ$  angle between stable positions is shown in Fig. 7.5

**BES1: A rotational bistable mechanism that has a  $40^\circ$  angle between two stable equilibria**

BES1 can be designed by using the same procedure applied to design BES2. Since greater actuation forces are required for BES1, four RL beams are used. Since four RL beam can be placed equally in a square, the maximum value of  $R_d$  is increased ( $\sim 5.5\text{mm}$ ). The radius of the rigid center is  $2.5\text{mm}$  and the required angle between two stable positions is  $40^\circ$ . From the obtained curves,  $L$  vs.  $n$  and  $R_d$  vs.  $\theta_{inc}$ , shown in Fig. 7.5, the following dimensions are chosen.

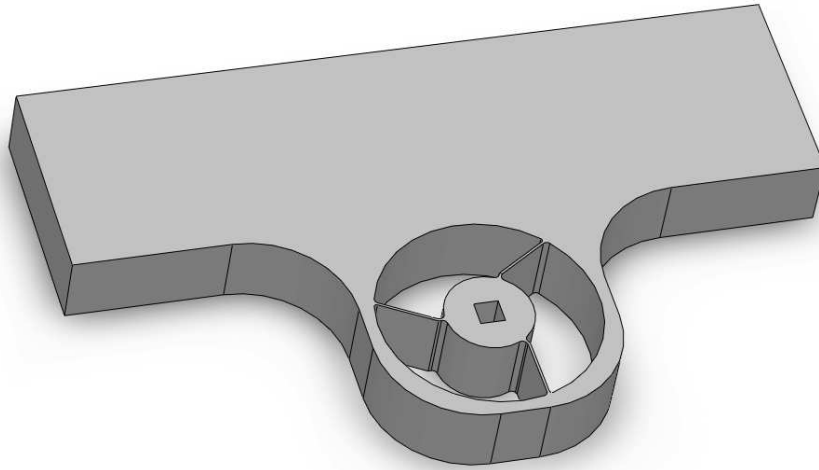


**Figure 7.5** BES2: a rotational bistable compliant mechanism with a 30° angle between stable positions

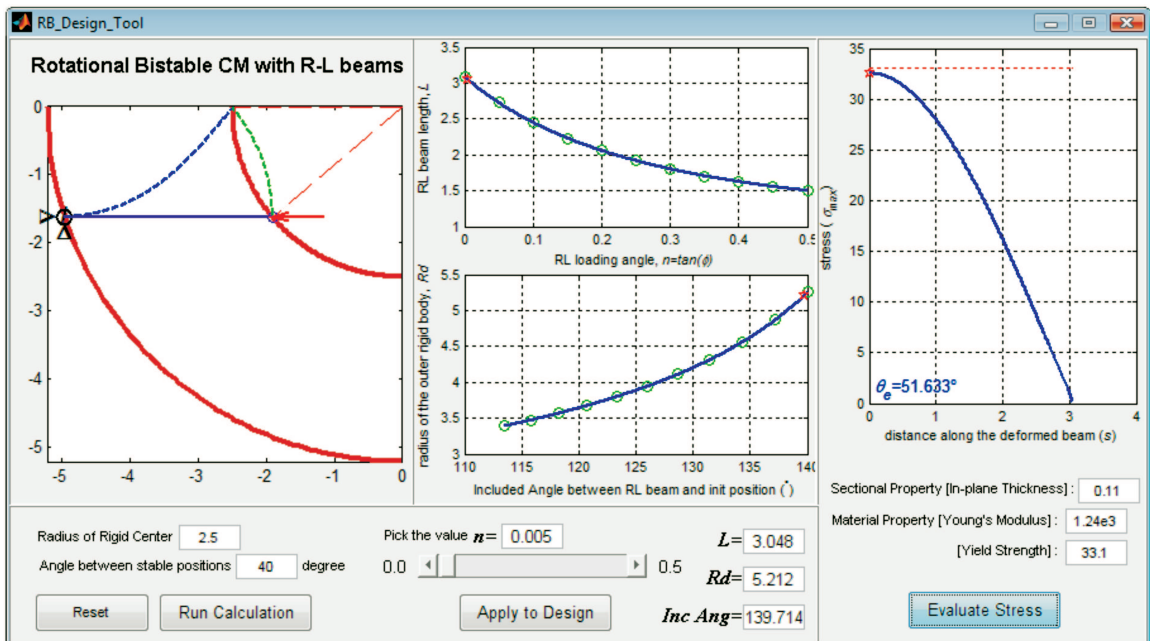


**Figure 7.6** Design and Analysis results of Rotational Bistable CM Design Tool for BES1.



$$\begin{aligned}
n &= 0.005 & (7.2) \\
L &= 3.048[mm] \\
R_d &= 5.212[mm] \\
\theta_{inc} &= 139.714^\circ
\end{aligned}$$

A 90 degree section of BES1 is displayed in Fig. 7.6 based on the above values. In the second design,  $h = 0.11\text{mm}$  is used.

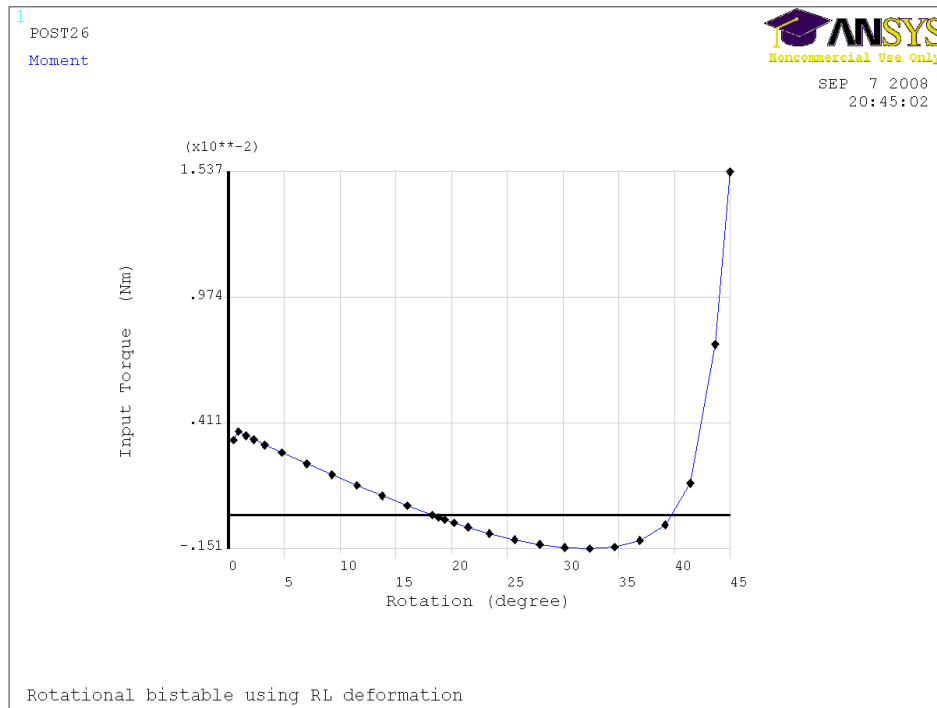
Fig. 7.7 shows the load-displacement and strain energy plots of BES1. As shown in the Fig. 7.7(a) and (b), the second stable position is located at the desired angle,  $40^\circ$ . The second stable position of BES2 is also located at  $30^\circ$  (Fig. 7.3). Note that as the slenderness ratio is decreased to below 20, the second stable position is decreased to below the desired value, and if the slenderness ratio is less than 10, the second stable position will disappear (Fig. 7.8). Therefore designers must consider the slenderness ratio to use RL deformations.

Two stable configurations of BES1 and Von Mises stress are shown in Fig. 7.9. In the figure, meshed elements represent the RL beam of BES2, and the solid line represents the inner rigid circle. Note that clockwise rotation is the positive direction.

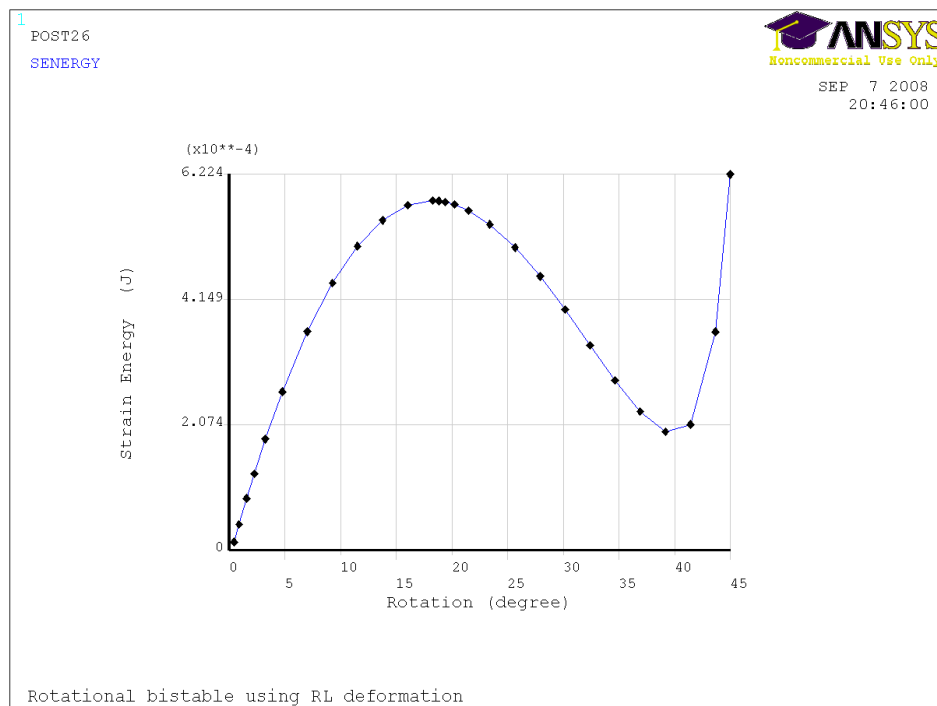
Four RL beams are placed equally in BES1. The same out-of-plane thickness is used. The final design of the rotational bistable compliant mechanism with  $40^\circ$  angle between stable positions is show in Fig. 7.10.

### 7.1.3 Design of a Rotational Multistable Compliant Mechanism

Two rotational bistable compliant mechanisms designed in the previous subsection are combined as described in Chapter 6. Combining the inner rigid circles of both bistable compliant mechanisms together provides the effect of series combination of two bistable behaviors. The combined configuration of two compliant mechanisms is shown in Fig. 7.11. Note



(a)



(b)

**Figure 7.7** Nonlinear FE analysis for **BES1** : (a) load-displacement response and (b) strain energy plot.

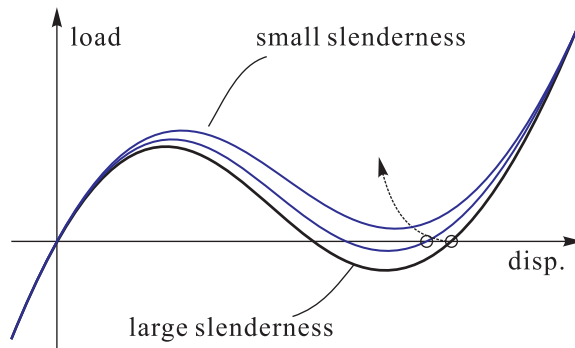


**Figure 7.8** Bistable behavior related to slenderness ratio.

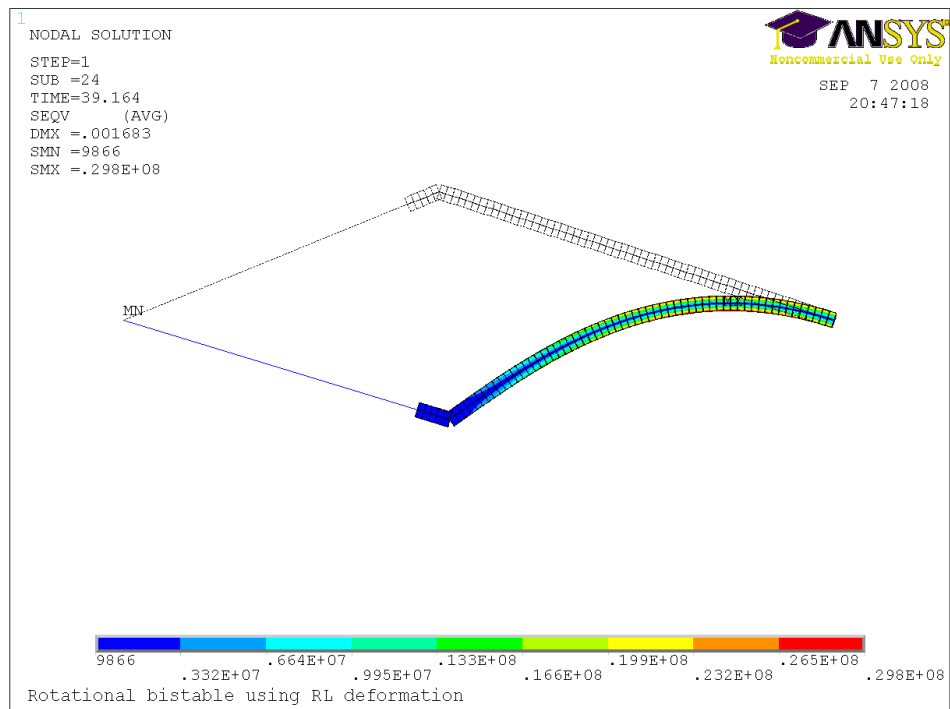


**Figure 7.9** Two stable positions of a RL beam of **BES1** and stress results.

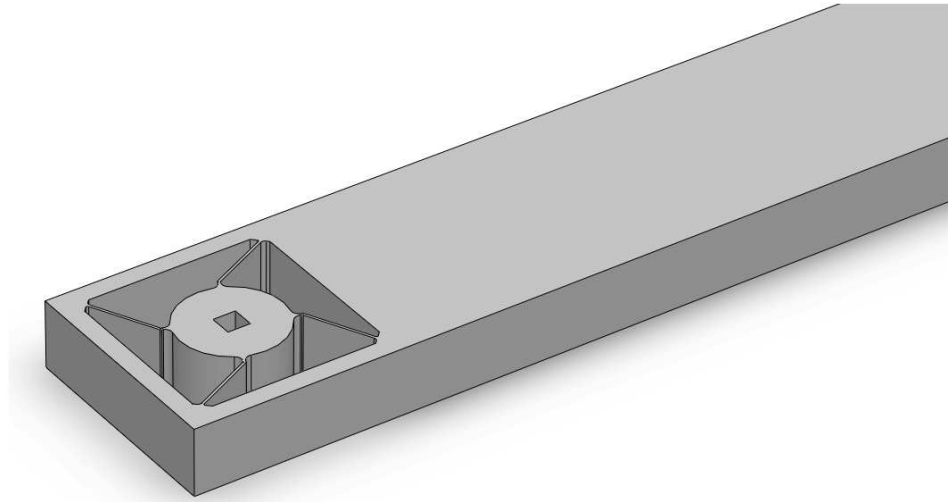


**Figure 7.10** BES1: a rotational bistable compliant mechanism with a  $40^\circ$  angle between stable positions

that combination types depend on orientations of the bistable compliant mechanisms, so the orientations should be carefully considered. This is also discussed in Chapter 6 (Fig. 6.24).

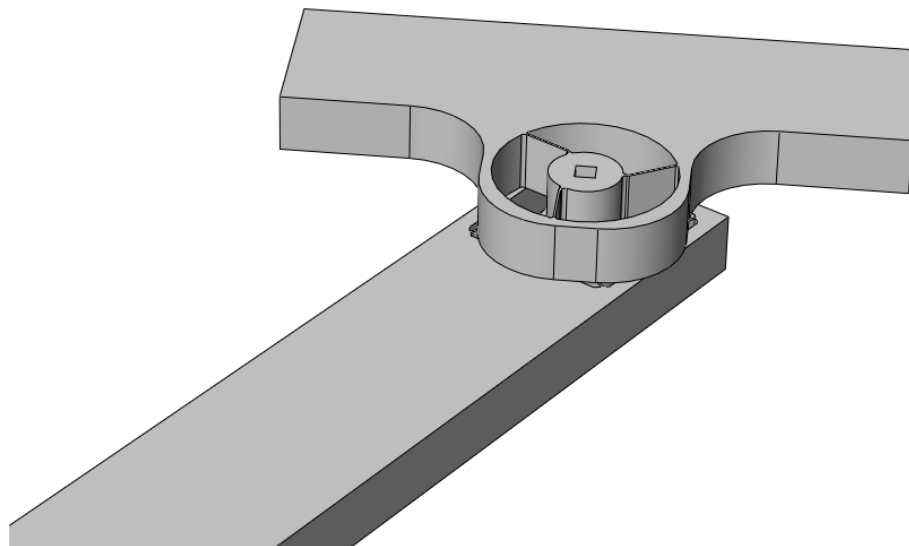


**Figure 7.11** The combined rotational multistable compliant mechanism.

Fig. 7.12 (a) and (b) show the load-displacement and strain energy plots of the combined rotational multistable compliant mechanism respectively. A nonlinear analysis with

a displacement control method is performed by using Ansys. The four stable equilibria can be obtained at the local minima of the strain energy curve. In the load-displacement curve, they are also located where the load inputs are zero and the slopes are positive.

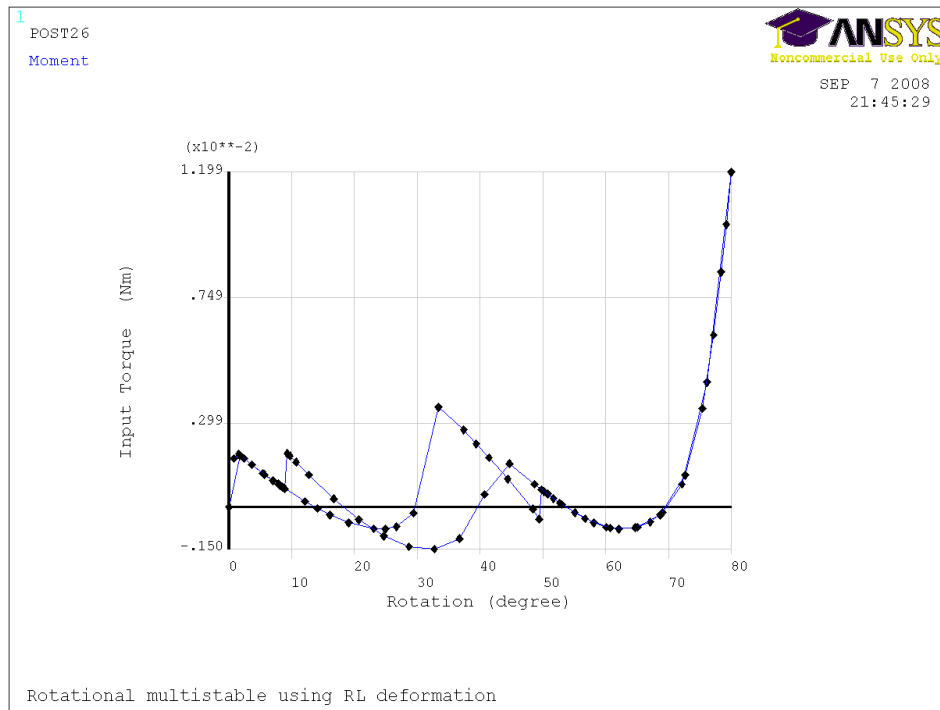
In general, multistable behaviors cannot be solved by using displacement control method because of the vertical jump shown in Fig. 6.10(a). In this example, vertical jumps are specially handled by adjusting the number of substeps in the nonlinear analysis. Note that these vertical jumps did not appear in the bistable behaviors of RL deformations. Users can take the advantage of the synthesis method described in Chapter 6, because nonlinear analysis is not required to evaluate the combined multistable compliant mechanism.

The first and the last stable configurations of the rotational multistable compliant mechanism are shown in Fig. 7.13. To visualize these configurations, the out-of-plane thickness of **BES1** is scaled to match the difference in the numbers of beams used for load sharing. Also, the Von Mises stress on the two RL beams is shown in Fig. 7.13. Note that the initial configuration of the RL beams are facing oppositely for **TYPE<sub>21</sub><sup>21</sup>**. **TYPE<sub>12</sub><sup>21</sup>** can be made by combining the two in the same orientation. The multistable behavior of **TYPE<sub>12</sub><sup>21</sup>** is shown in the third row of Table 6.2. **TYPE<sub>12</sub><sup>12</sup>** and **TYPE<sub>21</sub><sup>12</sup>** cannot be obtained from the two rotational bistable compliant mechanisms designed in this section because the actuation loads for BES1 is greater than the actuation loads for BES2.

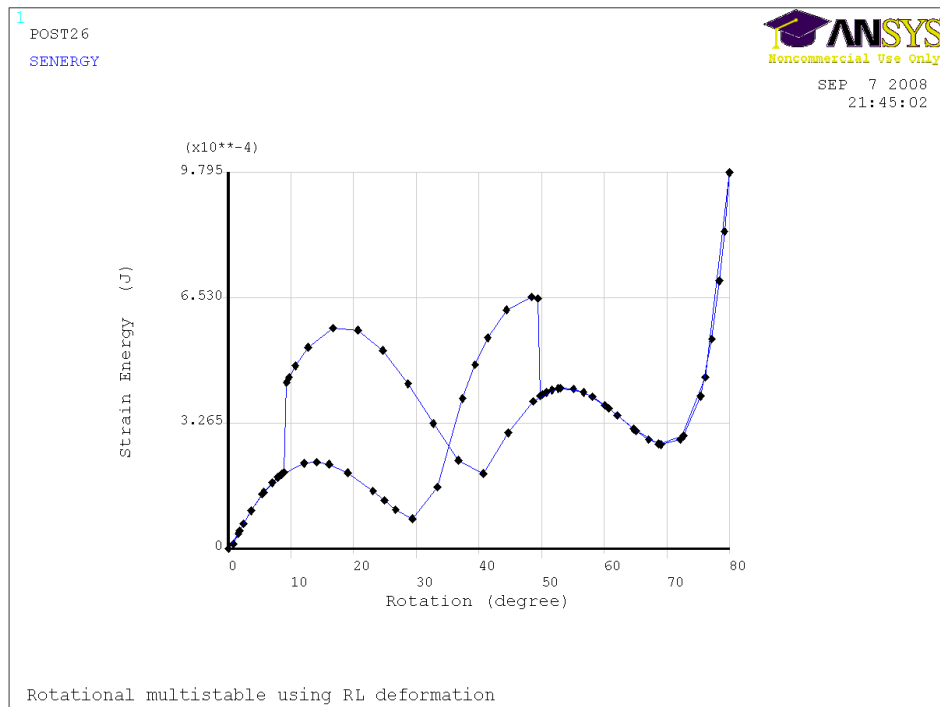
#### 7.1.4 Discussion

A detailed design procedure for a meso-scale rotational multistable compliant mechanism is presented in this section. Two rotational bistable compliant mechanisms, BES1 and BES2, were designed separately and combined using the synthesis method described in Chapter 6. **TYPE<sub>21</sub><sup>21</sup>** is used to obtain four stable equilibria. The final design has very thin cross sections ( $\sim 0.1\text{mm}$ ) of RL beams.

There are limitations to design of small-size multistable compliant mechanisms using RL deformations. They are



(a)



(b)

**Figure 7.12** Nonlinear FE analysis for the combined rotational multistable compliant mechanism : (a) load-displacement response , and (b) strain energy plot.

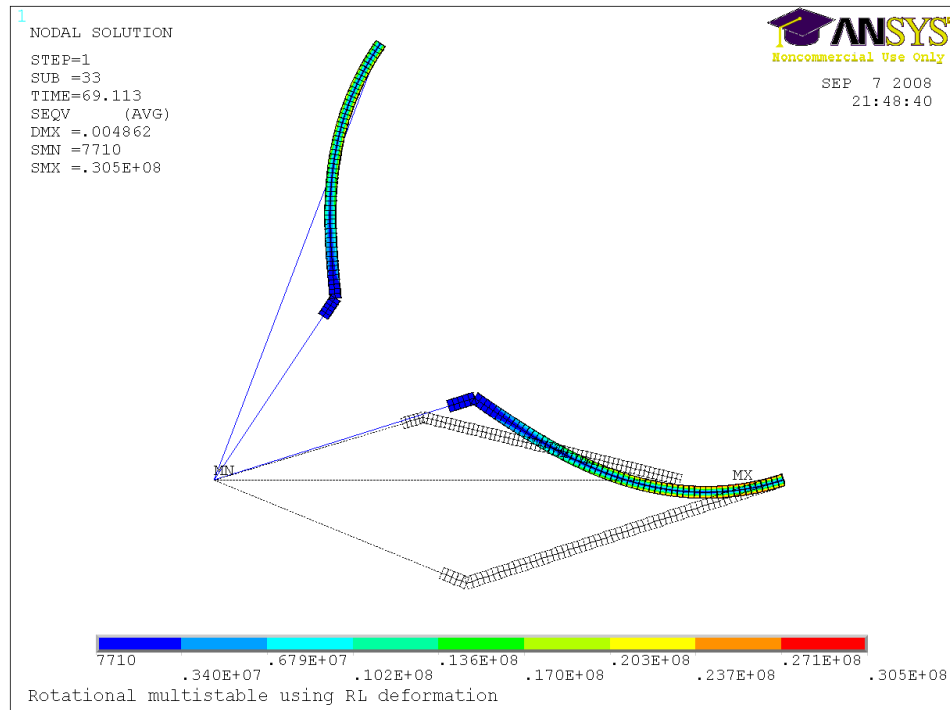


**Figure 7.13** The first and the fourth stable positions of the combined rotational multistable compliant mechanism and its stress results.

- i. *Limitation due to the slenderness ratio* : All design methods based on the Euler-Bernoulli have this limitation. The slenderness ratio must be greater than 15 (20 recommended) [5]. Using the recommended value of the ratio, designers can estimate the minimum thickness of RL beams once the overall size of design domain is defined.
- ii. *Limitation due to the minimum feature size* : This limitation is due to the manufacturing constraints.
- iii. *Limitation due to the stress constraint* : Although this is a critical constraint in many design problems, above two limitations are more critical in the design problem described in this section. This limitation is also dependent on the material properties.

Manufacturing processes of polypropylene can be achieved via extrusion or injection molding which are well suited for to mass productions.

## 7.2 Multistable Cargo Door Design using a Multistable Compliant Joint

The goal of this case study is to design a rotational multistable compliant mechanism that can tolerate a large input load. In general, living hinges are not applicable because they cannot sustain a large load. In this section, a buckled configuration is used to design a rotational multistable compliant mechanism.

The scope of the case study in this section is limited by the following assumptions:

- i. The bistable compliant mechanism will be designed by using the bistability of the buckled configuration shown in Fig. 4.23.
- ii. The magnitude of the load to be supported establishes the number of cyclic symmetric beams to be engaged for load sharing and the out-of-plane thickness.

### 7.2.1 Design Specifications

A cargo door is a door used to load or unload cargo. It is usually very heavy and requires a large amount of effort to open and close. Fig. 7.14 (a) shows the traditional cargo door with a pneumatic door opening system. In this section, a rotational multistable compliant mechanism will be designed to provide four stable positions of a cargo door as shown in Fig. 7.14 (b).

In this case study, design specifications for a rotational multistable compliant mechanism are following.

- i. *Footprint of the mechanism* : It is desired to be small enough so that it can be placed inside a vehicle along the hinge-line.
- ii. *Number of stable equilibria* : There are four open-positions of the cargo door. The four are equally distributed in the range of motion,  $75^\circ$ .
- iii. *Combination type* : In order to have four successive stable positions, combination **TYPE<sub>123</sub><sup>321</sup>** is desired. So three rotational bistable compliant mechanisms must be



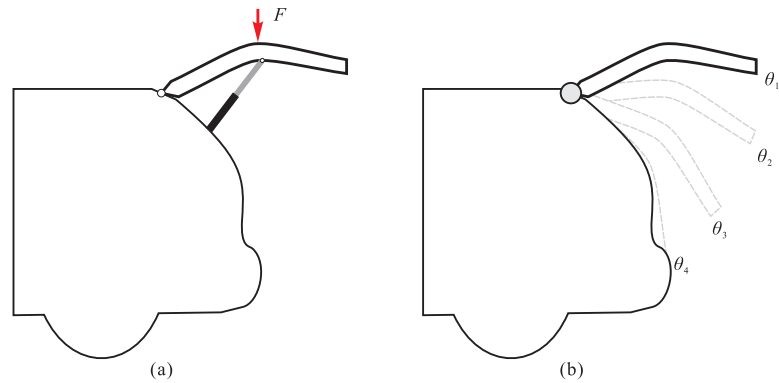


**Figure 7.14** Minivan cargo-door: (a) rigid-link mechanism with a pneumatic door opening system, and (b) rotational multistable compliant mechanism.

designed and combined. Combinations of three bistable behaviors are listed in Appendix C.

- iv. *Range of Motion* : Desired range of motion of combining three rotational bistable mechanisms is  $75^\circ$ . Three identical bistable compliant mechanisms that have  $26^\circ$  between two stable positions are used.
- v. *Materials* : A material which has a high ratio of yield stress to elastic modulus,  $\sigma_y/E$ , is desired. Titanium is used in this example. Table 7.1 has  $\sigma_y/E$  ratios of selected metals. Glass fiber reinforced polymer (GFRP) and carbon fiber reinforced plastic are other choices.
- vi. *Loading condition* : The height of the cargo door is 1.5 m ( $\sim 5$  feet), and its weight is 34.0 kg ( $\sim 75$  lb). The load due to the gravitational acceleration is applied to the center of the door. The maximum moment applied to the multistable compliant mechanism is 250 Nm.

## 7.2.2 Design of a Rotational Multistable Compliant Mechanism

Fig. 7.15 shows the input load due to the weight of the cargo door and the desired behavior of the multistable compliant mechanisms. The input load is a function of  $\theta$ , which is

**Table 7.1** Ratios of yield stress to elastic modulus of metals.

Material	Young's Modulus (GPa)	Yield Stress (MPa)	$\sigma_y/E \times 1E^3$
Aluminum	70	50	0.714
Copper	130	210	1.615
Gold	79	100	1.265
Iron	211	350	1.658
Lead	16	12	0.750
Nickel	170	195	1.147
Silver	83	170	2.048
Tantalum	186	200	1.075
Tin	47	200	4.255
Titanium	114	1170	10.263
Tungsten	411	620	1.508
Zinc	105	200	1.904

defined as an angle from the horizontal axis to the door. The input load is

$$M_{in} = M_{max} \cos \theta. \quad (7.3)$$

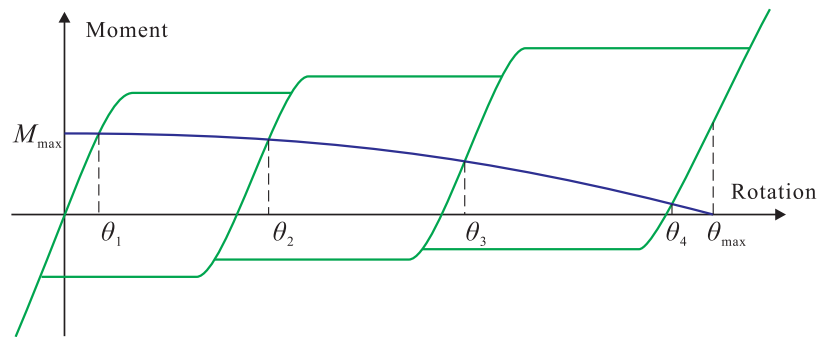


**Figure 7.15** Desired behavior of the multistable compliant mechanism and the door.

The cosine curve in Fig. 7.15 is decreased as  $\theta$  increases. The stable equilibria can be found wherever the two curves intersect each other. There are four stable equilibria,  $\theta_1 \sim \theta_4$ . Additionally, at  $\theta = \theta_{max}$ , the door is in its closed position.

Three rotational bistable compliant mechanisms will be combined based on the method introduced in Chapter 6. However, using **TYPE**<sub>123</sub><sup>321</sup>, three identical bistable compliant

mechanisms will be used. The rotational bistable mechanism shown in Fig. 4.23 is made of Titanium and has  $26^\circ$  angle between the two stable equilibria. The length of the beam is 8cm. The in-plane and out-of-plane thicknesses are 1mm and 4mm respectively. The actuation load of the bistable mechanism is 0.285 Nm. The load-displacement response of the bistable compliant mechanism is shown in Fig. 7.16. Note that the load is scaled to give a safety factor of 1.2. To match the scale, the out-of-plane thickness is increased to 10.4cm. Two rotational bistable mechanisms with 20 beams (load sharing) are used for each bistable behavior. The actuation load for the new rotational bistable mechanism is 296Nm.

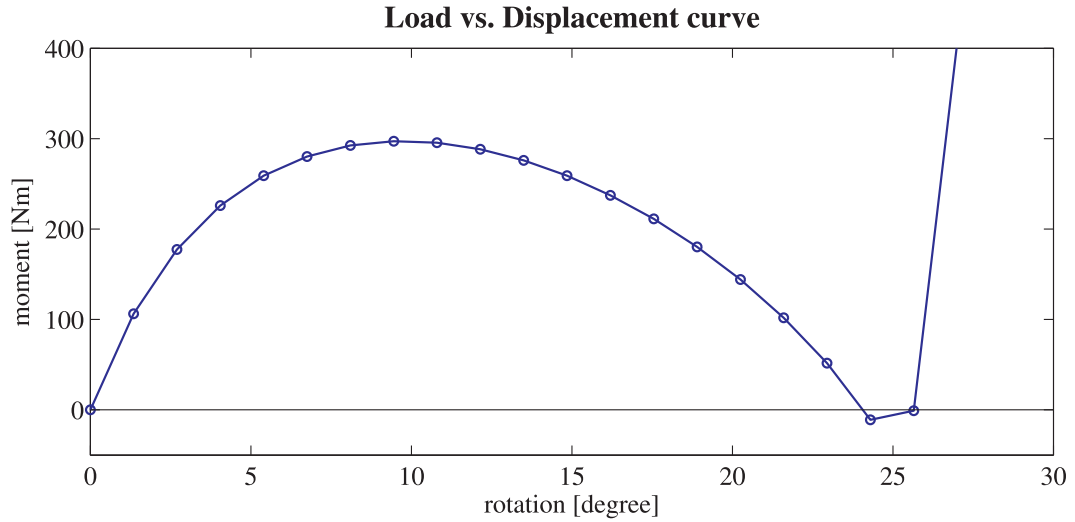


**Figure 7.16** Load-displacement curves of the multistable compliant mechanism and the door.

From the load-displacement curve in Fig. 7.16, the approximated piecewise continuous function is

$$M_i = \begin{cases} 60.0\phi_i - 3.0\phi_i^2 & \phi_i < 10 \\ -411.734 + 165.306\phi_i - 11.709\phi_i^2 + 0.229\phi_i^3 & 10 \leq \phi_i < 24 \\ 2145.0 - 180.0\phi_i + 3.7\phi_i^2 & 24 \leq \phi_i \end{cases} \quad (7.4)$$

The combined multistable behavior is plotted in Fig. 7.17. The entire range of motion

is about  $75^\circ$ , and the four stable equilibria are equally distributed with  $23^\circ$  angle.

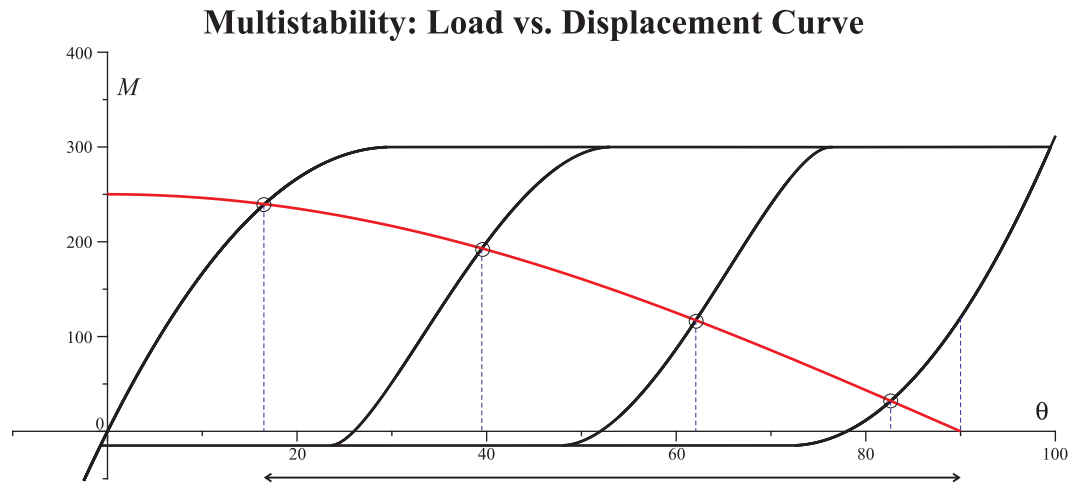


**Figure 7.17** Load-displacement curves of the multistable compliant mechanism and the door.

The combined rotational multistable compliant mechanism is shown in Fig. 7.17.

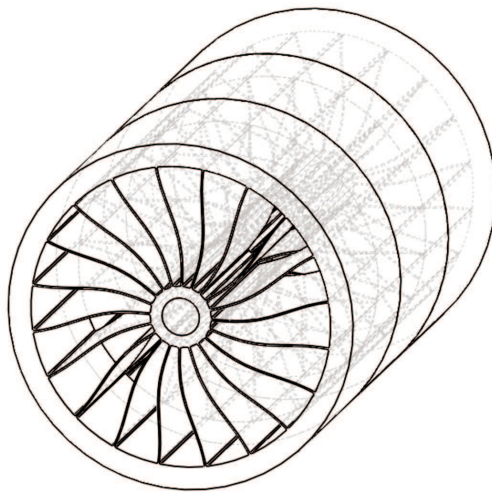


**Figure 7.18** A combined rotational multistable compliant mechanism. (diameter 23cm, length 36cm)

Fig. 7.18 shows how the multistable compliant mechanism can be attached to the cargo door.

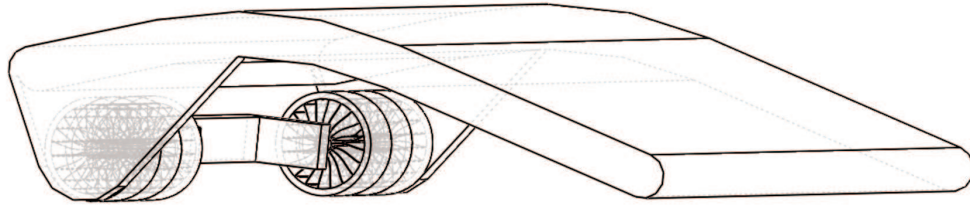


**Figure 7.19** A cargo door that has two rotational multistable compliant mechanisms located at both ends.

### 7.2.3 Discussion

This section presents the detailed design of a multistable compliant mechanism under a specified loading condition. The equilibria of the multistable compliant mechanism under a loading condition can be found by locating the intersection of two load-displacement curves. In order to design a rotational quadristable compliant mechanism which can be used as a multistable joint of a cargo door, three identical bistable compliant mechanisms were designed. They were combined to provide four stable equilibria. One of the advantages of using multiple identical bistable behaviors is that some of the stable equilibria are sharing their positions. Therefore manufacturing imperfections do not affect the stable positions. Rotational bistable compliant mechanisms are designed by using buckled configurations. A cyclic symmetric condition is applied to match the required actuation load. Also the out-of-plane thickness is scaled to match the required actuation load.

There can be some limitations to manufacture the rotational bistable compliant mechanism designed in this section due to the high aspect ratio. The limitations can cause manufacturing imperfections. However since there are many beams located cyclic symmetrically in the bistable compliant mechanism, sensitivity to the manufacturing imperfection is not critical.

## Chapter 8

### Conclusions, Contributions and Future Work

#### 8.1 Conclusions

The purpose of this dissertation is to establish a generalized mathematical framework for synthesis of multistable compliant mechanisms. A multistable compliant mechanism is a mechanism that can achieve multiple stable states within its range of motion through elastic deformation. It offers enormous advantages in terms of its stability, efficiency and accuracy. In addition, it has all the benefits that compliant mechanisms offer. In spite of attractive benefits and advantages, there has been no systematic method to design multistable compliant mechanisms. Existing methods to design multistability with conventional mechanisms require enormous computational time, and these methods do not apply to design compliant mechanisms that have more than two stable equilibria. Additionally, analysis of nonlinear behaviors of multistable compliant mechanisms is very complex and challenging. This research was motivated by the need to design multistable compliant mechanisms systematically without excessive computational complexity. This is accomplished by developing a mathematical formulation that captures the essential characteristics of nonlinear behaviors needed to design multistable compliant mechanisms.

The conclusion which can be drawn from this research is that synthesizing multistability can be decomposed into following two steps: (1) synthesizing bistabilities and (2) synthesizing multistability from the multiple bistabilities. In order to synthesize bistable compliant mechanisms, two new and systematic methods have been developed: (i) using

buckling modes as the initial stable configurations of the bistable compliant mechanisms, and (ii) utilizing the bistability of a clamped-pinned beam. The case studies in the chapters 4 and 5 demonstrated realization of the above two approaches. This study also introduced a mathematical approach to synthesize multistability by systematic combinations of bistable compliant mechanisms. Piecewise lower-order polynomials are used to represent nonlinear behaviors of bistable compliant mechanisms. The case studies in Chapter 6 demonstrated effectiveness of the method.

Some prototypes were fabricated and tested based on the case studies. The fabricated designs validated that the synthesis methodology introduced in this dissertation provides a viable method to create multistable compliant mechanisms from multiple bistable compliant mechanisms.

### **8.1.1 Summary of the Synthesis Methodologies**

#### **Synthesis of Bistable Compliant Mechanisms**

Two synthesis approaches for bistable compliant mechanisms were discussed in chapters 4 and 5. The first approach described in Chapter 4 utilized buckling configurations as initial configurations of bistable compliant mechanisms. In order to utilize buckling configurations, a modal strain energy formulation is introduced. The modal strain energy represents an energy barrier between two stable positions. Using topology optimization, topologies that satisfy desired bistabilities can be obtained by maximizing the modal strain energy. In topology optimization, design domains are discretized using modular ground structures. Unstable behaviors of beams are sensitive to imperfections, which may eliminate the desired bistabilities. Additional investigations regarding the effects of imperfections in Chapter 4 show how imperfections can eliminate bistabilities.

To reduce the manufacturing complexity and the sensitivity to imperfections, a reverse-lateral (RL) deformation of a clamped-pinned beam was introduced in Chapter 5. RL beams were used to design rotational and translational bistable compliant mechanisms in

the chapter. Bistable compliant mechanisms designed by using RL beams have robust bistabilities and are insensitive to imperfections. However, the drawback of using RL beams is that they require pin-joints. This can be overcome by utilizing flexures or living hinges instead of pin-joints to realize monolithic bistable compliant mechanisms.

### **Synthesis of Multistable Compliant Mechanisms**

The mathematical analysis introduced in Chapter 6 has demonstrated the validity of the hypothesis that combining bistabilities can generate multistabilities. Chapter 6 explains why a load-control method is effective and efficient to represent bistable behaviors compared to displacement-control and path-following methods. The load-control method was used to formulate the simplified mathematical expressions of bistable behaviors. This mathematical simplification enables designers to characterize bistable mechanisms by using piecewise lower-order polynomials and, in turn, synthesize multistable mechanisms.

Behaviors of combined multistable compliant mechanisms depend on combination types. Combination types were defined by the magnitude of actuation loads for each bistable behavior. The mathematical analysis performed in Chapter 6 showed that the number of stable equilibria as well as equilibrium paths is affected by combination types. Based on the combination types, combinations of two, three, and four bistable behaviors have been demonstrated. A library of feasible combinations was created. The methodology described in Chapter 6 can be extended to combine as many bistable behaviors as required. However, it seems reasonable to conclude that the combination table of three bistable behaviors is sufficient to design multistable compliant mechanisms with up to 8 stable equilibria.

### **8.1.2 Contributions**

This research is the first known attempt to develop a method to synthesize multistable compliant mechanisms which have more than two stable equilibria. Previous research in multistable compliant mechanism design is limited to design of bistable compliant mechanisms.



This is due to the fact that nonlinear analysis for multistable compliant mechanisms is much more complicated and limited by difficulties in numerical analysis including nonlinear finite element methods. Central to this research is a mathematical framework that captures the complex nonlinear behaviors of bistable and multistable compliant mechanisms. A key enabler for this is simplification of nonlinear behaviors in mathematical forms.

This dissertation provided three new and significant contributions to the following fields of compliant mechanism design.

1. *Synthesis of Multistable Compliant Mechanisms Using Combination of Multiple Bistable Compliant Mechanisms*: The methodology enables designers to (i) represent the design requirements in a mathematical expression, (ii) decompose the problem into feasible sub-problems, (iii) synthesize the desired multistable compliant mechanisms from combination libraries (e.g., Table 6.2 and Appendix C), and (iv) efficiently perform an evaluation without computationally intense nonlinear structural analysis.
2. *Topology Synthesis of Bistable Compliant Mechanisms Using Buckling Modes*: The method allows designers to (i) generate topologies of bistable compliant mechanisms using optimization methods, and (ii) perform analysis without nonlinear (large deformation) FEM.
3. *Topology Synthesis of Bistable Compliant Mechanisms Using Clamped-Pinned Beams*: The bistability of RL deformation provides the foundation to (i) design translational and rotational bistable compliant mechanisms using, and (ii) reduce imperfection sensitivity and hence robust designs of bistable and multistable compliant mechanisms.

Additional contributions of this work include:

- Optimization formulation for maximizing modal strain energy : Modal strain energy has been defined to represent energy barrier between two stable states. By maximizing modal strain energy, a designer can find the optimal topology which can provide

bistability.

- A Matlab based design tool for designing rotational bistable compliant mechanisms using RL deformation: Designers can use the tool to synthesize a rotational bistable compliant mechanism without solving the elliptic integral nor performing nonlinear analysis.
- Formulation of guidelines for designing translational bistable compliant mechanisms using RL deformation: Designers can use the chart (Fig. 5.10) to design a translational bistable compliant mechanism without solving either the elliptic integral or using nonlinear analysis.
- Analytical solution of an RL deformed beam and its visualization tool based on a Matlab environment: An analytical solution of RL deformation is implemented in a visualization tool. The visualization tool can be used to understand the behavior of RL deformation, such as deformed shapes, the path of the end of the beam, the load-displacement behavior, and the stress distribution.
- Digitizing bistability and multistability using binary number: The idea of digitizing multistability is that a unique binary number for each stable equilibrium can be identified by the corresponding equilibrium configuration of the combined bistable compliant mechanisms.
- Several novel bistable and multistable compliant mechanisms were designed. (Provisional patent filed)

## 8.2 Future Work

This study lays the foundation for future work on designing multistable compliant mechanisms. The future research can be divided into two main directions: (1) improving and expanding current methods of designing bistable and multistable compliant mechanisms and (2) exploring areas of application in multistable compliant mechanisms.

## 8.2.1 Improving Design Methodologies of Multistable Compliant Mechanisms

### Improving the Current Bistable Compliant Mechanism Synthesis Method

In Chapter 4, a Genetic Algorithm was applied to the topology optimization of bistable compliant mechanisms using buckling modes. A gradient based optimization is also applicable and reduces the computational time. When a gradient based optimization is used, the design variable can be the thickness of each beam of the ground structure. The upper and lower bounds of the design variables must be greater than zero, and the threshold value of the thickness can be chosen by the designer. The guidelines to acquire sensitivities of eigenvalues and eigenvectors of buckling analysis are described in Appendix E.

### Counterpart Design of Reverse Lateral Deformed Beam

In Chapter 5, rigid bodies and RL deformed beams were used as counterparts of RL deformation to generate bistable behaviors. However, the counterparts do not need to be limited to these two types. As explained in the chapter, counterparts of the RL deformation can be designed using nonlinear topology optimization. In this case, response behaviors of the counterpart mechanisms must match the load-displacement requirement for RL deformation, which are first established by solving elliptic integral.

### Decomposing Multistability to Multiple Bistabilities

The question as to how designer can select the best decomposition type remains open. A multistable compliant mechanism with  $n$  stable equilibria can be decomposed in many different types of combinations. For example, a quadristable behavior can be decomposed into either two (e.g. **TYPE**<sub>21</sub><sup>21</sup>) or three (e.g. **TYPE**<sub>321</sub><sup>123</sup>) bistable behaviors. The selection of the types of combinations depends on the application and the user preference.

## **Synthesis of Three Dimensional Multistable Compliant Mechanisms**

Multiple bistable compliant mechanisms can be synthesized in three-dimensional problems. Three-dimensional problems can be divided into single-DOF and multi-DOF problems. Single-DOF problems can be investigated by expanding the design theory of two-dimensional problems described in Chapter 6.

### **8.2.2 Areas of Applications**

Existing multistable mechanism (e.g. a multistable switch) that can benefit from compliant mechanisms should be explored to take advantage of the synthesis methodologies developed in this research. Space applications including pointing and orienting mechanisms, MEMS, flow control adaptive surfaces are other application of multistable compliant mechanisms. Ergonomic devices which require precise multistable behaviors are possible areas where multistable equilibrium compliant mechanisms can be well integrated.

## **Appendices**

# Appendix A: Combining Bistable Behaviors with Identical Actuation Loads

When the actuation load of each bistable system is identical, it is difficult to apply a previously defined types of combinations. Ideally, once the input load reaches the actuation load, each bistable system should be actuated at the same time. However, in the combined system, it is not possible to simultaneously make more than two bistable systems unstable. This problem can be illustrated by using a linear buckling analysis of two identical beams combined in series.

Fig. 1 illustrates two buckling problems and their boundary conditions: (a) has a single beam with an axial loading, and (b) has two identical beams combined in series. Only axial displacement is allowed at the end of each beam. The material and geometry properties are defined in the figure. The analytical solution of the eigenvalue problem of (a) is

$$P_{cr} = 4 \frac{\pi^2 EI}{L^2} = 65.7973,$$

where,  $P_{cr}$  is the critical load,  $E$  is Young's modulus,  $I$  is the area moment of inertia of the cross section, and  $L$  is the length of the beam. The critical load is obtained from the first or the smallest eigenvalue.

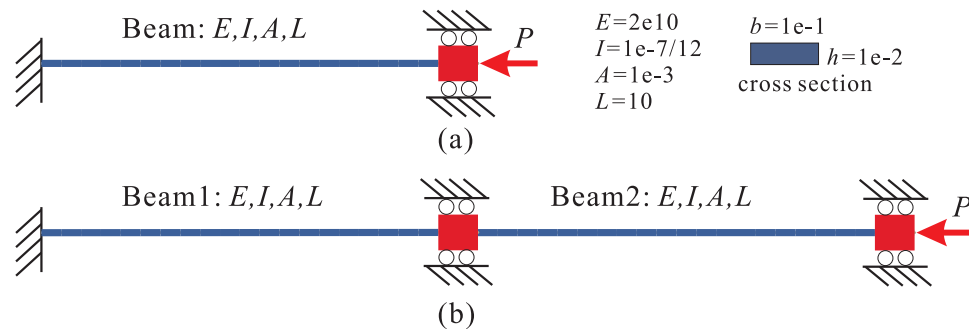


**Figure 1** Beam buckling analysis: (a) a single beam and (b) two beams in series.

The second problem can be solved with the same analytical method. The first and the second eigenvalues are the same. However, these repeated eigenvalues have different mode

shapes (orthogonal eigenvectors). Since only one mode shape is required to identify the buckled shape at the smallest eigenvalue, either one of the repeated eigenvectors can be used.

Fig. 2 describes the buckling mode shapes of the problems: (a) is the first buckling mode of the single beam, (b) is one of the smallest repeated eigenvalues of the combined problem, and (c) is the other buckling mode. The buckling mode shapes and the critical forces are obtained by using a finite element analysis with 20 elements per beam. Given that only one of the two subsystems is dominantly changed to its unstable status, we can deduce that after the initially actuated subsystem is fully collapsed, the other subsystem is turned into its unstable status.

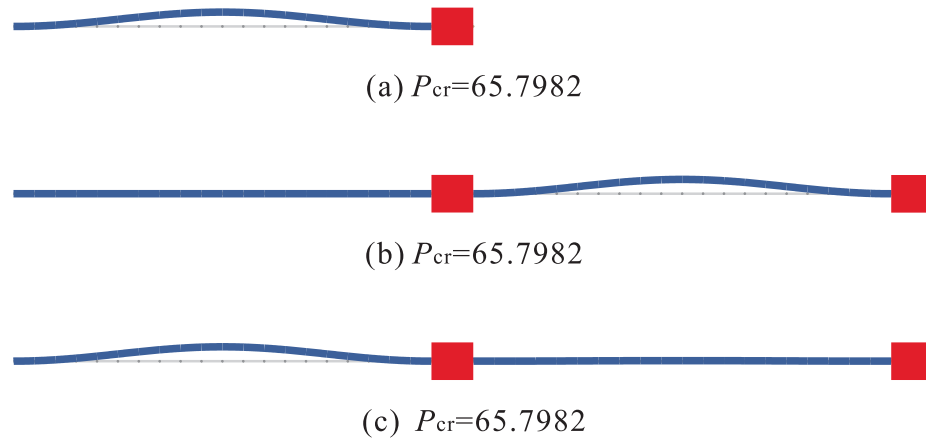
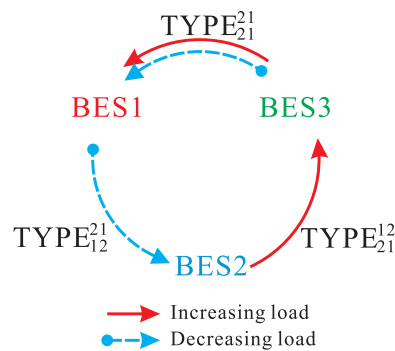


**Figure 2** Buckling modes and their critical loads: (a) one beam, (b)(c) two beams.

This behavior is even clearer when an imperfection is included in the analysis. Even though the designs of two bistable systems are identical, their actual behaviors are not be same with respect to the actuation loads and stable positions. This outcome is true because imperfections occur during manufacturing and in use. Whenever one of the actuation loads is smaller than the other, it is possible to apply the combination types defined in Chapter 6.

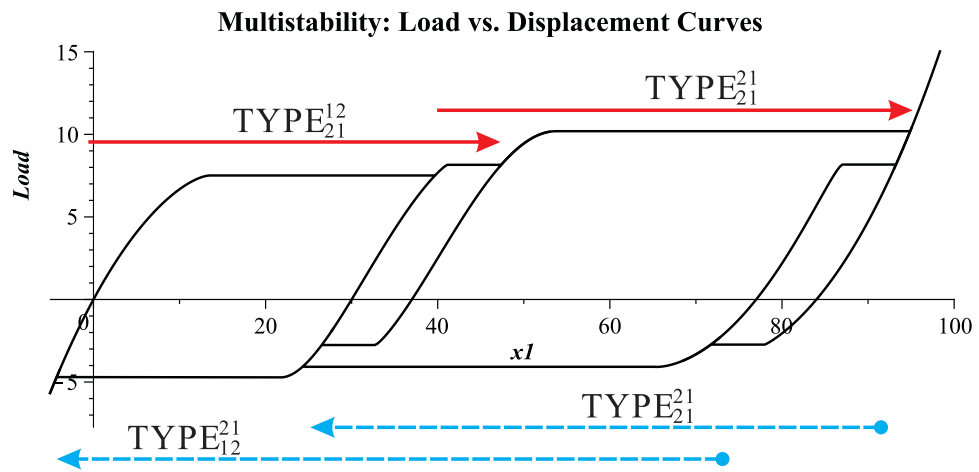
## Appendix B: Alternative Approach to Obtain Multistable Behavior

The combined multistable behavior in Fig. 6.15 is found by using the optimization procedure described in Chapter 6. Alternatively, the multistable behavior can be obtained by using the relations between two out of the three bistable behaviors (Fig. 3) and their combined behaviors in Table 6.2. The solid arrows in Fig. 3 and 4 indicate the direction in which the input load is increasing. The dotted arrows indicate that the load is decreasing. Whenever the input load increases or decreases, a pair of bistabilities with the two smallest actuation loads must be activated first. For example, when the load,  $F$ , increases in Fig. 6.12, the first pair includes BES2 and BES3. The corresponding type is  $\text{TYPE}_{21}^{12}$  as depicted in Fig. 3, and its behavior appears first as shown in Fig. 4. The second pair (BES1 and BES3), whose combination is  $\text{TYPE}_{21}^{21}$  has a higher load threshold and is activated only when the input load reaches this value. When the load decreases, the third pair (BES1 and BES3) has the two smallest actuation loads and appears first as  $\text{TYPE}_{21}^{21}$ . The other pair (BES1 and BES2) with the relation of  $\text{TYPE}_{12}^{21}$  is then derived when the load decreases further.



**Figure 3** Relationship chart between the two out of three bistable behaviors.

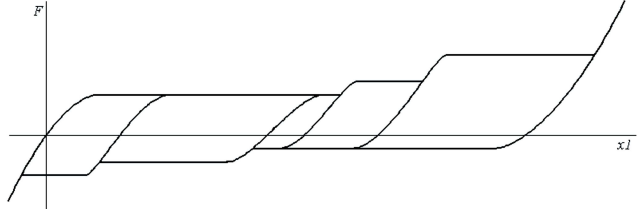
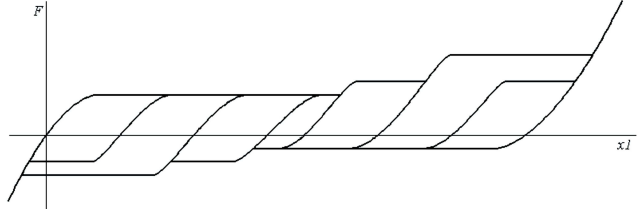
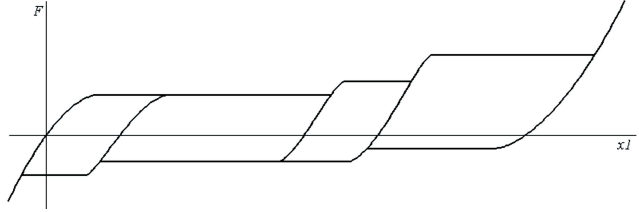
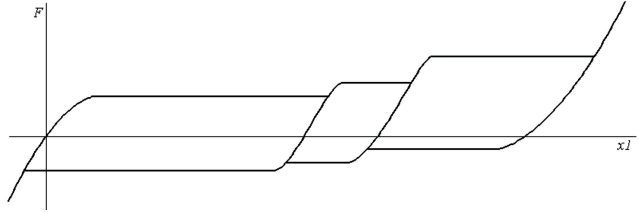
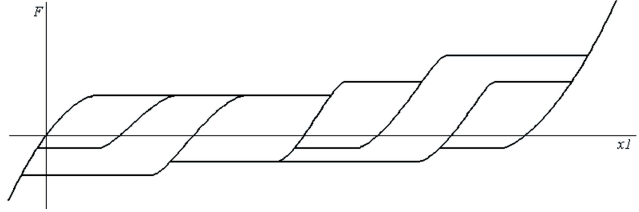
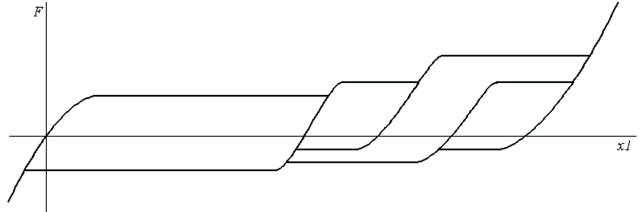


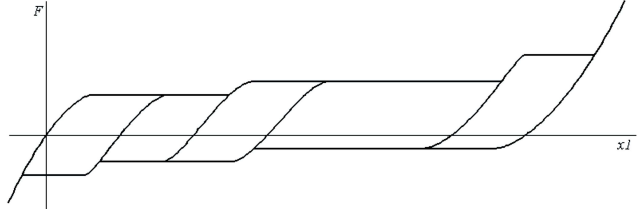
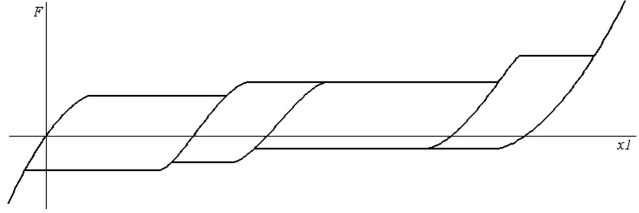
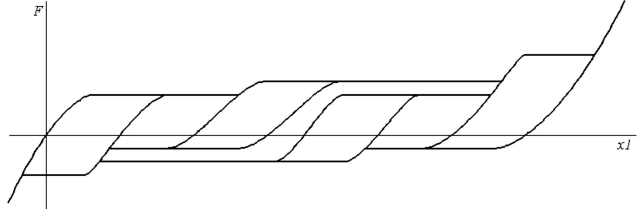
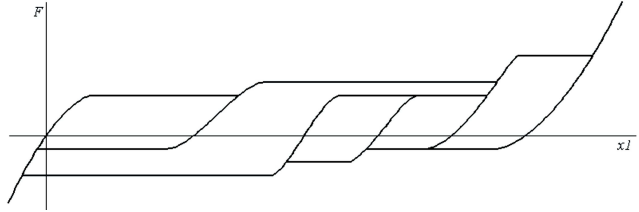
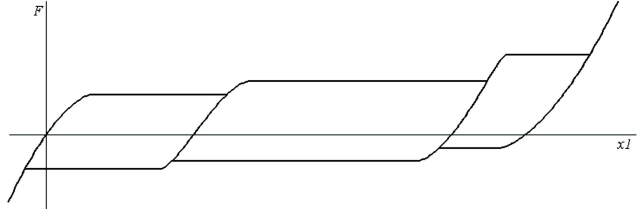
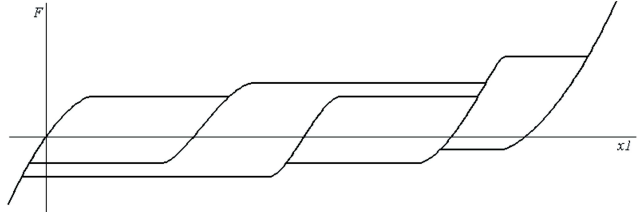


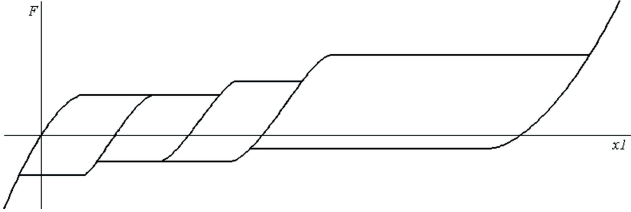
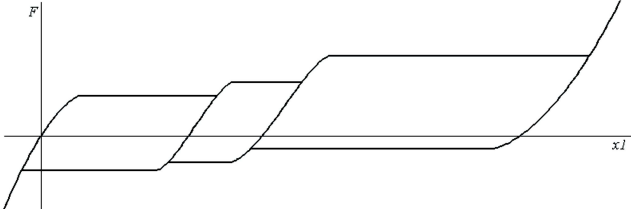
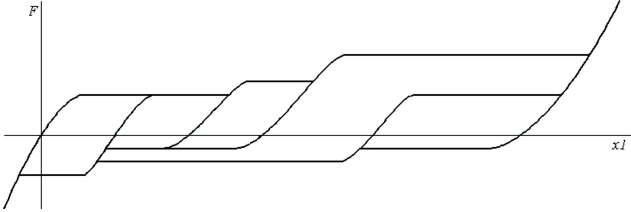
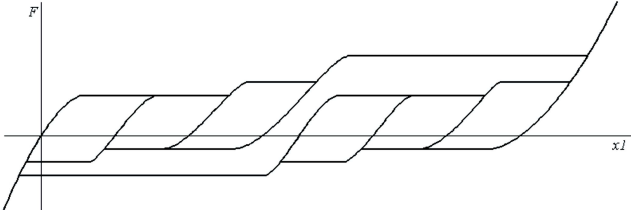
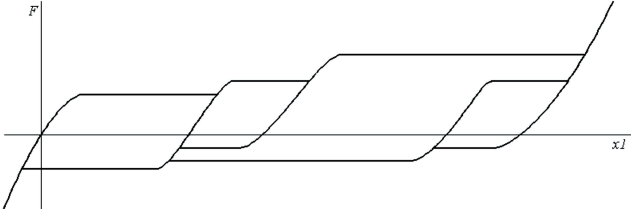
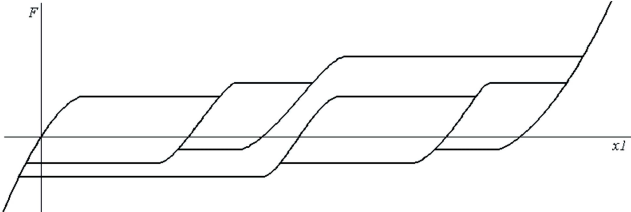
**Figure 4** Load-Displacement curve of  $TYPE_{312}^{231}$  and behaviors for two bistabilities in the curve.

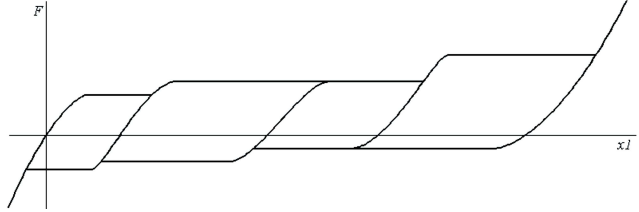
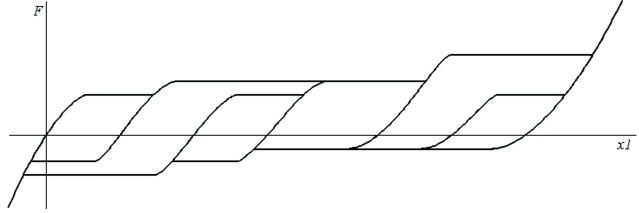
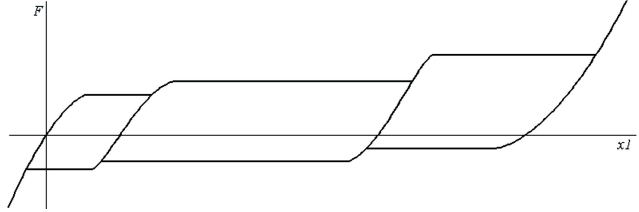
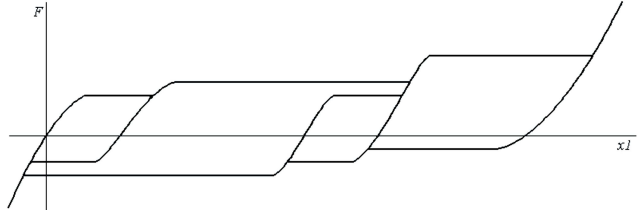
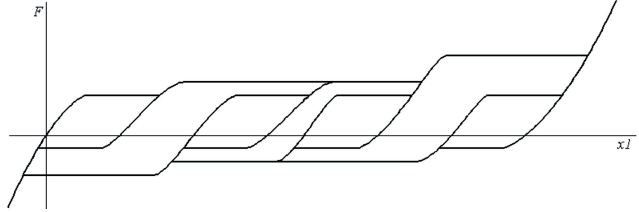
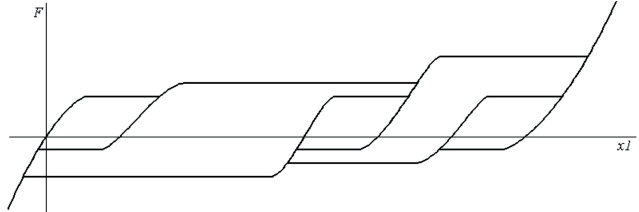
## Appendix C: Combinations of Three Bistable Behaviors ( $n = 3$ )

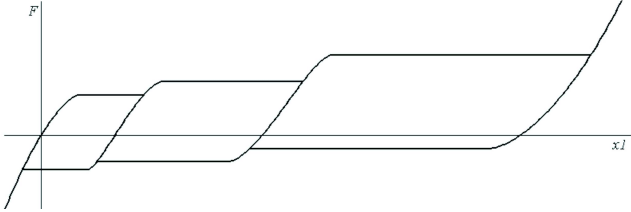
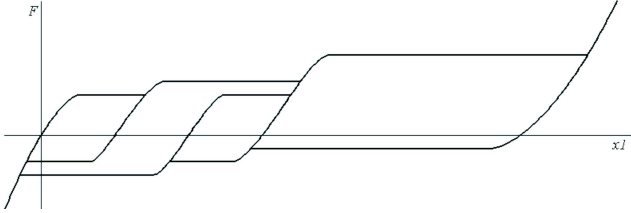
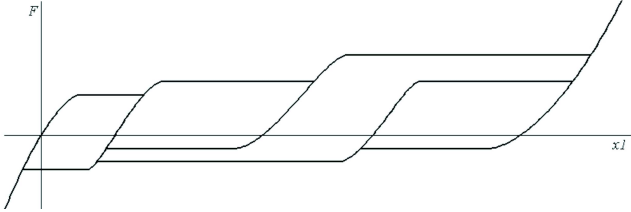
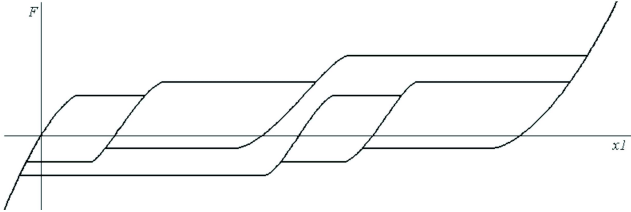
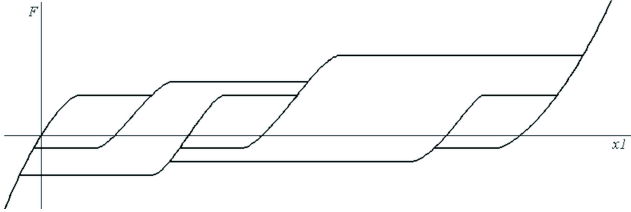
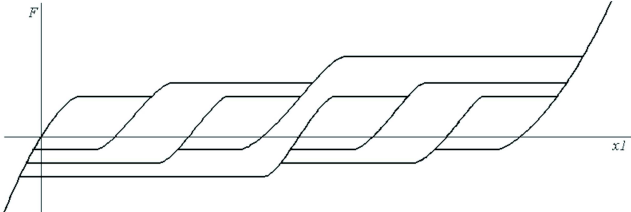
TYPE	Load-displacement Behavior	Number of Stable Equilibria
123 123		<b>8</b>
123 132		<b>6</b>
123 213		<b>6</b>
123 231		<b>5</b>
123 312		<b>5</b>
123 321		<b>4</b>

TYPE	Load-displacement Behavior	Number of Stable Equilibria
<p>132 123</p>	 <p>A graph with force <math>F</math> on the vertical axis and displacement <math>x_1</math> on the horizontal axis. It shows two curves: a loading curve (top) and an unloading curve (bottom). The loading curve has three distinct horizontal plateaus, and the unloading curve has three distinct horizontal plateaus. The curves intersect at six points, representing six stable equilibrium states.</p>	<p>6</p>
<p>132 132</p>	 <p>A graph with force <math>F</math> on the vertical axis and displacement <math>x_1</math> on the horizontal axis. It shows two curves: a loading curve (top) and an unloading curve (bottom). The loading curve has four distinct horizontal plateaus, and the unloading curve has four distinct horizontal plateaus. The curves intersect at eight points, representing eight stable equilibrium states.</p>	<p>8</p>
<p>132 213</p>	 <p>A graph with force <math>F</math> on the vertical axis and displacement <math>x_1</math> on the horizontal axis. It shows two curves: a loading curve (top) and an unloading curve (bottom). The loading curve has three distinct horizontal plateaus, and the unloading curve has two distinct horizontal plateaus. The curves intersect at five points, representing five stable equilibrium states.</p>	<p>5</p>
<p>132 231</p>	 <p>A graph with force <math>F</math> on the vertical axis and displacement <math>x_1</math> on the horizontal axis. It shows two curves: a loading curve (top) and an unloading curve (bottom). The loading curve has two distinct horizontal plateaus, and the unloading curve has two distinct horizontal plateaus. The curves intersect at four points, representing four stable equilibrium states.</p>	<p>4</p>
<p>132 312</p>	 <p>A graph with force <math>F</math> on the vertical axis and displacement <math>x_1</math> on the horizontal axis. It shows two curves: a loading curve (top) and an unloading curve (bottom). The loading curve has three distinct horizontal plateaus, and the unloading curve has four distinct horizontal plateaus. The curves intersect at seven points, representing seven stable equilibrium states.</p>	<p>7</p>
<p>132 321</p>	 <p>A graph with force <math>F</math> on the vertical axis and displacement <math>x_1</math> on the horizontal axis. It shows two curves: a loading curve (top) and an unloading curve (bottom). The loading curve has two distinct horizontal plateaus, and the unloading curve has three distinct horizontal plateaus. The curves intersect at five points, representing five stable equilibrium states.</p>	<p>5</p>

TYPE	Load-displacement Behavior	Number of Stable Equilibria
213 123	 <p>The graph shows force <math>F</math> on the vertical axis and displacement <math>x_1</math> on the horizontal axis. The load-displacement curve consists of three distinct stages, each with a horizontal plateau. The first stage has a single plateau. The second stage has two plateaus. The third stage has three plateaus. The total number of stable equilibria is 6.</p>	6
213 132	 <p>The graph shows force <math>F</math> on the vertical axis and displacement <math>x_1</math> on the horizontal axis. The load-displacement curve consists of three distinct stages, each with a horizontal plateau. The first stage has a single plateau. The second stage has two plateaus. The third stage has two plateaus. The total number of stable equilibria is 5.</p>	5
213 213	 <p>The graph shows force <math>F</math> on the vertical axis and displacement <math>x_1</math> on the horizontal axis. The load-displacement curve consists of three distinct stages, each with a horizontal plateau. The first stage has two plateaus. The second stage has three plateaus. The third stage has three plateaus. The total number of stable equilibria is 8.</p>	8
213 231	 <p>The graph shows force <math>F</math> on the vertical axis and displacement <math>x_1</math> on the horizontal axis. The load-displacement curve consists of three distinct stages, each with a horizontal plateau. The first stage has two plateaus. The second stage has two plateaus. The third stage has two plateaus. The total number of stable equilibria is 6.</p>	6
213 312	 <p>The graph shows force <math>F</math> on the vertical axis and displacement <math>x_1</math> on the horizontal axis. The load-displacement curve consists of three distinct stages, each with a horizontal plateau. The first stage has one plateau. The second stage has one plateau. The third stage has two plateaus. The total number of stable equilibria is 4.</p>	4
213 321	 <p>The graph shows force <math>F</math> on the vertical axis and displacement <math>x_1</math> on the horizontal axis. The load-displacement curve consists of three distinct stages, each with a horizontal plateau. The first stage has one plateau. The second stage has two plateaus. The third stage has two plateaus. The total number of stable equilibria is 5.</p>	5

TYPE	Load-displacement Behavior	Number of Stable Equilibria
231 123	 <p>The graph shows force <math>F</math> on the vertical axis and displacement <math>x_1</math> on the horizontal axis. The curve starts with a negative slope, crosses the <math>x_1</math> axis, and then exhibits four distinct regions of zero slope (horizontal segments) at increasing force levels, followed by a final region of positive slope.</p>	5
231 132	 <p>The graph shows force <math>F</math> on the vertical axis and displacement <math>x_1</math> on the horizontal axis. The curve starts with a negative slope, crosses the <math>x_1</math> axis, and then exhibits three distinct regions of zero slope (horizontal segments) at increasing force levels, followed by a final region of positive slope.</p>	4
231 213	 <p>The graph shows force <math>F</math> on the vertical axis and displacement <math>x_1</math> on the horizontal axis. The curve starts with a negative slope, crosses the <math>x_1</math> axis, and then exhibits five distinct regions of zero slope (horizontal segments) at increasing force levels, followed by a final region of positive slope.</p>	6
231 231	 <p>The graph shows force <math>F</math> on the vertical axis and displacement <math>x_1</math> on the horizontal axis. The curve starts with a negative slope, crosses the <math>x_1</math> axis, and then exhibits seven distinct regions of zero slope (horizontal segments) at increasing force levels, followed by a final region of positive slope.</p>	8
231 312	 <p>The graph shows force <math>F</math> on the vertical axis and displacement <math>x_1</math> on the horizontal axis. The curve starts with a negative slope, crosses the <math>x_1</math> axis, and then exhibits four distinct regions of zero slope (horizontal segments) at increasing force levels, followed by a final region of positive slope.</p>	5
231 321	 <p>The graph shows force <math>F</math> on the vertical axis and displacement <math>x_1</math> on the horizontal axis. The curve starts with a negative slope, crosses the <math>x_1</math> axis, and then exhibits five distinct regions of zero slope (horizontal segments) at increasing force levels, followed by a final region of positive slope.</p>	6

TYPE	Load-displacement Behavior	Number of Stable Equilibria
312 123	 <p>The graph shows force <math>F</math> on the vertical axis and displacement <math>x_1</math> on the horizontal axis. The curve starts with a negative slope, crosses the <math>x_1</math> axis, and then exhibits a series of three distinct hysteresis loops. Each loop consists of a loading path (upper curve) and an unloading path (lower curve). The final unloading path crosses the <math>x_1</math> axis at a point to the right of the origin, resulting in a total of 5 stable equilibrium points.</p>	5
312 132	 <p>The graph shows force <math>F</math> on the vertical axis and displacement <math>x_1</math> on the horizontal axis. The curve starts with a negative slope, crosses the <math>x_1</math> axis, and then exhibits a series of four distinct hysteresis loops. Each loop consists of a loading path (upper curve) and an unloading path (lower curve). The final unloading path crosses the <math>x_1</math> axis at a point to the right of the origin, resulting in a total of 7 stable equilibrium points.</p>	7
312 213	 <p>The graph shows force <math>F</math> on the vertical axis and displacement <math>x_1</math> on the horizontal axis. The curve starts with a negative slope, crosses the <math>x_1</math> axis, and then exhibits a series of three distinct hysteresis loops. Each loop consists of a loading path (upper curve) and an unloading path (lower curve). The final unloading path crosses the <math>x_1</math> axis at a point to the right of the origin, resulting in a total of 4 stable equilibrium points.</p>	4
312 231	 <p>The graph shows force <math>F</math> on the vertical axis and displacement <math>x_1</math> on the horizontal axis. The curve starts with a negative slope, crosses the <math>x_1</math> axis, and then exhibits a series of three distinct hysteresis loops. Each loop consists of a loading path (upper curve) and an unloading path (lower curve). The final unloading path crosses the <math>x_1</math> axis at a point to the right of the origin, resulting in a total of 5 stable equilibrium points.</p>	5
312 312	 <p>The graph shows force <math>F</math> on the vertical axis and displacement <math>x_1</math> on the horizontal axis. The curve starts with a negative slope, crosses the <math>x_1</math> axis, and then exhibits a series of four distinct hysteresis loops. Each loop consists of a loading path (upper curve) and an unloading path (lower curve). The final unloading path crosses the <math>x_1</math> axis at a point to the right of the origin, resulting in a total of 8 stable equilibrium points.</p>	8
312 321	 <p>The graph shows force <math>F</math> on the vertical axis and displacement <math>x_1</math> on the horizontal axis. The curve starts with a negative slope, crosses the <math>x_1</math> axis, and then exhibits a series of three distinct hysteresis loops. Each loop consists of a loading path (upper curve) and an unloading path (lower curve). The final unloading path crosses the <math>x_1</math> axis at a point to the right of the origin, resulting in a total of 6 stable equilibrium points.</p>	6

TYPE	Load-displacement Behavior	Number of Stable Equilibria
<p style="text-align: center;"><b>321</b> <b>123</b></p>		<b>4</b>
<p style="text-align: center;"><b>321</b> <b>132</b></p>		<b>5</b>
<p style="text-align: center;"><b>321</b> <b>213</b></p>		<b>5</b>
<p style="text-align: center;"><b>321</b> <b>231</b></p>		<b>6</b>
<p style="text-align: center;"><b>321</b> <b>312</b></p>		<b>6</b>
<p style="text-align: center;"><b>321</b> <b>321</b></p>		<b>8</b>

## Appendix D: Elliptic Integral Solution for Reverse Lateral Deformation

The following elliptic integrals have been derived by the elliptic integral tables of Byrd and Friedman [16].

Equation (17) is reduced to

$$\begin{aligned}\alpha &= \frac{1}{\sqrt{2}} \int_0^{\theta_e} \frac{d\theta}{\sqrt{n \sin \theta + \cos \theta - n \sin \theta_e - \cos \theta_e}} \\ &= \frac{1}{\sqrt{2}} H_1\end{aligned}$$

Equation (20) is reduced to

$$\begin{aligned}\frac{a}{L} &= \frac{1}{\sqrt{2}\alpha} \int_0^{\theta_e} \frac{\cos \theta d\theta}{\sqrt{n \sin \theta + \cos \theta - n \sin \theta_e - \cos \theta_e}} \\ &= \frac{1}{\sqrt{2}\alpha} (H_2 - p H_1 - n H_3)\end{aligned}$$

Equation (21) is reduced to

$$\begin{aligned}\frac{b}{L} &= \frac{1}{\sqrt{2}\alpha} \int_0^{\theta_e} \frac{\sin \theta d\theta}{\sqrt{n \sin \theta + \cos \theta - n \sin \theta_e - \cos \theta_e}} \\ &= \frac{1}{\sqrt{2}\alpha} H_3\end{aligned}$$



where,

$$\begin{aligned}
 H_1 &= g(F_k + F_{\lambda,k}) \\
 H_2 &= 2pg(E_k + E_{\lambda,k}) \\
 H_3 &= \frac{g}{p^2} \left( -\mu n(F_k + F_{\lambda,k}) - b(\mu + p)H_4\sqrt{2p(\mu + p)}\cos\lambda \right) \\
 H_4 &= \frac{1}{k^2} (E_k + E_{\lambda,k} - (1 - k^2)(F_k + F_{\lambda,k}))
 \end{aligned}$$

and,

$$\begin{aligned}
 \mu &= -(n \sin \theta_e + \cos \theta_e) \\
 p &= \sqrt{n^2 + 1} \\
 k &= \frac{\mu + n}{2p} \\
 g &= \sqrt{\frac{2}{p}} \\
 \lambda &= \text{sign}(n) \cdot \sin^{-1} \sqrt{\frac{p-1}{\mu+p}}
 \end{aligned}$$

$F_k = F(k)$  : Complete elliptic integral of the first kind

$F_{\lambda,k} = F(\lambda, k)$  : Incomplete elliptic integral of the first kind

$E_k = E(k)$  : Complete elliptic integral of the second kind

$E_{\lambda,k} = E(\lambda, k)$  : Incomplete elliptic integral of the second kind

where,  $n$  and  $\theta_e$  are defined in Fig. 5.2. The function,  $\text{sign}(n)$ , is defined as

$$\text{sign}(n) = \begin{cases} -1 & , \text{ if } n < 0 \\ 0 & , \text{ if } n = 0 \\ 1 & , \text{ if } n > 0 \end{cases}$$

## Appendix E: Sensitivity of Buckling Load and Corresponding Mode [28]

A linear prebuckling problem can be expressed as

$$[\mathbf{K} + \lambda \mathbf{G}] \Phi = \mathbf{0}. \quad (1)$$

where  $\mathbf{K}$  and  $\mathbf{G}$  are the global stiffness and geometry matrixes.  $\lambda$  and  $\Phi$  are the eigenvalue and corresponding eigenvector. The first eigenvalue is the critical load factor of the input load and the eigenvector is the buckling mode of the eigenvalue. This problem can be solved as the following:

$$\begin{aligned} [(\mathbf{K} + \mathbf{G}) + \gamma \mathbf{K}] \Phi &= \mathbf{0} \\ \mathbf{K}^{-1} (\mathbf{K} + \mathbf{G}) \Phi &= -\gamma \Phi \end{aligned} \quad (2)$$

where,

$$\gamma = \frac{1 - \lambda}{\lambda}. \quad (3)$$

Solving the eigenvalue problem of Eq. 2 yields

$$\lambda = \frac{1}{\gamma + 1}, \quad (4)$$

and the eigenvector can be calculated based on the following normalization.

$$\Phi^T \mathbf{G} \Phi = 1. \quad (5)$$

The sensitivity of the eigenvalue with respect to the design variables,  $\mathbf{x}$ , is

$$\begin{aligned}\frac{\partial \lambda}{\partial \mathbf{x}} &= \frac{-\Phi^T \left\{ \left( \frac{\partial \mathbf{K}}{\partial \mathbf{x}} + \lambda \frac{\partial \mathbf{G}}{\partial \mathbf{x}} \right) \Phi + \lambda \frac{\partial \mathbf{G}}{\partial \mathbf{u}} \Phi \frac{\partial \mathbf{u}}{\partial \mathbf{x}} \right\}}{\Phi^T \mathbf{G} \Phi (= 1)} \\ &= -\Phi^T \left\{ \left( \frac{\partial \mathbf{K}}{\partial \mathbf{x}} + \lambda \frac{\partial \mathbf{G}}{\partial \mathbf{x}} \right) \Phi + \lambda \frac{\partial \mathbf{G}}{\partial \mathbf{u}} \Phi \frac{\partial \mathbf{u}}{\partial \mathbf{x}} \right\}.\end{aligned}\quad (6)$$

The sensitivity of the eigenvector with respect to the design variables,  $\mathbf{x}$ , is

$$\frac{\partial \Phi}{\partial \mathbf{x}} = -\frac{1}{2} \left( \Phi^T \frac{\partial \mathbf{G}}{\partial \mathbf{x}} \Phi + \Phi^T \frac{\partial \mathbf{G}}{\partial \mathbf{u}} \Phi \frac{\partial \mathbf{u}}{\partial \mathbf{x}} \right) \Phi - \Phi^T \mathbf{G} \mathbf{y} \Phi + \mathbf{y} \quad (7)$$

where the vector,  $\mathbf{y}$ , can be calculated from the following equation.

$$\lambda \frac{\partial \mathbf{G}}{\partial \mathbf{u}} \Phi \mathbf{y} = - \left( \frac{\partial \mathbf{K}}{\partial \mathbf{x}} + \lambda \frac{\partial \mathbf{G}}{\partial \mathbf{x}} \right) \Phi + \frac{\partial \lambda}{\partial \mathbf{x}} \mathbf{G} \Phi + \lambda \frac{\partial \mathbf{G}}{\partial \mathbf{u}} \Phi \frac{\partial \mathbf{u}}{\partial \mathbf{x}} \quad (8)$$

## **Bibliography**

- [1] Multistability - nature.com. [http://www.nature.com/nrg/journal/v2/n4/glossary/nrg0401\\_268a\\_glossary.html](http://www.nature.com/nrg/journal/v2/n4/glossary/nrg0401_268a_glossary.html), 2008.
- [2] Multistability - wikipedia. <http://en.wikipedia.org/wiki/Multistable>, 2008.
- [3] Theoretical physics / complex systems - multistability. <http://www.icbm.de/kompl Syst/9905.html>, 2008.
- [4] ABAQUS.Inc. Abaqus analysis user's manual. *ABAQUS Version 6.6 Documentation*, 2006.
- [5] ABAQUS.Inc. Abaqus theory manual. *ABAQUS Version 6.6 Documentation*, 2006.
- [6] G. K. Ananthasuresh, S. Kota, and Y. Gianchandani. A methodical approach to the design of compliant micromechanisms. *Technical Digest. Solid-State Sensor and Actuator Workshop*, pages 189–92, 1994.
- [7] G. K. Ananthasuresh, S. Kota, and N. Kikuchi. Strategies for systematic synthesis of compliant mems. In *ASME Winter Annual Meeting - Symposium on MEMS, Dynamics Systems and Control*, volume 2, pages 677–686, 1994.
- [8] ANSYS.Inc. Nonlinear structural analysis. *ANSYS Documentation - Structural Analysis Guide*, 2005.
- [9] Shorya Awtar and Alexander H. Slocum. Constraint-based design of parallel kinematic xy flexure mechanisms. *Journal of Mechanical Design*, 129(8):816–830, 2007.
- [10] Shorya Awtar, Alexander H. Slocum, and Edip Sevincer. Characteristics of beam-based flexure modules. *Journal of Mechanical Design*, 129(6):625–639, 2007.
- [11] J Barber. *Intermediate Mechanics of Materials*. McGraw-Hill, Boston, 2001.
- [12] M. P. Bendsøe. Optimal shape design as a material distribution problem. *Structural and Multidisciplinary Optimization*, 1(4):193–202, 1989.
- [13] M. P. Bendsøe and N. Kikuchi. Generating optimal topologies in structural design using a homogenization method. *Comput. Methods Appl. Mech. Eng.*, 71(2):197–224, 1988.
- [14] P. A. Besselink. Bistable spring construction for a stent and other medical apparatus. *United States Patent 6,488,702*, (9/012,843), 2002.
- [15] K. E. Bisshopp and D. C. Drucker. Large deflection of cantilever beams. *Quarterly of applied Math*, 3(3):272–275, 1945.
- [16] Douglass L. Blanding. *Exact constraint machine design using kinematic principles*. ASME Press, New York, 1999.
- [17] P. F. Byrd and M. D. Friedman. *Handbook of Elliptic Integrals for Engineers and Physicists*. Springer-VerLag, Berlin, 1954.

- [18] J. Chessa. Programing the finite element method with matlab. Technical report, Northwestern University, 2002.
- [19] S. H. Crandall, N. C. Dahl, and T. J. Lardner. *An Introduction to the Mechanics of Solids*. McGraw-Hill, New York, 1978.
- [20] Martin L. Culpepper and Gordon Anderson. Design of a low-cost nano-manipulator which utilizes a monolithic, spatial compliant mechanism. *Precision Engineering*, 28(4):469–482, 2004.
- [21] N. Dixit and M. Campbell. Automated synthesis of bi-stable compliant relays. *46th AIAA/ASME/ASCE/AHS/ASC Structures, Structural Dynamics, and Materials Conference; Austin, TX; USA; 18-21 Apr*, page 1, 2005.
- [22] A. G. Erdman, S. Kota, and G. N. Sandor. *Mechanism design analysis and synthesis*. Prentice Hall, Upper Saddle River, N.J., 2001.
- [23] W. Fang and J. A. Wickert. Comments on measuring thin-film stresses using bi-layer micromachined beams. *Journal of Micromechanics and Microengineering*, 5(4):276–281, 1995.
- [24] C. A. Felippa. Nonlinear finite element methods - course note. <http://www.colorado.edu/engineering/CAS/courses.d/NFEM.d/>, 2007.
- [25] M. I. Frecker, G. K. Ananthasuresh, S. Nishiwaki, and S. Kota. Topological synthesis of compliant mechanisms using multi-criteria optimization. *Journal of mechanical design Transactions of the ASME*, 119(2):238–245, 1997.
- [26] F. B Friedman. Drinking tube. *United States Patent 2,094,268*, 1936.
- [27] A. Geisberger and M. D. Ellis. Storing mechanical potential in a mems device using a mechanically multi-stable mechanism. *United States Patent 7,012,491 B1*, 2006.
- [28] L. A. Godoy, E. O. Taroco, and R. A Feijoo. Second-order sensitivity analysis in vibration and buckling problems. *International Journal for Numerical Methods in Engineering*, 37(23):3999–4014, 1994.
- [29] P. Hajela and E. Lee. Genetic algorithms in truss topological optimization. *International journal of solids and structures*, 32(22):3341–3357, 1995.
- [30] R. H Harris. Buckling spring torsional snap actuator. *United States Patent 4,118,611*, 1978.
- [31] J. A. Hetrick, N. Kikuchi, and S. Kota. Robustness of compliant mechanisms topology optimization formulations. *SPIE*, 3667:244–254, 2000.
- [32] L L Howell. *Compliant Mechanisms*. John Wiley & Sons, Inc., 2001.

- [33] L. L. Howell and A. Midha. A method for the design of compliant mechanisms with small-length flexural pivots. *ASME Journal of Mechanical Design*, 116(1):280–290, 1994.
- [34] L. L. Howell and A. Midha. Parametric deflection approximations for end-loaded, large-deflection beams in compliant mechanisms. *ASME Journal of Mechanical Design*, 117(1):156–165, 1995.
- [35] L. L. Howell and A. Midha. Parametric deflection approximations for initially curved, large-deflection beams in compliant mechanisms. In *ASME Design Engineering Technical Conferences*, volume 96-DETC/MECH-1215, 1996.
- [36] L. L. Howell, A. Midha, and T. W. Norton. Evaluation of equivalent spring stiffness for use in a pseudo-rigid-body model of large-deflection compliant mechanisms. *ASME Journal of Mechanical Design*, 118(1):126–131, 1996.
- [37] L. L. Howell, S. S. Rao, and A. Midha. Reliability-based optimal design of a bistable compliant mechanism. *ASME Journal of Mechanical Design*, 116(4):1115–1121, 1994.
- [38] B. Jensen, M. Parkinson, K. Kurabayashi, L. Howell, and M. Baker. Design optimization of a fully-compliant bistable micro-mechanism. In *International Mechanical Engineering Congress and Exposition*, New York, NY, 2001. ASME.
- [39] B. D. Jensen and L. L. Howell. Identification of compliant pseudo-rigid-body four-link mechanism configurations resulting in bistable behavior. *ASME Journal of Mechanical Design*, 125:701–708, 2003.
- [40] B. D. Jensen, L. L. Howell, and G. M. Roach. Bistable compliant mechanism. *United States Patent 6,215,081 B1*, (US6215081B1), 2001.
- [41] B. D. Jensen, L. L. Howell, and L. G. Salmon. Introduction of two-link, in-plane, bistable compliant mems. In *Proceedings of the 1998 ASME Design Engineering Technical Conferences*. ASME, 1998.
- [42] J. Joo. *Nonlinear Synthesis of Compliant Mechanisms: Topology and Size and Shape Design*. PhD thesis, University of Michigan, 2001.
- [43] J. Joo and S. Kota. Topological synthesis of compliant mechanisms using nonlinear beam elements. *Mechanics Based Design of Structures and Machines*, 32(1):17–38, 2004.
- [44] J. Joo, S. Kota, and N. Kikuchi. Nonlinear synthesis of compliant mechanisms: Topology design. In *Proceedings of the 2000 ASME Design Engineering Technical Conferences*, 2000.
- [45] J. Joo, S. Kota, and N. Kikuchi. Large deformation behavior of compliant mechanisms. In *ASME Design Engineering Technical Conferences, DETC 2001*, 2001.

- [46] B. H. Kang and J. T. Wen. Design of compliant mems grippers for micro-assembly tasks. In *International Conference on Intelligent Robots and Systems*, Beijing, China, 2006.
- [47] B. H. Kang, J. T. Wen, N. G. Dagalakis, and J. J. Gorman. Design optimization for a parallel mems mechanism with flexure. In *2004 ASME Design Engineering Technical Conferences*, Salt Lake City, Utah USA, 2004.
- [48] C. King, J. J. Beanpan, S. V. Sreenivasan, and M. Campbell. Multistable equilibrium system design methodology and demonstration. *Journal of Mechanical Design (Transactions of the ASME)*, (6):1036, 2004.
- [49] C. W. King, M. I. Campbell, J. J. Beaman, and S. V. Sreenivasan. Synthesis of multistable equilibrium linkage systems using an optimization approach. *Structural and Multidisciplinary Optimization*, 29(6):477–487, 2005.
- [50] M. Kjell. Numerical results from large deflection beam and frame problems analysed by means of elliptic integrals. *International Journal for Numerical Methods in Engineering*, 17(1):145–153, 1981.
- [51] E. Kollata, C. King, and M. Campbell. Design synthesis of multistable compliant structures. *10th AIAA/ISSMO Multidisciplinary Analysis and Optimization Conference, Albany, New York, Aug. 30-1, 2004*.
- [52] Sridhar Kota and G. K. Ananthasuresh. Designing compliant mechanisms. *Mechanical Engineering-CIME*, v117(11):93–96, 1995.
- [53] W. H. Lee, B. H. Kang, Y. S. Oh, H. E. Stephanou, A. C. Sanderson, G. Skidmore, and M. Ellis. Micropeg manipulation with a compliant microgripper. In *IEEE International Conferences on Robotics and Automation*, 2003.
- [54] C. T. Leondes. *Intelligent Systems: Technology and Applications, Six Volume Set*. CRC Press, Inc., 2002.
- [55] A. A. Limaye, C. W. King, and M. I. Campbell. Analysis of multiple equilibrium positions in magnetostatic field. *Proceedings of the ASME Design Engineering Technical Conference*, 2 B:1289–1297, 2003.
- [56] N. Lobontiu. *Compliant mechanisms: Design of flexure hinges*. CRC Press, 2002.
- [57] K. J. Lu. *Synthesis of Shape Morphing Compliant Mechanisms*. PhD thesis, University of Michigan, 2004.
- [58] K. J. Lu and S. Kota. Design of compliant mechanisms for morphing structural shapes. *Journal of Intelligent Material Systems and Structures*, 14(6):379–391, 2003.
- [59] K. J. Lu and S. Kota. Topology and dimensional synthesis of compliant mechanisms using discrete optimization. *Journal of Mechanical Design*, 128(5):1080–1091, 2006.



- [60] M. P. Murphy and L. O'Neill. *What is Lift? The Next Fifty Years*. Cambridge University Press, New York, USA, 1995.
- [61] Y. S. Oh. Snap-fit based microassembly with a compliant gripper. Master thesis of mechanical engineering, Rensselaer Polytechnic Institute, 2003.
- [62] Y. S. Oh and S. Kota. Synthesis of multistable equilibrium compliant mechanisms using combinations of bistable mechanisms. In *Proceedings of the 2007 ASME Design Engineering Technical Conferences*, Las Vegas, NV, 2007. ASME.
- [63] Y. S. Oh and S. Kota. Robust design of bistable compliant mechanisms using the bistability of a clamped-pinned beam. In *Proceedings of the ASME 2008 International Design Engineering Technical Conferences*, New York, NY, 2008. ASME.
- [64] M. Ohsaki and S. Nishiwaki. Shape design of pin-jointed multistable compliant mechanisms using snapthrough behavior. *Structural and Multidisciplinary Optimization*, 30(4):327–334, 2005.
- [65] J. Park, Y. Lee, J. Song, and H. Kim. Safe link mechanism based on passive compliance for safe human-robot collision. *2007 IEEE International Conference on Robotics and Automation*, pages 1152 – 1157, 2007.
- [66] J. Park, Y. Lee, J. Song, and H. Kim. Safe joint mechanism based on nonlinear stiffness for safe human-robot collision. *2008 IEEE International Conference on Robotics and Automation*, pages 2177–2182, 2008.
- [67] J. M Paros and L. Weisbord. How to design flexure hinges. *Machine Design*, pages 151–156, 1965.
- [68] C. B. W. Pedersen, T. Buhl, and O. Sigmund. Topology synthesis of large-displacement compliant mechanisms. *International Journal for Numerical Methods in Engineering*, 50(12):2683–2705, 2001.
- [69] C. B. W. Pedersen, N. A. Fleck, and G. K. Ananthasuresh. Design of a compliant mechanism to modify an actuator characteristic to deliver a constant output force. *Journal of Mechanical Design*, 128(5):1101–1112, 2006.
- [70] J. Qiu, J. H. Lang, and A. H. Slocum. A curved-beam bistable mechanism. *Microelectromechanical Systems, Journal of*, 13(2):137–146, 2004.
- [71] L. Saggere and S. Kota. Static shape control of smart structures using compliant mechanisms. *AIAA Journal*, 37(5):572–579, 1999.
- [72] A. Saxena and G. K. Ananthasuresh. Topology synthesis of compliant mechanisms for nonlinear force-deflection and curved path specifications. *Transactions of the ASME, Journal of Mechanical Design*, 123(1):33–42, 2001.
- [73] H. G. Schaeffer. *MSC.Nastran Primer for Linear Analysis*. MSC.Software Corporation, 2001.

- [74] W. K. Schomburg and C. Goll. Design optimization of bistable microdiaphragm valves. *Sensors and Actuators*, 64:259 – 264, 1998.
- [75] Stuart T. Smith. *Flexures elements of elastic mechanisms*. Gordon & Breach, Amsterdam, 2000.
- [76] V. Steinberg. Hydrodynamics: Bend and survive. *Nature*, 420(6915):473, 2002.
- [77] B. Trease. *Topology Synthesis of Compliant Systems with Embedded Actuators and Sensors*. PhD thesis, University of Michigan, 2008.
- [78] B. Trease, Y. Moon, and S. Kota. Design of large-displacement compliant joints. *ASME Journal of Mechanical Design*, 127(4):788–798, 2005.
- [79] C. Vekar. *Generalized Synthesis Methodology of Nonlinear Springs For Prescribed Load-Displacement Functions*. PhD thesis, University of Michigan, 2008.
- [80] C. Vekar and S. Kota. Generalized synthesis of nonlinear spring for prescribed load-displacement functions. In *ASME Design Engineering Technical Conferences & Computer and Information in Engineering Conference*, volume DETC2006-99657, 2006.
- [81] C. J. Wood. Bistable hinge with reduced stress regions. *United States Patent 6,321,923*, 2001.